Bulletin of the Geological Society of Denmark

VOLUME 58 | DECEMBER 2010 | COPENHAGEN

DGF

Bulletin of the Geological Society of Denmark

is published by the Geological Society of Denmark (DGF, Dansk Geologisk Forening), founded in 1893

The *Bulletin* publishes contributions of international interest in all fields of geological sciences, with a natural emphasis on results of new work on material from Denmark and Greenland.

Contributions based on foreign material may also be submitted to the *Bulletin* in cases where the author is a member of the Society. The yearly rate of publishing is one volume, each consisting of two issues. All articles are issued as pdf-files after acceptance. The paper edition of each volume is issued at the end of the year.

Subscription

The annual subscription rate is DKK 350.00 excl. VAT and postage.

Instructions to authors:

See:
http://2dgf.dk/publikationer/bulletin/vejledning.html

Manuscripts will be reviewed by two referees and will appear approximately in the order in which they are accepted for publication. The final decision on whether or not a manuscript will be accepted for publication rests with the editor, acting, when necessary, on the advice of the editorial board. The final version of the manuscript should be submitted as a paper copy and as a digital file. If possible line drawings, tables, etc. should also be submitted as computer files.

Cover:
The type section of the Rørdal Member in the south-western wall of the Rørdal quarry. The exposed section is about 7 m high. Photo: Finn Surlyk.

Cyrtometopinid trilobites from the upper Volkhov and lower Lynna formations (lower Darriwilian) of NW Russia

THOMAS HANSEN

Hansen, T. 2010-16-02. Cyrtometopinid trilobites from the upper Volkhov and lower Lynna Formation (lower Darriwilian) of NW Russia. © 2010 by Bulletin of the Geological Society of Denmark, Vol. 58, pp. 1-13. ISSN 0011–6297. (www.2dgf.dk/publikationer/bulletin)

Two cyrtometopinid trilobite taxa from the lower Darriwilian of NW Russia are examined. A new species of the genus *Krattaspis* is described, extending the stratigraphical range of the genus into the lower Darriwilian (Middle Ordovician). *K. paraspinosis* n.sp. is the youngest representative of the genus, but is closest to forms assigned to *Cyrtometopus* and confirms the derivation of *Cyrtometopus* from *Krattaspis*. Ontogenetic studies of *K. paraspinosis* n.sp. and *Cyrtometopus clavifrons* Angelin, 1854, from the same beds indicates a forward displacement of the eyes with increasing size, which may be contrary to all other known members of the family Cheiruridae.

Keywords: *Cyrtometopus clavifrons*, *Krattaspis paraspinosus* n.sp., Cyrtometopinae, NW Russia, lower Darriwilian.

Thomas Hansen [th@geo.ku.dk], Department of Geography and Geology, Copenhagen University, Øster Voldgade 10, DK-1350 København K, Denmark.

The lower Darriwilian trilobites from Baltoscandia are described in several monographs (e.g., Dalman 1827; Angelin 1854; Linnarsson 1869; Schmidt 1881-1907; Brøgger 1882; Törnquist 1884; Lamansky 1905; Balashova 1953, 1976; Männil 1958; Přibyl, Vanek & Pek 1985; Nielsen 1995). These papers have resulted in an extensive knowledge of the geographical distribution of species, whereas the stratigraphical occurrences in most cases are known only at zonal or formational level. The biostratigraphy is thus from a modern point of view relatively coarse. Some initial steps have been taken in filling those gaps (e.g., Wandås 1984; Nielsen 1995; Hansen & Nielsen 2003; Ivantsov 2003), but much work remains to be done.

In the spring of 2000, intensive sampling was carried out at the Lynna River east of St. Petersburg, Russia (Fig. 1). The field work formed part of a larger project between St. Petersburg State University, the University of Copenhagen and the Geological Survey of Denmark and Greenland, with the main purpose to study the biostratigraphy of the Volkhov and Kunda stages (upper Dapingian to middle Darriwilian). The present study deals with the uppermost part of the $B_{II}\beta$, the entire $B_{II}\gamma$ and the lower part of the $B_{III}\alpha$ zones sensu Lamansky (1905), representing the upper part of the Volkhov Stage (B_{II}) and the lower part of the Kunda Stage (B_{III}). The studied section was divided into 11 beds and 50 sub-beds and sampled for fossils. This yielded 3920 mostly disarticulated trilobite specimens of which 151 or nearly four percent represented the subfamily Cyrtometopinae Öpik, 1937. The general biostratigraphic results for the trilobites have been treated elsewhere by Hansen & Nielsen (2003). The cyrtometopinid material contains three species, *Cyrtometopus clavifrons* Angelin, 1854, *Krattaspis paraspinosis* n.sp. and *Hemisphaerocoryphe platinflata* Hansen, 2005. *Hemisphaerocoryphe* Reed, 1896 has been treated elsewhere (Hansen 2005) and its taxonomical belonging to the cyrtometopinids is also not accepted by all (e.g. Congreve & Lieberman 2010). *C. clavifrons* was redescribed by Lane (2002) who observed some variation in morphology between various geographical areas, but did not find any systematic differences. This may, however, be because of coarse biostratigraphic resolution.

The aim of the present work is to present a description of the new species *Krattaspis paraspinosis* n.sp and how it supports the proposed relationship between *Krattaspis* and *Cyrtometopus*. Furthermore new data on ontogenesis and stratigraphically related changes in morphology of *Cyrtometopus clavifrons* are discussed.

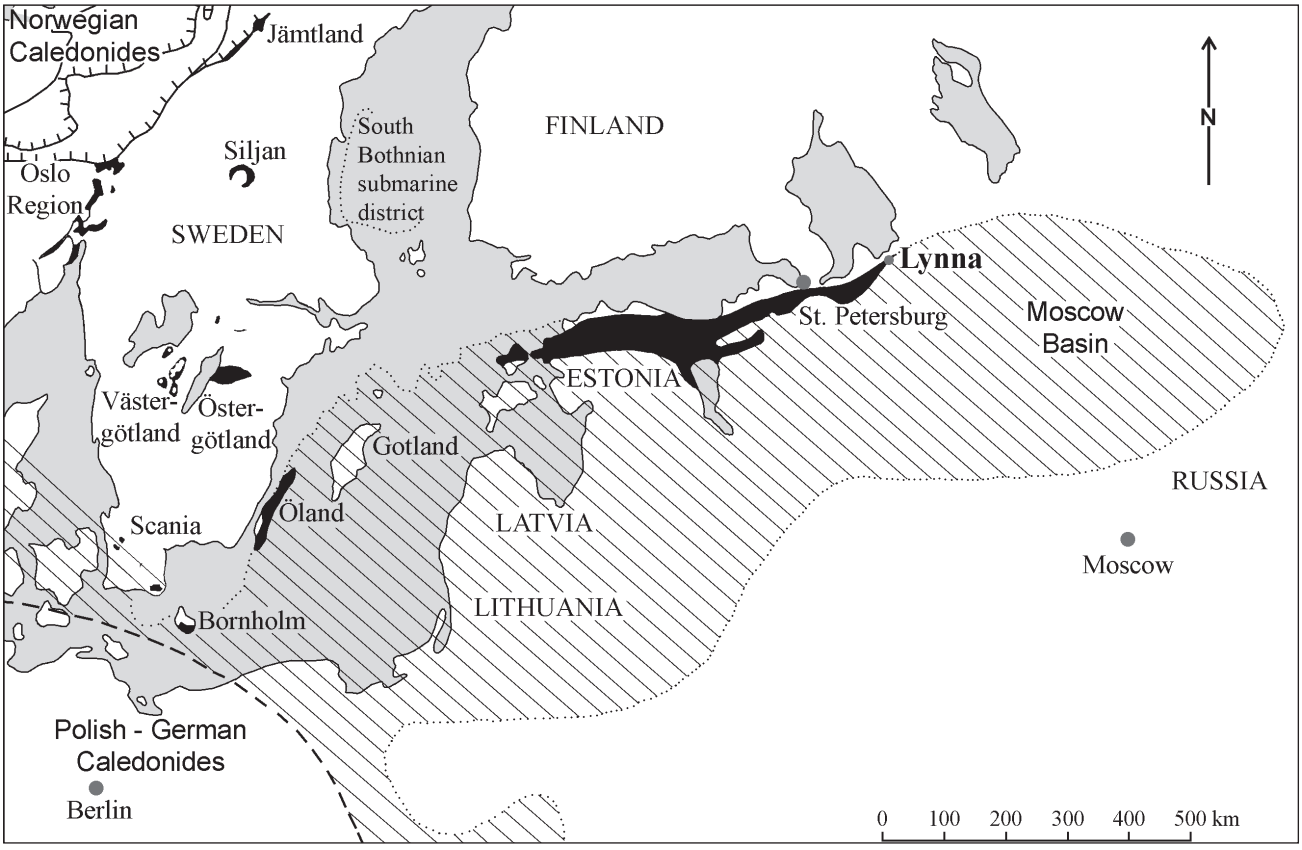

Fig. 1. Map showing distribution of Ordovician deposits in Baltoscandia. Outcrops are shown in black, while submarine and subsurface deposits are marked with diagonal stripes. The map is modified after Jaanusson (1982) and Nielsen (1995).

Geological setting

The studied exposure is located near the outlet of the Lynna River, about 150 km east of St. Petersburg, Russia (Fig. 1). The outcrop, which is more than 10 metres high, exposes Middle Ordovician rocks including the upper part of Volkhov Stage and the entire Kunda Stage. The section comprises yellowish to grey calcareous packstone and wackestone beds with numerous marl intercalations and high glauconite content in the lower half. This paper only deals with the lower 4.2 metres, which extend from the middle part of the Volkhov Formation (top of $B_{II}\beta$) to the basal part of the Lynna Formation (basis of $B_{III}\alpha$) (Fig. 2).

At the time of deposition the Baltic continent was situated in a temperate belt at about 50° S (Christiansen & Stouge 1999). The continent was largely covered by an epicontinental sea with only a few smaller land areas. Because of the low topography and extensive flooding the supply of terrigeneous sediments was extremely low. This together with a low cool-water carbonate production resulted in a very small net rate of sedimentation approximating 1 to 3 mm/1000 years (Jaanusson 1982). The low supply of terrigeneous sediments together with higher energy, reworking and removal of the clay particles resulted in extensive cool-water carbonate ramps in the shallow-watered Baltic area (Tolmacheva *et al*. 1999), whereas the outer shelf in south-western Scandinavia was characterized by siliclastic, muddy deposits (Jaanusson 1982, Nielsen 1995).

The sediments at Lynna were deposited below fair-weather wave base in a middle carbonate ramp environment containing a rich benthic fauna. Except for the constant alternation between marl and more coarse-grained limestone the succession is very uniform, indicating a largely stable environment. Even the sea level changes occurring throughout the period only resulted in slight changes such as a generally coarsening of the sediments and a variable glauconite and clastic content.

The area around Oslo, southern Norway, was characterized by deposition of impure carbonates through most of the Volkhov and Kunda stages and probably represents a mid shelf environment much like that found in the East-Baltic area, although influenced by a slightly higher terrigeneous input.

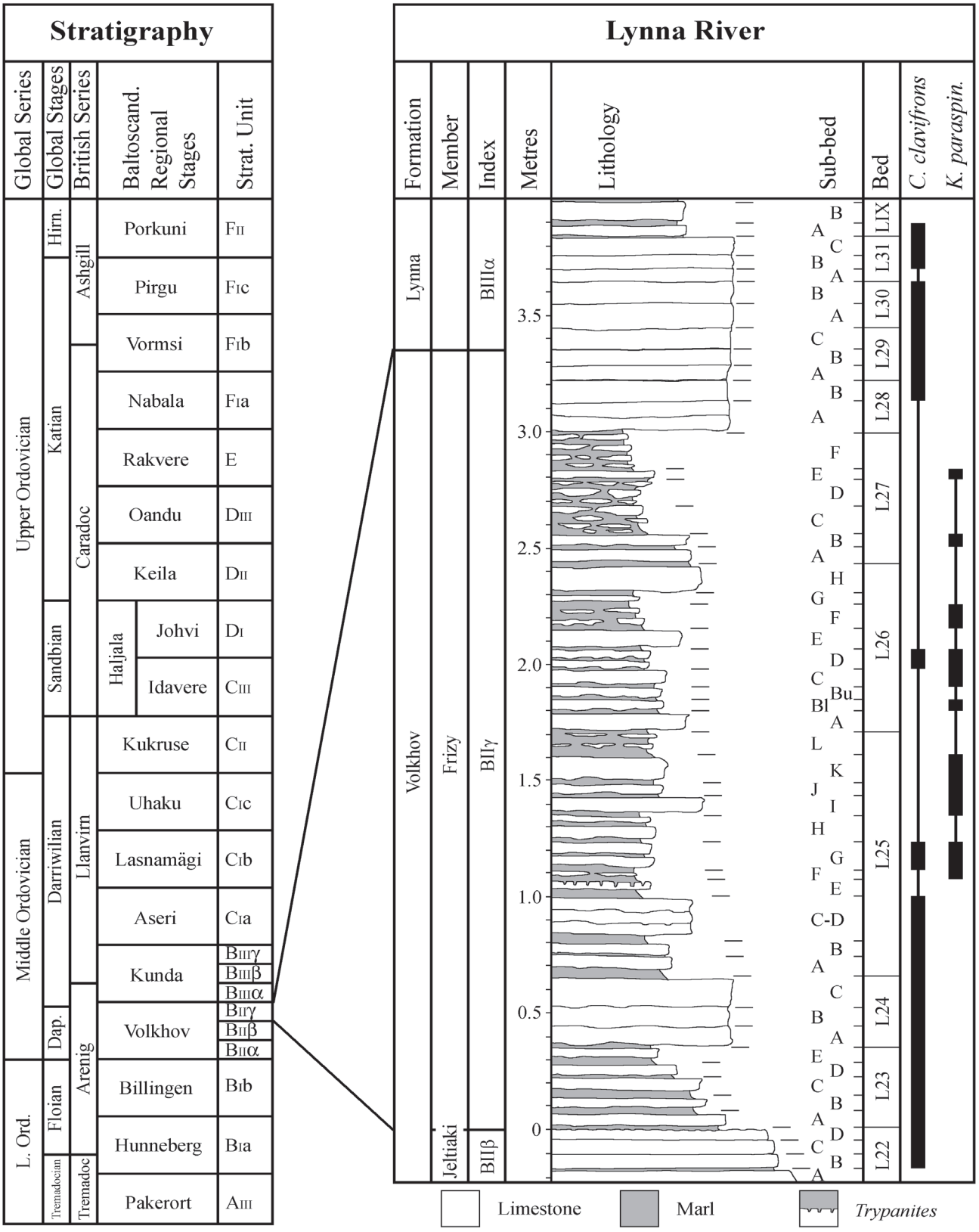

Fig. 2. Lithological log for the Lynna section. The log is based on data made available by Andrei Dronov. The formal lithological units on the right side column follow Dronov (1997). The stratigraphical units used for the Volkhov and Kunda Regional Stages on the left side column follow the subdivision proposed by Lamansky (1905). The rest follow the coarser system proposed by Männil (1966). The stratigraphical occurrences of the two species are shown on the right.

Measurements

All measurements were made using goniometric and measuring ocular, and are given to nearest half millimetre or, for the smallest specimens, with an accuracy of 0.1 mm. Cranidial measurements are shown on Fig. 3 and summarized in Tables 1 and 3 and the appendix. Glabella is defined as the area outlined by the occipital, axial and preglabellar furrows. The specimens were examined in random order in order to avoid measuring bias. A number of specimens selected at random were re-measured in order to estimate the measuring error. The error in general appears to be less than 5 % for the distance measurements and a couple of degrees for the angles. Increased variability of measurements related to systematic changes in preservation or deformation up through the studied interval are regarded as negligible.

Ontogenetic examinations were based on the cranidial length as size-indicator. The analysis was done with Reduced Major Axis on a double-logarithmic scale. The possibility of no correlation between size and morphometric ratio is given by p(uncorr.) together with the number of specimens measured, N, and Pearson´s product correlation-coefficient, r, which is negative when the line of best fit is negative and vice versa. In cases where two populations were compared statistically each population was initially tested with Shapiro-Wilks test for a normal distribution. If both populations were accepted ($p \geq 5$ %), the similarity was tested using the F- and t-test. In cases where the test for normal distribution was rejected for one or both populations, the similarity was tested with two distribution independent tests named Mann-Whitney U-test and Kolmogorov-Smirnov test. All tests were made with the statistical program Past (cf. Hammer, Harper & Ryan 2001).

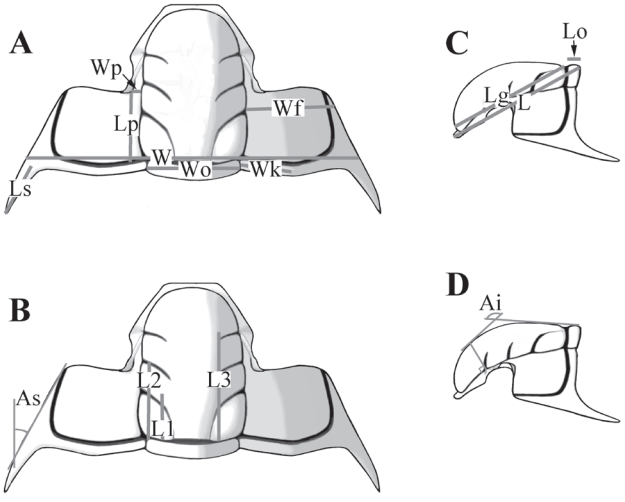

Fig. 3. Cranidial measurements. The bend on the posterior fixigenal border commented in the text is illustrated on Fig. 3B. The anterolateral border furrow is located at the fixigenal expansion opposite S3 (sub-fig. B). Abbreviations: **Ai** = angle of inflation, an angle formed between the sagittal line touching the occipital ring and posterior part of the glabella proper and the sagittal tangent to the glabella at the point, where a line perpendicular to the fixigena may be extended up from the lateral opening of S3 (high angles denotes cranidia with a small sagittal curvature) (Fig. 3D); **As** = angle between longitudinal axis of cranidium and anterior half of abaxial spine margin; **L** = cranidial length; **L2** = distance from occipital furrow to the opening of lateral glabellar furrow S2; **Lg** = glabellar length (excluding occipital ring); **Lo** = length of occipital ring; **Lp** = length between the pleuroccipital furrow and the posterior edge on the palpebral lobe; **Ls** = length of genal spine; **W** = cranidial width; **Wf** = width of fixigena; **Wk** = distance from axial furrow to the downwards bend on the posterior border; **Wo** = width of occipital ring; **Wp** = distance from the posterior edge on the palpebral lobe to the axial furrow.

Systematic palaeontology

Suborder Cheirurina Harrington & Leanza, 1957
Family Cheiruridae Hawle & Corda, 1847
Subfamily Cyrtometopinae Öpik, 1937

Cyrtometopinae was separated from the Cheiruridae by Öpik (1937). The subfamily is characterized by possessing a transverse furrow or line of pits across the thoracic pleurae. Lane (1971, 2002) considered the morphological variation within the group too large for a separation from the Cheirurinae Hawle & Corda, 1847 and Cyrtometopinae was therefore regarded as a junior synonym of this subfamily. The group was re-examined by Pärnaste (2003), who proposed a resurrection of the Cyrtometopinae but with fewer genera. These were *Actinopeltis* Hawle & Corda, 1847; *Cyrtometopella* Nikolaisen, 1961; *Cyrtometopus* Angelin, 1854; *Krattaspis* Öpik, 1937; *Reraspis* Öpik, 1937; *Sphaerocoryphe* (*Sphaerocoryphe*) Angelin, 1854 and *Sphaerocoryphe* (*Hemisphaerocoryphe*) (Reed, 1896). The emended diagnosis of Pärnaste (2003, p. 245) is followed here.

Genus *Cyrtometopus* Angelin, 1854
Type species.- *Calymene*? *clavifrons* Dalman, 1827 (designated by Schmidt 1881)

Cyrtometopus clavifrons Angelin, 1854
Fig. 3, 7A-E, Table 1, 2
1827 *Calymene*? *clavifrons* – Dalman, p. 260.

1854 *Cyrtometopus clavifrons*. Dalm. [partim] – Angelin, p. 32-33, pl. XXI: 4; pl. XXXIX: 9, a (non pl. XXI: 4a).
1869 *Ch.* (*Cyrtometopus*) *clavifrons* Dalm. – Linnarsson, p. 60, 86.
1881 *Cheirurus* (*Cyrtometopus*) *clavifrons* Dalm. – Schmidt, p. 152-157, pl. VIII: 4-6; XVI: 7-12.
1882 *Cheirurus clavifrons*, Dalm. [partim] – Brøgger, p. 131-134, pl. V: 1-4, 6-9 (fig. 5 belongs to *Nieszkowskia tumida gibba*).
1884 *Cyrtometopus clavifrons* Dalm. – Törnquist, p. 16.
1907 *Cyrtometopus clavifrons* Dalm. – Schmidt, p. 9, 91.
1936 *Cyrtometopus clavifrons* (Dalm.) – Poulsen, p. 48.
non 1952 *Cyrtometopus* cf. *clavifrons* (Dalman, 1826) – Skjeseth, p. 173-174, pl. IV: 3, 4, 6 (Assigned to *Cyrtometopus priscus* by Tjernvik (1956)).
1970 *Cyrtometopus clavifrons* (Dalman) – Tomczykowa & Tomczyk, p. 184, 190, tab. 9.
1984 *Cyrtometopus clavifrons* (Dalman, 1827) – Wandås, p. 235-236, pl. 13B, C, E.
1995 *Cyrtometopus* sp. – Nielsen, p. 71, fig. 33, 34, 36, 48, 49.
2002 *Cyrtometopus clavifrons* (Dalman, 1827) – Lane, p. 155-164, fig. 1, pls. 1-3.
2003 *Cyrtometopus clavifrons* – Hansen & Nielsen, p. 108, 110, fig. 3.
2009 *Cyrtometopus clavifrons* (Dalman, 1827) – Hansen, p. 142, pl. 27: 5-9.

Table 1. Table for the number of specimens (N), extremities (Min., Max.), average (μ) and scatter (σ) on *Cyrtometopus clavifrons*. Abbreviations are explained on Fig. 3.

	Cyrtometopus clavifrons (Dalman, 1826)				
	N	Min.	Max.	μ	σ
L (mm)	41	3,8	20	13,3	4,14
L/W	17	0,47	0,63	0,54	0,045
Wo/W	19	0,25	0,35	0,29	0,025
Lp/L2	35	0,79	1,02	0,9	0,056
Lp/Lg	30	0,41	0,48	0,45	0,021
Wp/Lp	38	0,3	0,52	0,41	0,061
As	9	27	34	30	2,8

A more complete synonymy list is presented by Lane (2002).

Emended diagnosis: The cranidium is defined by the central location of the maximal width and height of glabella and by the genal spines, directed approximately 30° outwards relative to the symmetric axis (modified from Angelin (1854) and Schmidt (1881)).

Type material: The type material is in the Swedish Museum of Natural History, Stockholm, Sweden. The lectotype cranidium RM Ar.17907 selected by Lane (2002) is from the Expansus or lower Raniceps Limestone of the Swedish Holen Limestone at Skarpåsen, Östergötland.

Material: The material from Lynna consists of 123 cranidia of which the 54 most well-preserved have been measured. The Russian material has been supplemented by 16 cranidia from Scandinavia, six of which are kept at the Natural History Museum, University of Oslo, Norway. The rest together with the material from Lynna are deposited at the Geological Museum, Natural History Museum of Denmark, University of Copenhagen.

Description: Modified from Schmidt (1881, p. 152-157) and Lane (2002, p. 158-164).

Examined cranidia between 3.8 and 20.0 mm long, averaging 13 mm. Cranidium trapezoidal in outline, width corresponding to nearly twice the length. Glabella subrectangular in outline with slightly convex flanks and evenly rounded front; highest point at L2. Glabella widest at anterior end of L2, width corresponding to approximately 75 % of glabellar length (occipital ring excluded). Anterior margin nearly straight with two sharp anterolateral edges. Posterior edge of palpebral lobe positioned between 79 % and 102 % of the distance between S2 and occipital furrow from pleuroccipital furrow. Distance from posterior edge to the axial furrow corresponding to between 30 % and 52 % of the distance between posterior edge and pleuroccipital furrow. Genal spine diverging posteriorly with an angle of about 30° to sagittal line.

The rest of the exoskeleton is described in full by Schmidt (1881) and Lane (2002).

Table 2. Ontogenetic investigations of selected morphometric ratios and angles. p(a = 1) is used to distinguish between allometric (p < 5 %) and isometric (p ≥ 5 %) distributions. p(uncorr.) is a test for non correlation between ratio and size indicator (usually L). r (Pearson´s product correlation index) is negative for decreasing distributions and visa versa.

	Ratio	Size indicator	Transf.	N	p(a = 1)	p(uncorr.)	r
C.cl.	Lp/Lg	L	Loglog	28	0	0,001	0,578
	Wk/Wf	L	Loglog	16	5,22E-22	0,003	0,699
K. pa.	Lp/Lg	L	Loglog	14	7,93E-3	0,008	0,676
	Lp/L2	L	Loglog	14	0	0,007	0,684
	Wk/Wf	L	Loglog	8	8,69E-9	0,062	0,683

Remarks: The specimen figured by Angelin (1854, Pl. XXI: 4a) does not belong to *C. clavifrons* because the eyes are located posterolaterally.

Ontogeny: The material represents only holaspids, but even so a clear forward movement of the eye is observed from small to large specimens (Tab. 2). Chatterton (1980) examined the ontogenetic variation within a large number of cheirurid species. A comparison with the material at hand reveals differences between *Cyrtometopus* and most other genera of Cheiruridae. The most pronounced difference concerns the location of the palpebral lobe. Chatterton (1980) found that nearly all the genera examined showed a retreating trend for the eyes during growth, whereas a few showed stasis. The eye on *Cyrtometopus* is in contrast located more anteriorly on the larger individuals. It may prove interesting to undertake similar examinations on the closely related *Cyrtometopella*, which may exhibit the same trend. At the moment the knowledge is too limited to make assumptions, but the observation may well prove valid for phylogenetic analysis. Unlike most genera examined by Chatterton (1980) no ontogenetic variations in the lateral placement of the eye or in the relative distance between the lateral glabellar furrows have been observed in the available material, but this may be due the small size of the material or that it contains only holaspids.

Morphostratigraphy: An examination of the stratigraphical variations in the cranidial length was negative and size-changes should thus not influence the stratigraphic variations in morphometry.

The cranidium of *C. clavifrons* is overall characterised by morphological stasis through time. Exceptions are found in the relative width of the occipital ring, which increases through time in the East Baltic area as shown by the two morphometric ratios Wo/W (Fig. 4) and Wp/Lp. The differences between the oldest and youngest population of both ratios were tested with an F- and t-test. The F- and t-test for Wo/W gave: F = 1.8103, p(same σ) = 0.395, t = -3.0893, p(same μ) = 0.00666. The t-test was rejected. The F- and t-test for Wp/Lp gave: F = 1.763, p(same σ) = 0.448, t = -3.3564, p(same μ) = 0.00187. The hypothesis that the difference in average was zero was rejected. The stratigraphic differences are thus significant. The same is the case for the angle of inflation, Ai, which is decreasing from basis to top of the Lynna section (Fig. 5), reflecting an increase in the sagittal curvature of the glabella. A mean change of more than 5 degrees from the lower to the upper population is too large to be explained by measuring errors, especially because the measurements were made in random order, and the observed changes are regarded as genuine morphological changes in the population through time. Because of the absence of the species in the central part of the Lynna section, it is impossible to tell whether the stratigraphic development is gradualistic or punctualistic, but a gradual change is hinted at in Fig. 5. Examinations of Norwegian material from the Dapingian to middle Darriwilian Huk Formation and basal Elnes Formation indicate that the stratigraphic changes of the Ai angle and Wo/W-value are very poorly expressed or missing in this region. The Norwegian material was measured on internal moulds in contrast to the better preserved Russian material, adding a possible source of error, but even so the observed changes appear to represent a local phenomenon, and are likely ecophenotypic in origin.

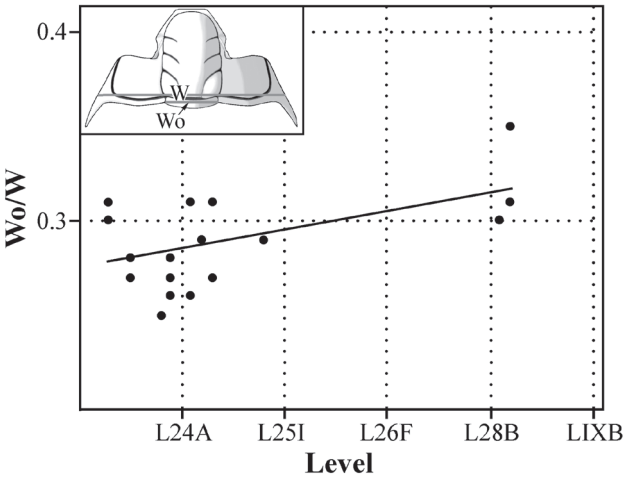

Fig. 4. Stratigraphical variations in the cranidial Wo/W-ratio on *Cyrtometopus clavifrons*. Only the numbers of every tenth sub-bed are shown.

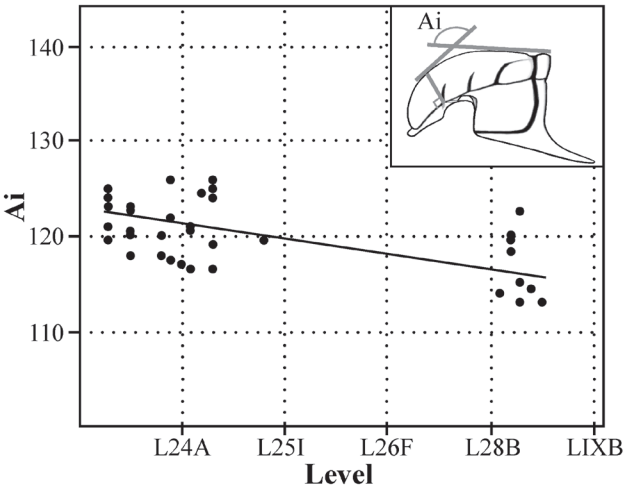

Fig. 5. Stratigraphical variations in the cranidial angle of inflation on *Cyrtometopus clavifrons*.

Occurrence: *Cyrtometopus clavifrons* is relatively common at the boundary between $B_{II}\beta$ and $B_{II}\gamma$ (sub-bed L22B to L25B) and again in the Volkhov-Kunda boundary interval at the top of the studied section (sub-bed L29A and upwards). In between it is nearly absent from sub-bed L25C-D to L28B (Fig. 2). The species is known from the Volkhov and Lynna formations (Glauconite limestone) and up into the Sillaoru and Obukhovo formations (Vaginaten limestone) in the East-Baltic (Schmidt 1881, 1907; Brøgger 1882), i.e. Volhkov-Kunda and maybe also top of the Billingen Stage. Lamansky (1905, p. 169) indicates an occurrence throughout B_{II}. However, this may well be too broad a stratigraphic interval and most probably includes the closely related but stratigraphically older *Cyrtometopus prisca* Tjernvik, 1956. Outside the East-Baltic area *C. clavifrons* is known from the Huk and lower Elnes Formation in the Oslo Region, Norway, where it ranges from the Dapingian *Megistaspis* (*Megistaspis*) *simon* Zone ($B_{II}\beta$) and up into the middle Darriwilian Aseri Stage (Brøgger 1882; Wandås 1984; Nielsen 1995; Hansen 2009; this study).

It is also found in the Komstad Limstone and Holen Formation in most of southern and central Sweden (Linnarsson 1869; Brøgger 1882; Törnquist 1884; Bohlin 1949; Nielsen 1995); in the Komstad Limestone at Vasagaard, Bornholm (Poulsen 1936; Nielsen 1995), and in the Polish Miedzygórz bed (Tomczykowa & Tomczyk 1970). In summary it ranges from the upper Dapingian to the middle Darriwilian.

Genus *Krattaspis* Öpik, 1937

Type species.- *Krattaspis viridatus* Öpik, 1937

The genus was redescribed and revised by Pärnaste (2003) and now includes the following species:

K. paraspinosis n.sp.
K. popovi Pärnaste, 2003
K. viridatus Öpik, 1937
K. vitalis Pärnaste, 2003

The inclusion of the new species allows the diagnosis of of the genus given by Öpik (1937) and Pärnaste (2003) to be emended thus: Glabella parallel-sided to slightly expanding, somewhat inflated; S3 furrows generally forward directed, describing an obtuse to weakly sharp angle to the preglabellar furrow. Eyes large; situated moderately close to glabella opposite L2 lobes and based on fairly high eye socle. Glabella and genal areas densely tuberculated.

The genus ranges from the Billingen Stage to the top of the Volkhov Stage (Floian to lower Darriwilian) and is geographically restricted to Baltoscandia (Pärnaste 2003; this study).

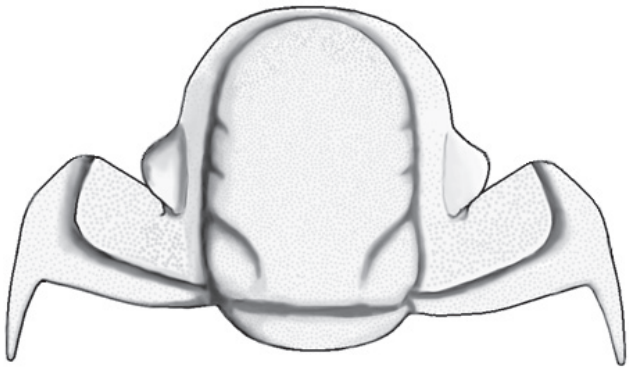

Fig. 6. Reconstruction of the cranidium of *Krattaspis paraspinosis* n.sp..

Krattaspis paraspinosis n.sp.
Fig. 6, 7F-L, Table 2, 3

Derivation of name: With reference to the genal spines, which diverge only slightly backward.

Diagnosis: Cranidium with slightly forward diverging axial sutures and short (sag.) occipital ring. Glabella low, S3 furrows directed slightly posteriorly. Genal spines short, diverging at about 15° from exsagittal line. Surface of cranidium with comparatively fine and dense granulation.

Material: The material at hand consists of 26 cranidia of which 18 well-preserved specimens have been selected for measurements. The description is largely based on these specimens. The holotype, MGUH 29201 (sample

Table 3. Morphometric ratios and angles for *Krattaspis paraspinosis* n.sp..

	Krattaspis paraspinosis n.sp.				
	N	Min.	Max.	μ	σ
L (mm)	16	3,3	9,7	6,6	1,8
L/W	9	0,56	0,76	0,64	0,06
Lo/Wo	14	0,21	0,29	0,24	0,024
Wo/W	10	0,33	0,38	0,36	0,015
Lp/L2	15	0,58	0,75	0,67	0,049
Lp/Lg	14	0,25	0,36	0,31	0,033
Wp/Lp	16	0,36	0,59	0,46	0,074
Wk/Wf	9	0,4	0,53	0,45	0,043
Ls/L	2	0,23	0,37	?	?
Ai	16	116	131	123	4,02
As	3	11,5	15	13	1,9

RL 2859) (Fig. 7G, H), is from sub-bed L26D in $B_{II}\gamma$. Paratype MGUH 29202 (sample RL 3784) was found in sub-bed L27E ($B_{II}\gamma$), whereas paratypes MGUH 29205, MGUH 29204 and MGUH 29203 (sample RL 2682, 3620 and 4315) were collected from sub-bed L26C, L27B and L29C ($B_{II}\gamma$) respectively. Two specimens, PMO 89691 and PMO 67269, from the Norwegian Huk Formation are housed at the Natural History Museum, University of Oslo. The rest of the material including all measured specimens, are deposited at the Geological Museum, University of Copenhagen, Denmark.

Description: Examined cranidia 3.3 to 9.4 mm long, averaging 6.4 mm. Length between 56 and 76 % of the width. Outline crescentic to rounded trapezoid; sagittal angle of inflation, Ai, around 123°; transverse inflation moderate to strong. Occipital ring relatively short (sag.), length between 21 and 29 % of the width; occipital ring occupies from 33 to 38 % of cranidial width. Glabella moderately inflated sagittally as well as transversely, but less so than in the other species within the genus. Glabella oblong rectangular in outline with frontal lobe describing neatly rounded dome; widest opposite S2, width corresponding to 75 % of glabellar length. Glabella highest at L2. Two anterior pairs of glabellar furrows shallow, posterior pair deeper. Posterior lobe, L1, bloated egg-shaped; L2 and L3 not inflated. Frontal glabellar lobe semi-elliptical in outline, width approximately twice the length. Axial furrow deep, describing, except for a slight curve around L1, a nearly straight line from posterior border to preglabellar furrow.

Fixigena with narrow palpebral area and broad posterior fixigenal field corresponding to approximately 40 % of cranidial length. Border short (sag.) with no or only indistinct frontal edges. Palpebral area very narrow, anteriorly bordered by normally indistinct eye-ridges running obliquely forwards to S3. Eye-ridge posteriorly transforming into relatively long and well developed palpebral lobe. Anterior part of lobe situated opposite S2 or posterior part of L3, posterior edge reaching back to a point between 58 and 75 % of length between S2 and occipital furrow from pleuroccipital furrow. Distance between posterior edge and axial furrow approximating 46 % of distance to pleuroccipital furrow. Posterior border on fixigena short (exsag.) bending sharply downwards about halfway to genal spine. Lateral border posteriorly continuing out into short genal spine with a length corresponding to between 23 and 37 % of cranidial length for the two measured specimen. Genal spine diverging from symmetric axis with about 13°. Facial sutures nearly parallel frontally, bending sharply outward and slightly forward immediately anteriorly of S1. Posterior branch sigmoidal, curving sharply backwards at lateral furrow, continuing in a nearly straight line to cranidial margin shortly anterior of genal spine.

Cranidial surface with relative fine and dense homogenous granulation; fixigena furthermore characterized by pits arranged in more or less distinct rows.

Thorax known only from specimen MGUH 29202 (Fig. 7F), showing the two anterior segments. Axial ring moderately inflated and relatively broad (tr.), length corresponding to approximately 20 % of axial width. Width (tr.) of pleurae corresponding to axial ring width. Inner half of pleurae divided into an equal anterior and posterior part by deep pleural furrow. Pleural furrow starting from axial furrow centrally (exsag.) on segment, continuing in a straight line abaxially, terminating nearly 40 % of axial ring width from axial furrow. Pleura distally narrowing into a sharply pointed spine.

Ontogeny: The morphometric examination showed that the eye move forward through ontogeny as seen on *C. clavifrons* (Table 2).

Discussion: *Krattaspis paraspinosis* n.sp. differs from the other assigned species by having less forward directed S3 furrows, a slightly narrower glabella, more backwardly directed genal spines and by having a generally more uniform and dense distribution of fine glabellar granules (see Pärnaste 2003). It is morphologically closest to *K. vitalis* Pärnaste, 2003, but differs in having a wider palpebral lobe and narrower (tr.) palpebral area.

The outline of the glabella together with the nearly perpendicular S3 furrow and the fine and uniform glabellar granulation places this species morphologically closer to *Cyrtometopus* than any of the earlier forms, but is still clearly separated by the larger and more posteriorly placed eyes; lack of anterolateral edges on the anterior cranidial border and by the arched and not conical glabellar cross-section. The large morphological and ontogenetic resemblance between species of *Cyrtometopus* and *Krattaspis paraspinosis* n.sp, the youngest species known, supports the idea proposed by Pärnaste (2003, p. 245) that *Krattaspis* gave rise to *Cyrtometopus*.

Occurrence: From sub-bed L25F to L27E in $B_{II}\gamma$ at Lynna (Fig. 2). It is relatively common and uniformly distributed throughout the interval. Additional material has been exmined from the contemporaneous Huk Formation in southern Norway.

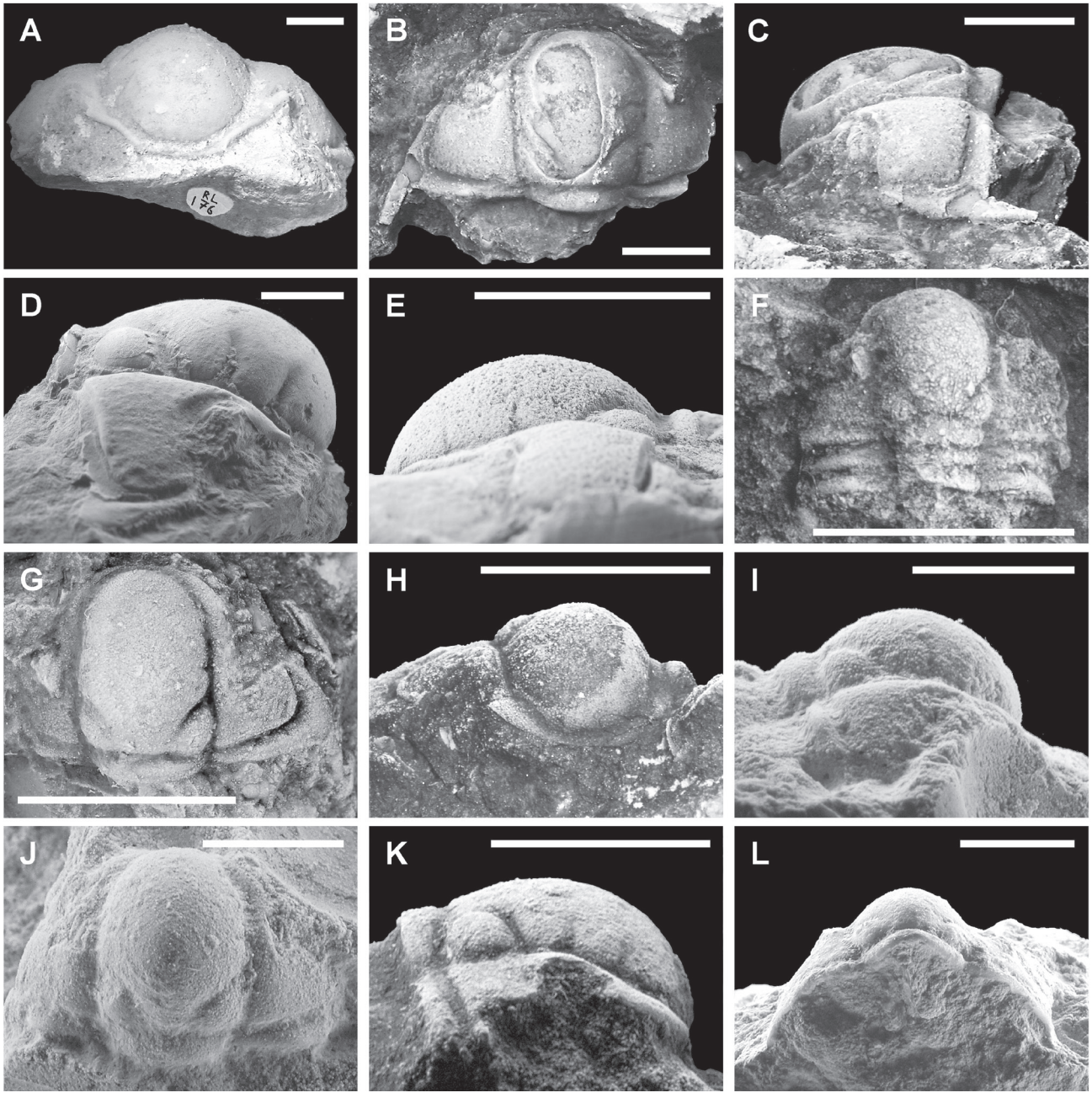

Fig. 7. ■ A-C. *Cyrtometopus clavifrons* Angelin. ■ A. Frontal view of cranidium. MGUH 29199 (sample RL176). Sub-bed L22C. $B_{II}\beta$. ■ B, C. Dorsal and lateral view of cranidium. MGUH 29200 (sample RL318). Sub-bed L23A. $B_{II}\gamma$. ■ D Lateral view of cranidium PMO 1994. Collected from the upper part of the Huk Formation at Huk, Bygdøy, Norway. ■ E. Lateral view of cast of cranidium PMO 102.474. Collected four to five metres above base of Elnes Fm. at Vikersund skijump, Modum, Norway. ■ F-L. *Krattaspis paraspinosis* n.sp.. ■ F. Cranidium and thoracic segments of early holaspid. Paratype MGUH 29202 (sample RL3784). Sub-bed L27E. $B_{II}\gamma$. ■ G, H. Dorsal and frontal view of cranidium. Holotype MGUH 29201 (sample RL2859). Sub-bed L26D. $B_{II}\gamma$. Note the nearly parallel genal spines; the lacking frontal edges and the posteriorly placed palpebral lobes. ■ I, J. Lateral and dorsal view of cranidium. Paratype MGUH 29203 (sample RL 4315). Sub-bed L29C. $B_{II}\gamma$. ■ K. Lateral view of cranidium. Paratype MGUH 29204 (RL 3620). Sub-bed L27B. $B_{II}\gamma$. ■ L. Posterior view of cranidium. Paratype MGUH 29205 (RL 2682). Sub-bed L26C. $B_{II}\gamma$. Scale bars represent five millimetres.

Appendix 1
Morphometric measurements on the cranidium of *Cyrtometopus clavifrons* and *Krattaspis paraspinosis* n.sp. from the locality at Lynna, Russia.

Sample	Taxon	Sub-bed	L	W	Lg	Wo	Lo	Lp	Wp	Wf	Ls	L2	Wk	Ai	As
RL4120	*C. clavifrons*	L29A	15,5	29,5	13,5	9	2	6,5	2,5	10	?	7	5	114	?
RL4157	*C. clavifrons*	L29B	8	?	7	4,5	1	?	?	?	?	3,5	?	119,5	?
RL4166	*C. clavifrons*	L29B	12,5	24	10,5	7,5	1,5	4,5	2	8	?	5,5	4	120	?
RL4173	*C. clavifrons*	L29B	13	21	11	7,5	1,5	4,5	2,5	7,5	?	5,5	?	118,5	?
RL1130	*C. clavifrons*	L24B	6,5	10,5	5,5	3	1	2,5	1	4	?	2,5	1,5	120,5	?
RL1759	*C. clavifrons*	L25G	6	11,5	5,5	3	1	2,5	1	4,5	?	2,5	?	119,5	?
RL992	*C. clavifrons*	L23E	?	?	?	?	?	4	1,5	7	4,5	?	?	?	?
RL4312	*C. clavifrons*	L29C	16	?	13,5	?	2,5	?	?	?	?	7	?	122,5	?
RL1267	*C. clavifrons*	L25A	12,5	22,5	9,5	6	2	4,5	1,5	7,5	6,5	5,5	3,5	124	27
RL282	*C. clavifrons*	L23A	?	28,5	?	8	2	6	2	9	?	6,5	4,5	?	?
RL4275	*C. clavifrons*	L29C	20	?	17	11	2,5	7,5	3	?	?	9	7	113	?
RL272	*C. clavifrons*	L23A	15,5	?	13	8,5	2	6	2	8,5	?	6,5	4,5	120,5	?
RL999	*C. clavifrons*	L23E	15	30	13	8	1,5	?	?	10	?	6,5	4	126	30
RL306	*C. clavifrons*	L23A	15,5	?	13	8	2	5,5	2	?	?	6,5	4	123	?
RL4458	*C. clavifrons*	L30B	4	?	3,5	2	?	1,5	0,5	?	?	16,5	?	?	?
RL132	*C. clavifrons*	L22C	18,5	?	17,5	11	2,5	?	?	?	?	8,5	6	125	?
RL896	*C. clavifrons*	L23E	9,5	19	8	5,5	1,5	3,5	1,5	6	?	4	2,5	117,5	33,5
RL1251	*C. clavifrons*	L24C	18,5	36	15,5	10,5	2,5	7,5	3,5	?	?	8	6,5	124,5	27
RL1601	*C. clavifrons*	L23C	?	?	?	?	?	6,5	3	?	?	6,5	4,5	?	?
RL1287	*C. clavifrons*	L25A	13,5	27,5	11,5	7,5	2	5	2	9	?	6	4	119	?
RL4464	*C. clavifrons*	L30B	10	?	8,5	5	1,5	?	?	?	?	4,5	?	113	?
RL4210	*C. clavifrons*	L29B	8,5	?	7,5	?	1	3,5	1,5	?	?	3,5	?	118,5	?
RL864	*C. clavifrons*	L23D	?	?	?	?	?	7	2,5	12,5	?	?	5	?	33
RL1062	*C. clavifrons*	L24A	18	?	17	?	?	?	?	?	?	8	?	117	?
RL291	*C. clavifrons*	L23A	16	?	13,5	8,5	2	?	?	?	?	6,5	?	118	?
RL871	*C. clavifrons*	L23D	15	32	13	8	2,5	6	2,5	11	?	6,5	5,5	118	30
RL1465	*C. clavifrons*	L25B	?	?	6	?	?	2,5	1	?	?	3	?	?	?
RL1137	*C. clavifrons*	L24B	20	?	17,5	9,5	2,5	8	2,5	?	?	8,5	?	116,5	?
RL318	*C. clavifrons*	L23A	11	20	10	5,5	1,5	4	1,5	6,5	?	4,5	3,5	122,5	27,5
RL4282	*C. clavifrons*	L29C	9	16,5	8	?	1	3,5	1,5	5,5	?	3,5	2,5	115	?
RL922	*C. clavifrons*	L23E	?	26,5	11,5	?	?	5,5	1,5	8	?	5,5	4	?	?
RL936	*C. clavifrons*	L23E	?	17	?	4,5	1	3,5	1	5,5	?	4	3	?	?
RL4526	*C. clavifrons*	L31B	?	?	11	?	?	?	?	?	?	5,5	?	?	?
RL182	*C. clavifrons*	L22C	11,5	?	10	5,5	1,5	4,5	2	7	?	5	3,5	123	?
RL1325	*C. clavifrons*	L25A	?	22	?	7	1,5	4,5	2	7	5,5	4,5	3	126	?
RL1123	*C. clavifrons*	L24B	14	24,5	12	7,5	1,5	?	?	8	?	6	4,5	121	?
RL1343	*C. clavifrons*	L25A	11,5	?	10	6,5	1,5	4	1,5	?	?	4,5	5	116,5	30
RL961	*C. clavifrons*	L23E	15,5	30	13,5	8,5	2	?	?	9	?	6,5	5	122	34
RL1322	*C. clavifrons*	L25A	11	?	10	6,5	1,5	4,5	2	?	?	4,5	3,5	125	?
RL176	*C. clavifrons*	L22C	18,5	34,5	16	10,5	2,5	7,5	3,5	?	?	7,5	6,5	119,5	?
RL1004	*C. clavifrons*	L23E	7,5	?	6,5	4	1	2,5	1,5	?	?	3	2,5	?	?
RL1336	*C. clavifrons*	L25A	14,5	?	13	8,5	2	6,5	2,5	?	?	6,5	4,5	116,5	?
RL163	*C. clavifrons*	L22C	18,5	?	16,5	9,5	2	?	3,5	?	?	7,5	?	?	?
RL340	*C. clavifrons*	L23A	13,5	?	11	8,5	2	5	2	?	?	6	4	?	?
RL1181	*C. clavifrons*	L24C	16	?	13,5	?	2	6	2	?	?	7	?	?	?
RL320	*C. clavifrons*	L23A	?	?	?	?	?	6	2	8,5	?	?	4	?	?
RL160	*C. clavifrons*	L22C	9	15	7,5	4,5	1,5	3,5	1,5	5,5	?	3,5	2,5	121	?
RL160	*C. clavifrons*	L22C	12,5	?	10,5	6,5	1,5	?	2	?	?	5	?	124	?
RL397	*C. clavifrons*	L23A	19,5	?	17,5	?	?	?	?	?	?	8	?	120	?
RL847	*C. clavifrons*	L23D	9	?	8	5	1	3,5	1	5,5	?	3,5	2,5	120	?
RL4523	*C. clavifrons*	L31B	?	?	?	?	1,5	3,5	1,5	6	?	4	2,5	?	?
RL4442	*C. clavifrons*	L30A	15	?	13,5	?	?	?	?	?	?	6,5	?	114,5	?
RL4060	*C. clavifrons*	L28B	?	?	15	?	?	?	?	?	?	7,5	?	?	?
RL4315	*K. paraspinosis*	L29C	7,5	?	6,5	4	1	2	1	?	?	3	2	121,5	?
RL2200	*K. paraspinosis*	L25J	9,5	15	8	5	1,5	2,5	1	5,5	?	4	2,5	123	12
RL1809	*K. paraspinosis*	L25G	6,5	9,5	5,5	3,5	1	1,5	0,5	3	?	2,5	1,5	122	?
RL3758	*K. paraspinosis*	L27E	7,5	11,5	6,5	4	1	2	1	3,5	?	3	1,5	126,5	?
RL2859	*K. paraspinosis*	L26D	5	8,5	4,5	3	1	1	0,5	2,5	?	2	1	123	11,5
RL4256	*K. paraspinosis*	L29C	8	?	6,5	?	1	2	1,5	?	?	3,5	?	116	?
RL2849	*K. paraspinosis*	L26D	6	8	4,5	2,5	1	?	?	?	?	2,5	?	126	?
RL3620	*K. paraspinosis*	L27B	7	?	6	4	1	2	1	?	?	3	?	122	?
RL1783	*K. paraspinosis*	L25G	8,5	?	7,5	?	1	2	1	?	?	3	?	125	?
RL2682	*K. paraspinosis*	L26C	7,5	13	6,5	4,5	1	2,5	1	4,5	?	3,5	2,5	122	?
RL3806	*K. paraspinosis*	L27E	5,5	9	4,5	3	1	1,5	1	3	?	2,5	1	128,5	15
RL3148	*K. paraspinosis*	L26F	4,1	?	3,6	2,4	0,5	1,1	0,5	?	?	1,7	?	117	?
RL1769	*K. paraspinosis*	L25G	6,5	9,5	5,5	3,5	1	1,5	1	3	1,5	2,5	1,5	122	?
RL2331	*K. paraspinosis*	L25K	?	13	?	4,5	1,5	2,5	1	4,5	2,5	3,5	2	?	?
RL1787	*K. paraspinosis*	L25G	?	13	?	?	?	2	1	4,5	?	?	?	?	?
RL3784	*K. paraspinosis*	L27E	3,3	?	2,8	1,8	0,5	0,7	0,3	?	?	1,2	0,6	120	?
RL1800	*K. paraspinosis*	L25G	4,3	7,5	3,7	2,6	0,6	1,1	0,5	2,5	1,6	1,8	1	128	?
RL2085	*K. paraspinosis*	L25I	9,5	?	8	5,5	1,5	?	?	?	?	4	?	131	?

Appendix 2
Morphometric measurements on the cranidium of *Cyrtometopus clavifrons* in Scandinavia.

Sample	Taxon	Locality	Stratigraphic index	Ai	W	Wo
A.564	*C. clavifrons*	Norway	BIIβ	107	?	?
A.1022	*C. clavifrons*	Norway	BIIβ-BIIγ (Lower)	116	?	?
A.1042	*C. clavifrons*	Norway	BIIβ-BIIγ (Lower)	114	?	?
A.1017	*C. clavifrons*	Norway	BIIβ-BIIγ (Lower)	114	?	?
A.327	*C. clavifrons*	Norway	BIIγ (Upper)	122	?	?
A.293	*C. clavifrons*	Norway	BIIγ (Upper)	111	?	?
A.384	*C. clavifrons*	Norway	BIIIα	108	?	?
K.1347	*C. clavifrons*	Sweden	BIIIα	114	~23,5	~6
PMO 1994	*C. clavifrons*	Norway	BIIβ-BIIIα	116	38	10
PMO 66338	*C. clavifrons*	Norway	BIIβ-BIIIα	?	26,5	7,5
PMO S.1601	*C. clavifrons*	Norway	BIIβ-BIIIα	102	?	?
PMO 106.073	*C. clavifrons*	Norway	BIIIγ-C1a	?	17,5	5
PMO 106.065	*C. clavifrons*	Norway	BIIIγ-C1a	?	29,5	~7,5
PMO 102.474	*C. clavifrons*	Norway	BIIIγ-C1a	114	16	4
PMO 105.984	*C. clavifrons*	Norway	BIIIγ-C1a	?	22	6,5
PMO 102.454	*C. clavifrons*	Norway	BIIIγ-C1a	116	?	?

Acknowledgement

The field work was sponsored by Carlsbergfondet grant 990311/10-1205 to Svend Stouge, GEUS, Denmark. Andrei Dronov, Department of Historical Geology, St. Petersburg State University, St. Petersburg, Russia, is thanked for his large help and organization of the fieldwork. Arne Thorshøj Nielsen, Geological Museum, Copenhagen, Denmark, is thanked for his support and review of this article and Helje Pärnaste, Institute of Geology at Tallinn University of Technology, Estonia, is thanked for discussions on the genus *Krattaspis*. David L. Bruton, Natural History Museum, University of Oslo, Norway has kindly read and helped improve the manuscript. Thanks are also due Per Ahlberg, Department of Physiology and Developmental Biology, Evolutionary Organismal Biology, University of Uppsala, Sweden for his valuable review.

Dansk sammendrag

Artiklen præsenterer en taksonomisk gennemgang af to midt ordoviciske trilobitarter, *Cyrtometopus clavifrons* Angelin, 1854, og *Krattaspis paraspinosis* n.sp., tilhørende underfamilien Cyrtometopinae. Undersøgelsen er hovedsageligt baseret på materiale indsamlet fra kalk- og mergelaflejringer ved bifloden Lynna´s udmunding cirka 150 kilometer øst for Skt. Petersborg, NV Rusland, men er suppleret med materiale af *Cyrtometopus clavifrons* fra Oslo området i Norge. *Krattaspis paraspinosus* n.sp. udgør den yngste art indenfor slægten. Den er morfologisk nærmere søsterslægten *Cyrtometopus* end slægtens andre arter og synes dermed at understøtte at *Cyrtometopus* nedstammer fra *Krattaspis* således som foreslået af Pärnaste (2003, s. 245). Undersøgelser af vækstændringer hos både *K. paraspinosus* og *C. clavifrons* indikerer en fremadrykning af øjets relative pladsering på hovedet i forhold til dyrets størrelse. Dette er modsat af hvad der ses hos andre repræsentanter af familien Cheiruridae.

References

Angelin, N. P. 1854: Palaeontologia Scandinavica. Pars 1. Crustacea Formationis Transitionis. Republished in revised form by G. Lindström (ed.) (1878), I-IX + 21-92, Pls. 25-41. Norstedt & Söner. Stockholm.

Balashova, E. A. 1953: K istorii razvitiya roda Asaphus v ordovike Pribaltiki. [On the history and evolution of the genus Asaphus in the Ordovician of the Baltic area.] Trudy VNIGRI, Nov. Ser. 78, 385-437. [In Russian.]

Balashova, E. A. 1976: Sistematika trilobitov Asaphina I ikh predstaviteli v SSSR. [Systematics of Asaphine Trilobites and their Representatives in the USSR.] 215 pp. Nedra, Leningrad. [In Russian.]

Bohlin, B. 1949: The Asaphus Limestone in Northernmost Öland. Bulletin of the Geological Institution of the University of Upsala 33, 529-570, Pls. I-II.

Brøgger, W. C. 1882: Die silurischen Etagen 2 und 3 im Kristianiagebiet und auf Eker. Universitätsprogramm. 376 pp. Kristiania.

Chatterton, B. D. E. 1980: Ontogenetic Studies of Middle Ordovician Trilobites from the Esbataothine Formation, Mackenzie

Mountains, Canada. Palaeontographica, Abteilung A, 171, 1-3, 1-74, Pls. 1-19.
Christiansen, J. L. & Stouge, S. 1999: Using Palaeo-oceanographical modelling in reconstructing Early Ordovocian palaeogeography. In: Kraft, P. & Fatka, O. (eds): Quo vadis Ordovician? Short papers of the 8th International Symposium on the Ordovician System. Acta Universitatis Carolinae. Geologica 43, 515-518.
Congreve, C. R. & Lieberman, B. S. 2010: Phylogenetic and biogeographic analysis of deiphonine trilobites. Journal of Paleontology 84, 1, 128-136.
Dalman, J. W. 1827: Om Palæaderna eller de så kallade Trilobiterna. Kongliga Svenska Vetenskaps-Akademiens Handlingar 1826, 2, 113-162 + 226-294, Pls. 1-6.
Dronov, A. 1997: Russian and International Bryozoan Conference "Bryozoa of the World": A Field Excursion Guide, St Petersburg, 1997. 52 pp.
Hammer, Ø., Harper, D.A.T., and P. D. Ryan, 2001. PAST: Paleontological Statistics Software Package for Education and Data Analysis. Palaeontologia Electronica 4, 1, 9 pp.
Hansen, T. 2005: A new trilobite species of Hemisphaerocoryphe from the Arenig of the St. Petersburg area, Russia. Norwegian Journal of Geology 85, 193-198.
Hansen, T. 2009: Trilobites of the Middle Ordovician Elnes Formation of the Oslo Region, Norway. Fossils and Strata 56, 215 pp.
Hansen, T. & Nielsen, A. T. 2003: Upper Arenig trilobite biostratigraphy and sea-level changes at Lynna River near Volkhov, Russia. Bulletin of the Geological Society of Denmark 50, 1, 105-113.
Harrington, H. J. & Leanza, A. F. 1957: Ordovician trilobites of Argentina. Department of Geology, University of Kansas, Special Publication 1, 1-276.
Hawle, I. and Corda, A. J. C. 1847: Prodrom einer Monographie der böhmischen Trilobiten. J. G. Calve, Prague, 176 pp., 7 pls.
Ivantsov, A. Yu 2003: Ordovician trilobites of the subfamily Asaphinae of the Ladoga Glint. Paleontological Journal 37, Suppl. 3, 229-337.
Jaanusson, V. 1982: Introduction to the Ordovician of Sweden. In: Bruton, D. L. & Williams, S. H. (eds): Field excursion guide. IV International Symposium on the Ordovician System. Paleontological Contributions from the University of Oslo 279, 1-9.
Lamansky, W. 1905: Die ältesten silurischen Schichten Russlands (Etage 8). Mémoires Comité Géologuque. Nouvelle Série, Livr. 20, 1-223.
Lane, P. D. 1971: British Cheiruridae (Trilobita). Monograph of the Palaeontographical Society. 1-95, Pls. 1-4.
Lane, P. D. 2002: The taxonomic position and coaptive structures of the Lower Ordovician trilobite Cyrtometopus. Special Papers in Palaeontology 67, 153-169.
Linnarsson, J. G. O. 1869: Om Vestergötlands cambriska och siluriska aflagringar. Kongliga Svenska Vetenskaps-Akademiens Handlingar 8, 2, 1-89, Pls. 1-2.
Männil, R. M. 1958: Trilobity semejstv Cheiruridae i Encrinuridae iz Estonii [Trilobites of the Families Cheiruridae and Encrinuridae from Estonia.] Trudy Instituta Geologii Akademii Nauk Estonskoj SSR 3, 165-212, Pls. 1-8.
Männil, R. M. 1966: Istoriya pazvitiya Baltijskogo bassejna v ordovike. [Evolution of the Baltic Basin during the Ordovician.] Eesti NSV Teaduste Akadeemia Toimetised, 1-201. Tallinn. [In Russian with English summary.]
Moberg, J. C. & Segerberg, C. O. 1906: Bidrag till kännedomen om Ceratopygeregionen med särskild hänsyn till dess utveckling i Fogelsångstrakten. Lunds Universitets Årsskrift. N. F. Afdelning 2, 2, 7. Kongliga Fysiografiska sällskapets Handlingar. N. F. 17, 7, 1-116, Pls. 1-7.
Nielsen, A. T. 1995: Trilobite systematics, biostratigraphy and palaeoecology of the Lower Ordovician Komstad Limestone and Huk Formations, Southern Scandinavia. Fossils and Strata 38, 1-374.
Nieszkowski, J. 1859: Zusätze zur Monographie der Trilobiten der Ostseeprovinzen, nebst der Beschreibung einiger neuen obersilurischen Crustaceen. Archiv für die Naturkunde Liv-, Ehst-, und Kurland, Serie I, 2, 345-384.
Nikolaisen, F. 1961: The Middle Ordovician of the Oslo Region, Norway, 7. Trilobites of the suborder Cheirurina. Norsk Geologisk Tidsskrift 41, 279-309, Pls 1-4.
Öpik, A. A. 1937: Trilobiten aus Estland. Acta et Commentationes Universitatis Tartuensis (Dorpatensis) A. Mathematica, Physica, Medica 32, 3, 1-163, Pls. 1-26.
Pärnaste, H. 2003: The Lower Ordovician trilobite Krattaspis: The earliest cyrtometopinid (Cheiruridae) from the Arenig of the East Baltic. Special Papers in Palaeontology 70, 241-257.
Poulsen, C. 1936: Übersicht über das Ordovizium von Bornholm. Meddelelser fra Dansk Geologisk Forening 9, 1, 43-66.
Přibyl, A., Vanek, J. & Pek, I. 1985: Phylogeny and taxonomy of family Cheruridae (Trilobita). Acta Universitatis Palackianae Olomucensis Facultas Rerum Naturalium Geographica-Geologica XXIV, 83, 107-193, Pls. 1-8.
Reed, F. R. C. 1896: Notes on the Evolution of the Genus Cheirurus. The Geological Magazine. New Series IV, III, 117-123.
Schmidt, F. 1881: Revision der ostbaltischen silurischen Trilobiten nebst geognostischer Übersicht des ostbaltischen Silurgebiets. Abtheilung I. Mémoires de l´Académie Impériale des Sciences de St-Pétersbourg VII, 30, 1, 1-237.
Schmidt, F. 1885: Revision der ostbaltischen silurischen Trilobiten. Abtheilung II. Acidaspiden und Lichiden. Mémoires de l´Académie Impériale des Sciences de St.-Petersbourg VII, 33, 1, 1-127.
Schmidt, F. 1886: Revision der ostbaltischen silurischen Trilobiten. Abtheilung III. Illaeniden. Mémoires de l`Académie Impériale des Sciences de St.-Petersbourg VII, 33, 8, 1-173.
Schmidt, F. 1894: Revision der ostbaltischen silurischen Trilobiten. Abtheilung IV. Calymmeniden, Proetiden, Bronteiden, Harpeiden, Trinucleiden, Remopleuriden und Agnostiden. Mémoires de l`cadémie Impériale des Sciences de St.-Petersbourg VII, 42, 5, 1-93.
Schmidt, F. 1898: Revision der ostbaltischen silurischen Trilobiten. Abtheilung V. Asaphiden; Lieferung I. Allgemeine Theil und Übersicht der Arten. Mémoires de l`Académie Impériale des Sciences de Dt.-Petersbourg VIII, 6, 11, 1-46.
Schmidt, F. 1901: Revision der ostbaltischen silurischen Trilobiten. Abtheilung V. Asaphiden; Lieferung II. Die Gattungen Asaphus sens. str., Onchometopus, Isotelus und Niobe enthatend. Mémoires de l`Académie Impériale des Sciences de St.-Petersbourg VIII, 12, 8, 1-113.
Schmidt, F. 1904: Revision der ostbaltischen silurischen Trilobiten. Abtheilung V. Asaphiden; Lieferung III. Enthaltend die Gattungen Ptychopyge (Pseudasaphus, Basilicus und Ptychopyge sens. str.), Ogygia und Nileus. Mémoires de l`Académie Impériale des Sciences de St.-Petersbourg VIII, 14, 10, 1-68.
Schmidt, F. 1906: Revision der ostbaltischen silurischen Trilobiten. Abtheilung V. Asaphiden; Lieferung IV. Enthaltend die Gattung Megalaspis. Mémoires de l`Académie Impériale des Sciences de St.-Petersbourg VIII, 19, 10, 1-62.
Schmidt, F. 1907: Revision der ostbaltischen Trilobiten. Abthei-

lung VI: Allgemeine Übersicht mit Nachträgen und Verbesserungen. Mémoires de l´Académie des Impériale des Sciences de St-Petersbourg VIII, 20, 8, 1-104.
Skjeseth, 1952: On the Lower Didymograptus Zone (3b) at Ringsaker, and contemporaneous deposits in Scandinavia. Norsk Geologisk Tidsskrift 30, 138-182, Pls. 1-5.
Tjernvik, T. E. 1956: On the Early Ordovician of Sweden, Stratigraphy and Fauna. Bulletin of the Geological Institutions of the University of Upsala 36, 107-284.
Tolmacheva, T., Holmer, L. E., Dronov, A., Egerquist, E., Fedorov, P. & Popov, L. E. 1999: Early Ordovician (Hunneberg-Volkhov) facial and faunal changes in the East Baltic. In: Kraft, P. & Fatka, O. (eds): Quo vadis Ordovician? Short papers of the 8th International Symposium on the Ordovician System. Acta Universitatis Carolinae. Geologica 43, 467-470.
Tomczykowa, E. & Tomczyk, H. 1970: Stratigraphy. In: Sokolowski, S. (ed.): Geology of Poland 1, Part 1, 1-651. Warsaw.
Törnquist, S. L. 1884: Undersökningar öfver Siljansområdets trilobitfauna. Sveriges Geologiska Undersökning. Serie C, 66, 1-101, Pls. 1-3.
Wandås, B. T. G. 1984: The Middle Ordovician of the Oslo Region, Norway, 33. Trilobites from the lowermost part of the Ogygiocaris Series. Norsk Geologisk Tidsskrift 63, 4, 211-267. [for 1983].

Postglacial sedimentary regime around northern Sylt, South-eastern North Sea, based on shallow seismic profiles

BOLDREEL, L.O., KUIJPERS, A., MADSEN, E. B., HASS, C., LINDHORST, S., RASMUSSEN, R., NIELSEN, M.G, BARTHOLDY, J. & PEDERSEN, J.B.T.

Boldreel[a], L.O., Kuijpers[b], A., Madsen[a], E. B., Hass[c], C., Lindhorst[d], S., Rasmussen[b], R., Nielsen[a], M.G, Bartholdy[a], J. & Pedersen[a], J.B.T.; 2010-04-08. Postglacial sedimentary regime around northern Sylt, South-eastern North Sea, based on shallow seismic profiles. © 2010 by Bulletin of the Geological Society of Denmark, Vol. 58, pp. 15-27. ISSN 0011–6297. (www.2dgf.dk/publikationer/bulletin)

During the past 5 years the coastal zone offshore the northern part of the island of Sylt, has been investigated by sparker seismics and high-resolution subbottom profiling. The North Sea sector of the area is characterized by northward-directed sediment bypass as a result of strong long-shore (tidal) currents heading towards the Lister Tief. The southern part of Lister Tief is characterized by the presence of a major dune field with up to 8 m high compound dunes with wavelengths up to 350 m indicative of easterly-directed sediment transport (flood dominated). Further to the northwest, in the outer delta, a dune field suggesting westerly-directed sediment transport is identified. The two dune fields appear to be separated by minor indefinite bed forms. The northern part of the Lister Tief is characterised by the presence of a channel with a depth of 20-30 mbsf (meter below sea level) (30-40 msec TWT (Two Way Traveltime)) and displaying erosion towards the north. At the western termination of the channel the sediment transport pathway appears to be divided into two directions; one towards the outer delta, and one towards the sediment depocenter SW of Rømø. The Lister Ley is characterized by the presence of minor dunes, indicative of flood-current control, apart from a central zone where ebb-tide is responsible for northward-directed sediment transport. Sparker seismic and Chirp III data are consistent with processes having been persistent throughout the Holocene. Based on the study a model for the current direction and sedimentation regime is suggested.

Keywords: Wadden Sea, postglacial sedimentary regime, Tidal area of Sylt and Rømø, sparker seismic, Chirp III sub-bottom profiling.

[a]*Department of Geography and Geology, University of Copenhagen, Øster Voldgade 10, DK-1350 Copenhagen K, Denmark, lob@geo.ku.dk.*
[b]*Geological Survey of Denmark and Greenland, Øster Voldgade 10, DK-1350 Copenhagen K, Denmark.*
[c]*Alfred-Wegener Institute for Polar- and Marine Research, Wadden Sea Station Sylt, Hafenstraße 43 D-25992 List.*
[d]*Institute of Geology and Palaeontology, University of Hamburg, Bundesstraße. 55, D-20146 Hamburg, Germany.*

Introduction

Sylt, the northernmost of the Frisian Islands in the German part of the Wadden Sea, is separated from the Danish island Rømø (Fig. 1) by the tidal inlet Lister Tief. The inlet has a diurnal mean tidal range of 1.86 m and a tidal prism of 627 106 m^3 (Kystinspektoratet, 1999). Water depths (Fig. 1) in the area are known from bathymetric maps and, in addition, in the Lister Tief sea floor topography is known from radar imaging (Hennings & Herbers 2006). The types of bed forms and their locations have predominantly been investigated by means of side scan, echo sounding and radar imaging (Ulrich & Pasenau 1973; Hennings et al. 2004; Hennings & Herbers 2006). These data sets were obtained during individual investigations but were not repeated annually. The orientation of the bed forms and large-scale sediment transport patterns have thus been based on limited side-scan sonar data and sea-clutter images (Hennings et al. 2004) although isolated parts of the Lister Tief have been imaged at greater detail (Ulrich & Pasenau 1973, Hennings & Herbes 2006). A systematic investigation of horizontal and vertical extent of bed forms, erosional features

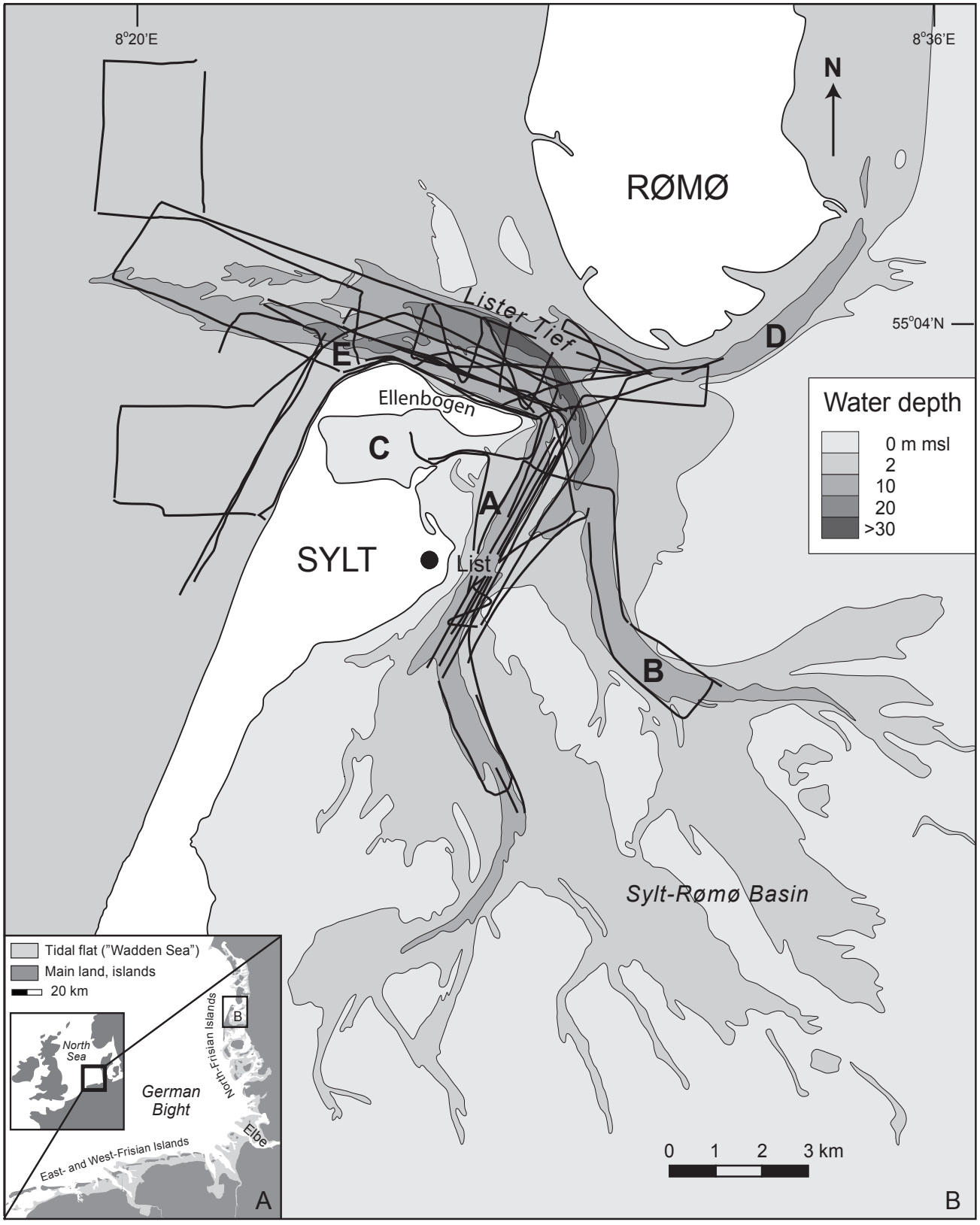

Fig 1: Overview map of the investigated area and bathymetry of the investigated area along with location of the sparker seismic profiles. The Chirp III data are located in the same area as the sparker data except for the area west of Sylt and the western most part of the Lister Tief. Bathymetry adapted from Lindhorst et al. 2008. The letters A, B, C and D designate Lister Ley, Højer Dyb, Könighafen and Rømø Dyb respectively. The letter E is referred to in the text.

and sediment by-pass, and their distribution, based on shallow seismic profiles has not previously been undertaken. To address this a large number of high resolution sparker-seismic profiles have been acquired offshore of the northern part of Sylt. These profiles cover the North Sea coastal zone and the adjacent Wadden Sea including the Lister Tief, Lister Ley, and Højer Dyb in the period 2004-2008 (Fig. 1). In order to improve resolution additional subbottom profiler data (Chirp III) were acquired in the Lister Tief and Lister Ley in 2009. From interpretation of the sparker and chirp III data, bed forms and areas of sediment by pass and erosion have been identified and mapped in this study. Based on the distribution of bed forms, erosional features and sediment by-pass signatures the overall transportation pattern around northern Sylt is interpreted and an overall model for the Holocene sediment transport regime is proposed.

Geological, physiographical and hydrographical setting

The present morphology of Sylt and adjacent areas are based on Mio-Pliocene sediments. These were deposited firstly under subtropical still-water conditions, in the form of silty clays, in a shallow sea near the coast. In the following period of lowering sea level, a sandy beach facies started to expand following the retreating sea. A riverine sandy facies followed and expanded in the Quaternary covering most of the Pliocene coastal sediments (Schwarzer, 1984). Glacial advances during the Pleistocene ice ages followed, however little is known of the extent that these affected the working area. Glaciers moved into the area for the last time during Saalian and dramatically changed its surface geomorphology. The facies units mentioned above were faulted, broke into pieces and were overthrusted (Schwarzer, 1984). They outcrop on the western and eastern sides of the central island. The western side became heavily eroded when the sea returned after the Weichselian sea-level low stand. Marine erosion started to affect the area from approx. 7 kaBP. Moraine deposits soon formed steep cliffs that retreated with the approaching North Sea and eroded materials started to form barrier spits to both the north and south. The northern recurved spit system grew predominantly due to swash bar accretion (Lindhorst et al., 2008), whereas the hooked-spit system that forms the northernmost part of Sylt, termed Ellenbogen, (Fig. 1) built up mainly as the result of longshore sediment transport ('beach drift') and accretion. The age of Ellenbogen is approximately 1300 years (Lindhorst et al., in press).

Coastal protection measures appear to have strongly influenced sedimentation along northern Sylt's coast line. Installation of groins in 1936 has most likely fixed the western coastline of Ellenbogen that was prone to strong erosion, and seaward progradation restarted. Paving of part of the beach in 1938 for bank protection purposes in NW Ellenbogen largely stopped erosion in this area but led to sediment bypass processes that also caused decreasing northward progradation of the system. Finally, beach nourishments to compensate for erosional loss were started in 1971 all along the west coast of Sylt. This caused growth rates in northern Ellenbogen to increase significantly due to enhanced sediment supply (Fürstenau, 2007; Lindhorst et al., in press).

While Sylt is subject to strong erosion along its western coast, Rømø is permanently gaining material – partly in the form of swash-bar accretion - and thus shows seaward progradation.

Today, the Sylt/Rømø tidal basin spans about 400 km^2; of which 67% is subtidal (10% above, 57% below –5 m in the channels) and 33% is intertidal (Lane et al., 2000). Tidal water exchange runs exclusively through the narrow Lister Tief tidal inlet. The inlet is the entrance to an artificial bight area as the free water flow is limited to the North as well as to the South by artificial dams connecting the islands of Sylt and Rømø to the mainland. The Lister Tief is the deepest (c. 40 m of water depth) of a set of three tidal channels (Rømø Dyb, Højer Dyb, Lister Ley, Fig. 1)) that merge from east into the List Tief. A volume of about 1100 m^3 of water passes the List Tief at maximum current speed of 1.3 ms^{-1} during one tidal cycle (Backhaus et al, 1998).

Due to the high-energy environment, medium and coarse sands (in places also including gravel and small boulders) dominate the channels, becoming gradually finer with decreasing water depth.

One of the most pronounced and prominent marine sand fields in the German coastal waters is found in the Lister Tief (Hennings & Herbers 2006). The area has been investigated over the years by various types of survey techniques. Ulrich & Pasenau (1973) carried out seven sounding profiles in a test area of the inlet and found that in the northern part most of the bed forms are ascribed to ebb-tide processs whereas in the southern part they are ascribed to flood-tide. They showed that sand dunes with a mean height of 3 m migrated approximately 60 m pr. year. Along the western coast of northern Sylt Ulrich & Pasenau indicate that sand drift is active. Bayer & Higelke (1994) presented an overview of Königshafen, a small sheltered bay on northern Sylt formed during the latest Holocene and suggested that input from dune sand from westerly directions and the formation of a sand spit system have caused substantial morphological changes up to

the present time. Before the formation of Ellenbogen 2250 to 1300 years ago, Königshafen was sheltered by a large sandy spit that developed between 5000 and 6000 years BP (Lindhorst et al., 2008). Ahrendt & Pesch (2001) applied GIS to illustrate the spatial distribution of sediment layers and suggested that offshore northern Sylt the base of the Holocene is situated at a depth of 20-30 mbsf. The sea bed morphology and the Lister Tief tidal channel show a complex configuration of different bed forms with moving sand waves. A sand-wave migration rate of 80 m pr. year has been measured (Hennings & Herbers 2006). Small-scale ripples and dunes are superimposed on large dunes up to 11 m high and often with a crest to crest distance that exceeds 300 m (Hennings & Herbers 2006). Hennings & Herbers also reported ebb dominated dunes to the north and flood dominated dunes to the south. Thus parts of Lister Deep have previously been investigated in some detail whereas the remaining area offshore northern Sylt has not been imaged in detail. This is in contrast to the rather detailed studies carried out onshore Sylt (Lindhorst et al., 2008; Lindhorst et al., in press.).

Bathymetry

Bathymetric and sparker seismic track data (Lindhorst et al. 2008, Fig. 1) and another recently published sea floor topographic map (Hennings & Herbers 2006) are in overall agreement with the depth-to-seabed map based on the acquired seismic profiles (Fig. 2). However, depth variations are shown in more detail in the bathymetric data (Fig. 2). West of Sylt the approximately uniform increase in depth to the west is

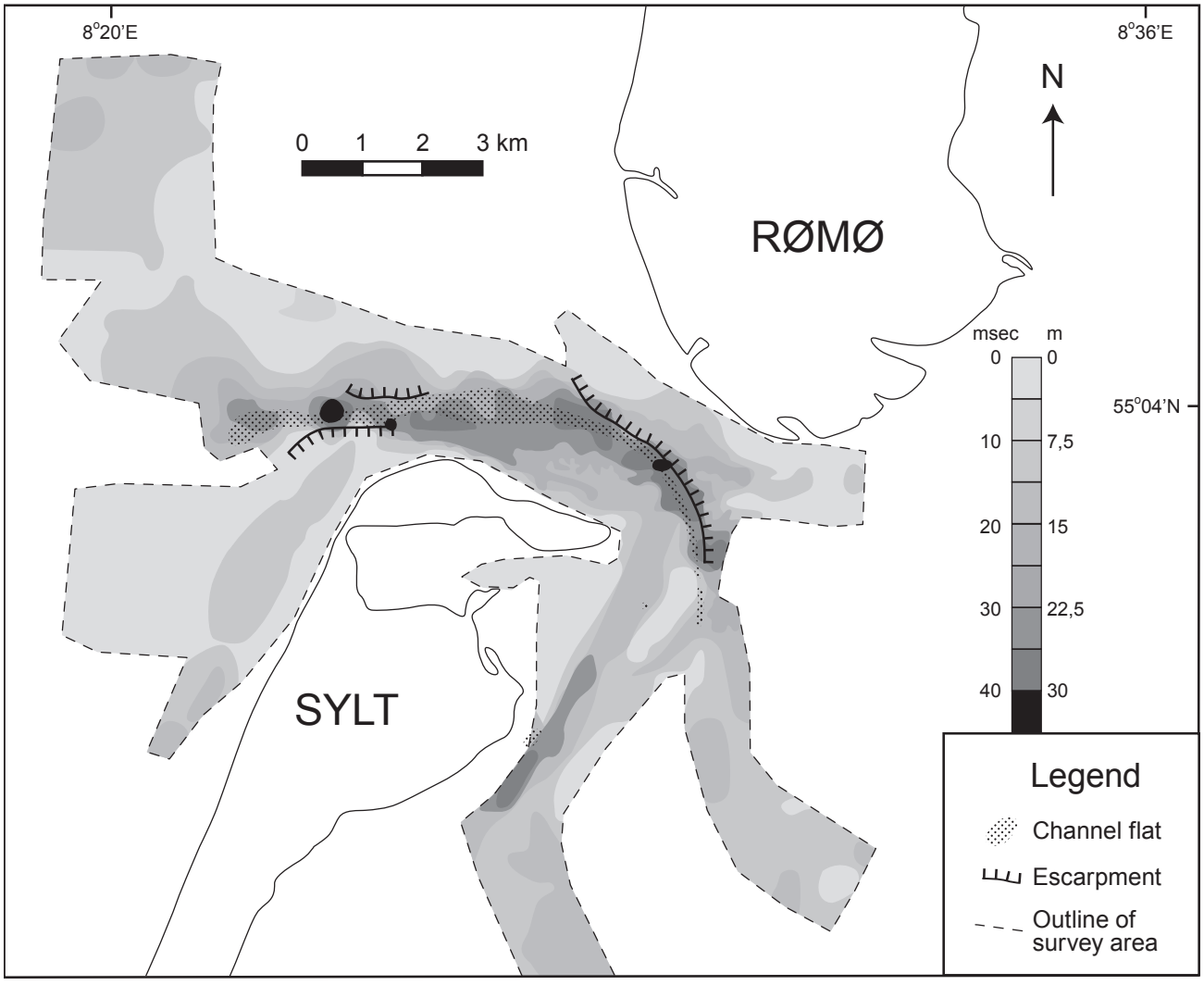

Fig. 2: Bathymetric map based on the sparker-seismic profiles acquired in this study along with locations of erosional escarpments and flatbased channel as interpreted on the sparker and Chirp III data. Depth in TWT sec. Depthlegend in TWT sec and m.

disrupted by a shallow channel striking approximately NNE-SSW (Fig. 2). The channel meets a NW trending topographic high (marked as E on Fig. 1), not connected to the island, located some 750 m from the coast NW of Sylt. Further seaward in a north-western direction, ca. 2.5 km off the coast, the seabed deepens to around 18 m and an ENE trending depression leads towards the main inlet of the Lister Tief. This channel area continues further to the NNE and becomes the Lister Tief. Bathymetric maps (Figs. 1 & 2) display that the sea-floor topography show a curved channel (marked as channel flat in Fig. 2) running in a SE-NW direction as also seen by Hennings & Herbers (2006). Channel depth locally reaches 35 m. On the eastern side of Sylt two additional channels are found: One parallel to the SSW-NNE strike direction of the island – the Lister Ley (marked as A on Fig. 1) - which is deepest (ca. 25 m) in its western part, the other – the Højer Dyb (marked as B on Fig. 1) - is found further to the East with a maximum depth of 14 m. The Königshafen tidal area at the northern part of Sylt (marked with a C on Fig. 1) consists of tidal flats separated by a meandering main channel. East of Lister Tief a narrow NE-SW trending channel – the Rømø Dyb (marked as D on Fig. 1) - is leading up along the SE coast of the Danish island of Rømø.

Data and Methods

High-resolution seismic data were acquired in 2006-2009 by the use of AWI (Alfred-Wegener Institute for Polar- and Marine Research, Wattenmeerstation Sylt, Germany) research vessel Mya, a small catamaran vessel with draught of 0.65 m. The data acquisition was part of a collaboration project between AWI, IGG (Department of Geography and Geology, Copenhagen University, Denmark), and GEUS (Geological Survey of Denmark and Greenland), with participation in 2005 by University of Kiel (RV 'Littorina') and in 2007 and 2009 by University of Hamburg. The weather conditions were excellent to very good for four of the five cruises whereas the 2007 data were acquired under more unfavourable sea state conditions.

The sparker data were acquired in 2005-2008 as single channel data. The ship speed was held at 5 Kts and the distance in time between consecutive shots was set to 0.5 sec. The vertical resolution of the data is approximately 0.5 m. The quality of the raw sparker data was improved by processing using the software ProMax. For the data acquired during the surveys carried out in 2005, 2006 and 2008 the processing included: Gain correction and Band Pass Filtering. In addition to these two processes the data acquired in 2007 were subject to F-X decon and dipscan in order to reduce noise. The data reveal a sub bottom depth penetration of 0.1 s TWT (Two Way Travel time) corresponding to 80 m applying a velocity of 1600 m/s for sediments. Sea floor multiples are present on all data and the data are single fold. The sparker-seismic data are measured in TWT s. Where depth in meters is mentioned, a velocity of 1470 m/s has been used for sea water.

For detailed investigations of the upper ca. 20 m of the sub-sea floor a high-resolution Chirp III sub-bottom profiler system was used in 2009 towed at a ship speed of 5 Kts. The Chirp III is able to operate in two frequency bands; 2-7 kHz and 10-20 kHz. The data were acquired with the low frequency band that provides a good compromise between sea-floor penetration and resolution of 15 cm. The Chirp III data are of good quality in spite of multiples and, in some cases, interference of the out and in going signal.

Both data sets were interpreted on a workstation using GeoGraphix software. The seismic profiles were interpreted applying the principles of seismic stratigraphy where boundaries of seismic units are mapped by the use of reflector terminations. The internal reflection pattern interpreted, along with the outer shape of the seismic units, enabled identification of individual geological structures e.g. bed forms and erosion scars. The large number of 2D profiles enables us to get a 2.5D image of local structures. In cases where dunes were crossed at right angles by the seismic profiles, the direction of the dune migration was interpreted as either flood or ebb oriented. However a number of poorly defined, often nearly symmetrical, dune structures are located outside the major dune fields and in these cases the dunes have been termed "indefinite". When present in areas clearly dominated by either flood or ebb transport, the sediment transport direction of these dunes has been concluded accordingly. Generally, our data confirm the bed form configuration observed in the Lister Tief by Ulrich & Pasenau (1973); Hennings et al. 2004 and Hennings & Herbers (2006).

The data, which were acquired during the 5 years field observations, show consistency in the location of the mapped larger structures, but the individual dunes can not be correlated on intersecting profiles of the various surveys. This is explained by the fact that the larger dunes move considerable distances per year (80 m/year Hennings & Herbers 2006 and 60 m/year Ulrich & Pasenau 1973).

Interpretation

From the interpretation of the seismic profiles we identify the following groups of structures: dunes of various sizes, escarpments and other erosional features, flat-channel-floor environments, large-scale foresets, and in addition, areas characterised by non-deposition interpreted as sediment by-pass corridors (Fig. 3).

1. Transverse dunes

A large number of dunes of various heights and lengths have been identified on the sparker and Chirp III profiles. Most of the dunes appear as individual structures on the sparker profiles but complex dunes where two or more individual structures merge are also present (Figs. 4-9). Smaller structures not resolved

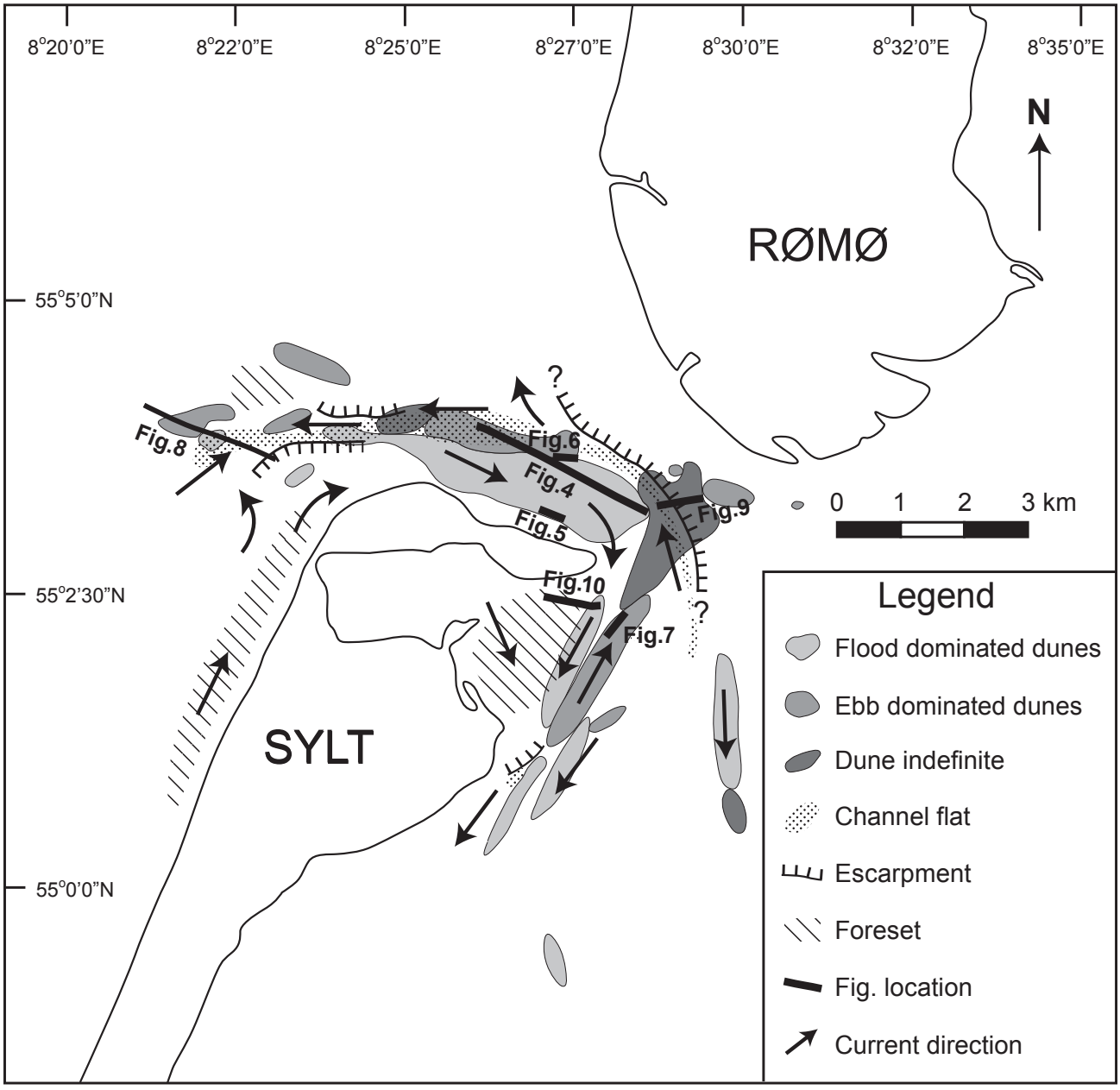

Fig 3: Facies map showing the distribution of observed bed forms, interpreted current directions and figure location.

at the seabed displayed in the sparker records can be documented by the Chirp III acoustic images (Figs. 5 & 7). Internal structure of the dunes and the underlying units can be studied in detail as available of the scale of seismic resolution (0.5 m for sparker profiles and 15 cm for Chirp III data). The Chirp III data, in particular, show remarkable details in the internal construction of dunes (Figs. 5, 6 & 7). The dunes have a slightly inclined stoss side and a rather steep lee side and display internal progradation (Figs. 4-8). In most cases the dunes overly older dune structures or were deposited on flat surfaces (Figs. 5-7) sometimes bounding well-defined foresets below (Fig. 8). They can also be found in the channel floor areas (Figs. 8-9). Dune structures showing similar orientations can be followed on parallel seismic profiles. This gives the overall orientation of the dunes as being transversal and oriented almost perpendicular to the coast, as can also be seen on sidescan data from Lister Tief and on acoustic soundings data (Hennings et al. 2004; Ulrich & Pasenau 1973). Along some of the seismic profiles parallel to the strike of Lister Tief and the Lister Ley the asymmetry of the dunes is in the opposite direction, indicating two apparent directions of sediment movement (Figs. 4 & 8). The geographical distribution of the dunes shows that the dunes are located in individual areas according to their orientation (Fig. 3). The dunes in the Lister Tief and Lister Ley seem to be oriented according to the direction of the flood and ebb dominated tides. Flood dominated structures are found in four individual areas: at the entrance to the Lister Tief and within the Lister Tief near the coast of Sylt in a large area up to approx. 4 km long and approx. 1 km wide, along the channel flanks in the central part of the Lister Ley, and in the Højer Dyb (Fig. 3). The length and height of the structures vary in such a way, that the smaller types are found in the sector of the dune field facing the incoming tide with a gradual increase in dune size in the inflow direction. The largest forms are found in the NE part of the dune field in the Lister Tief where the dunes wavelengths are up to 350 m (extension at the sea floor) and 8 m high (Fig. 4). Based on the results of Bartholdy et al. (2002, 2005) from a similar environment in an inlet north of the study area (Grådyb) this most likely signals a grain-size difference, where the largest compound dunes are formed in medium to coarse grained material.

Ebb dominated dunes are found in five areas; to the west and north of the inlet to the Lister Tief, in the western part of Lister Tief to the north of the flood dominated dune field, at the north-eastern part of Lister Tief, and in the middle and eastern side of the northern part of the Lister Ley (Fig. 3). The length and height of the structures vary but the dimensions of the ebb dominated dunes seem to be smaller than those of the flood dominated bed forms (Fig. 4).

From the 2D seismic sparker profiles a number of other dune structures are apparently lacking the characteristic shape that indicates direction of sediment transport movement (Figs. 4 & 9). Theses structures are found in four places: at the western part of the Lister Tief, in the eastern part of Lister Tief where it meets the Lister Ley, in the central part of the Lister Ley, and in the Højer Dyb (Fig. 3). At all these locations the structures are located in an area in between the flood and ebb dominated dune fields. The only exception is the Højer Dyb where the structures are located immediately to the south of the flood dominated dunes. This strongly suggests that either the structures have been crossed at too small an angle (unlikely), or that the structures are exposed to a varying current regime which shapes the structures such that they do not belong to either flood or ebb dominated environment. These structures are located in an area exposed to the interference of changing current systems.

2. Erosional features

The seismic stratigraphic interpretation shows that pronounced erosion of former deposits occurs as erosional truncation is observed at the sea floor at four locations. Two of these locations are found at the inlet of the Lister Tief, the third along the north-eastern part of Lister Tief, and the fourth in the Lister Ley close to List (Figs. 2, 3, 8 & 9). The erosional scar at the inlet of the Lister Tief, at the landward side of the flood dominated dunes of the inlet, cuts into the north-eastern part of the NW-trending high extending from Sylt. The scar zone is 600 m wide and is at about 20 m depth (Fig. 8). At the seaward side of the Lister Tief inlet, a scar is located west of the flood dominated dunes with evidence of erosional activity towards NE. The scar here is 150 m wide and 10 m high. Along the northern flank of the Lister Tief a pronounced erosional scar zone is observed to the north of the flood dominated and the "indefinite" dune area (Fig. 9). The zone is up to 26 m wide and up to 10 m high (Fig. 9). The northern and southern extension of the escarpment is outside the data coverage. At the eastern coast of Sylt, towards the north, an abrupt apparent erosional scar is found which is app. 120 m wide and up to 9 m high (Fig. 3). It can, however, not be excluded that this feature is part of a progradation system from a different direction.

3. Flat channel floor

On parts of the seismic profiles the sea floor is remarkably flat in two areas. Combining observations from all the seismic profiles it is found that a large continuous area with a flat channel floor is found from the inlet of the Lister Tief, along the northern flank of the Lister Tief and following the Lister Tief around the northeastern extremity of Sylt into the Højer Dyb (Figs. 2, 3 & 9). On the flat channel floor some dune structures are found (Fig. 9). The flat channel floor forms the deepest part of the surveyed area and is found immediately south of the continuous erosion scar observed in the Lister Tief (Fig. 3). At the seaward entrance to the Lister Tief the flat channel floor occurs west of the scar but landwards of the flood dominated dune field (Figs. 3 & 8). The width of the flat channel floor area is largest at the western inlet of the Lister Tief where it reaches approx. 270 m and narrows in an eastern direction being only 25 m at the entrance into the Højer Dyb. The other area of a seemingly flat channel floor is located in the western part of the Lister Ley close to List (Fig. 3).

At the entrance to the Lister Tief, ca. 300 m north of the main channel, the western part of an abandoned channel at least 300 m wide is located by one sparker profile. The channel extends to the north of the sparker profile. On the crossing profile, pronounced infill is seen in the channel. The inclination of the southern flank and the depth to the base of the abandoned channel resembles the present day channel south of here. The width of the two channels is also in the same range.

4. Large-scale Foresets

Large-scale foresets or clinoforms are observed in three areas (Fig. 3). The largest foreset system is found at the seaward side of the flat channel floor area at the North Sea inlet to the Lister Tief (Figs. 3 & 8). The direction of sediment movement is towards the East. Another group of foresets is found along the western coast of Sylt in the small NNE trending channel (Fig. 3). Here the foresets show that the direction of movement is to the NNE. The third location is in the Königshafen area (Figs. 3 & 10). Here the precise direction of foresets can not be estimated; however they seem to reflect sediment movement from the coast of Sylt into the Lister Ley.

5. Areas of non-deposition

In two areas no depositional features are present at the sea floor. One, in the westernmost part of the study area and the other, in the flat-channel-floor area, associated with the Lister Tief.

Discussion

Sparker data image the bedform configuration at the sea floor and display subsurface penetration to approx. 0.1 s TWT (ca. 75-100 mbsf (meters below sea floor)). These data are supplemented by Chirp III data that show details down to ca. 15-20 mbsf with a vertical resolution of approx. 3.5 times greater than that of the sparker data. From the interpretation of the seismic and subbottom profiler records a number of different geological structures can be identified. Among the observed bed forms, the dunes show sediment transport direction and prevailing sedimentation regime in the study area. The interpretation of the seismic profiles also reveals other large-scale, current-induced sedimentary systems enabling the compilation of a map illustrating an overall model for long-term sediment distribution and inferred bottom current regime responsible for sediment transport in the area (Fig. 3).

From the seismic data, the characteristic lee and stoss-side configuration of the dunes are identified and this is supported by information from sounding profiles and side scan sonar data (Ulrich & Pasenau, 1973; Hennings et al. 2004). Along some seismic profiles dunes indicating opposite current directions are found (Fig. 4). The spatial distribution of the transverse dunes shows two groups based on direction of sediment transport, which are ascribed to flood and ebb dominated tidal regimes as also suggested by Ulrich & Pasenau (1973), Hennings et al. (2004), and Hennings & Herbers (2006) (Fig. 3). Apart from these flood and ebb dominated dunes a third group of bed forms at the sea floor is identified. These are presumably also dunes, but were either crossed at oblique angles by the seismic profile or found in an environment strongly affected by both flood and ebb current activity and are therefore, called here "indefinite" dunes (Figs. 3, 4 & 9). Moreover, on some sparker profiles it is observed that some dunes are complex and appear to consist of a superimposed dune system, in contrast to most of the other dunes that seem to be singular, structures. Due to the higher resolution of the Chirp III data, these individual structures are identified as being made up of a number of smaller structures e.g. ripples or small scale dunes (Figs. 5 & 7) that all migrate in the same direction as the overall pronounced single standing dunes. Sometimes a merg-

ing of the small scale structures is observed. Similar findings based on sidescan data from the Lister Tief are also reported (Hennings & Herbers 2006).

As referred to before, in the Lister Tief the ebb dominated dunes are found located to the north of the flood dominated dunes and south of the flat channel floor area. This is expected as the flood oriented dunes most likely formed due to the Coriolis force acting on the flood current. In the northern part of the Lister Tief the ebb dominated dunes are found in the central part of the channel. In the Rømø Dyb the ebb dominated dunes are found in a shallow area NE of the large erosional scar.

Pronounced erosiononal scars are found at the sea floor where erosional processes cut into older deposits (Figs. 3, 8 & 9). From the entrance to the Lister Tief and along its northern boundary towards the entrance to the Højer Dyb a pronounced flat channel floor area, locally with some isolated dune structures, is found immediately south of the erosional scar. This area is located north of the flood-dominated dune fields (Fig. 3). The width of the channel varies and is largest in the western part of the Lister Tief, while narrowing markedly towards the NE.

Foresets are observed extending along the western coast of Sylt towards the entrance of the Lister Tief. They are also found at the seaward entrance of the Tief and in the Königshafen area (Figs. 3, 8 & 10).

In the seaward area our data indicates mainly non-deposition, i.e. sediment bypassing prevails in these areas.

Along the west coast of Sylt the presence of the elongate channel striking NE-SW indicates significant current action concentrated here. Accordingly, foresets observed here show a NE sediment transport direction all the way up to the northern end of Sylt where an elevated area acts as a barrier forcing the current transport path to bend seaward and/or to pass between this high and the coast of Sylt (Fig. 3).This reflects a northward sediment transport system along the coast of Sylt towards the Lister Tief. The flood-dominated dune field north of Sylt is seen in its overall form to be rather stable although individual structures do move. From side scan sonar (Hennings et al. 2004) data we see that the dunes are transverse and migrating, which concurs with our observations. The location of the dune field implies that a major deposition area is found in the Lister Tief immediately north of Sylt which is also reflected by the coastline configuration (Fig. 3).

North of this flood dominated dune field an ebb dominated dune field is located. The spatial extent of this dune field is smaller than found for the flood dominated dune field, whereas the individual dune structures are also smaller. Along the northern side of the ebb dominated dune field a flat channel floor area is found in the deepest part of the Lister Tief. As described before, the width of the flat channel floor area varies. This suggests that current speed is strongest in the areas where the channel is most narrow. From the observation of the distribution of the flood and ebb dominated dune fields in relation to the nature of the flat channel floor area and adjacent erosional scar, it is suggested that bottom current action here is dominated by the ebb tide, which due to Coriolis force, causes the strongest erosion at the northern slope of the Lister Tief (Fig. 3). More to the west, where the flat channel floor area and the erosional scar diverge, i.e. roughly midway in the Lister Tief, bifurcation of the sediment transport current is suggested. One branch continues westward through the Lister Tief where sediment are deposited as an ebb dominated dune field, whereas the other branch of the current continues in a northern direction along Rømø and loses speed here, leading to sediment deposition SW of Rømø.

Where the Lister Tief and Lister Ley meet at the NE extremity of Sylt, a large number of indefinite dune structures not attributable to either flood or ebb dominated processes are observed. These are located in an area where strong flood and ebb currents meet and this likely causes highly turbulent and complex hydrodynamic condition, with strong gyre formation, affecting the dune configuration in this area. Also, further south in the Lister Ley, indefinite dunes are observed that may reflect interaction between currents from the Lister Tief, Lister Ley and Højer Dyb combined with current processes originating from Königshafen Bay.

In the Königshafen area the water depth is very shallow and foresets point to a transportation direction from west to east in the platform areas, but as the area is virtually dry during ebb tides it is suggested that the foresets are not related to the present current regime but may be the result of older sedimentation processes (e.g. overwash, aeolian transport) originating from the west and directed towards the east, as suggested by Bayer & Higelke (1994). At the eastern termination of the foresets, flood dominated dunes are found in the Lister Ley and the dunes continue in a southward direction. An apparent erosional scar is located at the south western termination of the foreset area and the erosional scar and flood dominated dune structures concur with Corioli forcing of the incoming flood current controlling sediment transport here. In the central part of the Lister Ley a larger ebb dominated dune field is located showing that here northward directed currents are responsible for sediment movement. In the northern part of Højer Dyb flood currents controlling sediment movement appear to dominate again (Fig. 3)

The mapped bed form and channel configuration with the proposed sediment transport model for the Sylt Rømø area strongly resembles the overall model of an ebb tidal delta suggested by Hayes (1980). It was

suggested that well developed ebb tidal deltas occur in areas of large tides and smaller wave heights, which seems to apply to the Lister Tief area.

Furthermore, the results of the presented work show similarities to the work from ebb-tidal delta of Texel Inlet further south in the Wadden Sea (Sha 1990). The Marsdiep separates the barrier island Texel from the mainland at Den Helder. Using the results of the analysis of a large number of box and gravity cores, it was found that flood dominated bed forms are located along the coast of the mainland south of the inlet, and in the southern part of the Marsdiepnear Den Helder. In the northern part of Marsdiep ebb-dominated bed forms with a height of up to 3 m were found. It was shown that the flood dominated bed forms in the tidal inlet are up to 8 m high and thus considerably larger than the ebb dominated bed forms. Comparing the results of Sha (1990) and the present work shows, that Marsdiep and Lister Tief are comparable, both acting as ebb channels. The bed form distribution shows that flood dominated bed forms are located in the southern part of the inlet and that ebb dominated bed forms prevail in the north. In both areas the flood dominated bed forms are larger than the ebb dominated ones. A schematic diagram showing the morphology of ebb-tidal deltas based on examples from inlets of West Frisian Islands is shown by Sha (1990). Applying this diagram to the present study, reveals similarities suggesting that the Lister Tief is the main ebb channel. In the Sylt area, the flood channel is probably represented by the shallow channel and zone of non-deposition located along the west coast of Sylt. Landwards of the Lister Tief the flood and ebb current act on a smaller scale in the Lister Ley and the Højer Dyb, and still show flood, ebb and indefinite bed forms indicating the transitional zone between these two sediment transport current regimes. From the dataset it thus seems likely that the northern part of Sylt is building further to the north and Rømø is being enlarged to the southwest which may be associated with continued erosion at the escarpments and a further deepening of the Lister Tief.

Conclusion

A large number of high resolution 2 D seismic (sparker and Chirp III) profiles have been acquired during the period 2005 to 2009. The data reveal bedform configuration and sub-bottom structures to a depth of 75-100 mbsf for the sparker data and ca. 20 mbsf for the Chirp III data and thus add valuable information to previously obtained sidescan seabed information. The data show several geological and dynamic bed form features, i.e. flood and ebb dominated dune fields, flat channel floor areas, a large continuous erosional scar as well as evidence of smaller scale erosion. The dunes are transverse type with varying dimensions and a maximum length of up to 350 m and height up to 8 m. The investigation carried out here indicates that sediments are transported along the western coast of Sylt towards the entrance of the Lister Tief. In the Lister Tief near Sylt a very large, flood-dominated dune field is found. More to the north in the Lister Tief a flat channel floor area with a large erosional scar cutting the northern slope of the Tief and ebb dominated dunes have been found. This shows that ebb dominated currents control sediment transport and erosion processes in the northern sector of the Lister Tief. In the western part of the Lister Ley channel foresets prograde from the Königshafen area into the channel where they terminate in an area characterized by flood dominated dunes. In the eastern part of Lister Ley flood dominated dunes are also present, while in-between outgoing, northerly ebb currents govern sediment transport. Evidence for erosion and northward sediment transport along the west coast of Sylt with deposition along the north coast of Sylt is also reflected by the beach development in this area. The seismic data indicate narrowing and deepening of the Lister Tief at the same time as significant sediment deposition occur SW of Rømø. In the main, the proposed sediment transport model for the Lister Tief tidal inlet areas is in overall agreement with models suggested by Hayes (1980) and Sha (1990). The present study applying different acoustic techniques thus adds important information to our understanding of sediment transport patterns in a Wadden Sea tidal inlet.

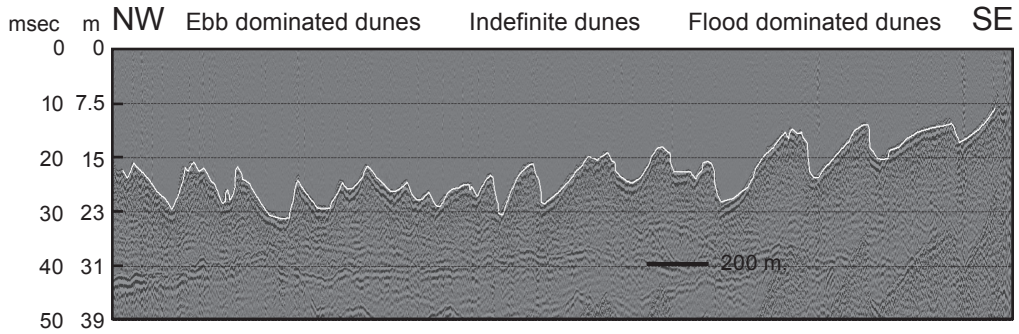

Fig. 4: Sparker profile from the central and western part of the Lister Tief showing flood and ebb dominated dunes. In between "indefinite" dune structures are located. Internal structures are seen in the upper part of the dunes. Vertical scale is in msec TWT and in m (velocity of soundwave in water 1500 m/s and 1600 m/s for sediments). For location of profile see Fig. 3.

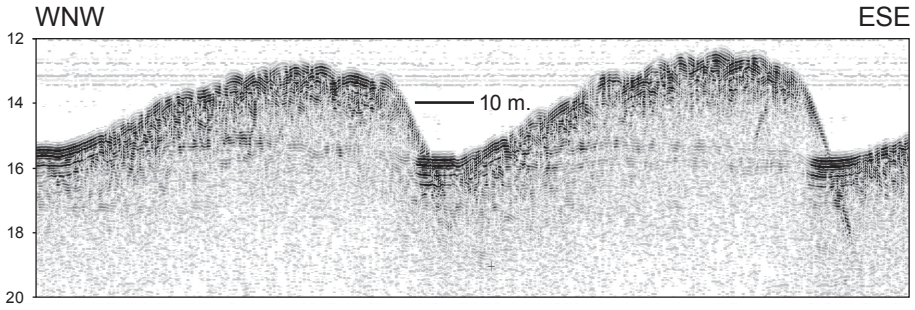

Fig. 5: Chirp III profile from the southern part of Lister Tief. This figure shows large, up to ca 3 m high dunes with an inferred sediment transportation to ESE indicative of flood dominated dune structure. The dune is located on top of a marked, horizontal reflector found at 15-16 m below present sea level. In several cases this reflector is seen to outcrop in the trough in between the dunes and presumably consists of a pavement of coarser sediment. Reflectors revealing internal structures are seen in the upper part of the dunes. The surface of the dunes is seen to be made up of smaller structures. Depth in m. For location of profile see Fig. 3.

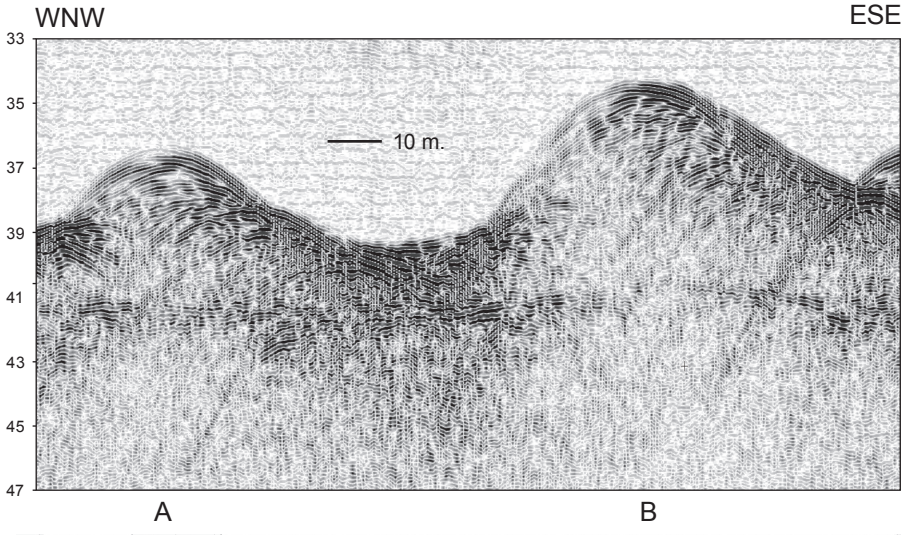

Fig. 6: Chirp III profile from the central part of the Lister Tief. The figure shows 4-5 m high dunes with a marked internal (foreset) reflection pattern typically indicating sediment transport conform to the topographic asymmetry of the dune which in this case is ebb dominated and thus towards the WNW. This is most clearly demonstrated in case of dune B at the ESE part of this profile. Note that in this case a mainly (sub) horizontal reflector is seen at a depth of 40-41 m, i.e. well below the depth of the horizontal reflector described in Fig. 5 and 7. In the case of dune A the reflector at a depth of 40-41 m is slightly upbending likely due to velocity pull up effect. Depth in m. For location of profile see Fig. 3.

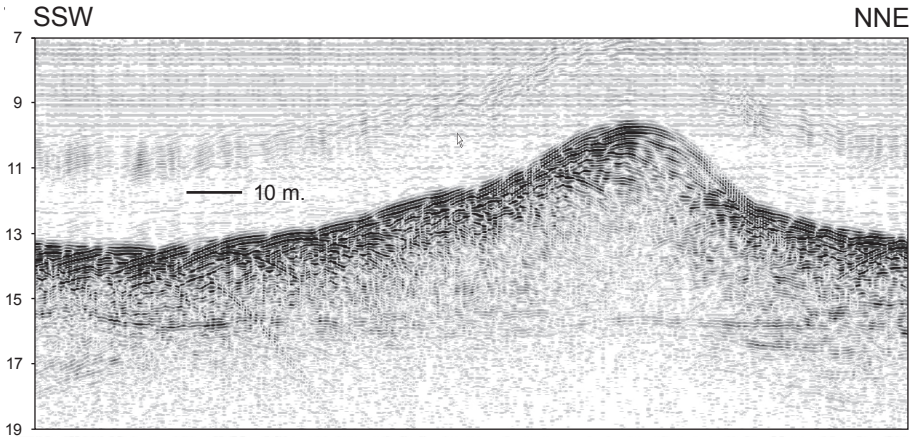

Fig. 7: Chirp III profile from the northern part of the Lister Ley. This figure shows a large, up to ca 3 m high dune with an inferred sediment transportation to NNE indicative of ebb dominated dune structure. Internal reflector pattern is seen within the dune indicating that the dune is migrating towards the NNE. The dune is located on top of a marked, horizontal reflector found at 15-16 m below present sea level overlain within the trough by a few meters of (sandy) sediments. This reflector which continues below the sand waves thus appears to form the base of the (migrating) dunes. From our data set it can not be determined with confidence, whether the reflector represents an older, early Holocene transgression horizon, or has been formed in relation to later dune formation and migrational processes. Depth in m. For location of profile see Fig. 3.

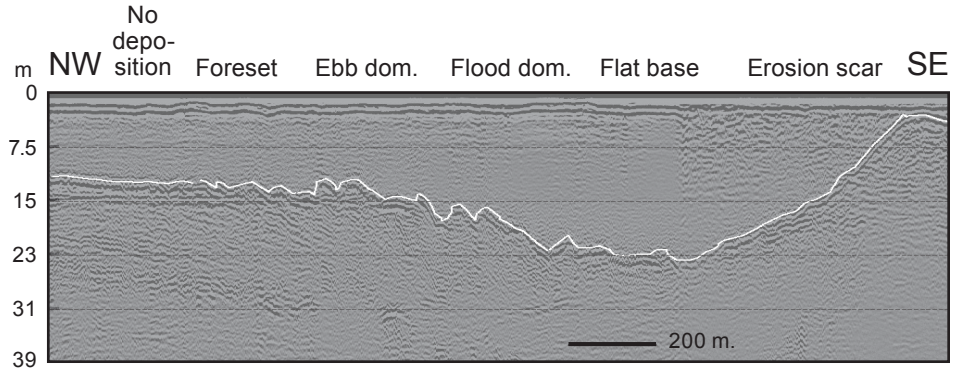

Fig 8: Sparker profile at the outer entrance to the Lister Tief showing erosion scar in relation to the topographic high NW of Sylt, a flat channel floor area, flood and ebb dominated dunes and area of no deposition. At the NW part foresets are seen in a depth interval of ca. 2-20 m below sea floor. Vertical scale is in msec TWT and in m (velocity of soundwave in water 1500 m/s and 1600 m/s for sediments). For location of profile see Fig. 3.

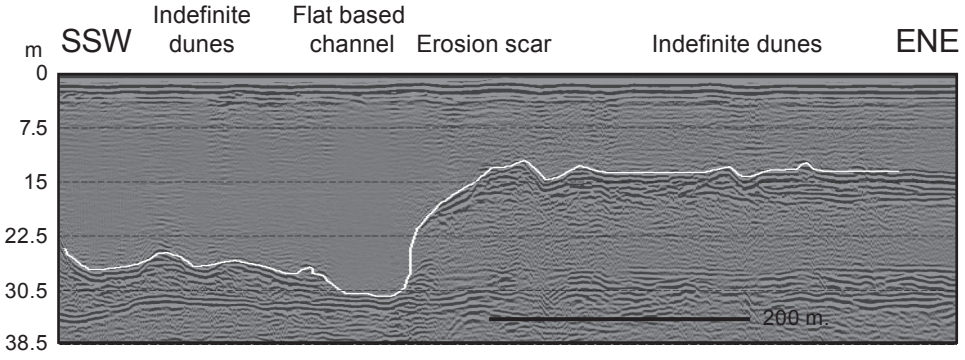

Fig 9: Sparker profile from the eastern most part of the Lister Tief showing a pronounced erosional scar, flat based channel, and "indefinite dunes" in the channel and at a higher level ENE of the erosional scar. Vertical scale is in msec TWT and in m (velocity of soundwave in water 1500 m/s and 1600 m/s for sediments). For location of profile see Fig. 3.

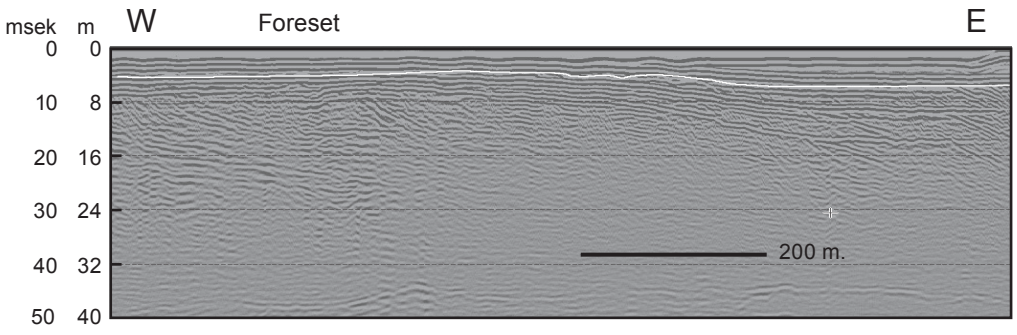

Fig 10: Sparker profile from the Königshafen area showing foreset indicating an eastern direction of sediment transport. Vertical scale is in ms TWT and in m (velocity of soundwave in water 1500 m/s and 1600 m/s for sediments). For location of profile see Fig. 3.

Acknowledgement:

Thanks are due to AWI for the opportunity of using their research vessel 'Mya' and to the crew for good cooperation. Thanks are also due to GEUS for making their sparker equipment available, to Langeland Museum and IGG for putting the Chirp III at our disposal and to the Institute for Baltic Sea Research ('IOW') for equipment support in 2007. Kiel University (Klaus Schwarzer) is acknowledged for support with RV 'Littorina' shiptime and equipment in 2005. Landmark is thanked for supplementing software for seismic interpretation and mapping through their University grant to IGG. We thank technicians at IGG and GEUS for their assistance with the acquisition of high-quality acoustic data and to B. Munch (IGG) for making the drawings. Thanks to the two reviewers Drs. H.Lykke-Andersen and J.B. Jensen for valuable comments. Thanks to Dr. W. Stratford for helpful correcting of English.

References

Ahrendt K. & Pesch, R. 2001: Das GIS als Methode für die Rekonstruktion geologischer Entwicklungen- Beispiel Sylt/Deutsche Bucht. Meyniana, 53, 5–30.

Aliotta, S. & Perillo, G.M.E., 1987: A sand wave field in the entrance to Bahia Blanca Estuary, Argentina. Marine Geology, 76, 1–14.

Backhaus, J., Hartke, D., Hübner, U., Lohse, H. & Müller, A., 1998: Hydrographie und Klima im Lister Tidebecken.- In: Gätje, C. & Reise, K. (eds.): Ökosystem Wattenmeer-Austausch-, Transport- und Stoffumwandlungsprozesse: 39–54; Berlin, Heidelberg (Springer).

Bartholdy, J., Bartholomä, A. and Flemming, B.W. 2002. Grain-size control of largecompound flow-transverse bed forms in a tidal inlet of the Danish Wadden Sea. Marine Geology Vol. 188, 391–413.

Bartholdy, J., Flemming, B.W., Bartholomä, A. Erntsen, V.B. 2005. Flow and grain size control of depth-independent simple subaqueous dunes. Journal of Geophysical Research-Earth Surface, 110, F04S16, doi:10.1029/2004JF000183.

Bayerl, K.-A. & Higelke, B., 1994: The development of the northern Sylt during the Latest Holocene. Helgoländer Meeresuntersuchungen, 48, 145–162.

Bot, S.L. & Trentesaux, A. 2004: Types of internal structure and external morphology of submarine dunes under the influence of tide- and wind-driven processes (Dover Strait, northern France). Marine Geology, 211, 143–168.

Fürstenau, J. (2007). Aufbau und Entwicklung eines holozänen Nehrungshakens – Ellenbogen/Sylt. Unpublished diploma thesis, University of Hamburg, 112 pp.

Hayes, M.O., 1980: General morphology and sediment pattern in tidal inlets. Sedimentary Geology, 26, 139–156.

Hennings, I. & Herbers, D. 2006: Radar imaging mechanism of marine sand waves at very low grazing angle illumination caused by unique hydrodynamic interactions. Journal of Geophysical research, Vol. 111, C10008, doi: 10.1029/2005JC003302,2006, 1–15.

Hennings, I, Lurin, B., Vernemmen, C. & Vanhessche, U., 2000: On the bahaviour of tidal current directions due to the presence of submarine sand waves. Marine Geology, 169, 57–68.

Hennings, I., Herbers, D., Prinz, K. & Ziemer, F. 2004: First results of the OROMA experiment in the Lister Tief of German Bight in the North Sea. EARSel proceedings 3, 1/2004, 86–104. et al. 2004).

Kystinspektoratet 1999: Morfologisk udvikling i Vadehavet, Lister Dybs Tidevandsområde og Vadehavsfronten. Trafikministeriet 38 pp.

Lane, A., Riethmüller, R., Herbers, D., Ryabaczok, P., Günther, H., Baumert, H. (2000). Observational data sets for model development. Coastal Engineering 41, 125–153.

Lindhorst, S., Fürstenau, J., Hass, H.C., Betzler, C. (in press). Anatomy and sedimentary model of a hooked spit (Sylt, southern North Sea). Sedimentology.

Lindhorst, S., Betzler, C., Hass, H.C., 2008. The sedimentary architecture of a Holocene barrier spit (Sylt, German Bight): Swash-bar accretion and storm erosion. Sedimentary Geology, 206, 1–16.

Schwarzer, K., 1984. Das Morsum-Kliff und seine Ausbreitung unter den nördlich vorgelagerten Wattsedimenten. In: Degens, E.T., Hillmer, G., Spaeth, C. (Eds.), Exkursionsführer Erdgeschichte des Nordsee-und Ostseeraumes. Geologisch-Paläontologisches Institut der Universität Hamburg, Hamburg, 251–282.

Sha, L.P., 1990: Surface sediments and sequence models in the ebb-tidal delta of Texel Inlet, Wadden Sea, The Netherlands. Sedimentary Geology, 68, 125–141.

Ulrich, J. & Pasenau, H., 1973: Morphologische Untersuchungen zum Problem der tidebededingten Sandbewegung im Lister Tief. Die Küste, 24, 95–112.

Yuepingia? sp., a ceratopygid trilobite from the upper Cambrian (Furongian) of Scandinavia

THOMAS WEIDNER & ARNE THORSHØJ NIELSEN

Weidner, T. & Nielsen, A.T., 2010-04-13. *Yuepingia*? sp., a ceratopygid trilobite from the upper Cambrian (Furongian) of Scandinavia. © 2010 by Bulletin of the Geological Society of Denmark, Vol. 58, pp. 29–33. ISSN 0011–6297. (www.2dgf.dk/publikationer/bulletin)

A single pygidium found in an ice-rafted loose boulder of coquinoid bituminous limestone represents an 'exotic' trilobite hitherto unknown from the Scandinavian Alum Shale Formation. The limestone, found on the east coast of Jutland, Denmark, also contains *Leptoplastus paucisegmentatus, Parabolina spinulosa* and *Orusia lenticularis* and derives from the upper Cambrian (Furongian) *Leptoplastus paucisegmentatus* Zone of Västergötland, south-central Sweden. The 'exotic' pygidium shows closest resemblance to the ceratopygid *Yuepingia glabra*, described from Alaska, and is treated as *Yuepingia*? sp. The Laurentian *Y. glabra* occurs in the *Ptychaspis-Prosaukia* Zone which corresponds in age to the Scandinavian *Leptoplastus* Superzone.

Keywords: Ceratopygid trilobite, Furongian, Alum Shale, Cambrian, Scandinavia.

Thomas Weidner [to.we@paradis.dk], Ravnholtvej 23, Rårup, DK-7130 Juelsminde, Denmark.
Arne Thorshøj Nielsen [arnet@snm.ku.dk], Geological Museum, University of Copenhagen, Øster Voldgade 5-7, DK-1350 Kbh K, Denmark.

The majority of glacial erratic boulders of Cambrian age found in Denmark and northern Germany derive from the Swedish provinces Västergötland, Scania and Öland and from the Danish island of Bornholm. They comprise sandstones, limestones and conglomerates as well as rare siltstones and shales, but which generally did not survive the long transportation. The Middle Cambrian–Tremadocian Alum Shale Fm is represented mostly by limestones, including the common so-called anthraconites (bituminous limestone/'orsten'), which occur as concretions and beds in the formation. The Furongian is represented almost exclusively by these bituminous limestones, which are often richly fossiliferous.

During the Furongian the major part of the Baltic platform was covered by a shallow sea with prevailing dysoxic conditions at the sea floor. The Furongian faunal assemblages are always monotonous and dominated by olenid trilobites adapted to this environment, in addition to a few agnostid taxa. Olenids often occur in great profusion, but with only 1–3 species occurring together. The fauna has been described from Sweden (e.g. Westergård 1922, 1939, 1944, 1947; Ahlberg *et al.* 2006; Terfelt 2003, 2006), Norway (Henningsmoen 1957a and references therein) and Bornholm, Denmark (notably Poulsen 1923). The same biofacies, dominated by olenid trilobites, is also known from Wales, eastern Canada and Argentina (e.g. Harringston & Leanza 1957, Holland 1971). Based on the abundant and short-ranging trilobites, a detailed biostratigraphic zonation has been established for Scandinavia (Westergård 1922, 1947; Henningsmoen 1957a). It was recently revised by Terfelt *et al.* (2008), who elevated the subzones of previous authors to zonal rank. In the present paper we treat the traditional Furongian zones of Westergård (1947) and Henningsmoen (1957a) as superzones (compare Terfelt *et al.* 2008, 2010).

In addition to the extremely abundant olenid-agnostid fauna, sparse 'exotic' trilobites, which are regarded as 'immigrants' from other biogeographic areas, are occasionally also found in the Alum Shale Fm and glacial erratic boulders of this unit (Westergård 1922, 1947; Henningsmoen 1957b; Buchholz 1998, 2005; Weidner 2001; Weidner & Żylińska 2005; Terfelt & Ahlgren 2007, 2009). These 'immigrants' are rare in the *Olenus* and *Parabolina* superzones and extremely rare in the *Leptoplastus* and *Peltura* superzones. The *Acerocare* Superzone has not yet yielded any 'exotic'

taxa. The 'immigrants' are potentially important for biostratigraphic correlation out of Baltica, providing a loose 'ghost stratigraphy' with ties to other continents (e.g. Westergård 1947; Terfelt & Ahlgren 2007; present paper).

In the present paper a trilobite new to the Alum Shale biofacies is described; the genus is elsewhere known from China and Alaska. The specimen was found in an erratic bituminous limestone boulder representing the basal *Leptoplastus paucisegmentatus* Zone of the Furongian *Leptoplastus* Superzone. The lithology and fossil assemblages of the local ice-rafted Cambrian boulders at As Hoved on the east coast of Jutland (Fig. 1) and the common presence of Kinnediabase clearly indicates that the material derives from the province of Västergötland, south-central Sweden (see also Houmark-Nielsen 1987, pp. 24–27).

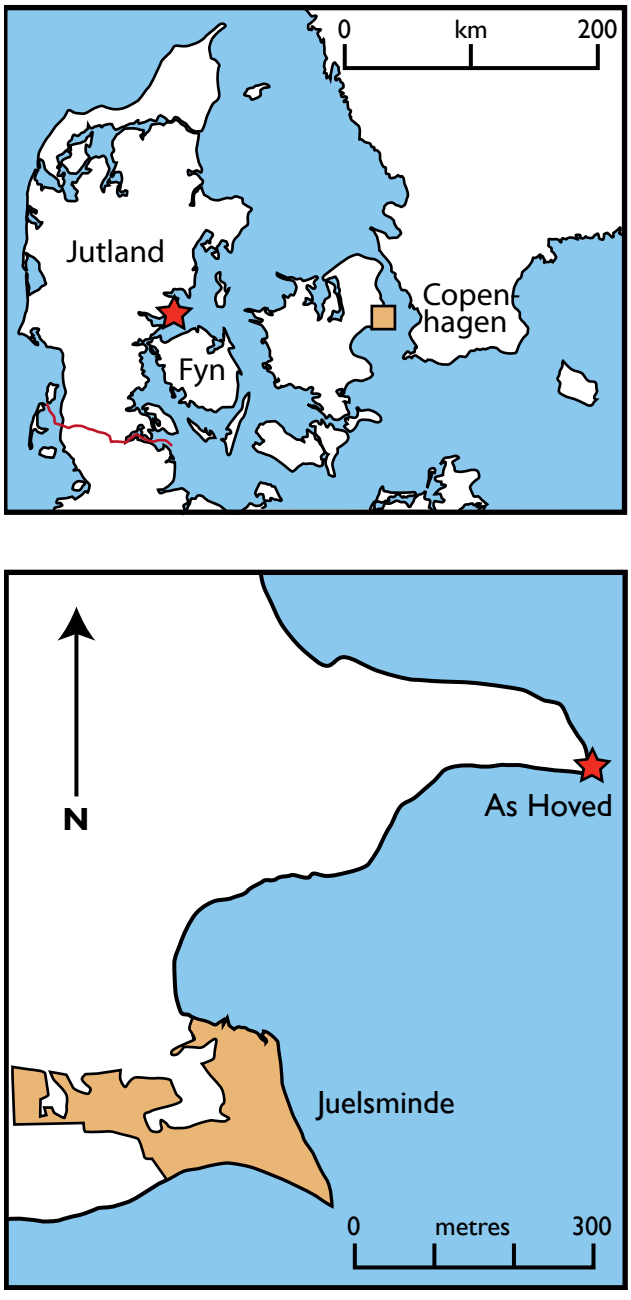

Figure 1. Map showing location of As Hoved shortly north of Juelsminde in eastern Jutland, Denmark. The ice-rafted boulder was found at UTM N 55° 44′ 43.93″, E 10° 4′ 18.10″.

Superfamily ASAPHOIDEA Burmeister, 1843

Family Ceratopygidae Linnarsson, 1869

Genus *Yuepingia* Lu, 1956

Yuepingia? sp.

Fig. 2: A–B

Material: One pygidium from an ice-rafted boulder found at As Hoved (Palsgård) cliff north of Juelsminde, Denmark (Fig. 1). The specimen is deposited at the Geological Museum, University of Copenhagen, as MGUH 29.196.

Accompanying fauna and age: *Leptoplastus paucisegmentatus* Westergård, 1922 (Fig. 2C–D), *Parabolina spinulosa* (Wahlenberg, 1818) and *Orusia lenticularis* (Wahlenberg, 1818). The faunal assemblage is unequivocally indicative of the *Leptoplastus paucisegmentatus* Zone of the Furongian *Leptoplastus* Superzone (see Westergård 1947; Henningsmoen 1957a; Terfelt *et al.* 2008, 2010).

Description: The spine-less pygidium is 4.2 mm long, semi-circular in outline and has a width:length ratio of about 1.6. The axis is strongly convex and consists of 6 or 7 rings (the anterior part of the specimen is damaged) in addition to the terminal piece and the articulating halfring. The axis occupies approximately 28% of the total width (tr.) at the first segment; it tapers evenly rearwards to about half the width at the posterior extremity. The axis is rather long, occupying approximately 80% of the total pygidial length (sag.), but extends only to the inner edge of the border; a postaxial ridge continues across the border. The axial furrows are distinct; the segmentation of the pleural fields is only very faintly discernible under oblique light. The border is weakly concave, descending quite steeply outwards, broadening slightly rearwards. The inner edge of the border is demarcated by a well-defined paradoublural ridge.

Remarks: The pygidium displays several general characteristics also seen in pygidia of ceratopygid

Yuepingia Lu, 1956, *Aplotaspis* Henderson, 1976 and *Charchaqia* Troedsson, 1937 and the asaphid *Golasaphus* Shergold, 1972.

Representatives of these genera occur in China, Australia and Alaska (Troedsson 1937; Lu *et al.* 1965; Palmer 1968; Shergold 1972; Henderson 1976). They all possess a spine-less, more or less semi-circular pygidium with a rather narrow and long convex axis delimited by distinct axial furrows; the axial and particularly the pleural fields show only faint segmentation and the border is relatively wide.

The specimen described in this paper has some features which differ from most representatives of the genera listed above: the weakly concave border is steeply sloping outwards and broadening slightly rearwards, the inner edge of the border is marked by a low but distinct paradoublural ridge, the axis does not extend beyond this ridge, but a faint postaxial ridge continues across the border. These features are shared with *Yuepingia glabra* (see Palmer 1968, pp. B56–57, pl. 13, figs 13, 16) described from the Hillard Peak area of Alaska. The associated Franconian–2 fauna includes species characteristic of the Laurentian *Ptychaspis-Prosaukia* Zone, which is considered coeval with the Scandinavian *Leptoplastus* Superzone (Geyer & Shergold 2000). The fauna also contains species with Asian affinities. It occurs in limestones deposited seawards of the continental shoreline in the outer detrital belt (Palmer 1968). The only apparent difference between the pygidium of *Y. glabra* and the specimen at hand concerns the axis, which in *Y. glabra* is almost totally effaced with only the anterior ring being discernible.

The type species of *Yuepingia, Y. niobiformis* Lu, 1956 from China (see Lu *et al.* 1965, pl. 102, fig. 13), has in comparison with the Scandinavian specimen a wide pygidium (width:length ratio 1.9 vs 1.6) with an axis extending onto the border, a strongly concave border and a slightly more pronounced segmentation of the pleural fields. We consider it questionable whether *Y. glabra* actually belongs to *Yuepingia* taking the different border outline, the shorter axis and the presence of a postaxial ridge into consideration. For this reason we treat the specimen at hand as *Yuepingia*? sp. The discussion of possible affinities would also greatly benefit from knowing the associated cranidium.

Hughes & Rushton (1990) suggested that *Yuepingia* Lu, 1956 is a junior synonym of *Haniwoides* Kobayashi, 1935, but see Choi *et al.* (2008, p. 196).

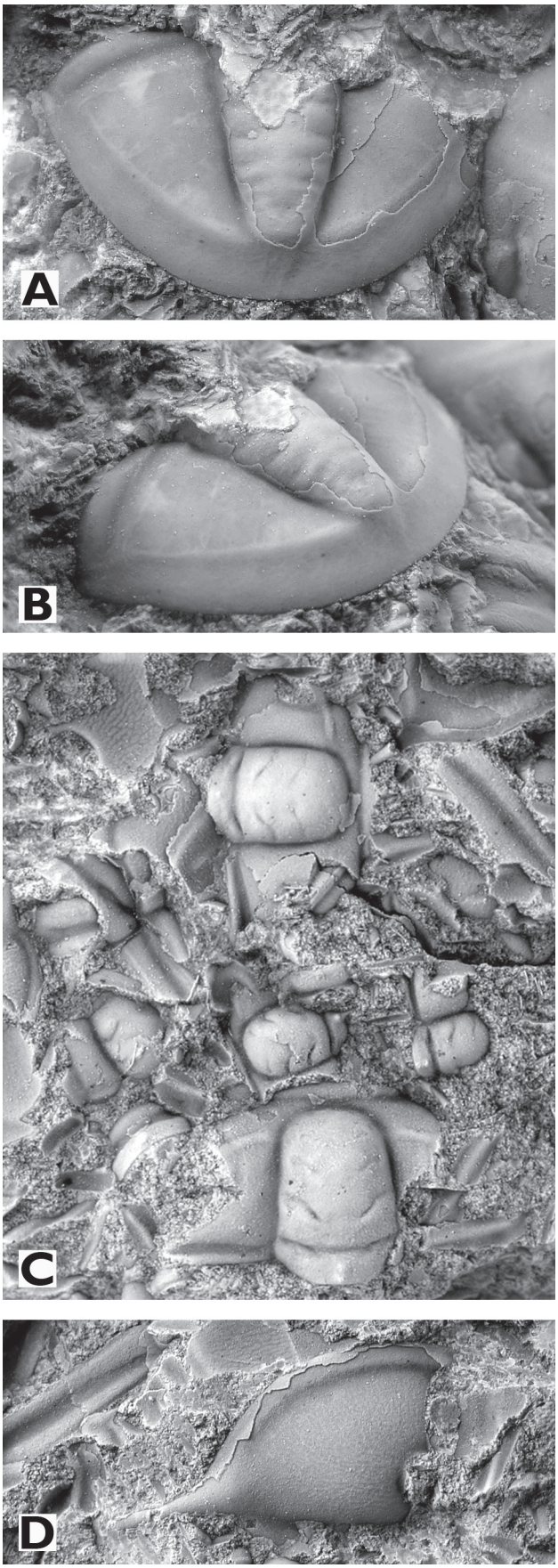

Figure 2. Trilobites from the erratic boulder found at As Hoved, east coast of Jutland, Denmark, all ×10. A–B. *Yuepingia*? sp., pygidium, MGUH 29.196 (A: Dorsal view, B: Oblique side view). C–D. *Leptoplastus paucisegmentatus* Westergård, 1922 (C: Group of cranidia, MGUH 29.197; D: Free cheek, MGUH 29.198).

The discussed Scandinavian pygidium also resembles that of *Golasaphus momedahensis* Shergold, 1972, in which, however, the pygidial width:length ratio approximates 2, and the axis is considerably narrower (cf. Shergold 1972, pl. 11, figs 1–5). *Yuepingia*? sp. may also be compared with the pygidium of *Aplotaspis erugata* (Whitehouse, 1939), as figured by Henderson (1976, pl. 49, figs 1, 3, 4), but which differs by having a strongly concave, wide border. *Aplotaspis* Henderson, 1976 was by Bao & Jago (2000) regarded as a junior synonym of *Charchaqia* Troedsson, 1937. Pygidia of *Charchaqia* (see *Charchaqia glabrescens* Peng, 1992, fig. 55 C, F; *Charchaqia halli* Jago, 1991, see also Bao & Jago 2000, pl. 2, figs 1–3, 6) differ from *Yuepingia*? sp. by having a longer, more strongly tapering axis.

The Scandinavian representatives of Asaphidae described from the *Peltura scarabaeoides* Superzone of the Alum Shale Fm (Westergård 1922, 1939), i.e. *Promegalaspides* and *Niobe* (*Niobella*), are readily distinguished from *Yuepingia*? sp. Species of *Promegalaspides* thus have an axis with strong segmentation and a concave, narrow border, whilst *Niobe* (*Niobella*) has a wide, strongly concave border. The oldest representative of the Asaphidae in Scandinavia is *Eoasaphus superstes* (Linnarsson, 1875), which is known only from one specimen found in the *Parabolina brevispina* Zone (Westergård 1922, pl. 2, fig. 20). The pygidial axis of this species resembles that of *Yuepingia*? sp., but the border is concave and the pleural fields exhibit faint segmentation.

Along with published as well as unpublished occurrences of *Anomocare*, *Drepanura*, *Elkanaspis*, *Irvingella*, *Jasmundia, Macropyge*, *Maladioidella, Pedinocephalus* as well as other genera of the Pterocephaliidae in the Alum Shale Fm (Westergård 1947; Henningsmoen 1957b; Buchholz 1998, 2005; Weidner & Żylińska 2005; Terfelt & Ahlgren 2007, 2009) the new finding provides another loose intercontinental biostratigraphic tie point, in this case with Laurentia.

Acknowledgements

We thank A. R. Palmer, Colorado, USA, and R. A. Fortey, Natural History Museum, London, for helpful advice on the identification of the described pygidium.

Referees P. Ahlberg, Geological Institution, University of Lund, and A. Żylińska, Institute of Geology, University of Warsaw, are thanked for many constructive corrections that improved the original manuscript.

References

Ahlberg, P., Månsson, K., Clarkson, E. N. K. & Taylor, C.M. 2006: Faunal turnovers in the upper Cambrian *Leptoplastus* Zone at Andrarum, southern Sweden. Lethaia 39, 97–110.

Buchholz, A. 1998: Jasmundia - eine neue Trilobitengattung aus einem oberkambrischen Konglomerat-Geschiebe Vorpommerns (Norddeutschland). Archiv für Geschiebekunde 2, 379–386.

Buchholz, A. 2005: Notizen zu einigen bemerkenswerten Trilobiten-Funden aus oberkambrischen Geschieben der Stufen 4 und 5 (*Leptoplastus*- und *Peltura*-Stufe) Mecklenburg-Vorpommerns (Nordwestdeutschland). Der Geschiebesammler 38, 15–32.

Bao, J.-S. & Jago, J. B. 2000: Late late Cambrian trilobites from near Birch Inlet, south-western Tasmania. Palaeontology 43, 881–917.

Choi, D. K., Kim, E.-Y. & Lee J. G. 2008: Upper Cambrian polymerid trilobites from the Machari Formation, Yongwol, Korea. Geobios 41, 183–204.

Geyer, G, & Shergold, J. H. 2000: The quest for internationally recognized divisions of Cambrian time. Episodes 23, 188–195.

Harrington, H. J. & Leanza, A. F. 1957: Ordovician trilobites of Argentina. Department of Geology, University of Kansas Special Publication 1, 1–276.

Henderson, R. A. 1976: Upper Cambrian (Idamean) trilobites from Western Queensland, Australia. Palaeontology 19, 325–364.

Henningsmoen, G. 1957a: The trilobite family Olenidae with description of Norwegian material and remarks on the Olenid and Tremadocian Series. Skrifter utgitt av Det Norske Videnskaps-Akademi i Oslo, I. Matematisk-Naturvidenskapelig Klasse 1957(1), 303 pp.

Henningsmoen, G. 1957b: A Trilobite with North American affinities from the Upper Cambrian of Sweden. Bulletin of the Geological Institutions of the University of Uppsala 37, 167–172.

Holland, C.H. (ed.) 1971: Lower Palaeozoic rocks of the New World, Volume 1, Cambrian of the New World. Wiley-Interscience, New York, 456 pp.

Houmark-Nielsen, M. 1987: Pleistocene stratigraphy and glacial history of the central part of Denmark. Bulletin of the Danish geological Society 36, 1–189.

Hughes, N. C. & Rushton, A. W. A. 1990: Computer-aided restoration of a Late Cambrian ceratopygid trilobite from Wales and its phylogenetic implications. Palaeontology 33, 429–445.

Jago, J. B. 1991: *Charchaqia halli*, a new species of Late Cambrian Trilobite from south-western Tasmania. Geological Society of India, Memoir 20, 131–139.

Lu, Y., Chang, W., Chu, C., Chien, Y. & Hsiang, L. 1965: Chinese fossils of all groups, Trilobita. Vol. 1, 1–362; vol. 2, 363–766. Science Publication Co., Peking. [In Chinese].

Palmer, A. R. 1968: Cambrian Trilobites of East-Central Alaska. U.S. Geological Survey Professional Paper 559-B, 1–115.

Peng, S. 1992: Upper Cambrian biostratigraphy and trilobite faunas of the Cili-Taoyuan area, northewestern Hunan, China. Memoirs of the Association of Australasian Palaeontologists 13, 1–119.

Poulsen, C. 1923: Bornholms Olenuslag og deres Fauna. Danmarks geologiske Undersøgelse, II Række, 40, 1–83.

Shergold, J. H. 1972: Late Upper Cambrian trilobites from the Gola Beds, western Queensland. Bureau of Mineral Resources, Geology and Geophysics, Bulletin 112, 1–127.

Terfelt, F. 2003: Upper Cambrian trilobite biostratigraphy and taphonomy at Kakeled on Kinnekulle, Västergötland, Sweden. Acta Palaeontologica Polonica 48, 409–416.
Terfelt, F. 2006: Review of uppermost Furongian trilobites from Scania, southern Sweden, based on type material. Palaeontology 49, 1339–1355.
Terfelt, F. & Ahlgren, J. 2007: *Macropyge* (*Promacropyge*) Scandinavica new species; the first macropyginid trilobite recorded from the Furongian of Baltica. Journal of Paleontology 81, 1516–1522.
Terfelt, F. & Ahlgren, J. 2009: The first remopleuridioidean trilobite and the earliest *Parabolinella* species recorded in the Furongian of Scandinavia. Journal of Paleontology 83, 299–306.
Terfelt, F., Ahlberg, P. & Eriksson, M. E. 2010: Complete record of Furongian trilobites and agnostoids of Scandinavia – a biostratigraphical scheme. Lethaia 10.1111/j.1502-3931.2009.00211.x.
Terfelt, F., Eriksson, M. E., Ahlberg, P. & Babcock, L. E. 2008: Furongian Series (Cambrian) biostratigraphy of Scandinavia – a revision. Norwegian Journal of Geology 88, 73–87.
Troedsson, G. T. 1937: On the Cambro-Ordovician faunas of Western Quruq tagh, Eastern T'ien-shan. Palaeontologica Sinica 106, 1–74.
Weidner, T. 2001: Vier Funde von Trilobiten der Familie „Pterocephaliidae" aus dem Oberkambrium Schwedens in Geschieben aus Dänemark. Der Geschiebesammler 34, 61–68.
Weidner, T. & Żylińska, A. 2005: "Exotic" trilobites from the Upper Cambrian Alum shales of Sweden. Meeting proceedings Lundadagarna i Historisk Geologi och Paleontologi IX. GFF 127, 60 (abstract).
Westergård, A. H. 1922: Sveriges Olenidskiffer. Sveriges Geologiska Undersökning Ca 18, 1–205.
Westergård, A. H. 1939: On Swedish Cambrian Asaphidae. Sveriges Geologiska Undersökning C 421, 1–16.
Westergård, A. H. 1944: Borrningar genom Skånes Alunskiffer 1941-1942. Sveriges Geologiska Undersökning C 459, 1–45.
Westergård, A. H. 1947: Supplementary notes on the Upper Cambrian trilobites of Sweden. Sveriges Geologiska Undersökning C 489, 1–34.

Geochemistry and petrology of mafic Proterozoic and Permian dykes on Bornholm, Denmark: Four episodes of magmatism on the margin of the Baltic Shield

P.M. HOLM, L.E. PEDERSEN & B. HØJSTEEN

Holm, P.M., Pedersen, L.E. & Højsteen, B., 2010–05–17. Geochemistry and petrology of mafic Proterozoic and Permian dykes on Bornholm, Denmark: Four episodes of magmatism on the margin of the Baltic Shield. © 2010 by Bulletin of the Geological Society of Denmark, Vol. 58, pp. 35–65. ISSN 0011–6297. (www.2dgf.dk/publikationer/bulletin)

More than 250 dykes cut the mid Proterozoic basement gneisses and granites of Bornholm. Most trend between NNW and NNE, whereas a few trend NE and NW. Field, geochemical and petrological evidence suggest that the dyke intrusions occurred as four distinct events at around 1326 Ma (Kelseaa dyke), 1220 Ma (narrow dykes), 950 Ma (Kaas and Listed dykes), and 300 Ma (NW-trending dykes), respectively.

The largest dyke at Kelseaa (60 m wide) and some related dykes are primitive olivine tholeiites, one of which has N-type MORB geochemical features; all are crustally contaminated. The Kelseaa type magmas were derived at shallow depth from a fluid-enriched, relatively depleted, mantle source, but some have a component derived from mantle with residual garnet. They are suggested to have formed in a back-arc environment.

The more than 200 narrow dykes are olivine tholeiites (some picritic), alkali basalts, trachybasalts, basanites and a few phonotephrites. The magmas evolved by olivine and olivine + clinopyroxene fractionation. They have trace element characteristics which can be described mainly by mixing of two components: one is a typical OIB-magma (La/Nb < 1, Zr/Nb = 4, Sr/Nd = 16) and rather shallowly derived from spinel peridotite; the other is enriched in Sr and has La/Nb = 1.0 - 1.5, Zr/Nb = 9, Sr/Nd = 30 and was derived at greater depth, probably from a pyroxenitic source. Both sources were probably recycled material in a mantle plume. A few of these dykes are much more enriched in incompatible elements and were derived from garnet peridotite by a small degree of partial melting.

The Kaas and Listed dykes (20-40 m) and related dykes are evolved trachybasalts to basaltic trachyandesites. They are most likely related to the Blekinge Dalarne Dolerite Group. The few NW-trending dykes are quartz tholeiites, which were generated by large degrees of rather shallow melting of an enriched mantle source more enriched than the source of the older Bornholm dykes. The source of the NW-trending dykes was probably a very hot mantle plume.

Keywords: Bornholm, dykes, Baltic Shield, petrology, geochemistry.

Paul Martin Holm [paulmh@geo.ku.dk], Department of Geography and Geology, University of Copenhagen, Øster Voldgade 10, DK-1350 Copenhagen K.

Geological setting

The Baltic Shield is separated from the Danish-Polish Basin by two major fault zones, the Sorgenfrei-Tornquist zone (STZ) and the Teisseyre-Tornquist zone (TTZ) (Fig.1). Bornholm island is situated just E of the Rønne Graben, which offsets the STZ and TTZ. The southern part of the island is covered by Phanerozoic sediments, while Proterozoic basement rocks are exposed in the northern part. The geology of Bornholm has been described by e.g. Callisen (1934), Münther (1973), Micheelsen (1961), Surlyk (1980) and Berthelsen (1989, 1992).

The basement gneisses of Bornholm have been considered to belong to the same province as the coastal gneisses in Blekinge (Sweden) north of Bornholm (Berthelsen, 1989). The latter were formed probably as juvenile crust in Gothian times around 1.8 – 1.7 Ga (Johansson & Larsen, 1989; Johansson et al., 2006). The gneisses are intruded by two generations of granites. The older granites have gradational contacts to the gneisses (Callisen, 1934), and Berthelsen (1989)

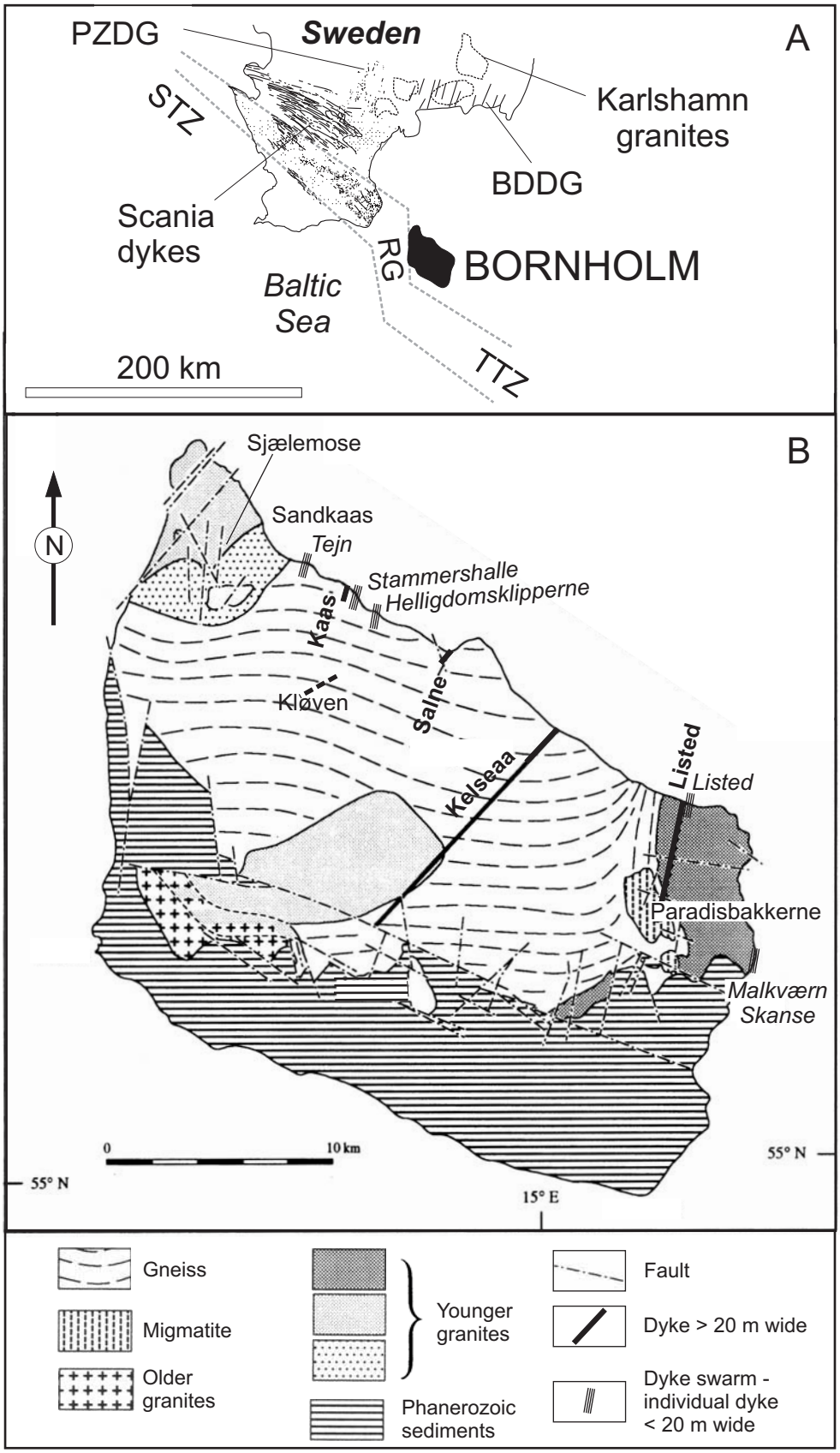

Figure 1: A: The location of Bornholm on the margin of the Baltic Shield. Also shown are three Swedish dyke swarms (PZDG – Protogine Zone Dolerite Group trending NNE, BDDG – Blekinge Dalarne Dolerite Group, Scania dykes), the Karlshamn granites, the Sorgenfrei-Tornquist Zone – STZ, the Teisseyre-Tornquist Zone – TTZ, and the Rønne Graben - RG. B: Geological map of Bornholm showing schematically the locations of large dykes (in bold) and dyke swarms (in italics). The geological map, apart from the dykes, is after Platou (1970). Modified from Abrahamsen & Lewandowski (1995). The authors have retained old spelling of place names related to dykes mentioned in the litterature. New spelling of Keldseaa is Kelse Å, Kaas is now Kås, and Strandkaas is Strandkås

suggested an origin by partial melting of the gneisses. The older granites are deformed. A younger generation of undeformed granites has sharp intrusive contacts to the gneisses. The granites were dated by Rb-Sr (Larsen, 1980) to 1400 ± 60 Ma (2σ) and subsequently by U-Pb (Tschernoster, 2000, Čečys, 2004). Recently, a much more restricted age range has been argued for the Bornholm gneisses and granites as more precise U-Pb analyses of zircon and titanite indicate that all granites crystallized in the interval 1475 - 1445 Ma, and that the orthogneiss country rocks have similar crystallization ages (Zariņš & Johansson, 2008). Gothian crust seems to be present only as inherited zircons in the gneisses (Zariņš & Johansson, 2008). The gneisses of Bornholm are therefore not equivalent to those of Blekinge which are Gothian with an age of 1.8 Ga (Johansson et al., 2006).

The deformation and granitic magmatism at c. 1.45 Ga is contemporaneous with similar events in Blekinge and elsewhere along the southwest margin of Baltica (Åberg, 1988; Obst et al., 2004; Johansson et al., 2006; Čečys & Benn, 2007; Bogdanova et al., 2008), which were termed the "Danopolonian orogeny" by Bogdanova (2001).

Extensional events in SW Sweden at around 1.2 Ga were accompanied by dyke intrusions at and parallel to the NNE-trending Protogine Zone (Fig. 1), and were correlated with a possible back-arc setting prior to the Sweconorwegian orogeny (Söderlund et al., 2005; Söderlund & Ask, 2006).

The Bornholm dykes

More than 250 mafic dykes have been intruded into the gneissic and granitic basement of Bornholm (Fig. 2), and their distribution and petrography have been described by Callisen (1934) and Münther (1945a, 1945b). Jensen (1966, 1988) has presented detailed petrography for a few selected dykes, and Obst (2000) discusses the petrology of the WNW- to NW-trending dykes. Abrahamsen (1977) and Abrahamsen & Lewandowski (1995) investigated the paleomagnetism of a wide range of dykes.

The dykes are mainly exposed along the north coast which is oblique to the trend of the dykes (Figs. 3 & 4a). The mafic dykes are estimated to have caused a minimum of 1.3% dilation along the c. 30 km long coast (Münther, 1945a, 1973). Almost all dykes strike between NNE and NNW (Fig. 4) and all are near-vertical. Among the exceptions are the Kelseaa dyke which strikes 40°, and a few WNW- to NW-striking dykes (Forchhammer, 1847; Münther, 1945b). Dykes exposed in inland areas and along the east and west coasts have similar orientations to the majority of dykes along the north coast. The width distribution of the dykes is strongly bimodal, in the sense that four dykes are 20 to 60 metres wide, whereas most of them are only a few metres wide (86 % are less than 3 m wide).

The Kelseaa dyke is the largest with a width of 60 m; it can be traced along strike for c. 20 km by detailed magnetic (Münther, 1973) and gravity measurements (Saxov, 1958). It is a significant gabbroic intrusion with an exposed area of almost 1.5 km^2. The Kaas dyke is

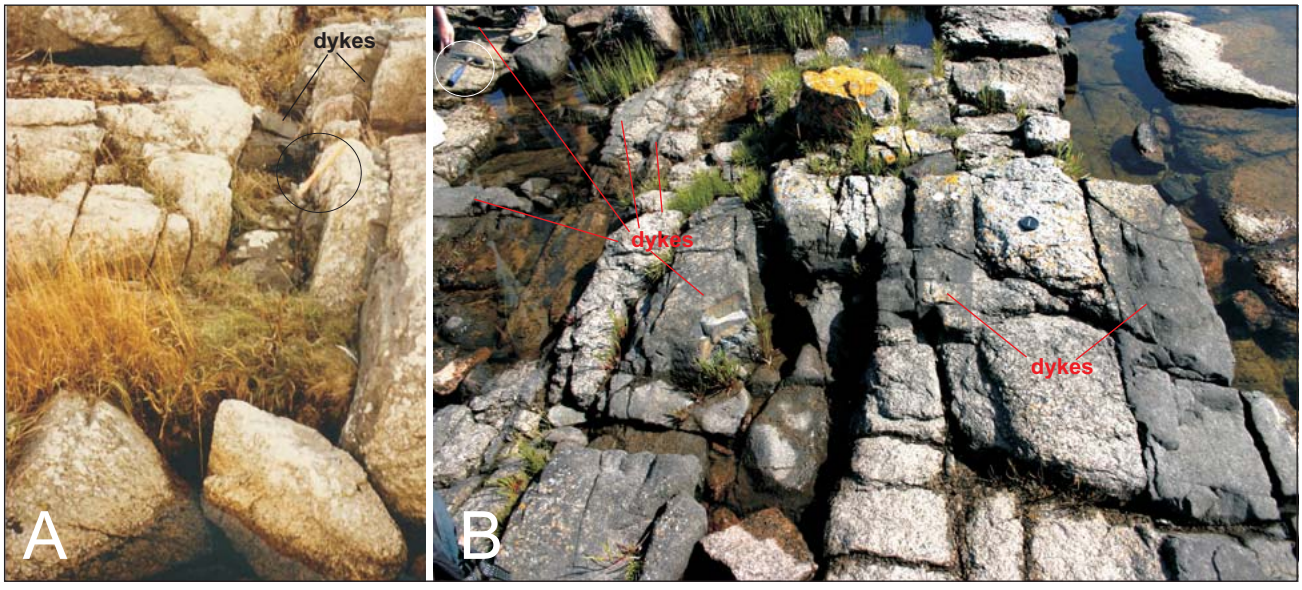

Figure 2: A) NNE-trending basaltic dykes cutting gneiss on the north coast of Bornholm. B) Part of the NNE-trending swarm on the east coast of Bornholm at Malkværn Skanse (hammer for scale in both photographs is 30 cm long) cutting the Svaneke granite.

40 m wide, but is exposed only over a short distance from the coast, whereas the 30 m wide Listed dyke can be traced 5 km inland. The Salne dyke is 22 m wide. Münther (1945a) lists four dyke swarms (Figs 3, 5): east of Tejn harbour where dykes make up around 20 % of the exposure over 150 m along the coast (Fig. 3A); around Stammershalle where > 16 dykes make up 7 % of the area for 300 m (Fig. 3B); in the Helligdomsklipperne area with 5 % dykes over 600 m of coast (Fig. 3C); and from east of Listed harbour to near the mouth of Vaseå stream dykes constitute c. 10 % of the crust over 550 m of coast line (Fig. 3G). However, the latter swarm includes the large dyke at Listed, which makes up 30 m of the 46.5 m total dyke width. The Listed dyke may be considerably younger than the other dykes (see below), which makes the concentration of the other, possibly penecontemporaneous, dykes in the area much lower (3.5 %) and they would probably not be considered to represent a swarm on their own. The easternmost dykes around Malkværn Skanse (Figs. 3H & 5b), on the other hand, constitute 7 % of the crust over a distance of 250 m in an ENE direction, and should therefore be considered a swarm. The term "dyke swarm" is used here for local concentrations that on Bornholm never represent more than 20 % crustal dilation. WNW- to NW-trending dykes are rare and constitute a relatively minor component of the mafic intrusions on Bornholm.

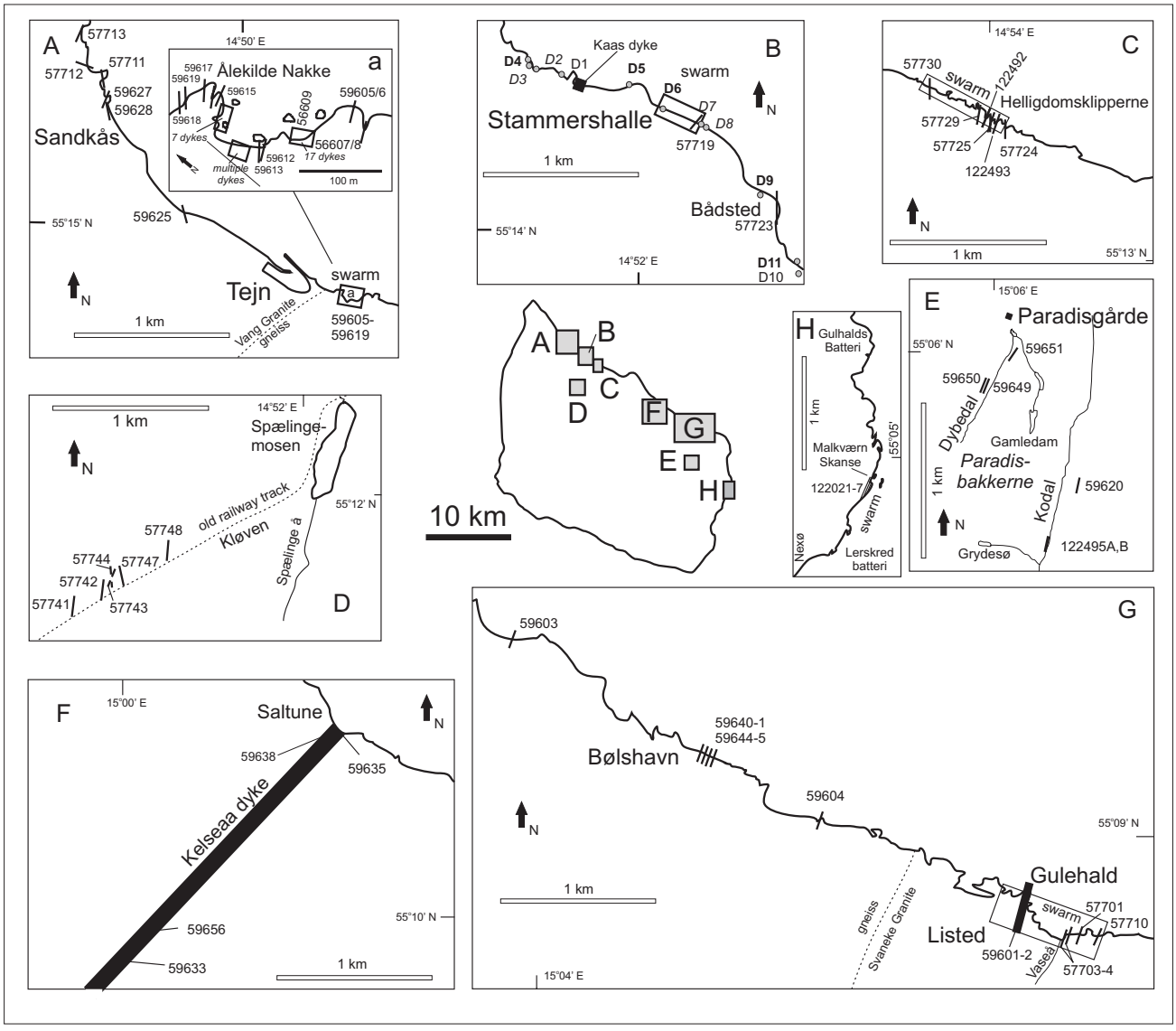

Figure 3: Location maps of the analyzed dyke samples. The positions of the detailed maps A-H are indicated in the central map of Bornholm. The inset (a) in (A) is an enlargement of the Tejn dyke swarm area. The locations of new samples and the dyke swarms as defined by Münther (1945a) are shown schematically. In B the approximate locations (marked D1, D2, etc.) of the samples used for palaeomagnetic age determination (Abrahamsen & Lewandowski, 1995) are shown. The Vang granite in (A) and Svaneke granite in (G) are two of the younger granites (see Fig. 1).

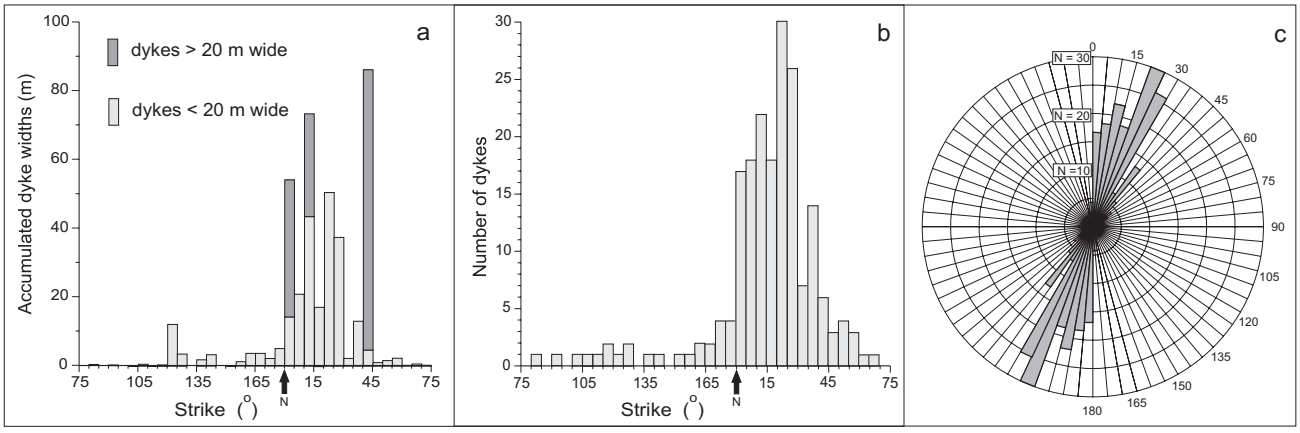

Figure 4: Distribution by orientation of the Bornholm dykes: (a) accumulated dyke widths per 5° strike intervals, (b) dyke frequency as a function of strike, and (c) Rose diagram of dyke frequency as a function of strike. NNE-striking dykes dominate in both number and width. Data from Münther (1945a).

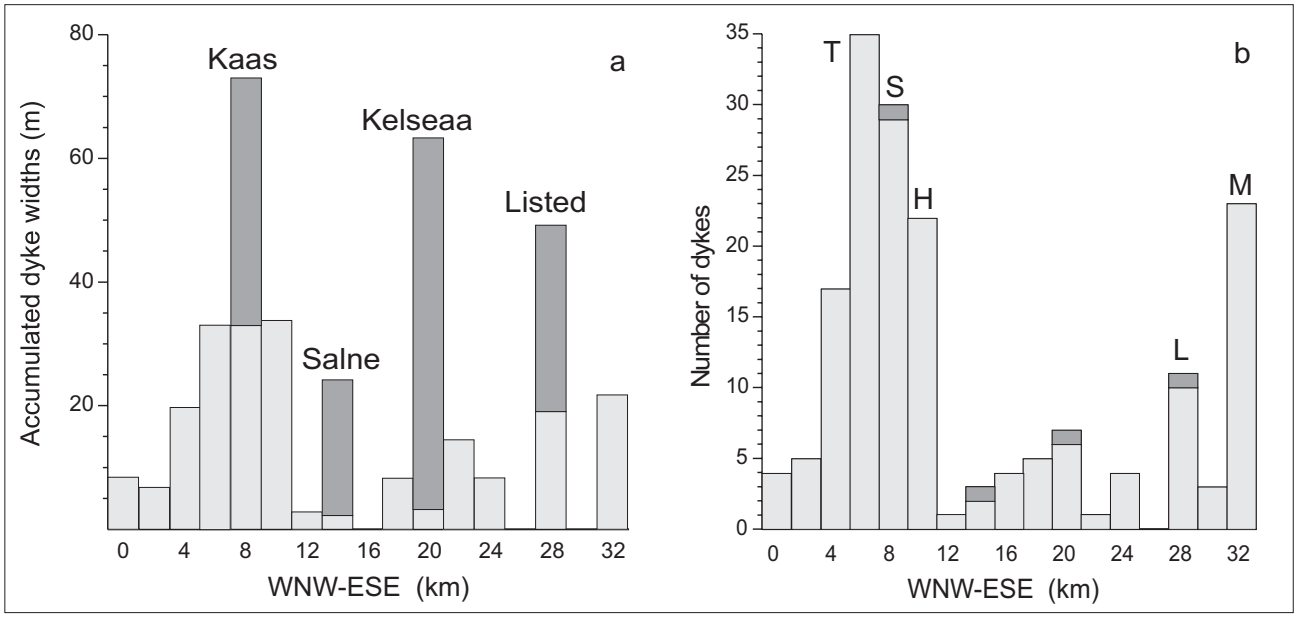

Figure 5: Distribution of the Bornholm dykes along a transect normal to the main orientation: (a) accumulated width per 2 km intervals and (b) frequency per 2 km intervals. Observations for the transect are mainly obtained along the north and east coasts of Bornholm with some contributions from inland locations and very few from the west coast. There is clearly an inhomogeneous distribution which led Münther (1945a) to define dyke swarms at (b): T – Tejn, S – Stammershalle, H – Helligdomsklipperne, L – Listed, and M – Malkværn Skanse. See text for discussion. The approximate locations of the four > 20 m wide dykes are shown with dark shading.

The four large dykes, Kelseaa, Kaas, Listed, and Salne, together make up a width of 152 m; the four dyke swarms have an accumulated width of 117 m; and 105 other individual dykes have a total width of 142 m wide according to the data of Münther (1945a, 1945b). This gives an absolute total dyke width of 411 m on Bornholm. We have analyzed 56 representative dykes with an aggregated width of 210 m out of the 411 m total. The dykes were sampled predominantly along the north coast of Bornholm but also at Kløven, Paradisbakkerne, along Kelse Å (Å = aa = stream) and along the east coast. Locations are shown in Fig. 3 and listed in Table 1.

On the basis of palaeomagnetic data Abrahamsen & Lewandowski (1995) concluded that Bornholm has remained in a fixed position relative to the Baltic Shield at least since the intrusion of the oldest dykes.

Table 1
Location and rock type of Bornholm dykes.

Sample	Area	Location	Width (m)	Strike	TAS field	Sub-field	CIPW norm ne, (q) (wt.%)
Kelseaa type (1)							
59633	Kelseaa	Kløvedal	60	40	basalt	medium-K ol tholeiite	0
59635	Kelseaa	Saltune	0.35	40	basalt	medium-K ol tholeiite	0
59656	Kelseaa	Hullegård	60	40	basalt	medium-K ol tholeiite	0
59638	Kelseaa	Saltune	-	-	basalt	ol tholeiite	0
57719	North coast	Stammershalle	1.7	42	basalt	ol tholeiite	0
Narrow dykes type (2)							
59644	North coast	Bølshavn	0.3	c. 20[1]	basalt	basaltic picrite	0
122022	East coast	Malkværn	3.1	25	basalt	basaltic picrite	0
59620	Paradisbakkkerne	Kodal	-	20	basalt	basaltic picrite	0
122025	East coast	Malkværn	0.7	25	basalt	alkali basalt	1
122023	East coast	Malkværn	0.35	25	basalt	alkali basalt	2
122021	East coast	Malkværn	0.6	25	basalt	alkali basalt	1
122026	East coast	Malkværn	0.4	25	basalt	ol tholeite	0
57751	Hammer granite	Sjælemose	0.4	12	basalt	medium-K ol tholeiite	0
122027	East coast	Malkværn	0.2	25	basalt	ol tholeite	0
122493	North coast	Helligdomsklipperne	0.5	10	basalt	medium-K ol tholeiite	0
122492	North coast	Helligdomsklipperne	2	20	basalt	medium-K ol tholeiite	0
57710	North coast	Vaseå	0.2	25	basalt	high-K ol tholeiite	0
57701	North coast	Vaseå	0.9	22	basalt	alkali basalt	5
59645	North coast	Bølshavn	2	c. 20[1]	basalt	alkali basalt	1
57748	Kløven	Old	0.7	4	basalt	alkali basalt	1
59618	North coast	Tejn	0.16	178	basalt	alkali basalt	3
59649	Paradisbakkkerne	Dybedal	0.35	24	basalt	alkali basalt	3
59612	North coast	Tejn	2.5	180	trachybasalt	hawaiite	2
59604	North coast	Helligkvinde	0.3	8	trachybasalt	hawaiite	6
59628	North coast	Storedal å	0.8	170	trachybasalt	hawaiite	2
59613	North coast	Tejn	0.3	22	trachybasalt	hawaiite	2
57724	North coast	Helligdomsklipperne	2	10	trachybasalt	hawaiite	0
59627	North coast	Sandkås	2	25	trachybasalt	potassic trachybasalt	1
59640	North coast	Bølshavn	0.7	c. 20[1]	trachybasalt	potassic trachybasalt	6
57711	North coast	Sandkås	0.65	170	trachybasalt	potassic trachybasalt	0
59650	Paradisbakkkerne	Dybedal	0.3	24	trachybasalt	potassic trachybasalt	5
59651	Paradisbakkkerne	Paradisgårde	0.4	34	trachybasalt	potassic trachybasalt	3
59619	North coast	Tejn	0.1	178	trachybasalt	potassic trachybasalt	2
59605	North coast	Tejn	0.4	14	trachybasalt	potassic trachybasalt	1
59606	North coast	Tejn	0.4	14	trachybasalt	potassic trachybasalt	0
59609	North coast	Tejn	2.5	22	trachybasalt	potassic trachybasalt	0
122495A	Paradisbakkkerne	Kodal	0.2	12	tephrite/basanite	basanite	1
57725	North coast	Helligdomsklipperne	2	20	tephrite/basanite	basanite	8
57729	North coast	Helligdomsklipperne	2	13	tephrite/basanite	basanite	6
59625	North coast	Sandkås	2.5	164	tephrite/basanite	basanite	4
122495B	Paradisbakkkerne	Kodal	0.1	12	tephrite/basanite	basanite	1
57741	Kløven		1.3	6	tephrite/basanite	basanite	4
57730	North coast	Helligdomsklipperne	1.2	13	phonotephrite	phonotephrite	5
57743	Kløven		0.65	178	phonotephrite	phonotephrite	3
57747	Kløven		0.5-3	169	phonotephrite	phonotephrite	4
Enriched narrow dykes type (2*)							
57703	North coast	Vaseå	0.7	22	basanite	potassic basanitic picrite	5
57704	North coast	Vaseå	0.3	22	basanite	potassic basanitic picrite	5
59607	North coast	Tejn	2	22	trachybasalt	potassic trachybasalt	6
59608	North coast	Tejn	2	22	trachybasalt	potassic trachybasalt	4
59615	North coast	Tejn	1	23	trachybasalt	potassic trachybasalt	5
59617	North coast	Tejn	0.1	24	trachybasalt	potassic trachybasalt	5
Kaas dyke type (3)							
57714	North coast	Kaas dyke	40	158	basaltic trachyandesite	shoshonite	(6)
57715	North coast	Kaas dyke	40	160	basaltic trachyandesite	mugearite	(1)
57750	North coast	Kaas	32	c. 160[1]	trachbasalt	potassic trachybasalt	(2)
57713	North coast	Sandkås	-	24	trachbasalt	potassic trachybasalt	(2)
57742	Kløven		0.8	20	basaltic trachyandesite	shoshonite	(3)
57744	Kløven		0.8	178	basaltic trachyandesite	shoshonite	(7)
Listed dyke (3)							
59601	North coast	Gulehald, Listed	30	14	basaltic trachyandesite	mugearite	(5)
59602	North coast	Gulehald, Listed	30	14	basaltic trachyandesite	mugearite	(4)
NW trending dyke (4)							
57712	North coast	Sandkås	1	110	basalt	medium-K quartz tholeiite	(5)

Footnote:
-) unknown due to insufficient outcrop
1) estimated strike due to insufficient outcrop

Age relations of the dykes and their relations to southern Sweden

Traditionally, the dykes have been considered to be related to major Proterozoic dyke swarms in southern Sweden (Berthelsen, 1989), e.g. the Central Scandinavian Dolerite Group (CSDG) and the Blekinge Dalarne Dolerite Group (BDDG) (e.g. Gorbatschev et al., 1979; Solyom et. al., 1992; Patchett et al., 1994).

Although the geochronology of the Bornholm dykes is poorly constrained, geological relations and palaeomagnetic and isotopic dating allow some inferences to be made. Some of the dykes, both large (Kelseaa and Listed) and small, cut the younger granites (Fig. 1), whereas the dykes in Paradisbakkerne cut the Paradisbakkerne migmatite. Most of the dykes are intruded into grey gneisses. The Listed dyke is cut by what has been referred to as 'sandstone dykes', which are sand-filled fractures in the basement rocks. The sandstone in these fractures is related to the Early Cambrian Nexø sandstone, the earliest preserved sedimentary deposit on Bornholm (Bruun-Petersen, 1975; Lewandowsky & Abrahamsen, 2003).

An U-Pb age of 1326 ±10 Ma (2σ) was obtained on baddeleyite from the Kelseaa dyke (Holm et al., 2005) in accordance with a previously published, less precise, estimate based on palaeomagnetic data (Abrahamsen, 1977). Further palaeomagnetic investigations of a suite of dykes from primarily two areas on Bornholm (Stammershalle and Listed), revealed that narrow NNW- to NNE-trending dykes were intruded around 1220 Ma, whereas the Kaas and Listed dykes were emplaced at c. 950 Ma with a possibility that the Listed dyke cooled at c. 700 - 800 Ma (Abrahamsen, 1977; Abrahamsen & Lewandowski, 1995). This links most of the dyke intrusions with two important igneous units in Sweden, the Protogine Zone Dolerite Group (PZDG, 1215-1221 Ma) and the Blekinge Dalarne Dolerite Group (BDDG, 100-870 Ma), respectively. A few dykes that trend WNW to NW seem to be of Permian age (Abrahamsen & Lewandowski, 1995). These have been described by Jensen (1988) and Obst (2000), who also consider them to be related to Permian dykes in Scania, southern Sweden (Fig. 1). Bornholm is situated along strike from the Scania dykes and their correlation seems straightforward.

Palaeomagentic and U-Pb results from Bornholm (Abrahamsen, 1977; Abrahamsen & Lewandowski, 1995; Holm et al. 2005) suggest at least four episodes of dyke injection: 1326 Ma (Kelseaa), c. 1220 Ma (some narrow dykes), c. 950 Ma (Kaas, and possibly Listed), and around 300 Ma (WNW- to NW-trending dykes). The fault pattern on Bornholm further suggests at least four episodes of horizontal movement (Münther, 1945a, 1945b) during which dyke emplacement could have occurred. As shown below, the geochemistry of the dykes may likewise be assigned to a number of discrete episodes of mafic magmatism, each with their own distinct character.

Three episodes of dyke emplacement have been recognized in southern Sweden (Fig. 1). The PZDG occurs in a 20 km-wide tectonic belt that extends N and NNE from southern Sweden into the central part of Scania (Klingspor, 1976). The age range of these dykes has been recently demonstrated by U-Pb analysis of baddeleyite to be 1215-1221 Ma (Söderlund et al., 2005). The BDDG extends over an area 700 km long and 150 km wide east of and parallel to the Protogine Zone and trend NNE north of Bornholm (Fig. 1). The intrusion age interval is indicated to be 1000 – 870 Ma (Patchett, 1978), and perhaps close to 930 Ma (Johansson & Johansson, 1990). The Permo-Carboniferous WNW- to NW-trending Scania dykes are widely distributed in the basement of central Scania (Klingspor, 1976). Dykes from a fourth mafic intrusive event that took place at 1270-1250 Ma are present in mid Sweden and western Finland, around 600 km to the north of Bornholm; this is the Central Scandinavian Dolerite Group (CSDG) (Söderlund et al., 2006).

Petrography

The petrographic descriptions below are based on our study of new samples combined with the detailed descriptions of some of the dykes mentioned by Callisen (1934) and Jensen (1966).

Petrographically we can divide the dykes into four main types: 1) Kelseaa type, 2) narrow dykes, 3) large dykes at Kaas and Listed, and 4) WNW- to NW-trending dykes (in the following referred to simply as the NW dykes). The relatively unaltered state of the Bornholm dykes in general is demonstrated by the common occurrence of well-preserved primary igneous minerals such as olivine and clinopyroxene.

Kelseaa

The Kelseaa dyke is a remarkably fresh, grey, massive rock (Fig. 6). The grain size varies from fine to medium and the texture is ophitic near the contact and coarsely gabbroic in the centre. Plagioclase, olivine (Fo_{60}), and augite are the main constituents with accessory amounts of Ti-magnetite, apatite, hypersthene, green uralitic amphibole, biotite, microcline, and quartz. Plagioclase in the centre of the dyke is zoned from labradorite (An_{70}) to oligoclase (An_{20}). Bytownite (An_{83}) and hypersthene occur near the contact. In the centre

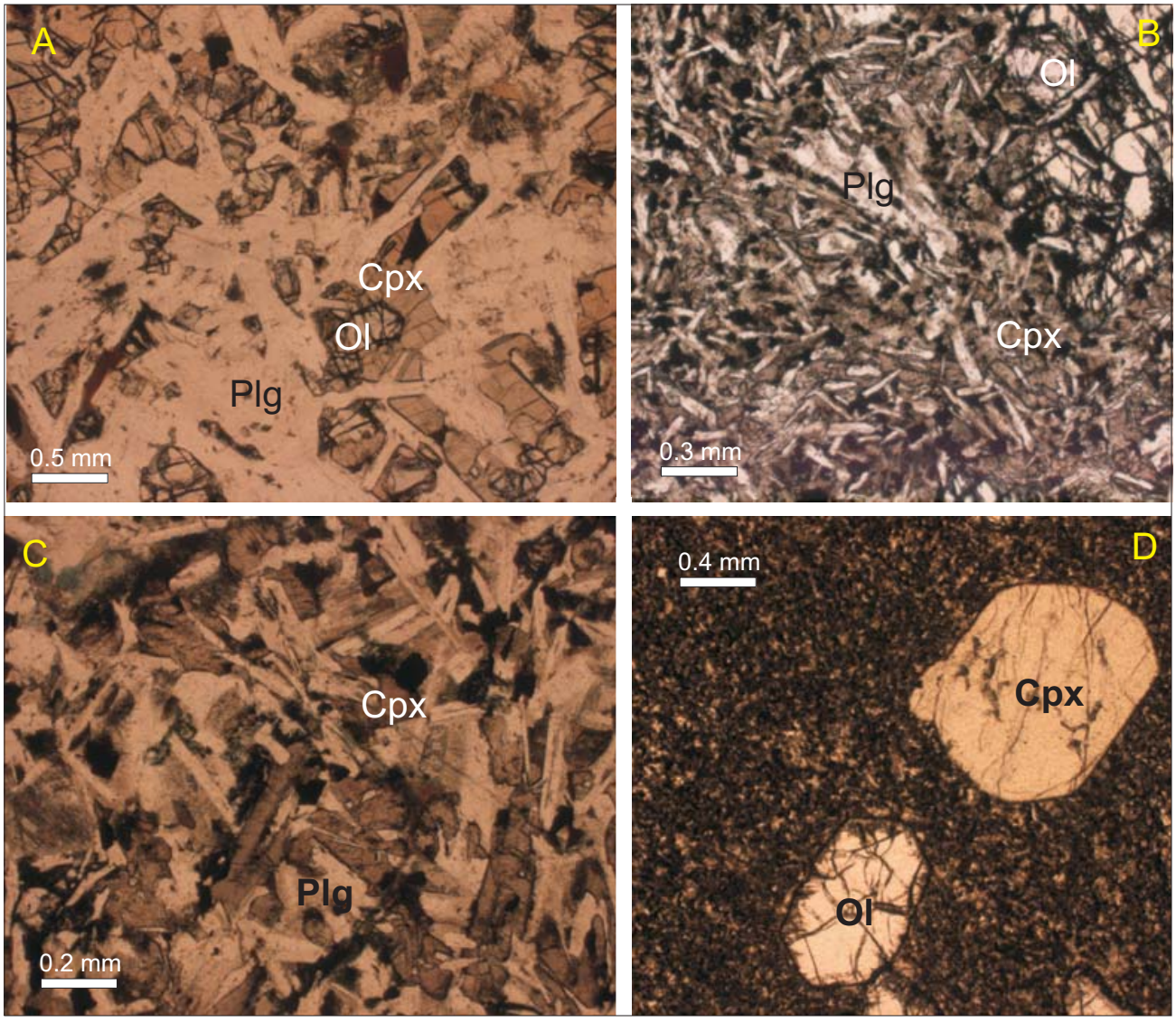

Figure 6: Photomicrographs (plane polarized light) of mafic dykes from Bornholm. A) the tholeiitic Kelseaa dyke (type 1) sample 59635: B-D alkaline dykes: B) narrow dyke 57751 (Type 2), C) narrow dyke 59605 (Type 2), D) enriched narrow dyke 59617 (Type 2*). Examples of minerals are indicated: ol – olivine, cpx – clinopyroxene, plg – plagioclase. See Tables 1 & 2 and text for details. Groups 3 and 4 are illustrated by Callisen (1934) and Jensen (1966).

small patches of fine grained microcline, oxides, and quartz occur interstitally between plagioclase laths, and are probably fractionation products. Small amounts of serpentine, chlorite, epidote and calcite are present as alteration products.

The narrow dykes

The narrow dykes are all fine grained; some are porphyritic and some are aphyric. The porphyritic samples all have less than 5 vol% phenocrysts. Two different phenocryst assemblages are present: (1) olivine (or pseudomorphs after olivine) and/or clinopyroxene (Fig. 6), or (2) olivine (or pseudomorphs) and plagioclase. The groundmass in the narrow dykes consists mainly of plagioclase, clinopyroxene and Fe-Ti oxide.

The Kaas-Listed dykes

The petrography of these evolved large dykes (Jensen, 1966) is quite similar to the Kelseaa dyke, but they do not have the coarse grained gabbroic central part. They have ophitic textures and are composed mainly of plagioclase, augite and olivine. The plagioclase is zoned from labradorite to oligoclase. Minor constituents are Fe-Ti oxides, biotite, quartz, and brown hornblende. Graphic intergrowths of quartz and feldspar

in the rims of plagioclase laths are common in the centre of the Kaas dyke. Augite is absent near the contact of this dyke, whereas in the Listed dyke olivine is absent near the contact.

The Listed dyke has a 3-4 m wide zone near the contact containing numerous elliptical plagioclase crystals or crystal aggregates. The presence of these plagioclase ovoids has been interpreted as resulting from the assimilation of country rock (Callisen, 1934; Jensen, 1966). However, as the large feldspar crystals in the wall rock are alkali feldspar, the plagioclase ovoids, if xenocrystic, must originate from a different rock type located deeper in the crust (Berthelsen, 1989). The zone of ovoids terminates abruptly towards the center of the dyke, implying that multiple intrusion has occurred.

NW-trending dykes

These relatively few basaltic dykes are plagioclase and clinopyroxene phyric, sometimes including small amounts of olivine. Phenocrysts often show resorption. Obst (2000) has described a 12 m-wide dolerite dyke that can be traced for over 3 km from Lindesdal. A trachytic dyke with the same trend is included in this group (Obst, 2000), and this dyke was suggested to be closely related to the so-called kullaites in NW Scania (Jensen, 1988).

Analytical methods

Sixty samples have been analyzed for major and trace elements by XRF. Major element analyses were acquired at the Geological Survey of Denmark and Greenland (GEUS) in Copenhagen. Analyses were made on glass discs prepared with sodium borate, except for Na_2O and MgO (atomic absorption), FeO (titration) and volatiles (calculated from loss on ignition).

Trace elements were determined by XRF (Rb, Ba, Sr, La, Ce, Nd, Y, Th, Zr, Nb, Zn, Cu, Co, Ni, Sc, V, Cr, and Ga) and 26 samples were additionally analyzed by INAA (La, Ce, Nd, Sm, Eu, Tb, Yb, Lu, U, Th, Ta, and Hf) by R. Gwozdz (Tracechem, Copenhagen), and 7 samples by ICP-MS (Sc, V, Cr, Co, Ni, Cu, Zn, Ga, Rb, Sr, Y, Zr, Nb, REEs, Hf, Ta, and Th) at Actlabs ©. The data is presented in Table 2. The major elements have been recalculated to 100 % on a volatile free basis. Analytical details are given in the appendix.

Geochemistry

Introduction

The mafic dykes on Bornholm are classified according to the IUGS classification using total alkali-silica (TAS) (Le Maitre et al., 1989; Le Bas, 2000). The rock classification (Fig. 7) is further detailed in Table 1. The majority of them range from basalts through alkali basalts (nepheline normative, Table 1) and trachybasalts to basanites. Potassic types dominate and most are nepheline CIPW normative, but sodic rocks (hawaiites) do occur, and three picrites are reported (Table 1). The compositions extend to very evolved types with a total range of MgO = 14.2 - 2.1 wt. % (Fig. 8). All major element analyses are in wt. % and will be expressed below as %. A total of 42 of the analyzed dykes are rather primitive with MgO > 5.8 %, and of these 30 have Mg# = 60 – 74 (Mg# = $Mg/(Mg+Fe^{2+})$ (atoms/atoms), Mg# calculated assuming $FeO/FeO^{total} = 0.8$ (Middlemost, 1989)), > 130 ppm Ni and > 225 ppm Cr (Figs. 8 & 9, Table 2). Silica concentrations for these rocks are 44 - 50 %. Fifteen of the dykes are more evolved with MgO = 2.1 – 5.5 %, and silica reaching 57 %. The relatively primitive nature of most of the dykes is in marked contrast to the distribution of compositions of the Swedish Proterozoic dykes which are generally quite evolved with just a small fraction exceeding 8 % MgO (Solyom et al., 1992).

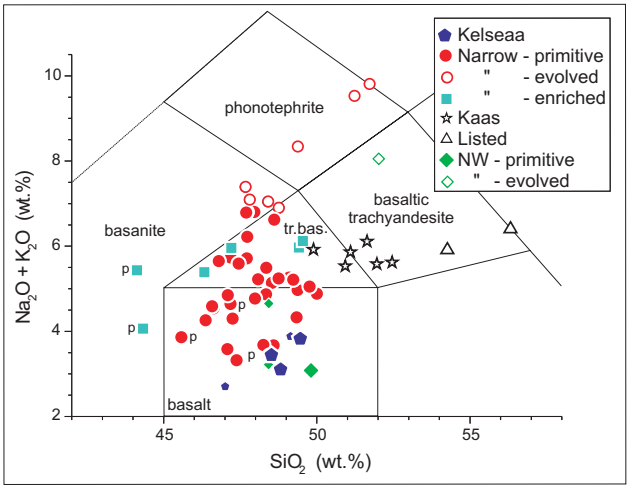

Figure 7: $Na_2O + K_2O$ vs. SiO_2 (TAS diagram) for the Bornholm dykes with the IUGS classification according to Le Maitre (1989) and Le Bas (2000); tr. bas. – trachybasalt. Filled symbols: rocks with MgO > 5.8 %, open symbols: evolved rocks (MgO < 5.8 %), small diamonds (3): NW-trending dykes from Jensen (1988) and Obst (2000); small hexagons (2): Kelseaa dolerite-like dykes; picrite samples are denoted by "p"; NW in legend: NW- to WNW-trending dykes. Rocks are further characterized in Table 1, and analytical data listed in Table 2.

Table 2
Geochemical compostion of Bornholm dykes

Sample id	59633	59635	59656	59638	57719	59644	122022	59620	122025	122023	122021	122026	57751	122027	122493	122492	57710
Location	Kelseaa	Kelseaa	Kelseaa	Cuts Kelseaa	Stammershl	Bølshavn	Malkværn	Paradisbk	Malkværn	Malkværn	Malkværn	Malkværn	Sjælemose	Malkværn	Helligdom	Helligdom	Vaseå
Type	1	1	1	1	1	2	2	2	2	2	2	2	2	2	2	2	2
Major elements (wt.%)																	
SiO_2	49.46	48.82	48.52	47.27	47.01	47.18	45.58	48.46	46.37	46.58	46.63	47.08	49.14	47.38	48.25	48.59	49.34
TiO_2	0.91	0.46	0.88	1.28	1.00	1.67	1.28	1.31	1.72	1.72	2.00	1.84	1.23	1.64	1.42	1.38	1.51
Al_2O_3	15.83	18.93	15.66	12.22	16.47	13.20	13.51	12.52	14.00	14.60	14.65	13.57	15.19	14.12	13.34	13.42	13.02
FeO^{total}	10.87	8.56	11.63	15.45	12.71	11.79	10.99	12.29	10.77	11.41	11.36	11.64	10.90	12.06	11.61	11.75	11.27
MnO	0.18	0.13	0.18	0.24	0.24	0.20	0.16	0.22	0.17	0.23	0.30	0.25	0.16	0.33	0.21	0.30	0.23
MgO	8.60	9.21	9.94	12.00	7.94	12.64	14.24	12.74	11.61	11.00	9.71	11.33	9.83	10.55	11.38	10.66	10.75
CaO	9.81	10.51	9.24	7.40	11.44	7.66	7.86	8.51	8.18	7.86	7.67	8.13	9.15	7.51	8.67	8.77	9.13
Na_2O	2.65	2.32	2.37	2.15	2.25	2.37	2.16	2.42	2.63	2.85	2.94	2.31	3.00	2.36	2.64	2.60	2.66
K_2O	1.17	0.78	1.06	1.25	0.45	2.26	1.70	1.01	1.63	1.75	1.60	1.27	0.88	0.95	1.04	1.07	1.66
P_2O_5	0.18	0.07	0.14	0.18	0.10	0.29	0.28	0.18	0.31	0.34	0.30	0.20	0.19	0.16	0.16	0.16	0.20
sum	100.00	100.00	100.00	100.00	100.00	100.00	98.98	100.00	98.58	99.60	98.44	98.90	100.00	98.41	100.00	100.00	100.00
volatiles	2.52	1.24	2.38	3.38	5.43	4.18	4.12	3.99	3.50	3.79	3.97	3.40	3.06	3.43	2.34	2.89	3.21
Fe^{2+}/Fe^{total}	0.72	0.78	0.72	0.68	0.72	0.44		0.75					0.73				0.82
Mg# (Fe^{2+}/Fe^{total} = 0.8)	64	71	66	63	58	70	74	70	71	68	66	68	67	66	69	67	68
Trace elements (ppm)																	
Sc	27	16	*28*	28	*24*	19	*22*	18	*23*	*22*	*23*	*23*	21	*22*	21	20	25
V	214	126	*179*	324	*246*	189	*152*	174	*194*	*195*	*205*	*211*	179	*217*	202	199	202
Cr	390	409	*314*	228	*364*	451	*699*	526	*674*	*520*	*531*	*632*	474	*570*	466	471	859
Co	67	76	*70*	90	*77*	74	*72*	86	*73*	*65*	*64*	*71*	65	*68*	65	67	73
Ni	259	310	*243*	430	*313*	393	*386*	480	*342*	*270*	*261*	*342*	257	*342*	357	384	267
Cu	114	109	*114*	117	*177*	177	*52*	76	*62*	*42*	*52*	*62*	59	*62*	66	63	59
Zn	84	59	*55*	101	*126*	134	*104*	117	*207*	*125*	*115*	*197*	78	*124*	108	109	125
Ga	20	15	*17*	19	*19*	20	*17*	16	*22*	*20*	*21*	*19*	19	*20*	19	19	19
Rb	50	33	*48*	60	*27*	172	47	64	58	52	51	42	37	34	69	73	124
Sr	145	148	*119*	111	*143*	142	561	385	595	635	604	423	464	359	397	389	426
Y	38.9	18.2	*32.2*	40	*29*	17	*9.39*	17.8	*15.55*	*11.44*	*16.67*	*14.5*	18.6	*12.43*	16.2	15.9	26.9
Zr	126	66	*103*	130	*91*	44	*117*	81	*138*	*148*	*134*	*96*	91	*106*	81	79	105
Nb	6.6	3.5	*4.0*	6.3	*0.6*	26.0	*15.7*	13.6	*18.7*	*18.7*	*19.8*	*14.5*	10.4	*10.4*	12.8	13.1	17.6
Ba	351	225	*370*	338	*71*	651	629	286	510	556	580	349	262	351	322	368	348
La	13.3	9.1	*10.10*	14.5	*1.47*	22.9	*21.1*	11.5	*25.3*	*25.5*	*26.0*	*13.3*	11.4	*10.7*	11.8	10.9	20.7
Ce	30.7	14.1	*20.80*	29.9	*3.47*	45.8	*43.9*	19.9	*52.8*	*53.8*	*54.6*	*29.5*	31.1	*24.3*	28.8	28.9	41.3
Nd	16.4	8.1	*11.40*	16.5	*3.81*	29.2	*19.0*	13.6	*22.7*	*23.1*	*23.8*	*15.5*	18.6	*14.3*	16.2	16.4	22.7
Sm	3.79	1.97	*3.09*		*1.87*		*3.86*	3.18	*4.87*	*4.78*	*5.21*	*3.83*	3.37	*3.63*			4.11
Eu	1.26	0.67	*1.04*		*0.83*		*1.31*	1.08	*1.60*	*1.58*	*1.77*	*1.35*	1.23	*1.24*			1.40
Tb	1.06	0.43	*0.75*		*0.48*		*0.52*	0.53	*0.62*	*0.62*	*0.73*	*0.62*	0.58	*0.52*			0.79
Yb	2.64	1.60	*2.53*		*1.19*		*0.94*	1.39	*1.35*	*1.25*	*1.35*	*1.35*	1.53	*1.45*			1.75
Lu	0.30	0.19	*0.37*		*0.18*		*0.17*	0.17	*0.19*	*0.17*	*0.20*	*0.19*	0.19	*0.20*			0.22
Hf	3.12	1.58	*2.39*		*1.31*		*3.23*	2.10	*3.84*	*4.05*	*3.75*	*2.80*	2.12	*3.42*			2.57
Ta	0.38	0.29	*0.39*		*0.06*		*1.04*	0.71	*1.24*	*1.35*	*1.35*	*0.93*	0.59	*0.73*			1.01
Th	2.7	2.0	*2.0*	2	*0.04*	1	*1.3*	1.0	*1.5*	*1.6*	*1.6*	*0.9*	1.2	*0.8*	1	1	2.4

Analytical method for trace elements: Normal font - XRF, italics - ICPMS, underlined - INAA. 1) T.E. Waight (pers. comm.) BH3A: North Coast, 50 m E of Kelseaa dyke, BH22: Dalegård Quarry, Olsker.

Table 2. Continued

Sample id	57701	59645	57748	59618	59649	59612	59604	59628	59613	57724	59627	59640	57711	59650	59651	59619	59605	59606
Location	Vaseå	Bølshavn	Kløven	Tejn	Paradisbk	Tejn	Helligkvinde	Sandkås	Tejn	Helligdom	Sandkås	Bølshavn	Sandkås	Paradisbk	Paradisbk	Tejn	Tejn	Tejn
Type	2	2	2	2	2	2	2	2	2	2	2	2	2	2	2	2	2	2
SiO_2	47.09	47.25	47.98	48.34	49.23	46.80	47.45	47.71	48.53	48.76	47.19	47.73	48.08	48.35	48.75	49.09	49.37	49.76
TiO_2	1.95	1.72	1.90	1.62	1.87	1.93	2.19	2.55	1.83	2.82	2.18	2.08	2.33	2.04	2.15	1.68	1.91	1.95
Al_2O_3	13.37	13.43	16.72	13.55	14.80	16.25	16.44	16.27	15.91	18.90	15.56	15.97	16.78	13.87	14.43	14.27	15.10	15.38
FeO^{total}	11.72	12.03	11.84	11.18	11.12	15.01	15.17	12.64	11.50	13.92	14.89	12.05	12.50	11.75	11.54	11.23	11.01	11.13
MnO	0.17	0.19	0.26	0.26	0.15	0.18	0.35	0.19	0.15	0.19	0.47	0.30	0.18	0.16	0.16	0.47	0.16	0.17
MgO	10.42	11.87	7.77	10.38	7.84	6.12	5.64	6.10	8.76	5.06	8.17	7.14	8.32	8.87	8.12	9.08	7.80	6.81
CaO	9.79	8.50	8.24	9.23	9.20	7.19	7.03	8.06	7.60	2.80	5.53	7.83	6.03	8.92	9.00	8.32	9.04	9.09
Na_2O	2.78	2.56	3.16	3.08	3.58	3.74	3.80	3.57	3.72	4.94	3.66	3.68	3.37	3.43	3.48	3.30	3.37	3.42
K_2O	2.07	1.73	1.61	1.79	1.62	1.91	1.79	2.15	1.42	1.95	2.07	2.54	1.86	2.06	1.76	1.96	1.60	1.63
P_2O_5	0.28	0.31	0.25	0.26	0.26	0.33	0.31	0.38	0.30	0.42	0.35	0.35	0.33	0.30	0.30	0.29	0.34	0.35
sum	100.00	100.00	99.99	100.00	100.00	100.00	100.00	100.00	100.00	100.00	100.00	100.00	100.00	100.00	100.00	100.00	100.00	100.00
volatiles	3.33	5.54	6.93	3.17	2.32	6.46	4.94	8.07	2.93	4.83	5.17	6.78	6.44	3.17	3.01	3.32	2.86	3.15
Fe^{2+}/Fe^{total}	0.72	0.70	0.80	0.75	0.74	0.66		0.72	0.80	0.84		0.75	0.84	0.81	0.74	0.75	0.75	0.75
Mg#	66	69	59	67	61	48	45	52	63	45	55	57	60	63	61	64	61	58
Sc	19	18	25	19	15	29	23	21	13	18	18	21	20	15	16	20	20	19
V	195	200	183	190	193	245	293	213	124	119	153	239	175	190	201	202	177	184
Cr	455	477	277	504	319	529	113	353	292	13	234	370	364	394	358	480	302	307
Co	66	72	61	70	56	68	62	58	71	55	76	54	68	69	60	70	61	63
Ni	270	361	161	309	150	220	59	234	186	44	178	145	185	228	185	269	184	186
Cu	71	10	42	66	57	60	45	51	35	21	31	58	37	59	58	61	51	58
Zn	82	148	103	111	105	140	129	129	78	218	133	172	152	106	110	137	89	101
Ga	20	21	18	22	22	24	24	25	22	24	24	25	22	25	24	21	21	24
Rb	63	100	95	52	53	57	55	83	31	59	67	151	85	77	86	61	34	35
Sr	619	533	569	599	604	645	553	596	732	603	731	561	666	645	662	603	569	575
Y	20.7	20.2	21.6	20.7	21.5	31.2	25.4	28	16.5	35.8	17.9	33.4	23.7	21.8	20.6	23.9	23.8	25.9
Zr	116	115	122	116	124	129	123	174	143	201	176	151	168	133	133	124	155	162
Nb	24.8	25.5	14.0	22.8	22.5	26.9	28.5	26.0	19.6	31.6	23.2	33.4	20.4	24.9	25.8	23.9	24.8	24.9
Ba	524	560	394	522	476	577	595	548	500	606	647	801	434	508	514	568	511	524
La	20.7	24.5	15.1	21.8	20.5	23.7	25.4	27.0	19.6	25.2	28.4	31.3	22.6	21.8	22.7	23.9	22.7	23.8
Ce	40.3	47.9	34.5	46.7	42.0	52.8	47.5	52.0	43.3	57.9	58.9	62.6	45.2	44.6	47.5	46.7	44.4	50.8
Nd	24.8	27.7	22.6	27.0	23.6	28.0	27.5	35.0	26.8	32.6	33.7	34.5	26.9	25.9	26.8	28.0	25.8	28.0
Sm	4.79	4.49		4.58		4.97	4.83		4.40		5.53		5.03	4.99	5.22			5.30
Eu	1.67	1.60		1.52		1.60	1.69		1.53		1.85		1.94	1.63	1.66			1.71
Tb	0.61	0.65		0.62		0.79	0.69		0.70		0.71		0.84	0.72	0.75			0.80
Yb	1.30	1.00		1.49		2.33	1.53		1.24		1.32		1.48	1.59	1.45			1.93
Lu	0.17	0.14		0.20		0.25	0.18		0.15		0.16		0.20	0.18	0.19			0.27
Hf	2.86	2.63		2.90		3.12	2.76		3.48		4.23		3.68	3.40	3.39			4.04
Ta	1.45	1.58		1.16		1.43	1.59		1.09		1.18		1.11	1.38	1.44			1.28
Th	2.5	1.9	1	2.1	3	2.0	1.9	3	1.1	1	1.4	1	1.3	2.1	2.2	1	1	2.0

Table 2. Continued

Sample id	59609	122495A	57725	57729	59625	122495B	57741	57730	57743	57747	57703	57704	59607	59608	59615	59617	57714	57715
Location	Tejn	Paradisbk	Helligdom	Helligdom	Sandkås	Paradisbk	Kløven	Helligdom	Kløven	Kløven	Vaseå	Vaseå	Tejn	Tejn	Tejn	Tejn	Kaas dyke	Kaas dyke
Type	2	2	2	2	2	2	2	2	2	2	2*	2*	2*	2*	2*	2*	3	3
SiO_2	50.00	47.67	47.69	47.81	47.96	48.41	48.61	49.38	51.23	51.72	44.33	44.13	46.33	47.21	49.41	49.55	51.64	51.10
TiO_2	1.76	2.70	2.41	2.53	2.30	2.71	2.39	2.92	1.65	1.60	2.50	2.40	2.44	2.56	1.99	2.04	3.96	3.04
Al_2O_3	14.25	18.23	16.35	17.09	16.38	18.19	16.58	17.67	18.07	18.40	12.37	12.18	13.10	14.57	12.34	12.64	16.35	15.72
FeO^{total}	11.41	13.08	11.78	12.43	12.01	12.84	12.15	12.79	11.72	11.43	12.87	12.70	12.96	13.07	10.67	10.62	12.03	11.80
MnO	0.14	0.19	0.16	0.17	0.15	0.23	0.22	0.19	0.18	0.27	0.18	0.21	0.17	0.15	0.17	0.17	0.08	0.14
MgO	8.11	4.76	6.99	4.73	7.05	4.54	6.11	3.88	2.24	2.09	13.36	13.92	9.57	7.09	10.22	9.41	2.93	5.40
CaO	8.73	4.11	7.11	6.70	6.49	4.16	6.37	3.93	3.67	2.98	9.72	8.46	9.15	8.45	8.56	8.74	5.45	5.95
Na_2O	3.45	4.09	4.25	4.83	3.99	4.72	4.40	4.85	4.88	5.58	1.68	1.12	3.20	3.58	3.41	3.42	3.79	3.97
K_2O	1.43	3.30	2.54	2.25	2.81	2.33	2.22	3.49	4.65	4.23	2.38	4.31	2.19	2.38	2.55	2.70	2.32	1.89
P_2O_5	0.25	0.42	0.46	1.15	0.59	0.43	0.59	0.55	1.18	1.22	0.30	0.30	0.42	0.46	0.43	0.44	0.96	0.67
sum	100.00	100.00	100.00	100.00	100.00	100.00	100.00	100.00	100.00	100.00	100.00	100.00	100.00	100.00	100.00	100.00	100.00	100.00
volatiles	3.52	2.19	5.26	4.03	4.42	2.89	4.15	2.45	2.59	2.13	4.86	4.19	3.51	3.15	2.78	2.47	1.98	2.51
Fe^{2+}/Fe^{total}	0.63		0.80	0.78	0.80		0.74	0.76	0.59	0.63	0.78	0.80	0.67	0.67	0.80	0.78	0.62	0.76
Mg#	61	45	57	46	57	44	53	40	30	29	70	71	62	55	68	66	35	50
Sc	16	16	18	16	18	17	14	9	8	7	19	18	16	16	16	17	27	16
V	208	127	138	89	141	108	121	65	8	7	256	243	192	219	162	174	209	167
Cr	444	9	225	90	239	7	167	7	4	1	481	525	339	328	410	395	39	155
Co	73	54	53	44	51	51	54	49	30	29	78	81	71	66	63	60	54	69
Ni	336	38	130	67	147	36	114	23	8	6	389	417	255	204	296	269	41	88
Cu	64	32	36	42	50	29	40	28	27	20	61	66	63	63	51	67	17	30
Zn	112	155	80	125	103	142	145	99	138	136	111	119	102	163	114	115	180	121
Ga	23	23	22	23	23	23	22	22	29	28	20	21	24	27	20	21	26	23
Rb	36	81	78	50	78	64	88	120	131	110	228	429	65	58	63	64	39	56
Sr	590	599	814	887	727	701	864	914	531	493	519	384	907	915	753	791	564	600
Y	17	32.8	21.2	27.1	20	24.2	18.9	30.9	36.1	34.9	20	20.9	21.9	20	25.8	25.8	44.9	32.8
Zr	106	185	209	200	186	190	214	240	394	401	122	122	149	146	182	183	332	241
Nb	21.0	29.1	29.6	34.5	29.0	29.9	32.6	36.0	58.8	60.5	32.6	32.3	39.6	42.0	40.2	41.3	20.4	19.5
Ba	443	582	637	731	710	747	909	830	1609	1406	700	655	868	1020	765	813	761	673
La	18.0	26.3	29.6	39.7	32.0	27.6	33.6	39.1	61.9	61.6	20.0	22.9	29.1	31.0	37.1	35.1	35.7	28.7
Ce	42.0	62.9	68.8	87.7	67.0	62.8	75.6	82.3	138.2	130.3	43.1	45.9	60.4	64.0	65.0	66.1	86.7	67.7
Nd	22.0	34.1	36.0	49.1	35.0	34.7	39.9	46.3	72.2	70.8	26.3	25.0	33.3	36.0	35.1	37.2	56.1	40.0
Sm								7.09	11.80	10.70	4.82		6.19		6.56		9.90	7.53
Eu								2.36	2.91	2.84	1.79		2.05		2.05		3.15	2.55
Tb								0.90	1.35	1.30	0.78		1.02		1.03		1.55	1.23
Yb								1.81	2.50	2.32	0.94		1.02		1.85		2.86	2.17
Lu								0.21	0.35	0.29	0.13		0.14		0.23		0.36	0.28
Hf								4.90	8.26	7.71	3.00		3.44		4.17		7.98	5.44
Ta								2.09	3.20	3.39	2.04		2.20		2.49		1.04	1.32
Th	2	1	1	1	2	2	1	2.2	2.6	3.2	2.2	1	2.5	4	4.3	1	1.9	2.1

Table 2. Continued

Sample id	57750	57713	57742	57744	59601	59602	57712	BH3A[1]	BH22[1]
Location	Kaas	Sandkås	Kløven	Kløven	Listed dyke	Listed dyke	Sandkås	Gneiss	Granite
Type	3	3	3	3	3	3	4	Basement	Basement
SiO_2	49.89	50.93	51.96	52.46	56.32	54.26	49.81	73.08	73.81
TiO_2	3.80	3.64	3.50	3.58	2.19	2.31	3.23	0.44	0.34
Al_2O_3	16.36	15.31	14.68	14.88	15.81	16.74	13.46	13.27	13.06
FeO^{total}	13.07	12.51	12.58	12.47	9.19	9.62	13.71	2.45	1.82
MnO	0.12	0.15	0.16	0.16	0.21	0.15	0.22	0.06	0.04
MgO	3.23	4.29	4.06	3.85	3.57	3.85	6.01	0.46	0.26
CaO	6.19	6.51	6.36	5.57	5.63	6.45	9.73	1.37	1.23
Na_2O	3.95	3.71	3.50	3.66	4.25	3.98	2.34	2.86	3.16
K_2O	1.97	1.82	2.08	1.96	2.15	1.93	0.74	5.38	5.36
P_2O_5	0.90	0.84	0.87	0.88	0.46	0.44	0.33	0.13	0.07
sum	100.00	100.00	100.00	100.00	100.00	100.00	100.00	99.50	99.15
volatiles	2.87	2.22	1.80	1.57	1.31	1.74	2.31	3.00	4.00
Fe^{2+}/Fe^{total}	0.63	0.78	0.82	0.62	0.78	0.74	0.73	-	-
Mg#	35	43	42	41	46	47	49	7	4
Sc	25	21	18	21	22	21	29	6	4
V	189	178	186	197	151	162	358	14	6
Cr	36	31	35	36	32	31	126	-	-
Co	61	64	57	55	46	54	68	92	73
Ni	53	46	42	41	33	43	98	-	-
Cu	24	20	14	18	6	16	239	-	-
Zn	217	126	153	152	120	110	116	-	-
Ga	25	24	24	23	20	23	24	-	-
Rb	28	29	38	43	49	48	20	199	256
Sr	591	586	539	529	456	559	333	135	103
Y	47.6	42	44	45.8	46.7	40.4	40.8	39	62
Zr	290	278	305	309	304	232	218	297	307
Nb	17.6	17.4	18.4	19.3	15.2	12.1	24.5	14.5	17.0
Ba	756	712	818	781	630	622	173	914	736
La	32.1	30.7	34.8	36.6	35.6	26.3	24.5	51.1	93.9
Ce	80.7	76.9	82.9	83.4	81.3	62.6	61.2	104.0	186.0
Nd	49.6	48.2	54.2	51.9	44.7	38.4	34.7	37.9	62.4
Sm				9.61	8.21				
Eu				3.15	2.39				
Tb				1.64	1.40				
Yb				3.54	3.32				
Lu				0.45	0.46				
Hf				7.33	6.93				
Ta				1.03	0.92				
Th	1	1	1	1.8	3.5	3	1	22	33

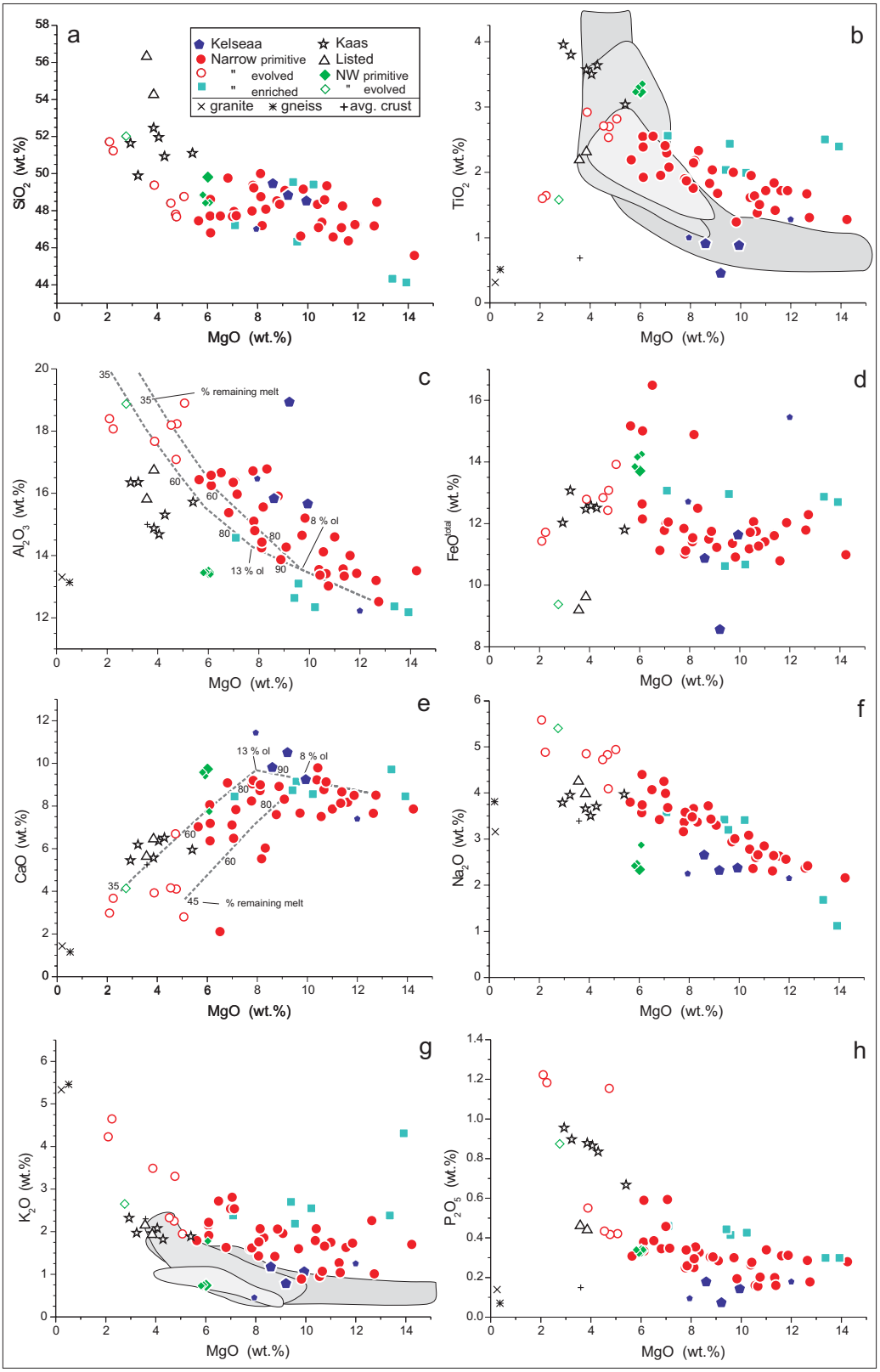

Figure 8: Major element variations for the Bornholm dykes. Symbols as in Fig. 7 except: x: basement gneiss; *: Hammer granite (data: T. E. Waight pers. comm.); +: average middle continental crust (Rudnick and Gao, 2003). In (c) and (e) are shown examples of magmatic evolution modelled by fractional crystallization of sample 59620; see text for details. In (b) and (g) fields for Central Sweden Dolerite Group (pale grey), Protogine Zone Dolerite Group (medium grey) and Blekinge Dalarne Dolerite Group (darkest grey) are shown (Solyom et al., 1992).

Geochemically five main types of mafic dykes can be distinguished on Bornholm. Type 1 (tholeiitic basalts) is represented by three samples from the Kelseaa dyke, a dyke from Stammershalle with strike 42°NE (57719), and a dyke intruded into the Kelseaa dyke.

Type (2) comprises most narrow dykes, and is by far the largest group (46 samples). These are transitional to alkaline, predominantly potassic alkali basalts, trachybasalts and basanites. Type (2*) represents a group of six narrow dykes distinctly more enriched in incompatible elements than other type 2 dykes.

An evolved type (3) consists of samples from the Listed and Kaas dykes, two smaller dykes located not far from the Kaas dyke and probably closely related to it, and two dykes from Kløven south of Kaas. Kaas and related dykes are shoshonites and potassic trachyandesites, and the more sodic Listed dyke samples are mugearites. Samples from the last of the large dykes, the Salne dyke, are all very altered and have largely been left out of this study. This dyke seems to have been a duct for hydrothermal fluids. We note the unusual NE orientation of the Salne dyke that is similar to the Kelseaa dyke.

The WNW- to NW-trending dykes are also geochemically distinct. Type (4) comprises the only quartz tholeiites on Bornholm (Table 1; Obst, 2000). They have relatively low alkali and Al_2O_3 contents and high CaO and TiO_2 for their MgO contents.

Although most of the dykes petrographically appear rather fresh, postmagmatic alteration processes, such as hydrothermal activity, may have disturbed the distribution of, in particular, the more easily mobilized elements K, Rb, Sr, and Ba. However, Ba correlates well with Nb and therefore does not appear to have been significantly mobilized. By contrast, Rb, K, and to a limited extent Sr, show more scatter (not shown). Immobile Zr, though, correlates broadly with K_2O (not shown) and attests that alteration effects are quite limited. We therefore suggest that, although some disturbance has occurred by secondary processes, it has only affected the most mobile elements, and the geochemistry of the dykes is thought to largely reflect magmatic processes. This is despite the fact that less than half of the samples have volatile contents below 3 %, and ten samples have 5 – 10 % volatiles. These elevated volatile contents may partially reflect that the sampled dykes were emplaced as un-degassed magma at considerable depth. Measured $Fe^{2+}/Fe^{total}_{average} = 0.74 \pm 0.07$ (1σ, N = 50, mafic samples only) is typical for alkaline magmas (Middlemost, 1989). The tight normal distribution of this ratio does not indicate large scale secondary oxidation. Low temperature alteration, apparent from petrographic studies, however, is probably the cause of spuriously high values of MnO in nine rocks (MnO = 0.25 – 0.48 %), and occasionally high FeO^{total} values.

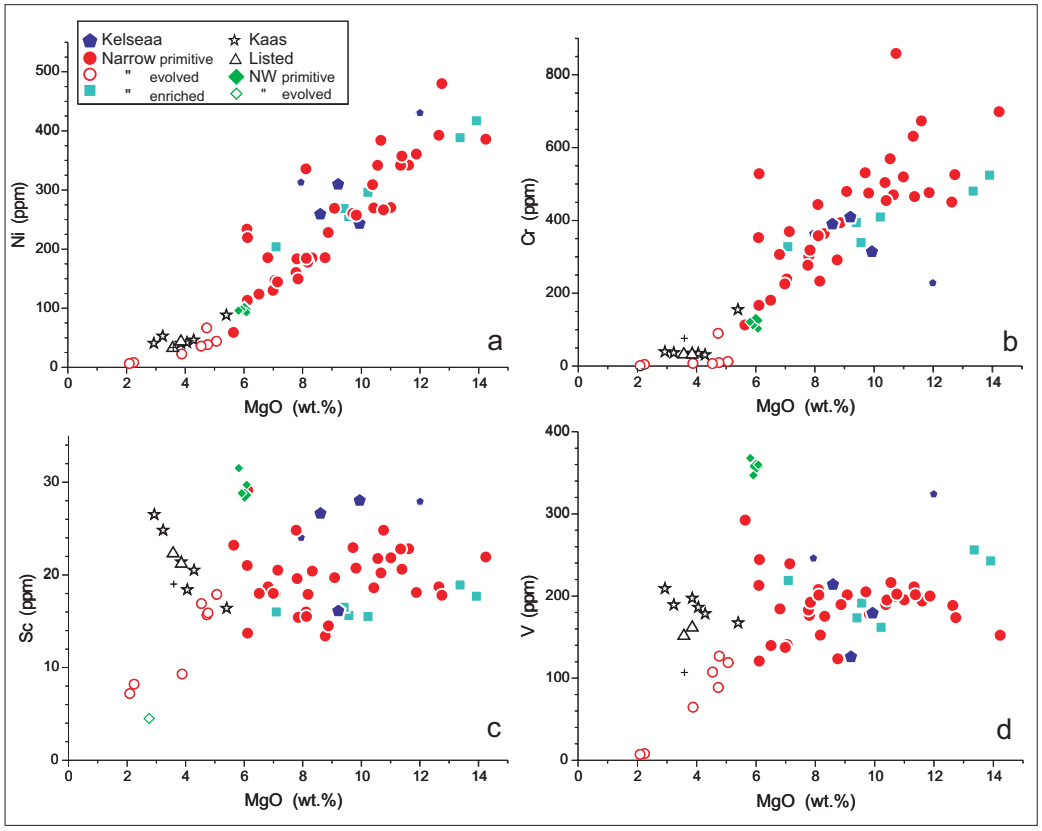

Figure 9: Variation diagrams for selected compatible trace elements vs. MgO. Symbols as in Fig. 8.

Kelseaa-like dykes (type 1)

Three samples from the Kelseaa dyke have been analyzed. They are olivine tholeiites with high MgO contents (8.5 - 12 %), Mg# (0.69 - 0.74), Ni (250 - 430 ppm) and Cr (225 - 400 ppm). SiO_2 concentrations are 47.3 - 49.5 %. The internal geochemical variation in the dyke may reflect differentiation processes during cooling or repeated magma injection in the dyke. Some of the gabbroic rocks in its central part are partial cumulates. The high Al_2O_3 and low FeO^{total} of sample 59635 can be ascribed to the effect of 20 % plagioclase accumulation, although Sr is not high. The concentrations of the incompatible trace elements Rb, Ba, La, Ce, Nd, Y, Zr, and Nb in 59635 are about half of those in 59633. This, together with relatively high Ni and Mg# in 59635, indicates that around 50 % plagioclase and olivine cumulus crystals are present in this rock, which also explains its relatively low V-concentration. Samples 59633 and 59656, from near the dyke margin, are almost identical and may best represent the magma composition. Kelseaa and related magmas have lower TiO_2 (0.5-1.3 %), Sr and Nb than other Bornholm dykes and also have relatively low Na_2O, K_2O, and P_2O_5 (Figs. 8 & 10).

The Kelseaa samples have negative Sr, P, and Ti anomalies in Fig. 11a. Apatite is an early precipitating phase in the Kelseaa dyke (Callisen, 1934), and accu-

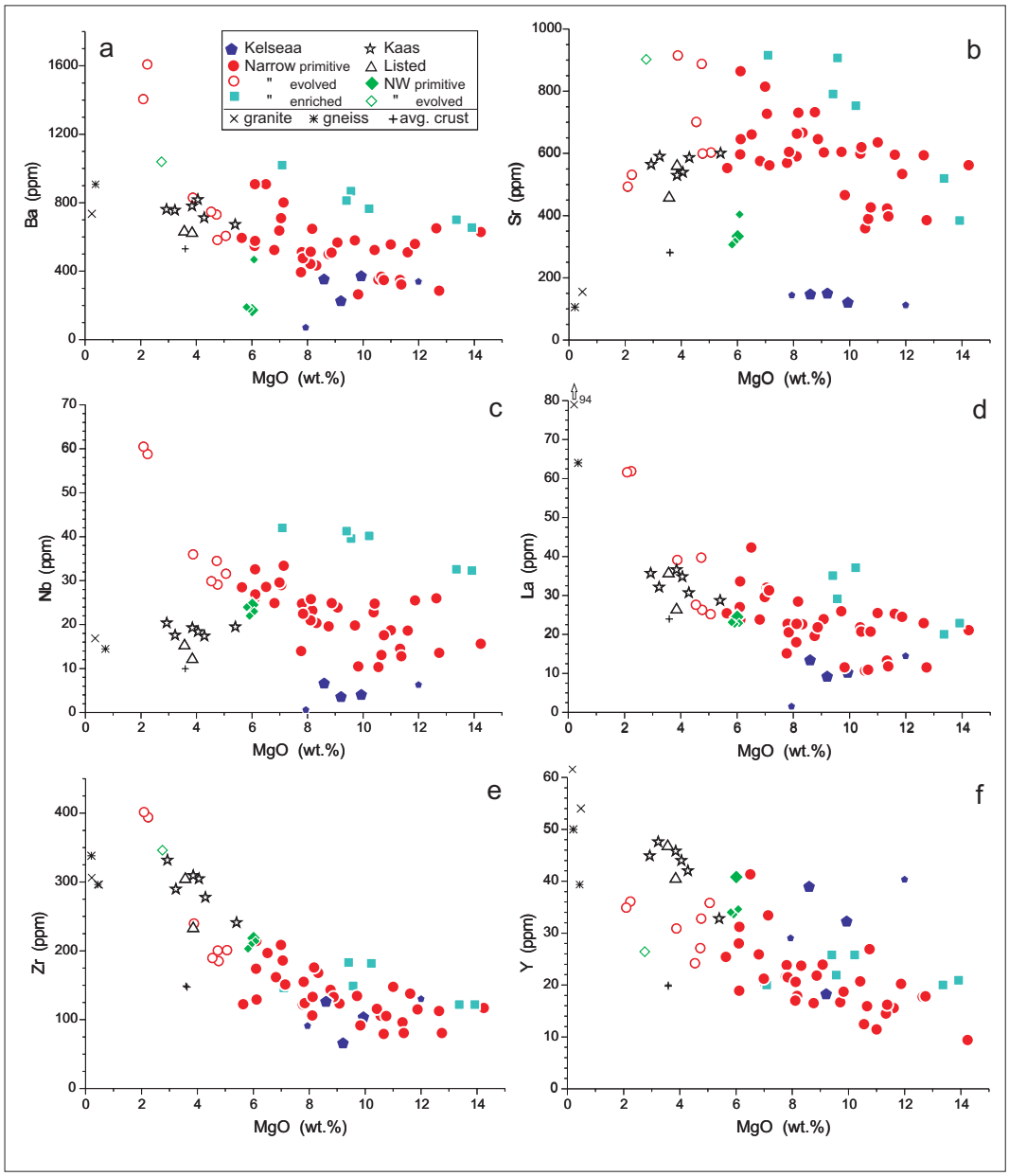

Figure 10: Variation diagrams for selected incompatible trace elements vs. MgO. Symbols as in Fig. 8.

mulation/fractionation of this mineral in the magma chamber could have generated these anomalies, whereas it cannot explain the negative Th anomaly. The heavy REEs are relatively variable having Tb/Yb_N = 1.2-1.8, which indicates an origin by mantle melting at shallow to intermediate depth.

Sample 57719 has very low concentrations of incompatible elements, apart from Rb, Ba, K and Sr (Fig. 11a). The trend is even more depleted than average N-type MORB (Normal-type Mid Ocean Ridge Basalt), but a Tb/Yb_N ratio of 1.8 is higher than in MORB, indicating deeper mantle melting.

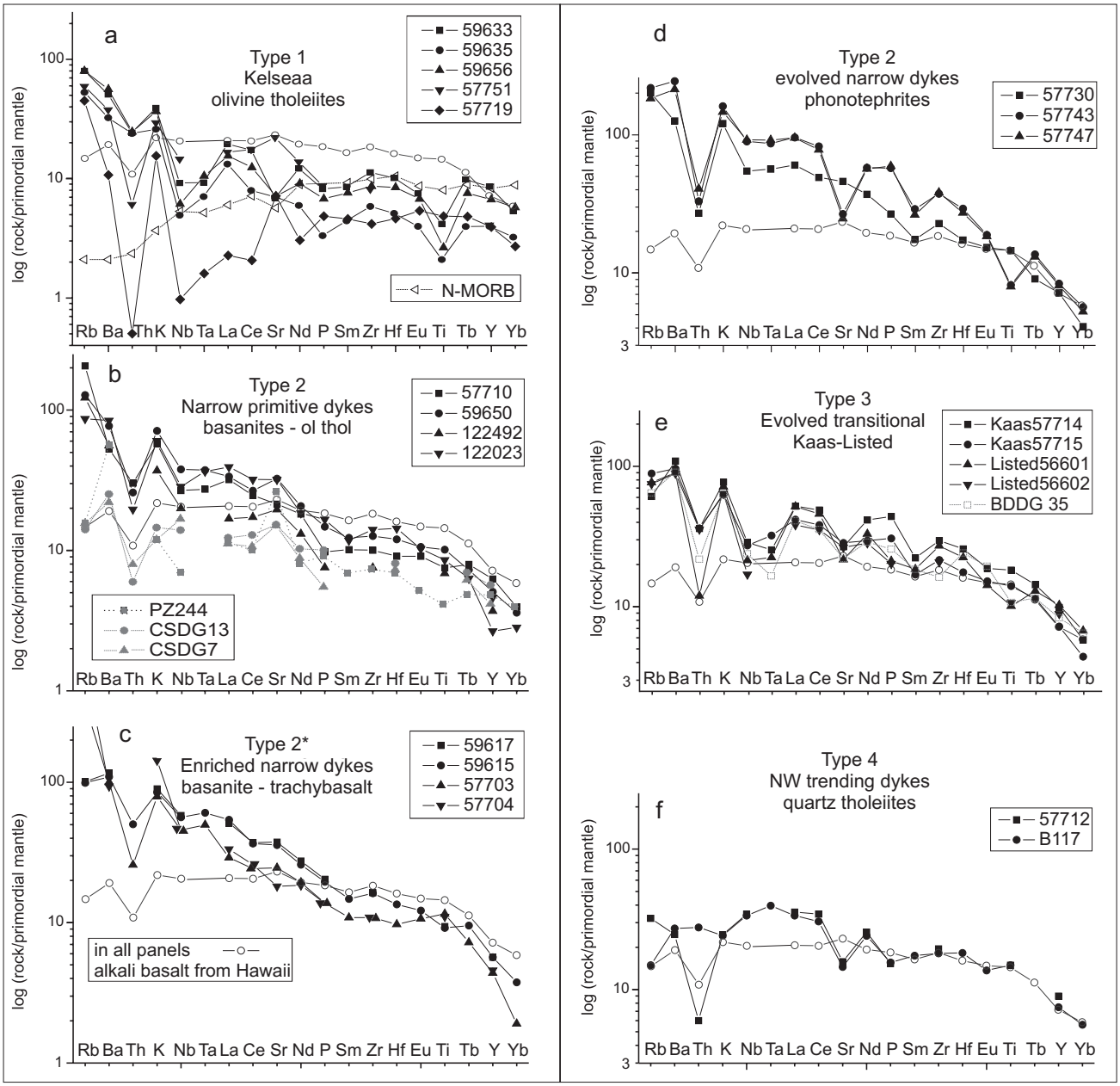

Figure 11: Trace element variation diagrams (spider diagrams) for the mafic dykes. (a) the Kelseaa type; (b) the narrow type with three examples of primitive mid Proterozoic Swedish dykes from the Protogine Zone Dolerite Group (PZDG) and the Central Swedish Dolerite Group (CSDG) (Solyom et al., 1992); (c) most enriched samples of the narrow type; (d) the most evolved narrow dykes: phonotephrites; (e) evolved rocks of the Kaas type and Listed dyke. Also shown is a dyke from the Blekinge Dalarne Dolerite Group (BDDG) which has comparable major element composition (Solyom et al., 1992); (f) NW-trending dyke type. B117 is from Obst (2000). Compositions have been normalized to mantle from Sun & McDonough (1989). An alkali basalt, Honolulu Series, Oahu, Hawaii (sample 65KPO-1, Clague & Frey, 1982) is shown for comparison on all diagrams. (a) also shows an N-type MORB (Hofmann, 1988). Note that the vertical scale differs.

The narrow mafic dykes (type 2) and enriched narrow dykes (type 2*)

The trace element compositions of the narrow dykes are distinctly different from the Kelseaa dyke. The narrow dykes comprise a wide compositional range. They vary in alkalinity from transitional to basanitic, with a few evolved phonotephrites and tephriphonolites. These rocks have very variable MgO contents (2 - 14 %). Among the most magnesian samples three are picrites, and several others have high Cr (> 500 ppm), Ni (> 400 ppm), and Mg# > 65, and may represent near-primary mantle-derived magmas (Table 2, Figs. 8 & 9).

There is a correlation between major element concentrations and petrographic groups. The olivine ± clinopyroxene-phyric samples have primitive compositions with high MgO (> 8 %) and CaO, while the aphyric samples are relatively evolved with MgO < 8 %. The olivine + plagioclase-phyric dykes, which do not include the alkaline dykes, are in many respects intermediate between the other two petrographic groups, although most samples have lower MgO (< 8 %) and CaO, and higher Al_2O_3 than the other two groups.

The narrow dykes have relatively smooth spider diagram patterns except for the LIL (Large Ion Lithophile) elements (Fig 11b). Some of the samples display small positive Sr anomalies. A positive Sr spike is developed in highly magnesian samples that have presumably experienced the least extent of crystal fractionation. Only the most evolved phonotephrites with MgO concentrations of 2.1 and 2.2 % have troughs at Sr, Eu, and Ti. The element patterns therefore do not suggest fractional crystallization of plagioclase until MgO < 4 % during late stages of differentiation. A lack of fractionation-related troughs persists even in samples with low MgO-contents, e.g. samples 59604 (5.64 % MgO, hawaiite) and 57730 (3.88 % MgO, phonotephrite).

Differentiation of the narrow dykes was by fractionation of olivine ± clinopyroxene. The plagioclase phenocrysts in samples with > 4 % MgO are accordingly considered to be related to late stage crystallization of the magmas; plagioclase was not involved in fractionation. Initial crystallization probably took place in a shallow magma chamber, subsequent to some fractionation at greater depths. Constant V-concentrations with decreasing MgO show that Fe-Ti oxides did not fractionate. This also suggests that clinopyroxene was the dominating phase in the extract (K_D,$V^{cpx\text{-}liq} = 0.9$, (Ulmer, 1989)). Compared to some of the few published primitive compositions from southern and central Sweden (one dyke from the Protogine Zone Dolerite Group and two from the Central Swedish Dolerite Group (Solyom et al., 1992)), the Bornholm dykes are enriched in incompatible elements and show a more fractionated pattern (Fig. 11b), as evident by the generally lower Zr/Nb ratios of 4-10 in type 2 rocks compared to 7-22 in PZDG and CSDG samples.

Phonotephritic magmas are late fractionation products of highly alkaline magmas and relate samples 57730, 57743 and 57747 to the narrow basanitic dykes.

The two most magnesian samples are potassic basanitic picrites (57703 and 57704) with much lower silica than the rest. Four potassic trachybasalts are also particularly K-rich and incompatible element enriched (high also in P_2O_5, Ba, LREE (Light Rare Earth Elements), Zr, and Nb), but less SiO_2-depleted, and low in Al_2O_3 (Fig. 8 & 10, Tables 1 & 2), as is also apparent in the spider diagram (Fig. 11c). These 6 samples will be treated separately as subtype 2* in the discussion.

The Kaas, Kaas-like and Listed dykes (type 3)

This group of evolved rocks is transitional to slightly quartz normative and potassic. The more sodic Listed samples deviate in most diagrams from the trends defined by the Kaas dyke and the Kaas-like dykes. Mineralogical variations across the Kaas and Listed dykes have been described in detail by Jensen (1966).

The 40 m wide Kaas dyke displays some internal variation. Sample 57715 has higher MgO, Ni, Cr and Sc and lower SiO2 than 57714. This may be caused either by in situ fractionation or (not evident in the field) by multiple injection. Two dykes from Kløven (57742 and 57744), one from Sandkås (57713) and one close to the Kaas dyke (57750) have Kaas-like compositions that distinguish them from evolved type 2 dykes, and include relatively high TiO2, P2O5, and V (Figs. 8 & 9).

The Listed dyke has higher SiO_2 contents (54.3-56.3 %) than the Kaas-like dykes (49.9-52.5 %), and lower concentrations of FeO^{total}, TiO_2, and P_2O_5. The two samples from the 30 m-wide Listed dyke (59601 and 59602) are from the contact and center of the dyke, respectively, and show a small, systematic difference indicating that some differentiation took place between injection of the outer and inner parts of the dyke, as is also implied by their different feldspar phenocryst assemblages.

The spider diagram patterns of the evolved dykes (Fig. 11d) are in many respects similar to that of the Kelseaa dyke, the difference being mainly a higher degree of enrichment of LREEs and HFSEs (High Field Strength Elements) in the evolved type 2 dykes. Concentrations of the LIL elements are only slightly

higher than in Kelseaa. Concentrations of heavy rare earth elements are similar, although the HREE are slightly more fractionated (Tb/Yb_N = 1.8-2.4) than in the Kelseaa dyke, and therefore indicate a deeper melt extraction. Some Blekinge Dalarne Dolerite Group (BDDG) rocks resemble the type 3 dykes (Fig. 11d).

NW-trending dykes (type 4)

The Sandkås sample 57712 (strike: 110°), as well as three other samples from northern Bornholm (Obst, 2000), and a trachytic (kullaite) dyke from central Bornholm (Jensen, 1988), have trends between WNW and NW. Sample 57712 is very similar in composition to those reported by Obst (2000). These are distinct from other Bornholm dykes in having lower Al_2O_3, Na_2O, K_2O and higher Sc, V and Cu (Figs. 8-10). Together with the more evolved Listed and Kaas-type dykes the NW-dykes are the only quartz normative examples on Bornholm. The incompatible element patterns of these rocks show less enrichment in very incompatible elements than type 2 rocks, and they have negative Sr anomalies (Fig. 11e).

Discussion

Geochronology

Both field relations and palaeomagnetic studies suggest that the dykes were intruded in four or five episodes between the formation of the younger granites (c. 1.45 Ga, Zariņš & Johansson, 2008) and the Permian (Münther, 1945a; Abrahamsen, 1977; Abrahamsen et al., 1995; Lewandowski & Abrahamsen, 2003). These four events at c. 1326 Ma, c. 1220 Ma, 950-900 Ma and ≈300 Ma can be correlated to the Kelseaa dyke, the narrow dykes, the Kaas dyke, and the-NW trending dykes, respectively. The Listed dyke has been suggested to be somewhat younger than the Kaas dyke (700 – 800 Ma, Abrahamsen, 1977), and may accordingly represent a separate intrusive episode. As its age is uncertain, however, and because the Listed dyke has compositional affinities to the Kaas-like dykes, we group them together. The geochemistry of the dykes indicates that (a) the Kelseaa, (b) the narrow dykes, (c) the evolved Kaas and Listed dykes and (d) the NW-trending dykes define four distinct compositional types (types 1-4) which is in accord with the above sequence of intrusion. In the following we will discuss the geochemistry of the dykes based on the hypothesis that each intrusive event represents a distinct episode of mafic magmatism.

Fractional crystallisation

Kelseaa (type 1). The variation among the Kelseaa dyke samples in terms of major elements suggests multiple intrusion in the dyke. This has not been substantiated by field evidence, possibly due to poor exposure. Although petrographic observations suggest differentiation during solidification, the compositions of the samples cannot be related by simple fractionation processes. The geochemistry suggests that magmas of variable and independent derivation were involved.
Narrow dykes (type 2). These make up rather well defined trends in the variation diagrams (Figs. 8-10) and are here considered as products of similar crystallization histories of a range of primitive magmas. Overall initial fractionation of olivine +/- chromite is indicated for magmas with > 9 % MgO by the decrease with MgO of only Ni, Co, and Cr (Fig. 9), and the increase of several other elements not present in olivine, e.g. Na_2O and Zr (Figs. 8 & 10). Clinopyroxene + olivine fractionation is indicated as the melts evolved through 9-8 % MgO by decreases in CaO, SiO_2, and Sc, together with the continued decrease of Ni and a more pronounced increase of excluded elements such as TiO_2, Al_2O_3, Na_2O, K_2O, and P_2O_5. Clinopyroxene and olivine are joined by Fe-Ti oxide fractionation very late in the magmatic development for the few samples with MgO < 5.6 %, as shown by strong decreases in FeO, TiO_2 and V (Figs. 8 & 9). Plagioclase and apatite are not significant fractionating phases since Na_2O, P_2O_5, LREEs, and Sr increase into the most evolved samples (Figs. 8 & 10). The late onset of feldspar crystallization is typical for highly silica undersaturated (basanitic and nephelinitic) magmas that fractionate towards phonolitic compositions (e.g. Holm et al., 2006).

The simple fractionation scheme that encompasses the majority of the narrow dyke magmas was modelled quantitatively from a starting melt compostition using picrite sample 59620 as an example (Fig. 8c, e). This sample may have accumulated some olivine (the sole phenocryst phase) but correction for this would not be well constrained and would only change the modelling very slightly as regards the amount of crystallization involved. Equilibrium olivine and clinopyroxene were calculated for each fractionation increment of 1 %. The model shows that after initial fractionation of 8-13 % olivine, clinopyroxene started to crystallize and the cotectic proportions are indicated to have been around 1 ol:5 cpx. Most samples are described by < 20 % fractionation. The interval 13 - 6 % MgO is covered by c. 40 % fractionation. The most evolved phonotephrite compositions can be modelled as samples with 35-45 % residual melt (Fig. 8c, e).

Kaas-Listed (type 3). These rocks have high concentrations of Sc as well as TiO_2 and P_2O_5, which show well-defined negative correlations with MgO (Figs. 8 & 9), implying that neither clinopyroxene, Fe-Ti oxides nor apatite fractionated in significant amounts from these magmas over the restricted compositional range sampled. Negative Sr anomalies in the spider diagram (Fig. 11d) suggest that plagioclase fractionated in the precursory magmas. Low Ni, together with low MgO in these rocks, indicate that olivine was also important in the fractionate. Because some BDDG rocks resemble the Kaas-Listed dykes we have used a primitive BDDG sample (#56) with 11.4 % MgO and 49.9 % SiO_2 (Solyom et al., 1992) as the parental composition for fractionation modelling. This shows that Kaas-like type 3 magmas with 4 % MgO may result from 53 % crystal extraction of 11 % olivine (covering the range 11.4 to 7.0 % MgO) followed by 29 % plagioclase + 11 % olivine + 0.5 % clinopyroxene + 0.1 % Fe-Ti oxide (7.0 to 4.0 % MgO). It is noted that Kaas-like samples have twice the TiO_2 and P_2O_5 concentrations of the Listed samples and their parental magmas were therefore probably much more enriched. Moreover, as seen from the SiO_2- and TiO_2-contents, the Listed and Kaas magmas also evolved differently, possibly because their magma chambers were emplaced at different depths.

Compositional considerations indicate that the evolved type 3 dykes had a different parental magma type from the Kelseaa (type 1). The Kelseaa dyke has higher CaO but lower Sr-concentrations than the evolved dykes, which is not compatible with derivation of the latter by fractionation of plagioclase and olivine from a magma geochemically similar to type 1. Furthermore, petrographic observation of the Kelseaa dyke suggests that apatite was an early crystallizing phase, in contrast to the differentiation history of the evolved dykes.

NW-trending dykes (type 4). The medium-K basalts of the NW-trending dykes show very little variation. These rocks are quite evolved with Mg# around 49. The slightly silica undersaturated Bjergebakke mugearite (Table 7 in Jensen, 1988) would be difficult to derive from these highly hypersthene normative basalts by fractional crystallization, and they are not likely to be comagmatic.

Contamination

Contamination of mafic magmas commonly takes place in crustal magma chambers accompanying fractional crystallization. For three of the dyke types discussed, Kelseaa, Kaas-Listed and the NW-trending dykes, quantitative modelling of possible contamination is not feasible because only a very restricted compositional range is available. Instead the effects of adding crustal material to mantle melts are considered on the basis of element ratios that typically have a significant contrast between continental crust and mantle melts. Ratios such as Ba/Nb and La/Nb are sensitive to contamination with crust-derived material which typically has high Ba, LREE, and low Nb, as exemplified by the Bornholm gneiss and a Hammer granite (Table 2), compared to mantle melts, exemplified by oceanic basalts (Fig. 12). Moreover, these ratios do not change significantly during fractionation of the observed mineral assemblages.

Kelseaa (type 1) and Kaas-Listed (type 3) dykes. The

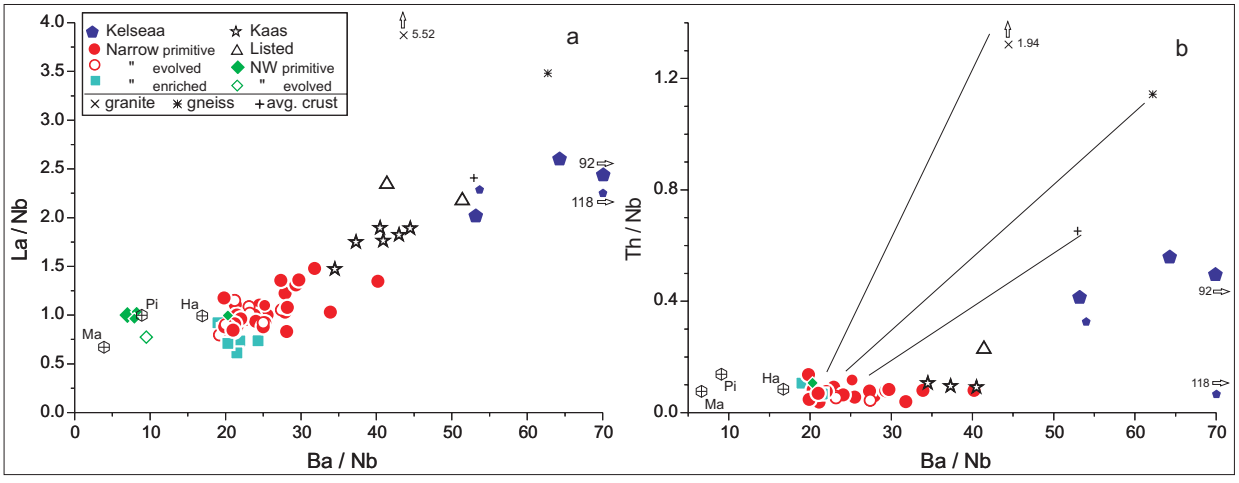

Figure 12: (a) La/Nb versus Ba/Nb; (b) Th/Nb versus Ba/Nb. Examples of OIB hot spot magmas are shown as hexagons with plus: Ha –Hawaii (same as in Fig.9); Ma – Mangaia HIMU-type OIB, sample M13 (Woodhead, 1996); Pi – Pitcairn Island EM1-type OIB, sample Pit89-1 (Eisele et al., 2002). (b) includes mixing trajectories between low Ba/Nb dykes and various crustal compositions. The trend of Kelseaa type and Kaas-Listed type dykes towards high Ba/Nb and La/Nb seems unrelated to assimilation of local basement compositions. See text for discussion. Other symbols as in Fig. 8.

Kelseaa (type 1) dykes consistently have the highest values of both Ba/Nb (54-111) and La/Nb (2.0-2.6) (Fig. 12), whereas the Kaas-Listed dykes have ratios (33-45, 1.4-2.0, respectively) intermediate between Kelseaa and the narrow dykes (Ba/Nb = 19-32, except for a few outliers). The Kelseaa dykes are also enriched in Rb, Ba, Th and K that are usually high in felsic crustal rocks, and we conclude that significant crustal contamination of the magmas has taken place. Sample 57719 is relatively enriched in the fluid-mobile elements Rb, Ba, K, and Sr. This, and the very high Ba/Th ratio of 1700, suggest that the N-MORB pattern was modified by addition of a fluid-borne agent, which may also have influenced sample 57751 (type 2). The Kaas-Listed magmas seem somewhat less contaminated.

The Kaas-Listed magmas cannot have developed from magma similar to the Kelseaa dyke by means of AFC (assimilation coupled with fractional crystallization) processes because they have lower Ba/Nb but much higher Ba-concentrations, and alkali feldspar is not considered a possible liquidus phase. The Kaas-Listed dykes evolved from magmas more Nb-enriched than the Kelseaa magmas, if it is accepted that the geochemistry of the Kelseaa samples mainly reflects a melt composition rather than a cumulate, as it was argued at least for sample 59656.

The Listed samples have higher La/Nb and Ba/Nb than the Kaas and Kaas-like dykes and may be more contaminated. It is noted, however, that the enrichment in Ba and LREE is not accompanied by Th enrichment (Fig. 12b). The difference between the two Listed samples may be caused by multiple injection, as indicated petrographically, of variably contaminated magmas.

Specific contaminants for the dykes may be the exposed crustal rocks. These may be approximated by the grey granitic gneiss and Hammer granite (the northernmost younger granite, Fig. 1, Table 2). In Fig. 12b we also show the composition of these and a global average of middle continental crust (Rudnick & Gao 2003). Because only amphibolite facies gneisses are exposed (Callisen, 1934), upper crustal rocks are not common below the present exposure level and are probably not relevant for discussion of the Bornholm dykes, since contamination would have involved the middle or lower crustal rocks. Mixing of two components in this type of diagram will produce straight lines (Fig 12b). Type 1, 2 and 3 samples are situated on a broad trend in Fig. 12a, which includes the crustal average but not the local basement. If an average type middle crust was assimilated by the Kelseaa and Kaas-Listed magmas, very high proportions are indicated for Kaas-Listed, whereas the Kelseaa samples exceed crustal values. Assimilation of the local basement with high La/Ba ratio is only indicated for one sample of the Listed dyke that lies above the main trend in Fig. 12a. Either crustal contamination is not generally related to the locally exposed basement, or a different process caused the high Ba/Nb and La/Nb ratios in type 1 and 3 magmas.

The narrow dykes (type 2). The variation of the narrow dykes does not indicate much local continental crustal assimilation as they have Ba/Nb and La/Nb ratios close to those of mantle rocks and oceanic basalts (Fig. 12). Ba, Th and Nb were all very incompatible in the dyke magmas. The variation of ratios of these elements in type 2 dykes is not towards the crustal rocks, as demonstrated in particular by the constant and mantle-like Th/Nb ratio (Sun & McDonough, 1995). Sr is also incompatible in most type 2 magmas, and the correlation of ratios Ba/Nb and Sr/Th with Sr/Nb does not appear to be related to assimilation of relatively evolved crust (with high Th and low Sr), but

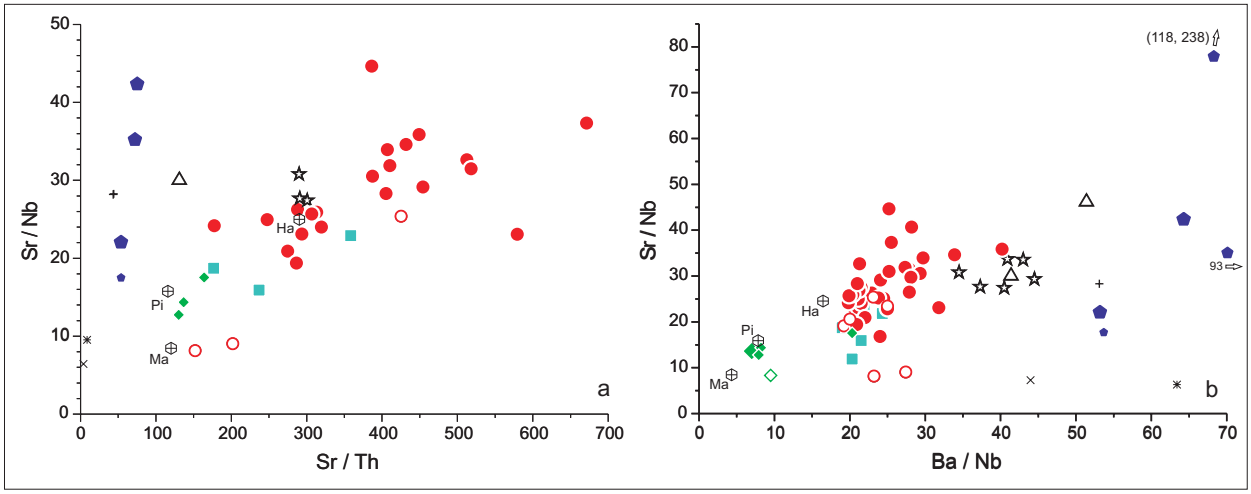

Figure 13: (a) Sr/Nb versus Sr/Th; (b) Sr/Nb versus Ba/Nb. Symbols as in Fig. 12. Sample 57719 is not shown in (a) due to extremely high and uncertain Sr/Th due to Th concentration close to the detection limit (Table 2).

rather some agent rich in Ba, Sr, and LREEs (Figs. 12 & 13). The rocks enriched in Sr, Ba, and La have both a small negative Nb-anomaly and a positive Sr-anomaly in spider diagrams (Fig. 11b). These are the type 2 rocks with the highest Zr/Nb (= 6 - 10). There is no relation between any of these ratios and degree of magmatic differentiation, and modification of type 2 melts with relatively low Zr/Nb (4-6) was therefore not by assimilation and fractionation processes involving crust that typically has high Zr/Nb. HFSE ratios are generally not thought to be affected by post magmatic processes. It therefore seems that the elevated Zr/Nb ratios must have been acquired in the mantle.

Mantle melting and source compositions

The folowing discussion of melt generation is mainly based on the modelling in Figs. 14 & 15. Fig. 16 is an attempt to graphically illustrate the models with simplified sketches.

Kelseaa (type 1)

Significant fractionation of the heavy rare earth elements, such as Tb and Yb, in basaltic magmas can only be accomplished by melt-garnet interaction. Three samples of the Kelseaa dyke have Tb/Yb_N = 1.2 - 1.8 (Fig. 14a). A Tb/Yb_N ratio of 1.2 is in accordance with melting in the spinel stability field (see below), whereas the higher ratio of 1.8 requires the presence of garnet in the source. This is an additional indication of the presence of two magmas in the Kelseaa dyke, and it requires the Kelseaa melts to be variably derived over a depth range.

REE-modelling of melting of mantle peridotite in the garnet and spinel stability fields is shown in Fig. 14a. The melts are modelled by aggregated non-modal batch melting. A mantle source (termed DPM) somewhat depleted relative to primitive mantle (McDonough & Sun, 1995) was used. Its composition was calculated as depleted mantle, DM (McKenzie & O'Nions, 1991), enriched by 5 % partial melts generated by 0.5 % melting of a depleted garnet peridote (Tainton & McKenzie, 1994). Such a source can account for the samples with the highest Tb/Yb_N ratios on Bornholm. The Kelseaa samples 59656 and 59635 with Tb/Yb_N = 1.2 – 1.3 fall below the model curve and must have been generated from a source more depleted than that of the model. A depleted type mantle is also inferred from the geochemistry of the Kelseaa dyke in general with Nb_N and $MREE_N$ < 10 (Middle Rare Earth Element), and low TiO_2 < c. 1 % giving a flat trace element spectrum, apart from the enrichment in LILE and LREE (Fig. 11).

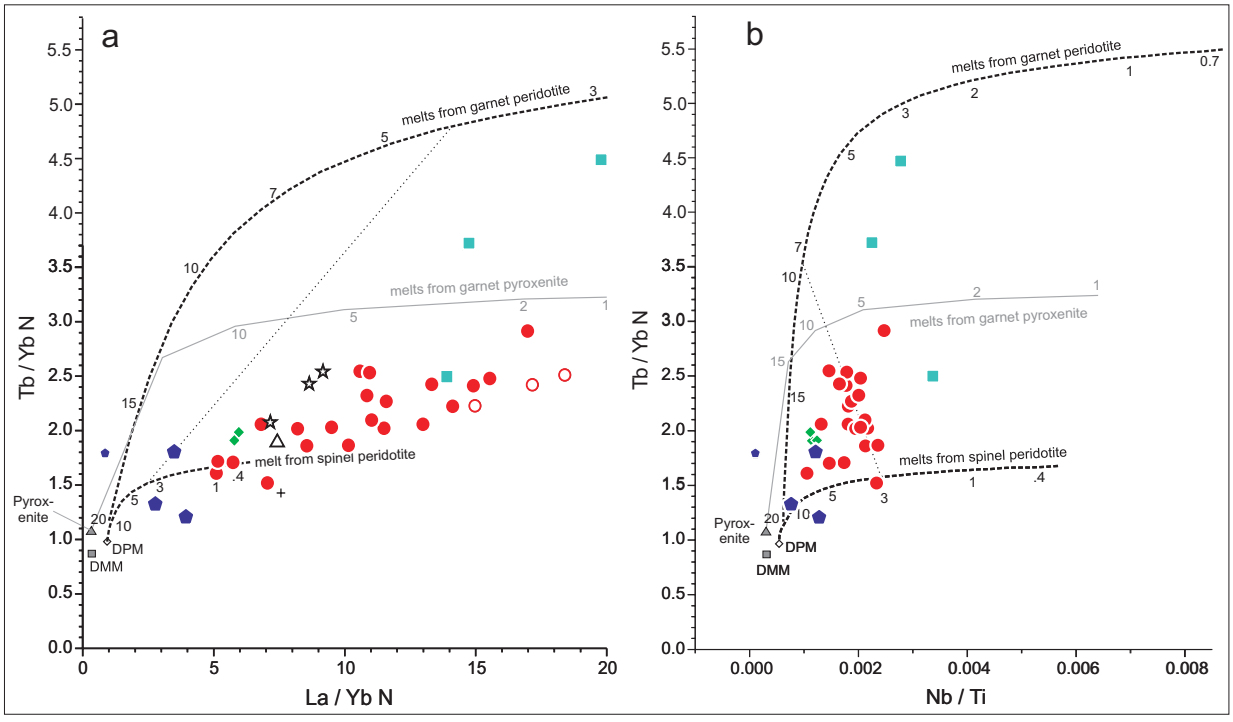

Figure 14: (a) Tb/Yb_N vs. La/Yb_N. (b) Tb/Yb_N vs Nb/Ti. Modelling of melting of a hypothetical mantle source in the spinel peridotite and garnet peridotite stability fields, respectively. Sources are: DMM – depleted MORB mantle; Pyroxenite is recycled MORB mantle, and DPM (mantle somewhat depleted relative to primordial mantle). See text for explanation. La/Yb and Tb/Yb are normalized to chondrite (Anders & Grevesse, 1989). Only primitive samples are shown in (b). Symbols as in Fig. 7.

Depleted sample 57719 with very low La/Yb_N = 0.85 has rather high Tb/Yb_N = 1.8 and it must have been generated at high pressures from garnet-bearing mantle (Fig. 14). The high $Fe_2O_3^{total}$ compared to MORB is also an indication of relatively deep extraction (Klein & Langmuir, 1987).

Sample 59633 with high Tb/Yb_N = 1.8 and La/Yb_N = 3.5 could be generated from the model source by mixing of partial melts from the garnet and spinel stability fields, or by melting during decompression of rising mantle through the garnet-spinel transition. Mixing of melts generated by around 4 % melting would be mixed in the ratio 1 garnet peridotite:12 spinel peridotite. With a more depleted mantle source, a larger proportion of the magma would stem from garnet-bearing mantle. There are no other significant geochemical differences between the Kelseaa samples with higher and lower Tb/Yb, and one depleted source is inferred for them all.

The Bornholm lithosphere at the time of the Kelseaa intrusion was 300 Ma old and thus would be expected to be more than 100 km thick even though it was strongly modified at 1.45 Ga during formation of the granitic crust. Thus, as melting to a large extent took place in the spinel stability field at depths less than 75-90 km, the source must have been located in, but not restricted to, the lithospheric mantle or, alternatively, the lithosphere had been thinned at the time of melt generation. With the apparently unique occurrence of the Kelseaa type a hotspot is hardly indicated, and general heating of the lithosphere would also be expected to yield more magmas. Furthermore, the quite depleted mantle source for the Kelseaa dyke infers melting by decompression, because refractory lithospheric mantle is less likely to melt by conductive heating.

The ultimate source of the Kelseaa dyke, however, cannot have been depleted mantle of the same type as inferred to generate mid-ocean ridge basalts. Although Zr/Nb in the Kelseaa samples is high (20-26) (Fig. 11, Table 2), it is still slightly lower than in typical N-MORB (> c. 30) (Hofmann, 1988). Crustal contamination would not tend to decrease this ratio. Using Nb/Ti as a parameter for the degree of melting (see explanation below for type 2 modelling), the model indicates a relatively high degree of melting (5-10 %) (Fig. 14b), so it is clear that a mantle source that is slightly more enriched than that of N-MORB is required. Incompatible element depleted sample 57719 (believed to represent a melt composition) with its high Zr/Nb = 142 and Th, Nb and LREE-depletion is an indication that MORB asthenosphere was involved in the formation of the Kelseaa (type 1) magmas.

We propose a back-arc extensional regime for these magmas. This may allow MORB-like magmas to be derived in a rifting continental setting. A back-arc setting would also explain the enrichment in fluid-mobile elements and in Th, as discussed above. The very limited amount of magmatism, however, suggests that this extensional process did not progress far.

The narrow dykes (type 2)

The narrow dykes have a wide range of Tb/Yb_N of 1.5-2.9 (enriched subtype 2* has up to 4.5) and a large group of samples form a general trend ranging to Tb/Yb_N = 2.5 and La/Yb_N to 17 (Fig. 14a), suggesting that melting took place across the garnet-spinel stability boundary and, for most dykes, a considerable component was derived in the garnet stability field. These primitive magmas therefore likely formed below the Bornholm lithosphere, either from relatively hot mantle, or from mantle with a relatively low solidus temperature such as other lithologies than peridotite, e.g. pyroxenite, or from hydrous mantle. Extension and lithospheric thinning, as indicated by the preferred dyke orientation, might have assisted the melting, but residual garnet is still required and thus rather deep melting at > 80 km.

Very high La/Yb_N (up to 17) at the high Tb/Yb-end of the main trend would point to very small degrees of melting (below 1 %) of garnet peridotite, whereas the other end of the trend would indicate c. 1 % spinel source melting (Fig. 14a). However, bearing in mind that some of these rocks are preferentially enriched in Ba, Sr, and LREEs, the La/Yb ratios may not only be related to melting of a homogeneous source, and the derived melting proportions may therefore be invalid.

In an attempt to circumvent this problem we have modelled melting using Nb/Ti, which is also a ratio of a highly to intermediately incompatible element. Because both are HFSEs this ratio would not be significantly influenced by the variable enrichment, which is dominated by LILEs and LREEs. The resulting melting curves (Fig. 14b) are broadly similar to those in Fig. 14a. However, a negative trend for type 2 magmas is evident, suggesting much larger degrees of melting: 3 % in the spinel field and around 10 % in the garnet field. If one common source is assumed, then a decrease in the amount of melting with declining pressure requires a lowering of temperature for decompression melting. Only a small temperature change is expected for asthenospheric processes which are mainly adiabatic. Alternatively, the melts could have been generated from two sources with different Nb/Ti ratios and different solidus temperatures and different degrees of melting would be expected at the same temperature.

If a source composed of peridotite with pyroxenite

veins rises, the pyroxenite has the lower solidus temperature, and therefore starts to melt at deeper levels (Stracke & Bourdon, 2009). At a given potential mantle temperature, pyroxenite will melt to a higher degree than peridotite. Results of batch melting of pyroxenite can be compared to the peridotite melting already discussed (Fig. 14). As is apparent in Fig. 14b, unrealistically small degrees of melting are modelled at low pressure, whereas garnet pyroxenite melting may be a viable alternative to peridotite. A mixed source, then, would allow for the two lithologies to have have different Nb/Ti ratios and could explain a higher degree (c. 7 %) of garnet pyroxenite melting and a lower degree (c. 3 %) of melting of spinel peridotite, and would not require a variation in source temperature. From Zr-Nb modelling (Fig. 15a) rather similar degrees of melting are suggested: 2 – 3 % for the low Zr/Nb samples which have low Tb/Yb, and around 5 % for the high Zr/Nb (6 – 10) samples.

The narrow dykes reflect a mantle composition which has certain similarities to the source of some ocean island basalts. The dykes with low La/Nb (0.8 - 1.2), Zr/Nb (4 - 6) and Ba/Nb (19 - 26) (Figs. 12, 15) are comparable to young oceanic islands like St Helena, Tubuaii, and Pitcairn Island (e.g. Weaver et al., 1987, 1991; Palacz & Saunders, 1986; Dupuy et al., 1988; Eisele et al., 2002) which represent mantle end members (Zindler & Hart, 1986). These mantle end members have been interpreted to represent recycled oceanic lithosphere which, after subduction, have contributed to OIB (Ocean Island Basalt) melts as parts of rising mantle plumes. The dykes from Bornholm include, however, samples more enriched in LIL elements relative to HFSE and LREE than most oceanic basalts. This is particularly evident in those dykes with La/Nb = 1.2 – 1.6 which also have high Ba/Nb = 30-41, and in those with positive Sr anomalies (Fig. 11b). Thus, if the low LREE/HFSE ratios of the source are derived from typical OIB mantle, the LILE enrichment must have been added from other sources available at the same time, sources which were demonstrated above not to be derived from the crust.

Most type 2 rocks form a well-defined trend that suggests mixing of two distinct end-member compositions (Figs. 12a, 13, 14, 15b). One has high La/Nb, Ba/Nb, Sr/Nb, Sr/Th, Zr/Nb, and Sr/Nd = c. 30. The other end-member has much lower Sr/Nd = c. 16, which is typical for MORB and some OIB (Hofmann, 1997). The high Sr/Nd end-member is suggested to be recycled gabbroic oceanic crust enriched in Sr by plagioclase accumulation. Such a component has also been suggested to be part of some mantle plumes (e.g. Chauvel & Hémond 2000; Kokfelt et al. 2006). This end-member is identical to the type 2 dyke component with relatively high Tb/Yb and low Nb/Ti identified above, which was characterized by a relatively low solidus temperature, as expected from a gabbroic composition.

Because the more enriched subtype 2* dykes that have even more extreme OIB signatures (Zr/Nb = 3 - 4, La/Nb = 0.6 - 0.9, Ba/Nb = 20 - 25) also have higher Tb/Yb_N = 2.5 - 4.5 they were generated at greater depth. These dykes extend from type 2 towards higher Nb/Ti and compositions derived by c. 2 % melting of garnet peridotite (Fig. 14b). Along with incompatible element ratios (Figs. 12 &13) and the lack of a positive Sr anomaly this demonstrates that they had a different source than the predominant type 2 magmas. The apparently small scale of this igneous activity indicates that no major rifting is associated, and melting seems to have taken place under a more or less intact continental lithosphere. Therefore, the

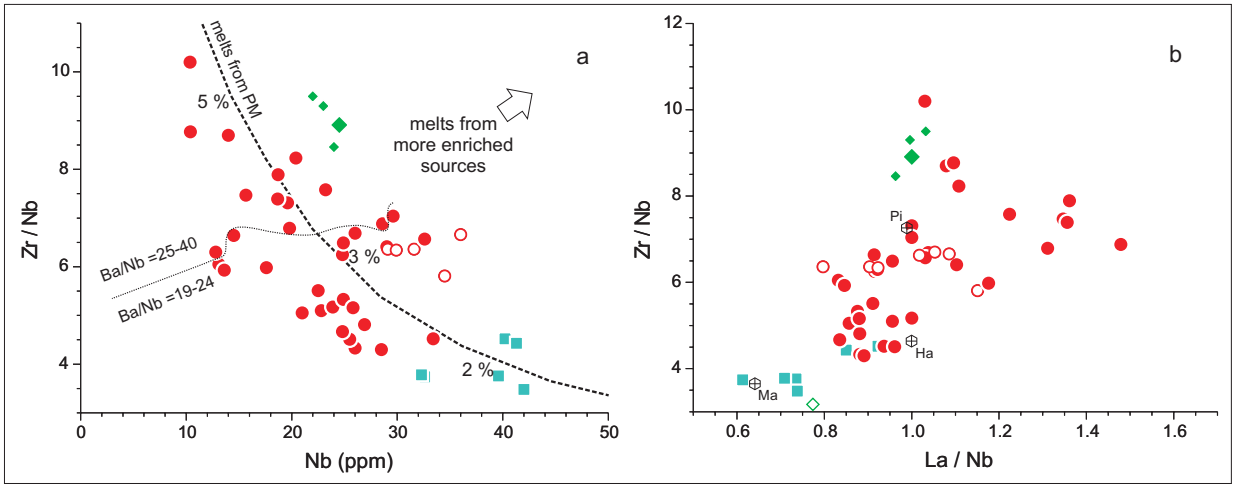

Figure 15: (a) Zr/Nb vs Nb. (b) Zr/Nb vs. La/Nb. In (a): curve for melts from aggregated incremental batch melting of PM (= primordial mantle; Sun & McDonough, 1995) is shown for reference. Thin dotted line separates samples with Ba/Nb higher and lower than 25. Symbols as in Fig. 12. See text for discussion.

most likely cause for magma generation was the presence of extraordinarily hot mantle under Bornholm at this time, and a different event than that which generated type 2 magmatism may be indicated.

Contemporaneous Protogine Zone magmas have a different geochemistry from type 2 magmas and may well have been generated differently. A rifting event at this time in southern Sweden that did not extend to Bornholm, based on the relatively low dyke intensity, may have led to lithospheric thinning and been the trigger for melting in abnormally hot mantle with a composition different from MORB-source asthenosphere, and a plume source under Bornholm may be indicated.

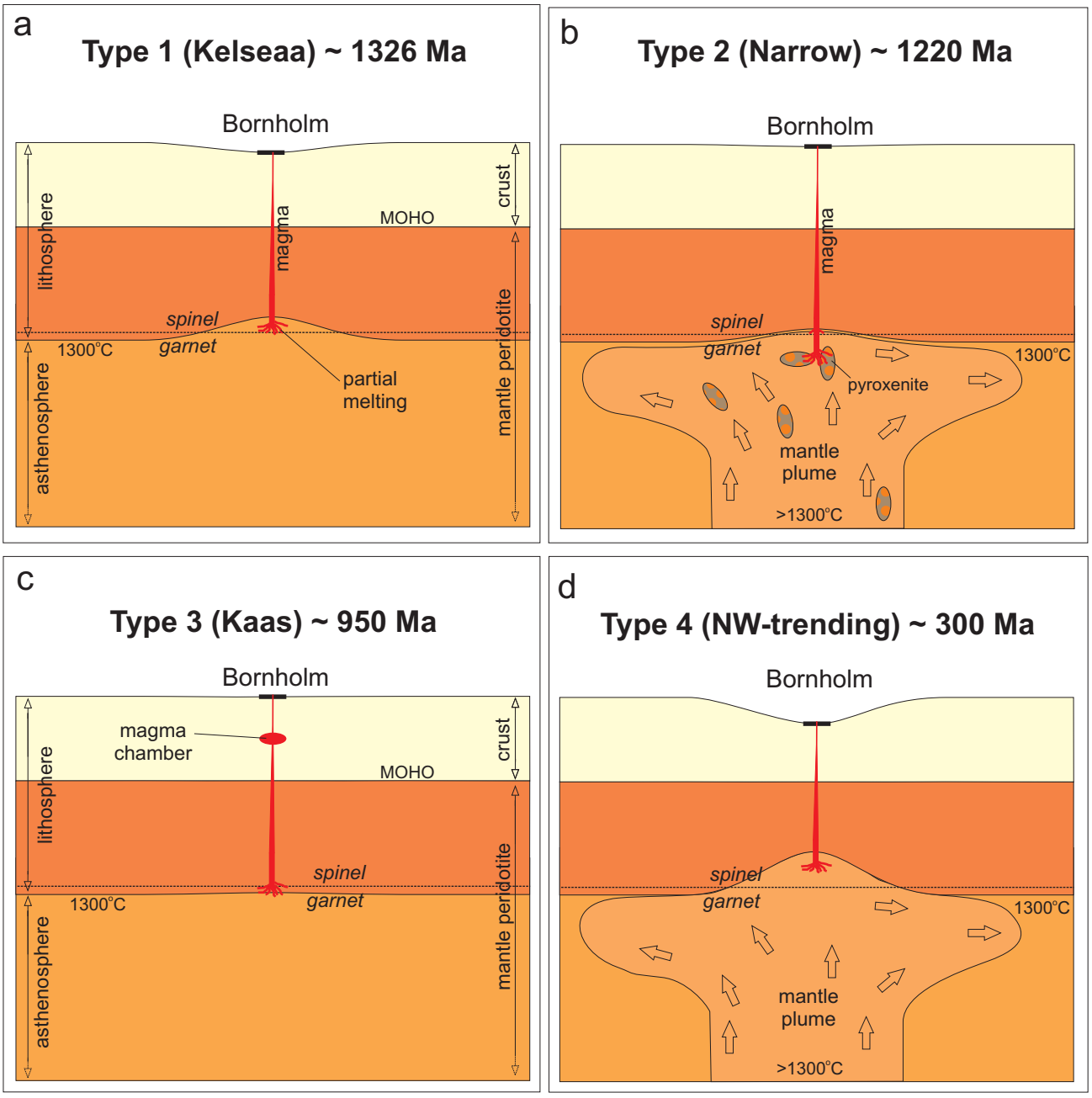

Figure 16: Simplified schematic models for the melting regime for Bornholm mafic magmas. a) Melting mainly of depleted asthenospheric peridotite in the spinel stability field at c. 1326 Ma probably during an extensional tectonic environment in the lithosphere; b) melting of an abnormally hot (> 1300°C) pyroxenitic and peridotitic mantle plume mainly in the garnet stability field at c. 1220 Ma; c) melting of both garnet and spinel peridotite around 950 Ma; d) melting of enriched spinel peridotite probably in a mantle plume under a dilated lithosphere at c. 300 Ma. MOHO is the Mohorovic crust-mantle discontinuity; the 1300°C isotherm is used as the transition between lithospheric and asthenospheric mantle; the depth of the spinel-garnet transition is located at 70-90 km depending on the local temperature gradient.

Kaas and Listed (type 3)

The geochemistry of the evolved type 3 magmas is far removed from precursory mantle melts and may hold no clear indication of their origin. However, the HREE ratios would be expected to be relatively less changed during crustal residence in a magma chamber than more incompatible elements. From the appearance in Fig. 14a these magmas may have originated in a mantle source with a considerable proportion of melts derived from the garnet stability field. Because of their evolved and contaminated nature it is not possible to constrain the possible mantle source(s) further.

NW-trending dykes (type 4)

The Permian dykes seem to have been derived at somewhat shallower depths than type 2 magmas, $Tb/Yb_N < 2$ (Fig. 14), and by slightly larger degrees of melting, provided they had a similar mantle source. This is also suggested by their quartz normative nature and from Zr-Nb modelling (Fig. 15a). Significant lithospheric thinning probably took place at this time. Type 4 magmas were generated from a source with low Ba/Nb (< 10) and more enriched in HFSE than that of other Bornholm magmas, and comparable to the source of several hot spots (Figs. 11, 12, 13, 15). Together with the rather shallow, and high degree of melting indicated from REEs (Fig. 14), this strongly suggests that a hot plume source rose in the Permian.

Bornholm and the evolution of the Baltic shield

The Kelseaa dyke was intruded about 100 Ma after a major rejuvenation of the Gothic crust at 1.45 Ga according to the extensive data base for the gneiss and granites of Bornholm (Tschernoster, 2000; ĜĞŷs, 2004; Obst et al., 2004, Zariņš & Johansson, 2008). It therefore seems most likely that this major dyke marks a NE-trending rifting event of Baltica at around 1326 Ma. The N- to NE-trending Kungsbacka bimodal suite (1.34-1.30 Ga) south of Lake Vänern and west of the Protogine Zone and related dolerite with an age of just under 1.30 Ga have recently been suggested to be emplaced during a continental rifting event (Austin Hegardt et al., 2007; Söderlund et al., 2008). Although these occurrences are > 200 km apart, they are the only reported events at the time of the Kelseaa intrusion. In the case of the Kelseaa magma, rifting most likely developed in a back-arc setting.

The events forming the CSDG took place in the interval 1270-1250 Ma and have been explained as being related to extension behind an active margin with subduction along the Laurentia-Baltica continental margin preceding Rodinia formation (Söderlund et al., 2006). Solyum et al. (1992) considered that the CSDG was intracratonic and unrelated to continental rifting. However, the CSDG seems to be somewhat earlier than the type 2 dykes (c. 1220 Ma) of Bornholm.

Datings of zircon and baddeleyite from ultramafic, mafic and felsic intrusions including N-S trending dolerites in the Protogine zone define two distinct magmatic events at c. 1204 and c. 1220 Ma (Söderlund et al., 2004; Söderlund et al., 2005, Söderlund & Ask, 2006), significantly older than the c. 1180 Ma previously suggested by Johansson & Johansson (1990). These events then seem contemporaneous with the type 2 Bornholm dykes. The Protogine Zone magmatic events were thought to be related to back-arc spreading during the closure of an ocean from 1.25 Ga until 1.13 Ga at the beginning of the Sveconorwegian orogeny (Söderlund & Ask, 2006). The new precise age information for the Protogine Zone magmatism separates this from both the Gardar and the MacKenzie events (LeCheminant & Heaman, 1989; Upton et al., 2003). However, the composition of the Protogine Zone Dolerite Group (PZDG) (Solyum et al., 1992) is very different from the type 2 dykes of Bornholm, for which we suggest a mantle plume origin, and they were probably not related.

The Blekinge Dalarne Dolerite Group (BDDG) was intruded at 978-945 Ma based on U-Pb and Lu-Hf on baddeleyite and zircon (Söderlund et al., 2004, Söderlund et al., 2005). This is somewhat earlier than the c. 930 Ma based on Sm-Nd whole rock isochrons (Johansson & Johansson, 1990) which are in accordance with most of Rb-Sr age determinations of Patchett (1978). These dykes occur in a zone parallel to the Protogine Zone and extend for 700 km from Dalarne in the north to the south coast of Blekinge where they trend approximately N-S just north of Bornholm (Fig. 1). The Sveconorwegian and Grenvillian orogenies took place in the period 1.13 – 0.95 Ga (Andréasson & Rohde, 1990) with peak metamorphism at 972 Ma (Johansson et al., 2001). Solyum et al. (1992) considered that the BDDG were emplaced as part of the earliest phase of a late Proterozoic rifting of Baltica which encompassed graben formation in the Protogine Zone (Andréasson & Rodhe, 1990). Söderlund & Ask (2006) described the intrusion of the BDDG as contemporaneous with exhumation of the high-grade rocks of the orogeny and taking place in the Sveconorwegian foreland, and suggested that the graben formation at lake Vättern in the Protogine Zone was an analogue to the Permian Oslo rift. The Kaas and Listed dykes are quite similar to some BDDG dykes and may be part of these events.

The NW-trending Permian dykes, including the

trachytic Bjergebakke dyke, have been correlated with the Scania dykes of similar age (Obst et al. 2000), and are thus related to the Oslo rift and other rifts in the Skagerrak and the North Sea, and in general to the breakup of Pangea.

Conclusions

The more than 250 dykes on Bornholm represent significant events of mafic magmatism related to rifting at the edge of the Baltic craton in the mid to late Proterozoic and Permian. The dykes occur in all basement rocks, although more rarely in the granites than in the gneisses. In four dyke swarms basaltic materials constitute 10 - 20 % of the crust. The dykes comprise four distinct types based on age information, mode of occurrence, petrography and geochemistry:

1) The Kelseaa dyke and Kelseaa-like dykes at 1326 Ma are NE-trending olivine tholeiites comprising the 60 m Kelseaa gabbroic-doleritic dyke and two others.

The Kelseaa magmas were derived from depleted mantle enriched in fluid-mobile elements and contaminated in the crust, probably in a back-arc setting. One Kelseaa-like dyke has N-MORB character.

2) More than 200 narrow NNW- to NNE-trending dykes probably intruded around 1220 Ma. Most of them are alkali basalts-trachybasalts-basanites with potassic character. A few differentiates range to phonotephritic compositions. One subtype of basanitic or potassic trachybasaltic composition is particularly enriched in incompatible elements.

The magmas of the narrow dykes may be related by fractionation of olivine, followed by olivine + clinopyroxene to a few more evolved dykes. They were mainly derived from a mantle plume. The plume source of recycled oceanic crust consisted of typical OIB-type peridotite and probably a garnet pyroxenite of gabbroic origin. A more enriched subgroup was derived at greater depths by a few percent melting of peridotite, probably at higher temperatures. The narrow dykes may be contemporaneous with the Protogine Zone Dolerite Group of southern Sweden, but have a different origin.

3) The large dykes at Listed and Kaas, and some Kaas-like smaller dykes, comprise a group of evolved transitional rocks (shoshonites and mugearites) intruded around 950 Ma.

The source of the Kaas-Listed dykes was rather depleted, probably sublithospheric mantle. Geochemically they resemble the c. 950 Ma Blekinge Dalarne Dolerite Group and may be closely related to these.

4) A few WNW- and NW-trending dykes are Permian (c. 300 Ma old) quartz tholeiites.

The magmas injected in the NW-trending dykes were derived at rather shallow depths by relatively high degrees of melting of most likely a hot mantle plume. The source displays a distinct OIB-type geochemistry different from the narrow dyke sources, and was more enriched than sources for other Bornholm dyke magmas.

Acknowledgements

We thank John Bailey for trace element XRF analyses and Raymond Gwozdz for INA analyses. We are grateful for the help from Trine Dirks with collection of some of the samples and for company in the field of B. and H. Viuf and B. and H. Jensen. Niels Abrahamsen and Asger Ken Pedersen contributed with contructive reviews that improved the paper, and the comments and editorial handling of J. Richard Wilson are greatly acknowledged.

Dansk sammendrag

Bornholms mafiske gange repræsenterer mellem proterozoiske til permiske magmatiske hændelser i randen af Det Baltiske Kraton. Flere hundrede gange er intruderede i det prækambriske grundfjelds gnejser og graniter. Feltforhold og 60 nye kemiske analyser af hoved- og sporgrundstoffer præsenteres. Gruppering baseret på evidens fra felten, geokemi og petrologi indikerer at gangintrusionerne kan korreleres med begivenheder for henholdsvis 1326 Ma (Kelseaa gangen), 1220 Ma (de smalle gange), 950 Ma (Kaas-Listed gangene) og 300 Ma (NW- eller WNW-strygende gange) siden. Den største gang ved Kelseaa (60 m bred) og nogle relaterede gange er primitive olivin tholeiiter af hvilke en har N-MORB (normaltype midtoceanrygsbasalt) geokemiske træk; alle er skorpekontaminerede. Kelseaa-type magmaer blev dannet i ret ringe dybde fra en fluid-beriget relativt forarmet kappekilde, men nogle har en komponent, som er dannet fra en kappekilde med residual granat. Deres dannelse foreslås at være i et backarc-miljø.

De mere end 200 smalle gange er olivin tholeiiter (hvoraf nogle er pikritiske), alkali basalter, trachybasalter og basaniter (hvoraf nogle er pikritiske), og omfatter kun få udviklede phonotephriter. Magmaerne udvikledes ved olivin og olivin + clinopyroxenfraktionering. De har sporgrundstof geokemiske karaktertræk, som kan beskrives hovedsaglig ved to komponenter, af hvilke en er et typisk OIB-magma (OIB = oceanøbasalt) (La/Nb < 1, Zr/Nb = 4, Sr/Nd = 16) og afledt fra spinel peridotit i et temmelig højt kappeniveau, hvorimod den anden er beriget på Sr,

har La/Nb = 1.0-1.5, Zr/Nb = 9, Sr/Nd = 30, og var afledt fra større dybde fra en oprindeligt gabbroisk kilde. Begge kilder var sandsynligvis recirkuleret materiale i en kappediapir. Et mindre antal af disse gange er meget mere beriget i inkompatible grundstoffer og blev dannet fra granatperidotit ved en lav grad af opsmeltning. De få andre store gange (20-40 m) og relaterede gange er alle udviklede trachybasalter og basaltiske trachyandesiter. De synes at være relaterede til Blekinge-Dalarne doleritgruppen. De få NW-gående gange er kvarts tholeiiter, som blev dannet ved en høj grad af opsmeltning under relativt lavt tryk af en mere beriget kappe end andre bornholmske gange. Dette implicerer at kappen formentlig var en meget varm diapir.

References

Åberg, G. 1988: Middle Proterozoic anorogenic magmatism in Sweden and worldwide. Lithos 21, 279-289.

Abrahamsen, N. 1977: Palaeomagnetism of 4 dolerite dykes around Listed, Bornholm Denmark . Bulletin of the Geological Society of Denmark 26, 245-264.

Abrahamsen, N. & Lewandowski, M. 1995: Palaeomagnetism of Proterozoic dykes from Bornholm, Denmark. Geophysical Journal International 121, 949-962.

Anders, E. & Grevesse, N. 1989 Abundances of the elements: Meteoritic and solar. Geochmica Cosmochimica Acta 53, 197-214.

Andréasson, P.-G. & Rodhe, A. 1990: Geology of the Protogine Zone south of lake Vättern, Southern Sweden: a reinterpretation. Geologiska Föreningens i Stockholm förhandlingar 112, 107-126.

Austin Hegardt, E., Cornell, D.H., Hellström F.A. & Lundqvist, I. 2007: Emplacement ages of the mid-Proterozoic Kungsbacka Bimodal Suite, SW Sweden. Geologiska Föreningens i Stockholm förhandlingar 129, 227-234.

Berthelsen, A. 1989: Bornholms grundfjeld. Varv 1989,1, 3-39.

Berthelsen, A. 1992: Mobile Europe. In: D. Blundell, R. Freeman & S. Mueller (Editors), A Continent Revealed: The European Geotraverse. Cambridge University Press, Cambridge, pp. 11-32.

Bogdanova, S.V. 2001: Tectonic settings of 1.65-1.4 Ga AMCG magmatism in the western East European Craton, western Baltica. Journal of Conference Abstracts 6, 769.

Bogdanova, S.V., Bingen, B., Gorbatschev, R., Kheraskova, T.N., Kozlov, V.I., Puchkov, V.N. & Volozh, Y.A. 2008: The East European Craton Baltica before and during the assembly of Rodinia. Precambrian Research 160, 23-45.

Bruun-Petersen, J. 1975: Origin and correlation of the sandstone dykes at Listed, Bornholm Denmark. Bulletin of the Geological Society of Denmark 24, 33-44.

Callisen, K. 1934: Das Grundgebirge von Bornholm. Danmarks Geologiske Undersøgelse, II. række 50, 266 pp.

c̆c̆s, A. 2004: Tectonic implications of the ca. 1.45 Ga granitoid magmatism at the southwestern margin of the East European Craton. Unpublished Ph. D. thesis, University of Lund, Sweden, 115 pp.

c̆c̆s, A. & Benn, K. 2007: Emplacement and deformation of the c. 1.45 Ga Karlshamn granitoid pluton, southeastern Sweden, during ENE-WSW Danopolonian shortening. International Journal of Earth Sciences 96, 397-414.

Chauvel, C. & Hémond, C. 2000: Melting of a complete section of recycled oceanic crust: trace element and Pb isotopic evidence from Iceland. Geochemistry, Geophysics, Geosystems 1, 1999GC000002.

Clague, D.A. & Frey, F.A. 1982: Petrology and Trace Element Geochemistry of the Honolulu Volcanics, Oahu: Implications for the Oceanic Mantle below Hawaii. Journal of Petrology 23, 447-504.

Dupuy, C., Barsczus, H.G., Liotard, J.-M. & Dostal, J. 1988: Trace element evidence for the origin of ocean island basalts: An example from the Austral Islands. Contributions to Mineralogy and Petrology 98, 293-302.

Eisele, J., Sharma, M., Galer, S.J.G., Blichert-Toft, J., Devey, C.W. & Hofmann, A.W. 2002: The role of sediment recycling in EM-1 inferred from Os, Pb, Hf, Nd, Sr isotope and trace element systematics of the Pitcairn hotspot. Earth and Planetary Science Letters 196, 197-212.

Forchhammer, G. 1847: Gebirgsbildung des Königsreichs Dänemarks. Copenhagen.

Gorbatschev, R., Solyom, Z. & Johansson, I. 1979: The Central Scandinavian Dolerite Group in Jämtland, central Sweden. Geologiska Föreningens i Stockholm förhandlingar 101, 3, 177-190.

Hofmann, A.W. 1988: Chemical differentiation of the Earth: the relationship between mantle, continental crust, and oceanic crust. Earth and Planetary Science Letters 90, 297-314.

Hofmann, A.W. 1997: Mantle geochemistry: the message from oceanic volcanism. Nature 385, 219-229.

Holm, P.M., Heaman, L.M. & Pedersen, L.E. 2005: First direct age determination for the Kelseaa Dolerite Dyke, Bornholm, Denmark. Bulletin of the Geological Society of Denmark 52, 1-6.

Holm, P.M., Wilson, J.R., Christensen, B.P., Hansen, L., Hansen, S.L., Hein, K.M., Mortensen, A.K., Pedersen, R., Plesner, S. & Runge, M. 2006: Sampling the Cape Verde Mantle Plume: Evolution of Melt Compositions on Santo Antão, Cape Verde Islands. Journal of Petrology 47, 145-189.

Jensen, A. 1966: Mineralogical variations across two dolerite dykes from Bornholm. Meddelelser fra dansk geologisk Forening 16, 370-455.

Jensen, A. 1988: The Bjergebakke dyke - a kullaite from Bornholm. Bulletin of the Geological Society of Denmark 37, 123-140.

Johansson, L. & Johansson, Å. 1990: Isotope geochemistry and age relationships of mafic intrusions along the Protogine Zone, southern Sweden. Precambrian Research 48, 395-414.

Johansson, L., Möller, C. & Söderlund, U. 2001: Geochronology of eclogite facies metamorphism in the Sveconorwegian Province of SW Sweden. Precambrian Research 106, 261-275.

Johansson, Å. & Larsen, O. 1989: Radiometric age determinations and Precambrian geochronology of Blekinge, southern Sweden. Geologiska Föreningens i Stockholm förhandlingar 111, 1, 35-50.

Johansson, Å., Bogdanova, S. & c̆c̆s, A. 2006: A revised geochronology for the Blekinge Province, southern Sweden. Geologiska Föreningens i Stockholm förhandlingar 128, 287-302.

Klein, E.M., & Langmuir, C.M. 1987: Global correlation of ocean ridge basalt chemistry with axial depth and crustal thickness. Journal of Geophysical Research 92, 8090-8115.

Klingspor, I. 1976: Radiometric age-determination of basalts, dolerites and related syenite in Skåne, southern Sweden. Geologiska Föreningens i Stockholm förhandlinger 98, 195-216.

Kokfelt, T.F., Hoernle, K., Hauff, F., Fiebig, J., Werner, R. & Garbe-Schönberg, D. 2006: Combined Trace Element and Pb-Nd-Sr-O Isotope Evidence for Recycled Oceanic Crust (Upper and Lower) in the Iceland Mantle Plume. Journal of Petrology 47, 9, 1705-1749.

Larsen, O. 1980: Geologisk aldersbestemmelse ved isotopmålinger. Dansk Natur - Dansk Skole, årsskrift for 1980, 89-106.

Le Bas, M.J. 2000: Reclassification of the high-Mg and picritic volcanic rocks. Journal of Petrology 41, 1467-1470.

LeCheminant, A.N. & Heaman, L.M. 1989: MacKenzie igneous events, Canada: middle Proterozoic hotspot magmatism associated with ocean opening. Earth and Planetary Science Letters 96, 38-48.

Le Maitre, R. W. 1989: A Classification of Igneous Rocks and Glossary of Terms. Blackwell Scientific Publications, Oxford, 193 pp.

Lewandowski, M. & Abrahamsen, N. 2003: Paleomagnetic results from the Cambrian and Ordovician sediments of Bornholm (Denmark) and Southern Sweden and paleogeographical implications for Baltica. Journal of Geophysical Research 108, 2516, doi: 10.1029/2002JB002281.

McDonough, W.F. & Sun, S.-s. 1995: The composition of the Earth. Chemical Geology 120, 223-253.

McKenzie, D., & O'Nions, R.K. 1991: Partial Melt Distribution from Inversion of Rare Earth Element Concentrations. Joural of Petrology 32, 1021-1091.

Micheelsen, H.I, 1961. Bornholms grundfjæld. Meddelelser fra dansk geologisk Forening 14, 308-347.

Middlemost, E.A.K. 1989: Iron oxidation ratios, norms and the classification of volcanic rocks. Chemical Geology 77, 19-26.

Münther, V. 1945a: Diabasgangene paa Bornholm: En undersøgelse af de vigtigste bornholmske Sprækkedale og en redegørelse for Diabasens Relation til Granitens Forkløftning, 217pp. Unpublished prize paper. University of Copenhagen, Copenhagen.

Münther, V. 1945b: Sprækkedale og diabasintrusioner på Bornholm. Meddelelser fra dansk geologisk Forening 10, 641-645.

Münther, V. 1973. Dominerende forkastninger på Bornholm. Danmarks Geologiske Undersøgelse, II. række 85, 161 pp.

Obst, K. 2000: Permo-Carboniferous dyke magmatism on the Danish island Bornholm. Neues Jahrbuch der Geologie und Paläontologie Abhandlungen 218, 243-266.

Obst, K., Hammer, J., Katzung, J. & Korich, D. 2004: The Mesoproterozoic basement in the southern Baltic Sea: insights from the G 14-1 off-shore borehole. International Journal of Earth Sciences 93, 1-12.

Palacz, Z. & Saunders, A.D. 1986: Coupled trace element and isotope enrichment in the Cook-Austral-Samoa islands, southwest Pacific. Earth and Planetary Science Letters 79, 270-280.

Patchett, P. J. 1978: Rb/Sr ages of Precambrian dolerites and syenites in southern and central Sweden. Sveriges Geologiska Undersökning, ser. C 747, 63pp.

Patchett, P.J., Lehnert, K., Rehkämper, M. & Sieber, G. 1994: Mantle and crustal effects on the geochemistry of Proterozoic dikes and sills in Sweden. Journal of Petrology 35: 1095-1125.

Platou, S.W. 1970: The Svaneke granite complex. Bulletin of the Geological Society of Denmark 20, 93-133.

Rudnick, R.L. & Gao, S. 2003: Composition of the Continental Crust. In: Turekian, K.K. & Holland, H.D. (Editors.) Treatise of Geochemistry. Elsevier, Chapter 3.01, 64pp.

Saxov, S. 1958: Keldseå Diabas Dike and Gravity, Geodætisk Institut Meddelelse No. 35.

Söderlund, U. & Ask, R. 2006: Mesoproterozoic bimodal magmatism along the Protogine Zone, S Sweden: three magmatic pulses at 1.56, 1.22 and 1.205 Ga, and regional implications. Geologiska Föreningens i Stockholm förhandlingar 128, 303-310.

Söderlund, U., Patchett, P. J., Vervoort, J. D. & Isachsen, C. E. 2004: The decay constant of ^{176}Lu determined from Lu-Hf and U-Pb isotope systematics of terrestrial Precambrian high-temperature mafic intrusions. Earth and Platetary Science Letters 219, 311-324

Söderlund, U., Isachsen, C.E., Bylund, G., Heaman L.M., Patchett, P.J., Vervoort, J.D. & Andersson U.B. 2005: U-Pb baddeleyite ages and Hf, Nd isotope chemistry constraining repeated mafic magmatism in the Fennoscandian Shield from 1.6 to 0.9 Ga. Contributions to Mineralogy and Petrology 150, 174-194.

Söderlund, U., Elming, S.-Å., Ernst, R.E. & Schissel, D. 2006: The Central Scandinavian Dolerite Group – Protracted hotspot activity or back-arc magmatism? Constraints from U-Pb baddeleyite geochronology and Hf isotopic data. Precambrian Research 150, 136-152.

Söderlund, U., Hellström F.A. & Kamo S.L. 2008: Geochronology of high-pressure mafic granulite dykes in SW Sweden: tracking the P-T-t path of metamorphism using Hf isotopes in zircon and baddeleyite. Journal of Metamorphic Geology 26, 539-560.

Solyom, Z., Lindqvist, J.-E. & Johansson, I. 1992: The geochemistry, genesis, and tectonic setting of Proterozoic mafic dyke swarms in southern and central Sweden. Geologiska Föreningens i Stockholm förhandlingar 114, 47-65.

Stracke, A. & Bourdon, B. 2009: The importance of melt extraction for tracing mantle heterogeneity. Geochimica Cosmochimica Acta 73, 218-238.

Sun, S.-s. & McDonough, W.F. 1989: Chemical and isotopic systematics of oceanic basalts: implications for mantle composition and processes. In: A.D. Saunders & M.J. Norry (Editors) Magmatism in the ocean basins. Geological Society of London Special Publication 42, 313-345.

Surlyk, F. 1980: Denmark. In: Geology of the European Countries, Proceedings of the 26th International Geological Congress, Paris. Graham & Trotman Ltd, Bordas, pp.1-50.

Tschernoster, R. 2000: Isotopengeochemische Untersuchungen am Detritus der Dänisch-Norddeutsch-Polnischen Kaledoniden und deren Vorland. Unpublished Ph.D. thesis, Rheinisch-Westfälischen Technischen Hochschule, Aachen, 128 pp.

Tainton, K.M. & McKenzie, D. 1994: The generation of kimberlites, lamproites, and their source rocks. Journal of Petrology 35, 787-817.

Ulmer, P. 1989: Partitioning of high field strength elements among olivine, pyroxenes, garnet and calc-alkaline picrobasalt: experimental results and an application. Annual Report of the Director of the Geophysical Laboratory 1988/1989: 42-47.

Upton, B.G.J., Emeleus, C.H., Heaman, L.M., Goodenough, K.M. & Finch, A.A. 2003: Magmatism of the mid-Proterozoic Gardar Province, South Greenland: chronology, petrogenesis and geological setting. Lithos 68, 43-65.

Weaver, B.L. 1991: The origin of ocean island basalt end-mem-

ber compositions: trace element and isotopic constraints. Earth and Planetary Science Letters 104, 381-397.
Weaver, B.L., Wood, D.A., Tarney, J. & Joron, J.-L. 1987: Geochemistry of ocean island basalts from the South Atlantic: Ascension, Bouvet, St. Helena, Gough and Tristan da Cunha. In: J.G. Fitton & B.G.J. Upton (Editors), Alkaline Igneous Rocks. Geological Society of London Special Publication 30, 253-267.
Woodhead, J.D. 1996: Extreme HIMU in an oceanic setting: the geochemistry of Mangaia Island (Polynesia), and temporal evolution of the Cook-Austral hotspot. Journal of Volcanology and Geochermal Research 72, 1-19.
Zariņš, K. & Johansson Å. 2008: U-Pb geochronology of gneisses and granitoids from the Danish island of Bornholm: new evidence for 1.47-1.45 Ga magmatism at the southwestern margin of the East European Craton. International Journal of Earth Sciences. doi 10.1007/s0531-008-0333-0.
Zindler, A. & Hart, S.R. 1986: Chemical geodynamics. Annual Reviews in Earth and Planetary Sciences 14, 493-571.

Appendix

Comparison between measured and reference values for some standards, internal analytical precision and detection limits for XRF, INAA and ICP-MS trace element analyses.

	XRF				INAA					ICP-MS							
Element	Precision rel% (1•)	LLD$ meas@ ppm	Standard AGV-1 meas@ ppm	AGV-1 Ref.* ppm	Precision rel% (1•)	LLD$ meas@ ppm	Standard BHVO1 meas@ ppm AVG	1•• ppm N=5	Ref.* ppm	LLD$ meas@ ppm	Blank meas@ ppm	Standards DNC-1 meas@ ppm	DNC-1 Ref.* ppm	W-2a meas@ ppm	W-2a Ref.* ppm	BIR-1a meas@ ppm	BIR-1a Ref.* ppm
Sc	5	<1	13	12.1	0.2	0.006	31.7	0.5	31.8	1		31	31	36	36	43	44
V	5	<3	119	123						5		156	148	281	262	336	313
Cr	5	<3	11	12						20	< 20	290	285	90	92	380	382
Co	4	<1	12.5	15						1	< 10	56	54.7	43	43	50	51.4
Ni	2	<1	14	17						20	< 30	260	247	60	70	150	166
Cu	5	<2	58	60						10	< 1	100	96	110	110	120	126
Zn	5	<1	84	88						30	< 0.5	120	66	130	80	100	71
Ga	5	<1	20	20						1	< 5	14	15	17	17	14	16
Rb	2	<0.5	66	67						2	< 1	4	4.5	20	21	< 2	0.25
Sr	1	<0.5	652	662						2		142	145	195	190	108	108
Y	5	<1	20	21						2	< 20	13	18	17	24	11	16
Zr	2	<1	223	225						4	< 1	47	41	98	94	23	16
Nb	2	<0.5	14.4	15						1	< 0.2	1	3	7	7.9	< 1	0.6
Ba	2	<1	1204	1221	8	26	139	16		3		102	114	168	182	7	7
La	2	<1	38	38	0.7	0.07	16.3	0.4	13.8	0.1	< 0.05	3.6	3.8	10.2	10	0.7	0.62
Ce	2	<2	69	66	0.4	0.45	39	3	39	0.1	< 0.05	8	10.6	22.5	23	2	1.95
Nd	4	<1	34	34	10	5	27.1	1.9	25.2	0.1	< 0.05	4.7	4.9	12.1	13	2.2	2.5
Sm					0.6	0.05	6.2	0.4	6.2	0.1	< 0.01	1.4	1.38	3.1	3.3	1	1.1
Eu					0.6	0.009	2.07	0.03	2.06	0.05	< 0.005	0.59	0.59	1.08	1	0.52	0.54
Tb					8	0.07	1.03	0.1	0.96	0.1	< 0.01	0.4	0.41	0.7	0.63	0.4	0.36
Yb					5	0.1	1.6	0.2	2.02	0.1	< 0.01	2	2.01	2	2.1	1.6	1.65
Lu					5	0.02	0.27	0.05	0.291	0.04	< 0.002	0.3	0.32	0.3	0.33	0.25	0.26
Hf					0.6	0.05	4.4	0.2	4.38	0.2	< 0.1	1.1	1.01	2.6	2.6	0.7	0.6
Ta					1	0.03	1.17	0.08	1.23	0.1	< 0.01	0.1	0.098	0.5	0.5	< 0.1	0.04

*) Govindaraju, k. (1994) Geostandards Newsletter 18, Special Issue, 1-158. $) LLD = Lower Limit of Detection. @) Measured value

A new echinoderm faunule from the Lower Jurassic (Pliensbachian) of southern Sweden

AARON W. HUNTER & JAN REES

Hunter, A.W. & Rees, J. 2010–xx–xx. A new echinoderm faunule from the Lower Jurassic (Pliensbachian) of southern Sweden. © 2010 by Bulletin of the Geological Society of Denmark, Vol. 58, pp. 66–73. ISSN 0011–6297. (www.2dgf.dk/publikationer/bulletin)

In Sweden, Jurassic echinoderms are extremely rare. This present study documents an Early Jurassic echinoderm assemblage collected from a temporary exposure near Helsingborg in Skåne, southern Sweden, which includes a previously undescribed species of isocrinid crinoid, *Isocrinus ranae* sp. nov., and an acrosaleniid echinoid. The Swedish specimens demonstrate that even limited echinoderm material from small exposures can be assigned to a high systematic level and provide data of considerable significance to the evolution of the group as a whole.

Keywords: crinoids, echinoids, taphonomy, palaeoecology, Lower Jurassic, Skåne, Sweden.

Aaron W. Hunter[a.hunter@nhm.ac.uk], Department of Earth and Planetary Science, University of Tokyo, Hongo, Tokyo, 113-0033, Japan. & Department of Palaeontology, Natural History Museum, Cromwell Road, London SW7 5BD United Kingdom. Jan Rees [jan.rees@kau.se], Department of Biology, Karlstad University, SE-651 88 Karlstad, Sweden.

Echinoderms are uncommon in the Jurassic of the Nordic countries, owing to the areas of outcrop largely being restricted to southern Sweden and the island of Bornholm (Denmark). As a result, very few Jurassic crinoids have been formally described from Scandinavia, with Simms (1989) only mentioning one *nomen dubium* from this area. Moberg (1888) first mentioned the existence of up to four species of '*Pentacrinus*' in the 'Lias' of southeastern Skåne, exposed at Kurremölla, including the new species *P. patulus* Moberg, 1888.

Simms (1989) regarded *P. patulus* as *nomen dubium* and the specimens referable to the genera *Balanocrinus* and/or *Isocrinus*. The other three taxa in Moberg (1888) are *P.* cf. *basaltiformis*, (now included in *Isocrinus*; Simms 1989), *P.* cf. *subteroides* (now referred to the genus *Balanocrinus*; Simms 1989) and *P.* sp. The deposits in this area have yielded a few ammonites indicating Sinemurian and/or early Pliensbachian age (Moberg 1888; Reyment 1959). In a monograph on the Early Jurassic of north-west Skåne, Troedsson (1951) recorded both the above-mentioned taxa found by Moberg (1888) in the southern part of Skåne and also discovered *P. scalaris* and *P. basaltiformis* in a temporary section through the Sinemurian and parts of the Pliensbachian. Here, we re-examine these early occurrences of Early Jurassic crinoids from Sweden and describe new material collected from a temporary outcrop exposing Pliensbachian strata. This study attempts to demonstrate that these occurrences, however localised and poorly preserved, are significant in the documentation of the Early Jurassic normal marine echinoderm fauna more commonly associated with England, France and Germany (Jäger 1985a & b Simms 1989, Jäger 1990, 1991). We shall not only attempt to identify the disarticulated remains, but will also try to judge their palaeoecological and palaeoenvironmental significance, despite their geographical disparity to other regions under investigation.

Geology and stratigraphy

In Sweden, Upper Triassic and Jurassic strata occur exclusively in the southernmost province of Skåne (Fig. 1), and the largest continuous area is situated in the northwestern part of the province. Smaller areas of Jurassic surface bedrock are also located in central Skåne and the Vomb Trough in southern Skåne. The

most complete Lower Jurassic succession can be found in the northwesterly area overlying mainly deltaic and floodplain deposits of the Hettangian Höganäs Formation, are marine sandstones, siltstones and clays deposited through much of the remaining Early Jurassic. These sediments are included in the Rya Formation, and range in age from the Sinemurian to the Aalenian (e.g. Norling *et al*. 1993). Large portions of this marine succession are richly fossiliferous, including both ammonites and foraminifera, and the stratigraphy is well established (Reyment 1959; Norling 1972). Sinemurian sedimentation started with the deposition of coarse-

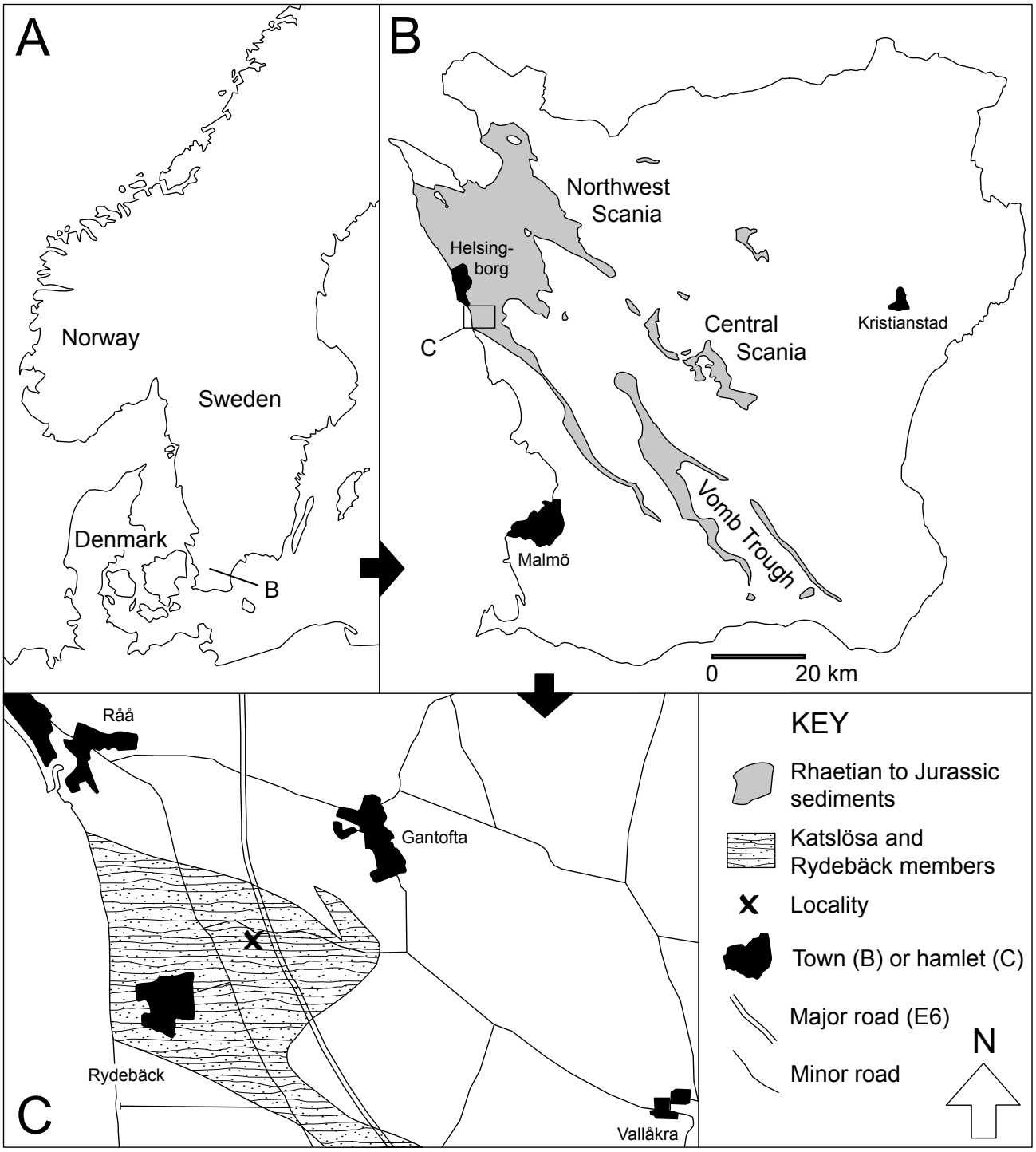

Fig. 1. A, the location of Skåne in Scandinavia. B, the extension of Rhaetian and Jurassic sediments in the province (based on map Ba 43 from the Geological Survey of Sweden). C, Katslösa and Rydebäck members as surface bedrock in the enlarged area (based on map Af 149 from the Geological Survey of Sweden) and the locality at the X. Modified from Rees (2000).

grained sandstones and siltstones, and these are followed by clays and marls that were laid down throughout the rest of the Sinemurian and Pliensbachian, with the exception of a short interval of terrestrial deposits in the Pankarp Member (Norling 1972; Norling *et al*. 1993). Strata of the Katslösa Member and Lower Jurassic portion the Rydebäck Member were deposited in a quiet environment below wave base (Norling *et al*. 1993). Crinoid columnals have previously been recorded by Troedsson (1951) from the Katslösa Member (see above).

The samples which yielded the echinoderm material described herein were collected from a temporary exposure accessible during the construction of a railway bridge over the road between the hamlets of Råå, Rydebäck and Gantofta (55°58′32″N, 12°47′36″E). The strata exposed included dark grey, poorly lithified silts and clays with patches of shell debris. Bioturbation was observed to be extensive within these sediments, and no other sedimentary structures were recorded. In addition to echinoderm remains, the samples yielded frequent belemnite rostra, bivalves, ostracods, foraminifera and fish remains, including shark teeth (Rees 2000). Ammonites were rare and fragmentary in the section sampled, but the rich foraminiferal fauna show strata to belong to the *Margaritatus* and *Spinatum* Zones in the late Pliensbachian (British Charmouthian or Domerian (see Simms 1989)), although some of the species recorded do suggest the slightly older *Davoei* Zone (E. Norling, pers. comm. 2000). It is thus likely that the samples collected encompass more than one ammonite zone.

Systematic palaeontology

The material described and figured is deposited in the Natural History Museum (Naturhistoriska riksmuseet) in Stockholm and numbered RM PZ X.

Class Crinoidea Miller, 1821
Subclass Articulata von Zittel, 1879
Order Isocrinida Sieverts-Doreck, 1952
Family Isocrinidae Gislén, 1925

Genus *Isocrinus* Agassiz, 1836;
[Syn. *Chladocrinus* Agassiz, 1836, see Simms 1989]

Type species. Isocrinus pendulus Agassiz, 1836 (see Simms 1989).

Diagnosis. After Simms (1989), a robust isocrinid. Stem pentalobate to pentagonal. Noditaxes of moderate length. Cirral scars of moderate size, directed outwards and slightly upwards. Symplectial areoles elliptical to slightly pyriform. Adradial crenulae of adjacent areolae generally separate and at slight angle to each other except near lumen. Cryptosymplectial articula with first and second order crenulae. Radial pores in proximal columnals indistinct. Basals small, separate, projecting slightly to overhang top of stem. Arms stout. Brachitaxes short to moderate length. Fulcral ridge of muscular articula often projected.

Isocrinus ranae sp. nov.
Figs 2.1-2.6

Holotype. The columnal Fig.2B (RM PZ 31445a) and pluri-columnals Fig.2D (RM PZ 31445b) are the named holotypes Fig.2A (RM PZ 31446a), Fig.2C(RM PZ 31446b), Fig.2E (RM PZ 31446c), Fig.2F (RM PZ 31446d) are named as paratypes.

Etymology. After Rán, the sea goddess in Norse mythology, who is the keeper of the drowned and the consort of Ægir, the ruler of the sea.

Type locality. Temporary exposure at a railway underpass between the hamlets of Råå, Rydebäck, and Gantofta (55°58′32″N, 12°47′36″E).

Type horizon and Bio-Zone. Temporary exposure, Pliensbachian, most likely *Margaritatus* or *Spinatum* zones(no ammonites found at the sampling area).

Material. Collection of disarticulated material from sieved mudstones, the residues include 58 pluricolumnals (RM PZ 31447a), eight columnals (RM PZ 31447b) and 10 brachials (IIBr) (RM PZ 31448). The specimen is described from columnals and using the classification defined by Simms (1989).

Diagnosis. 4-6 columnals per noditaxis. Columnal latera smooth, especially the interradii, some carinate tuberculation on the strongly developed radial epifacets. Interradii sharp to stellate and pentalobate, with low columnals. Adradial crenulations diminish in size towards the lumen. Crenulations are wide.

Description. Distal internodals are stellate (Fig. 2A-B) to pentalobate (Fig. 2C). The maximum internodal diameter is 6 mm and the smallest specimen has a diameter of 4 mm. No nodals are preserved. Nodal spacing is unclear, distal noditaxes with between five and seven columnals per noditaxis (Fig. 2D-F). Internodal height is low compared with internodal diameter. The latera of the columnals avaliable are slightly inflated between the margins (Fig. 2D), but are otherwise unornamented. A small epifacet is developed in

the radius with some tubercles developed on the epifacet (Fig. 2D & F). The tubercles on the epifacet are not continuous around each internodal. All internodals have symplectial articulations (Fig. 2A-C). The arrangement of crenulae on these is typical of the genus. No dorsal cup, cirri, or pinnules are found in the residue and the brachials are abraded but can be asigned to genus.

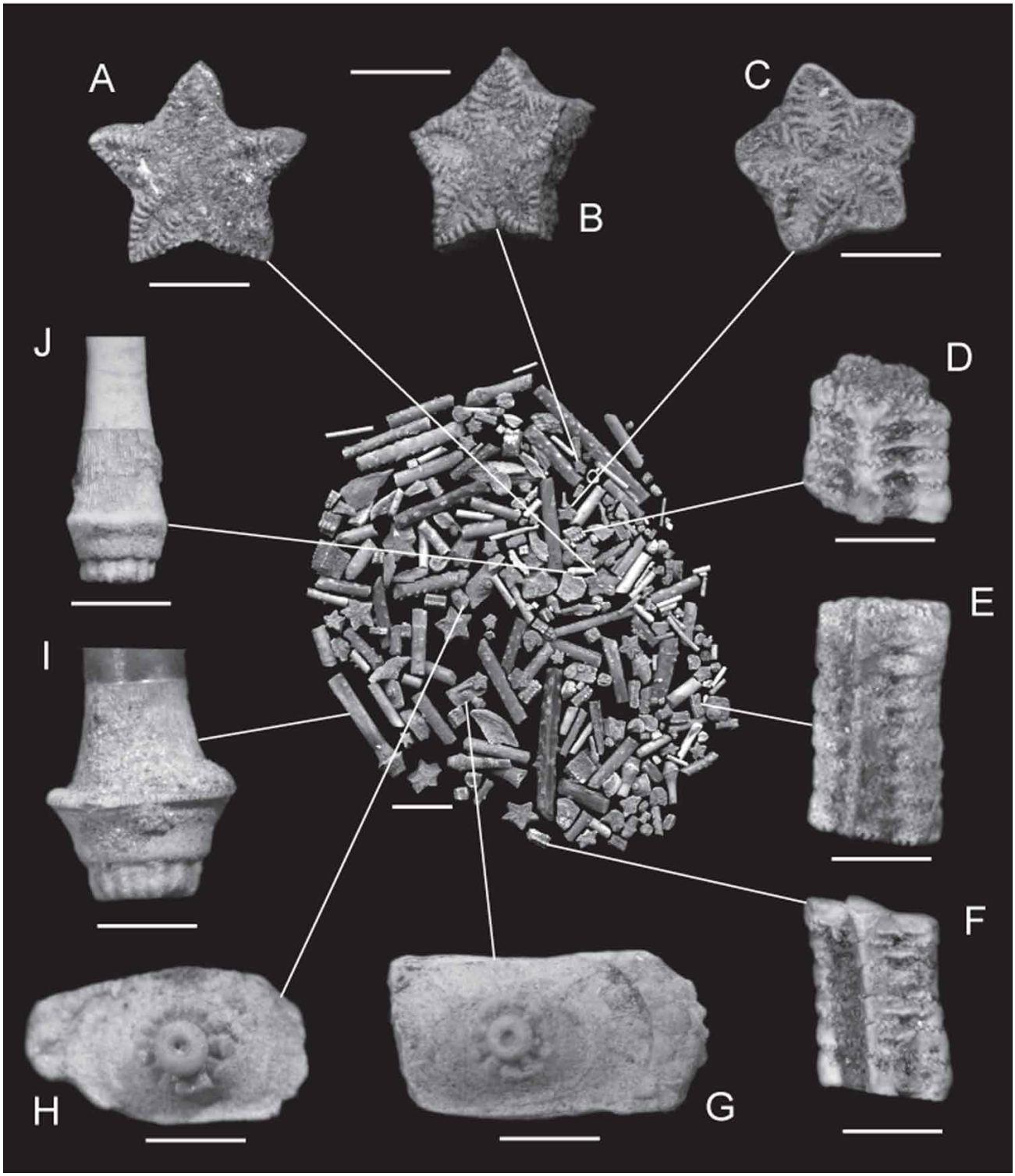

Fig. 2. Residue of the picked echinoderm material (centre, scale bar 10 mm). Specimens of *Isocrinus ranae* sp. nov. (A-C columnals (RM PZ 31447a), D-Fpluricolumnals (RM PZ 31447b)) and of ?Acrosaleniidae indet. Interambulacral G-H (RM PZ 31449a-b)- primary radioles (with bases) I-J (RM PZ 31450a-b)Scale bars 2 mm.

Remarks. It is quite possible that Moberg (1888) assigned the different conspecific columnals to separate species, as there are at least four species in his monograph, of which two can now be regarded as *nomina dubia*. There is a high morphological variation in crinoid columnals not recognised at that time, and members of the same species can have different shapes or even small variations in the crenulation pattern. The descriptions in Moberg (1888) are not very informative and it has not been possible to study his specimens during this investigation. Troedsson (1951) also clearly identified four species and hinted at two other morphotypes that share many of the diagnostic characters of *I. ranae*, such as smooth columnal latera, carinate tuberculation on the radial epifacets and low columnals. Troedsson (1951) recorded an unfigured specimen of *Pentacrinus scalaris* (now *Hispidocrinus scalaris*; Simms 1989), and illustrated specimens of *P. basaltiformis*, *P.* cf. *basaltiformi* and *P.* cf. *subteroides* (the latter is transferred to *Balanocrinus*; Simms 1989) at Katslösa. As these specimens were not studied first hand, it is difficult to confirm these designations. On examination of the plates in Troedsson (1951), we believe that *Balanocrinus subteroides* is correctly identified but we found no evidence of this species in our recently collected samples. It is common, however, for associated facies in the Lower and Middle Jurassic to have representatives of at least two genera of crinoids (Hunter & Zonneveld 2008). In addition, we believe that Troedsson (1951) provided few conclusive characters to provide a clear distinction between the 'pentagonal' *P. basaltiformis* and the more rounded *P.* cf. *basaltiformis* (now *Isocrinus basaltiformis*; see Simms 1989) which together are very likely to constitute the new species, *Isocrinus ranae*.

In comparison with other Isocrinidae from England and continental Europe, *Isocrinus ranae* is similar to the pre-Toarcian *Isocrinus psilonoti* (Quenstedt, 1858) in lacking ornament on columnal latera but the number of columnals per noditaxis is significantly lower. The new species differs from *Isocrinus tuberculatus* (Miller, 1821) in that it does not have tuberculate columnal latera and that the interradii are more rounded and tubercles less spinose in *I. tuberculatus* than in *Isocrinus ranae*. The number of columnals per noditaxis in *Isocrinus ranae* is only slightly lower than in *Isocrinus robustus* (Wright, 1858) and *I. basaltiformis* (Miller, 1821). *Isocrinus ranae* most closely resembles *I. robustus* in having tuberculate columnal latera with distinct epifacets but these epifacets are much more weakly developed in the *Isocrinus ranae* and are not continuous over the interradii (Fig. 2D). Both *I. ranae* and *I. basaltiformis* have sharp, commonly carinate interradii, with the absence of a continuous epifacet over the interradii, but *I. ranae* does not have spinose columnal latera (Fig. 2E). Consequently, *I. ranae* closely resembles both *I. basaltiformis* and *I. robustus*, with which it is roughly contemporaneous. Simms (1989) states that "the sharpness of the interradii and the relatively tall columnals are typical features of immature *Isocrinus*, and immature columnals of *I. robustus* are frequently difficult to distinguish from those of *I. basaltiformis*". The very low and flat columnals of *I. ranae*, however, clearly belong to an adult stage distinct from *I. basaltiformis* (Fig. 2F). *Isocrinus ranae* also displays many in common characters with the early Toarcian *I. rollieri* (de Loriol, 1886), particularly the shorter noditaxes and the general lack of tuberculation on columnal latera. It is distinct from *I. nudus* (Quenstedt, 1876), also from the Lower Toarcian, as it does not have inflation of columnal radii around the position of the radial pores.

Superorder Echinacea Claus, 1876
Order Salenioida Delage & Hérouard, 1903
Family ?Acrosaleniidae Gregory, 1900

Diagnosis. Primary spines relatively stout and fusiform, with cortex. Upper parts spinose, prominent crenulated tuberculation (Smith Echinoid Directory 2009).

Genus and species indet.
Fig. Interambulacral plates 2G-H (RM PZ 31449a-b)-primary radioles (with bases) 2I-J (RM PZ 31450a-b)

Material. 10 interambulacral plates (RM PZ 31451), 12 primary radioles (with bases) (RM PZ 31452), 53 primary radioles (RM PZ 31453). The plates are poorly preserved. Eight test plates preserving mamelons but lacking ambulacra, and 53 primary spines.

Description.
This specimen is described only from the preserved interambulacra and primary radioles.

Interambulacra plate boundaries are difficult to determine, as they are slightly abraded but rectangular (Fig. 2G). Some large granules are preserved on each plate. Scrobuler circles are separated by a prominent grove (Fig. 2G). The primary tubercles are perforated, and have 10-14 crenulations (Fig. 2G-H). no smaller tubercles are preserved. The primary tubercles are convex, rising from a sub-rounded flattened basal terrace (Fig. 2G). The mamelons have slightly undercut necks. The primary spines are long and spinose (7cm) flattened or circular in cross-section, the distal part of the spine is flattened and ornamented by rows of thorns. The proximal surface has longitudinal lines towards the base (Fig. 2I). The spine tapers proximally into a short neck and ends in a slightly ex-

panded base with small longitudinal groves around the sides (Fig. 2I).

Remarks. The tentative designation to the acrosaleniids is based on characters from the base of the spines and interambulacral test fragments, but with no ambulacral or apical plates preserved, designation beyond family level is not possible at this stage. Members of the Acrosaleniidae can be distinguished from other echinoids by having a single primary tubercle to each interambulacral plate; will all tubercles perforate and crenulate (Fig. 2G-H). Primary spines relatively stout and fusiform, with a cortex (Fig. 2I-J). Although the upper part of each spine is spinose or 'cidaroid' like, most members of the Cidaridae do not have strong crenulations on the tubercles.

Discussion

Moberg (1888) and Troedsson (1951) identified at least four species of crinoids within the Lower Jurassic (Sinemurian-Pliensbachian) of southern Sweden, along with several echinoid fragments, which even now are difficult to assign confidently. The poor preservation of the echinoid fragments means that we feel that we can discuss their significance any further. In response to more recent developments in crinoid taxonomy, we have found that these can be revised to be at least two species, *Balanocrinus subteroides* and the new species *Isocrinus ranae*, and possibly a third taxon, *Hispidocrinus scalaris*, but we have no conclusive evidence of the last named taxon. This makes the Lower Jurassic crinoid fauna of Sweden comparable with that of the Lower Jurassic of England (see Simms 1989).

It is clear that despite the geographic separation, the Early Jurassic crinoids and echinoids described herein have clear taxonomic affinities with contemporary representatives of the British faunas. The preservation of the echinoids means that it is difficult to resolve the details of their significance. Nevertheless, this is an isolated occurrence and thus any interpretation must be approached with caution. Hunter & Zonneveld (2008) developed a classification of Jurassic crinoids, and although they used Middle Jurassic groups, it has some relevance to this study. The residues described herein for both the echinoids, and the crinoids belong to taphofacies 2 (Hunter 2006; Hunter & Zonneveld 2008); that is para-autochthonous articulated columnals, unabraded, and exposed to minimum transport.

Simms (1989) noted that many of the Early Jurassic crinoids he described could be either intermediate forms or evolved through neoteny, such as in *I. basaltiformis*. Although *I. ranae* shares many characters with *I. basaltiformis* and could have originated by neoteny from a theoretical ancestor, it is difficult to quantify this due to lack of data. It is clear, however, that *I. ranae* shares many characters that were considered intermediate between two Early Jurassic species described by Simms (1989), which are found associated with the same muddy substrate. For instance, the late Sinemurian *I. tuberculatus* with its weak tubercles and radial epifacets is thought to be intermediate between *I. psilonoti* (Hettangian) and *I. robustus* (Pliensbachian), as the latter has distinctive tuberculation and radial epifacets, while *I. psilonoti* is largely smooth and devoid of such characters. However, *I. ranae*, which is Pliensbachian in age, shares many characters with *I. tuberculatus,* despite being contemporaneous with *I. robustus*. Thus, the new species could prompt a reanalysis of the species concept among the Lower Jurassic *Isocrinus*. Despite the apparent separation from the basin where most of these described groups occur, this species could indeed be related to the same evolutionary lineage identified by Simms (1989).

Acknowledgments

Tatsuo Oji and Simon Darroch (University of Tokyo), Dave Lewis (Natural History Museum, London), and Christina Frenzen (Naturhistoriska riksmuseet, Stockholm) are thanked for their helpful comments and suggestions on earlier versions of this manuscript. Additional thanks go to John W.M. Jagt (Natuurhistorisch Museum, Maastricht, The Netherlands) for critical and helpful review comments. Dr. Mike Reich (University of Göttingen Museum, Germany) is thanked for help in finding the more obscure German literature.

References

Agassiz, J.L.R. 1836. Prodrome d'une monographie des radiaires ou échinodermes. Mémoires de la Société Neuchâteloise des Sciences Naturelles 1, 168-199.

Claus, C.F.W. 1876. Grundzüge der Zoologie (3rd ed.). N.G. Elwert'sche, Universitäts Buchhandling Marburg & Leipzig. 1254pp.

Delage, Y.M. & Hérouard, E. 1903. Les Echinodermes, *In*: Traité de Zoologie concrète 3, Les échinoderme Schleicher frères, Paris. 496 pp.

Gislén, T. 1925. Some Mesozoic Comatulids. Annals and Magazine of Natural History 9(16), 1-30.

Gregory, J.W. 1900. The Echinoidea. *In:* Lankester, E.R. (ed.). A Treatise on Zoology. Part 3: The Echinoderma, 282-332. Adam & Charles Black, London.

Hunter, A.W. 2006. Model for the palaeoecology of echinoderms from the Middle Jurassic (Bathonian) marginal marine facies of Great Britain, France, and the United States, Unpublished PhD thesis, Birkbeck College, University of London, 347 pp.

Hunter A.W. & Zonneveld J.-P. 2008. Palaeoecology of Jurassic encrinites: reconstructing crinoid communities from the Western Interior Seaway of North America. Jurassic Marine Palaeobiology Special Issue, 263, 58-70.

Jäger, M. 1985a. Saurier und Seelilien: Versteinerungen aus dem Jurameer (Posidonienschiefer), Schriften des Bodenseee-Naturkundemuseums. Seekreis Verlag, Konstanz. 36pp

Jäger, M. 1985b. Die Crinoiden aus dem Pliensbachium (mittlerer Lias) von Rotttorf am Klei und Empelde (Süd-Niedersachsen), Naturhistorisch Gesellschaft zu Hannover, Berichte. 128, 71-151

Jäger, M. 1990. Lias epsilon von Dotternhausen. Fossilien 7, 274-277

Jäger, M. 1991. Lias epsilon von Dotternhausen. Fossilien 8, 33-36

Loriol, P. de. 1886. Paléontologie française, ou description des fossiles de la France, série.1, Animaux invertébrés. 11. Crinoïdes. Terrain jurassique: G. Masson, Paris. 1207pp.

Miller, J.S. 1821. A Natural History of the Crinoidea or Lily-Shaped Animals, with observations on the genera *Asteria*, *Euryale*, *Comatula* and *Marsupites*. Bryan & Co, Bristol. 150pp.

Moberg, J.C. 1888. Om Lias i sydöstra Skåne. Sveriges Geologiska Undersökning C 99, 1-86.

Norling, E. 1972. Jurassic stratigraphy and foraminifera of western Scania, southern Sweden. Sveriges Geologiska Undersökning Ca 47, 1-120.

Norling, E., Ahlberg, A., Erlström, M. & Sivhed, U. 1993. Guide to the UpperTriassic and Jurassic geology of Sweden. Sveriges Geologiska Undersökning Ca 82, 1-71.

Quenstedt, F. A. 1858. Der Jura. Laupp'she Buchhandlung, Tübingen. 842 pp.

Quenstedt, F. A. 1876. Petrefactenkunde Deutschlands; Erste Abtheilung Vierter (4) Band, Echinodermen, Asteriden und Encriniden, Atlas zu den Asteriden und Encriniden, Fues Verlag, Leipzig. 742 pp.

Rees, J. 2000. A new Pliensbachian (Early Jurassic) neoselachian shark fauna from southern Sweden. Acta Palaeontologica Polonica 45, 407-424.

Reyment, R.A. 1959. On Liassic ammonites from Skåne, southern Sweden. Stockholm Contributions in Geology 2(6), 103-157.

Sieverts-Doreck, H. 1952. Ueber die sogenannten "Deckplaettchen" gotlaendischer Cyathocrinidae. Neues Jahrbuch für Geologie und Paläontologie, Monatshefte 9, 420-430.

Simms, M.J. 1989. British Lower Jurassic crinoids. Palaeontographical Society Monographs 142, 103 pp.

Smith, A. B., *Salenioida*. In: Smith, A. B. (editor) 2005.*The Echinoid Directory.* World Wide Web electronic publication. http://www.nhm.ac.uk/palaeontology/echinoids [03/03/09]

Troedsson, G. 1951. On the Höganäs series of Sweden (Rhaeto-Lias). Lunds Universitets Årsskrift N.F. 47, 1-268.

Wright, T. 1858. Notes on the Fossils collected by Mr Geikie from the Lias of the Isles of Pabba, Scalpa and Skye. Quarterly Journal of the Geological Society of London, 14, 24-36.

Zittel, K.A. von., 1879. Handbuch der Paläontologie, 1. Paläozoologie. R. Oldenbourg, München & Leipzig. 557 pp.

Eudialyte decomposition minerals with new hitherto undescribed phases from the Ilímaussaq complex, South Greenland

S. KARUP-MØLLER, J. ROSE-HANSEN & H. SØRENSEN

S. Karup-Møller, J. Rose-Hansen & H. Sørensen. 2010-11-10. Eudialyte decomposition minerals with new hitherto undescribed phases from the Ilímaussaq complex, South Greenland. © 2010 by Bulletin of the Geological Society of Denmark, Vol. 58, pp. 75–88. ISSN 0011–6297. (www.2dgf.dk/publikationer/bulletin)

Eudialyte is a distinctive mineral in the agpaitic group of peralkaline nepheline syenites. The paper describes the alteration of eudialyte from the Ilímaussaq complex, South Greenland, which is the type locality for eudialyte, as well as for agpaitic rocks.

Two types of alteration are distinguished: alteration of eudialyte to catapleiite is widespread in the complex, whereas alteration to zircon only occurs in strongly altered rocks. Additionally, the following minerals have been identified in the altered eudialyte: aegirine, K-feldspar, albite, analcime, fluorite, monazite, apatite, allanite, Y-fergusonite, Ce-fergusonite, fersmite, nacareniobsite-(Ce), uranothorianite, neptunite and grossularite. Some unidentified Nb and/or REE minerals have been distinguished.

The different styles of alteration can be explained by different late- and post magmatic conditions at different settings in the complex. Alteration to zircon is caused by fluids of external origin or by fluids expelled from intersecting lujavrite and pegmatite dykes. Alteration to catapleiite is caused by late-magmatic interstitial fluids. The alteration has resulted in distinct fractionation of some elements; Zr is, for instance, located only in zircon and catapleiite, Nb and REE in separate minerals.

Keywords: Ilímaussaq complex, South Greenland eudialyte decomposition products, marginal pegmatite, kakortokites, unidentified Nb- and REE-minerals.

S. Karup-Møller [svka@env.dtu.dk] Department of Environmental Engineering. Technical University of Denmark, Lyngby, Denmark; J. Rose-Hansen [rose-hansen@dadlnet.dk] and H. Sørensen [kimik@compaqnet.dk], Department of Geography and Geology, University of Copenhagen, Denmark.

Introduction

The Ilímaussaq alkaline complex is the type locality of agpaitic nepheline syenites (Ussing 1912) as well as of eudialyte (Stromeyr 1819). Agpaitic rocks are peralkaline nepheline syenites containing complex minerals such as eudialyte instead of simple minerals such as zircon.

The Ilímaussaq complex consists of four main intrusive phases. Phase 1 is a partial rim of augite syenite, phase 2 is alkali granite and quartz syenite in the roof zone of the complex, phase 3 consists of pulaskite, foyaite, sodalite foyaite and naujaite and phase 4 of kakortokites and lujavrites (e.g. Rose-Hansen & Sørensen 2002, Sørensen 2006, Sørensen et al. 2006).

A unit called marginal pegmatite (Ussing 1912, Westergaard 1969, Bohse et al. 1971, Steenfelt 1972) consists of agpaitic nepheline syenite and short pegmatitic veins. It forms a rim between the country rocks and the kakortokite and the lowermost lujavrites of the complex and between country rocks and naujaite in the upper part of the complex (Sørensen 2006).

The matrix of the marginal pegmatite is generally a massive-textured, homogeneous agpaitic nepheline syenite, which is locally layered. It consists of K-feldspar, nepheline, eudialyte, aegirine, arfvedsonite and locally sodalite. Where it is in contact with the lowermost lujavrites it is thoroughly altered, K-feldspar and nepheline being replaced by analcime and pigmentary material/sericite, and arfvedsonite and green aegirine by brown aegirine (Sørensen 2006).

The pegmatitic veins, which are a few metres long and up to about 0.5 m wide, consist of microcline, albite, nepheline, sodalite, eudialyte, aegirine, arfvedsonite, aenigmatite, biotite, rinkite, astrophyllite,

tundrite, lithium mica and fluorite (Bohse *et al.* 1971).

Eudialyte in the matrix of the marginal pegmatite is altered in various degrees to zircon or catapleiite and a host of other minerals that are described in the present paper. Selected analyses of eudialyte completed during the present study and by other scientists are listed in Table 1.

Alteration of eudialyte

Ussing (1898, 1912) gave a detailed description of the eudialyte from the Ilímaussaq complex and identified alteration of this mineral to zircon, and more commonly to catapleiite. This observation was confirmed by Bøggild (1953) who also described other types of alteration of eudialyte from the Ilímaussaq complex and the adjacent Igaliko complex. Sørensen (1962) described the alteration of eudialyte to catapleiite and noted that in some lujavrites, eudialyte was substituted by steenstrupine. Semenov (1969) described alteration of eudialyte to a yellowish powder of an amorphous substance known under the name zirfesite (Kostyleva 1945) and suggested the general formula $Fe_2Zr_3Si_4O_{17}\cdot 15H_2O$ for the Ilímaussaq variety. Zirfesite has later been discredited as a mineral name. Sørensen & Larsen (2001) distinguished agpaitic eudialyte-

Table 1. Electron microprobe analyses (XRF and INA: IG 109269 and D7-34.5 m) of eudialyte and zirfesite from the Ilímaussaq complex

	Eudialyte	Eudialyte	Eudialyte	Eudialyte	Eudialyte	Eudialyte	Zirfesite
	Kakortokite IM 109269 Layer-9, red Bohse pers. com	Naujaite D7-34.5 m # Bohse pers. com	Johnsen & Gault 1997	Kakortokite Layer +1 This paper	Kakortokite Layer +9 This paper	Kakortokite Layer +16 This paper	Semenov 1961
SiO_2	48.90	49.01	48.82	49.76	49.66	50.07	31.75
ZrO_2	13.40	13.29	11.65	11.76	11.78	11.79	21.08
ThO_2	n.d	n.a	n.d	0.02	0.02	0.01	
TiO_2	0.06	0.07	0.00	0.09	0.10	0.09	
Nb_2O_5	0.91	1.09	0.77	0.67	0.66	0.67	0.79
La_2O_3	0.34	*0.30	0.47	0.64	0.47	0.48	
Ce_2O_3	*0.77	*0.66	0.90	1.44	0.95	0.97	
Nd_2O_3	*0.32	*0.26	0.41	0.61	0.39	0.41	
Pr_2O_3	*0.09	*0.08	n.a	0.19	0.13	0.13	
Sm_2O_3	*0.06	*0.05	n.a	0.18	0.11	0.13	
Eu	*0.09	n.a.	n.a	n.a.	n.a	n.a.	
Gd_2O_3	*0.07	0.06	n.a	0.17	0.06	0.14	
Y_2O_3	*0.42	0.28	0.44	0.74	0.46	0.47	
Al_2O_3	0.38	0.68	0.50	0.19	0.24	0.24	1.23
Fe_2O_3							11.30
Total Fe as FeO	6.21	6.08		5.29	6.05	6.20	
MnO	0.85	1.07	0.47	1.16	0.60	0.65	
MgO	n.a	0.03	n.a	n.a	n.a	n.a	
CaO	9.87	10.48	9.61	9.82	10.16	9.63	3.01
Na_2O	13.26	13.24	15.46	13.27	14.87	15.34	
K_2O	0.39	0.25	0.36	0.57	0.26	0.27	
P_2O_5	n.a	n.a	n.a	0.00	0.01	0.01	
Cl	1.28	1.33	1.34	1.07	n.a	1.34	
F	n.a	n.a	n.a	0.03	0.06	0.05	
H_2O	n.a.		0.22	n.a	n.a	n.a.	15.56
HfO_2	0.23	n.a	0.58	n.a	n.a	n.a	
Ta_2O_5	0.05	0.06	n.a	n.a	n.a	n.a	
RE_2O_3							8.03
Total	97.95	98.37	92.00	97.67	97.04	99.09	92.75

* INAA analyses of separated minerals; # D7= drill core 7; n.a = not analysed.

bearing lujavrites and steenstrupine-bearing hyperagpaitic lujavrite varieties. Sørensen (2006) noted that eudialyte was substituted by zircon in the most altered parts of the marginal pegmatite. These studies were carried out by traditional microscopy and chemical analyses of separated minerals.

The chemical composition of eudialyte shows no significant changes throughout the kakortokite series (Bohse et al. 1971, Steenfelt & Bohse 1975, Kogarko et al. 1988, Sørensen 1992, Pfaff *et al.* 2008) and our analyses (Table 1).

Examples of investigation of eudialyte alteration by electron microprobe analyses are presented by Coulson (1997) from the Igaliko complex and by Mitchell & Liferovich (2006) from the Pilansberg Complex, South Africa. This is also the method applied in

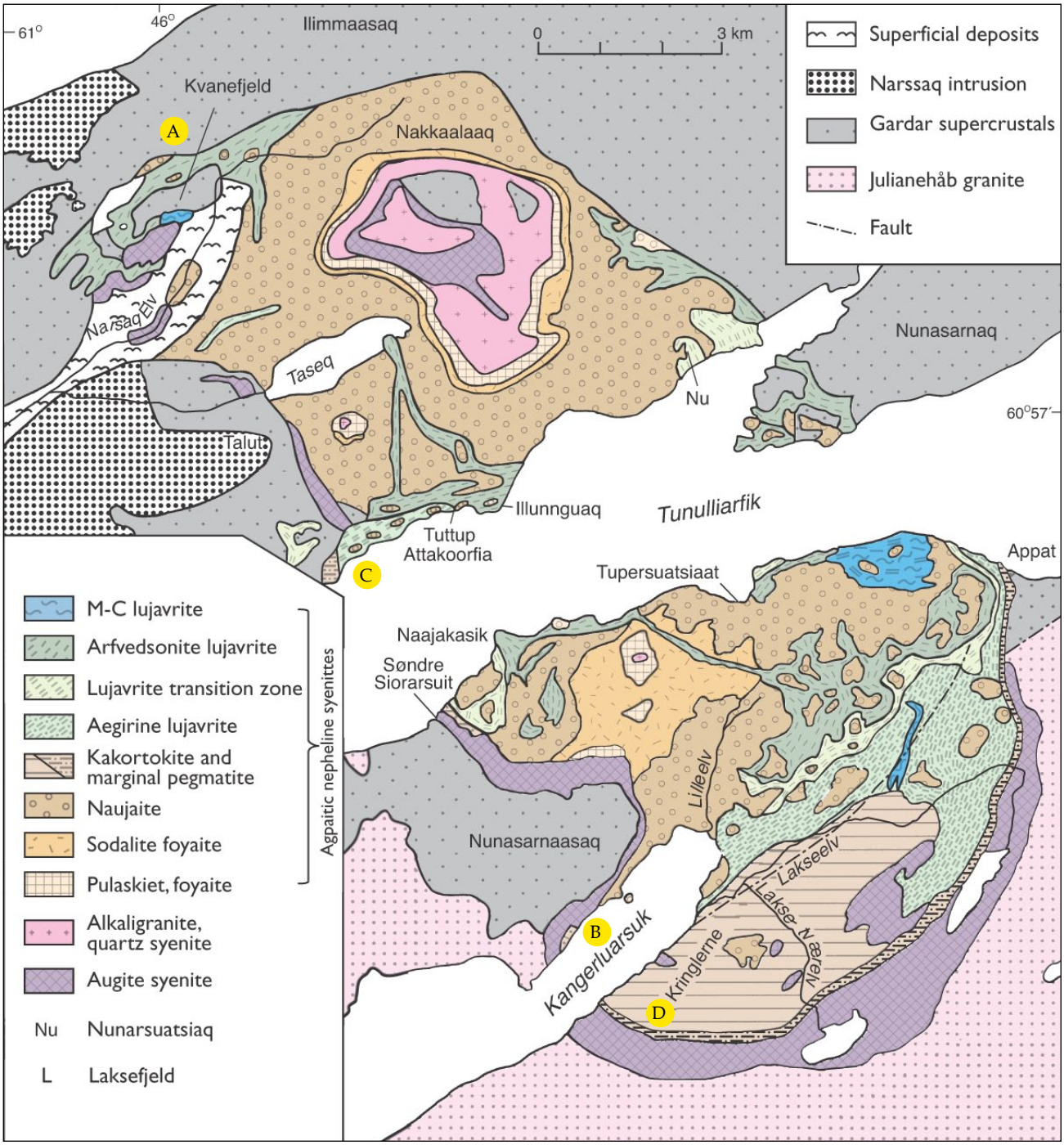

Fig. 1. Simplified geological map of the Ilímaussaq complex based on Ussing (1912), Ferguson (1964), Andersen *et al.* (1988) and ongoing studies by the "Ilímaussaq group".

our examination of minerals from the marginal pegmatite since the grain size of the alteration products is generally less than 10 micrometers in diameter.

Description of the geological setting of the investigated localities

The examined material was collected at four localities (Fig. 1) within the marginal pegmatite that have been petrographically described by Sørensen (2006).

The alteration to catapleiite was studied at locality A (GI.104380) from the Kvanefjeld area in the northernmost part of the complex, and at locality D (GI. 104563) from near the south-west contact of the complex. Alteration to zircon was described at locality B (GI. 104361) from the north coast of Kangerdluarsuq and at locality C (GI. 109302 and 109303) from the north coast of Tunulliarfik.

At locality A, the marginal pegmatite is the marginal facies of the naujaite and forms a partial rim between this rock and the basaltic country rocks. Its matrix is poikilitic, similar to the texture of naujaite, but with massive-textured patches similar to the matrix of the marginal pegmatite from localities B and C. It is locally rich in eudialyte. We have examined the macroscopically massive-textured matrix variety which consists of microcline, nepheline, arfvedsonite, aegirine and eudialyte. Thin section studies reveal that arfvedsonite, aegirine and aggregates of eudialyte crystals poikilitically enclose nepheline and aegirine crystals. The eudialyte is practically unaltered.

At locality D the marginal pegmatite passes inwards into kakortokite, but has sharp contacts against the external margin of augite syenite. Masses of naujaite occur between the marginal pegmatite and the augite syenite. The sample examined is a small lenticular body of a rather fine-grained, massive-textured rock which forms a pocket in a pegmatite and is interpreted as a sample of quenched pegmatitic melt (Sørensen 2006). It is rich in eudialyte which, because of the sheltered location of the body, is only slightly altered. It belongs to a lower stratigraphic level of the complex than the pegmatite at the other three localities.

Localities B and C are both located between the lower part of the lujavrite sequence and its country rocks. At locality B, the country rocks are the augite syenite and outside it the granitic basement; at locality C, the volcanic country rocks. At both places, eudialyte, nepheline, arfvedsonite and aegirine are strongly altered. Alteration at locality B may be related to the many intersecting thin lujavrite dykes, at C to swarms of parallel pegmatite veins. The microcline is partly substituted by albite, the nepheline by sericite and analcime, the arfvedsonite by aegirine, and the eudialyte by zircon.

The matrix rock at locality C displays the same features as the examined rock at locality B, but is slightly less altered.

Mineralogy of the altered eudialyte

Methods

Electron microprobe analyses were carried out at the Department of Geography and Geology, University of Copenhagen, using a JEOL 733 superprobe in wavelength dispersive mode with an online correction program supplied by JEOL. The excitation voltage was 15 kV, beam current 15 nA and beam diameter 1 micron. Wavelengths and standards used were Na *Kα* (albite), K *Kα* ($KAlSi_3O_8$), Ca *Kα* and Si *Kα* ($CaSiO_3$), Mn *Kα* ($MnTiO_3$), Fe *Kα* (Fe_2O_3), Al *Kα* (Al_2O_3), Ce *Lα* (CeO_2), La *Lα* (La-18), Nd *Lα* (Nd_3Ga_5), Pr *Lα* ($Pr_3Ga_5O_{12}$), Sm *Lα* ($SmFeO_3$), Y *Lα* ($Y_3Al_5O_{12}$), Gd *Lα* ($GdFeO_3$), P *Lα* and F *Kα* (apatite-wilberforce), Nb *Lα* (columbite), Th *Mα* (ThO_2), Cl *Kα* (sodalite). The estimated detection limit was 0.02 wt.% for all elements. Up to 10 analyses were completed on each phase in a

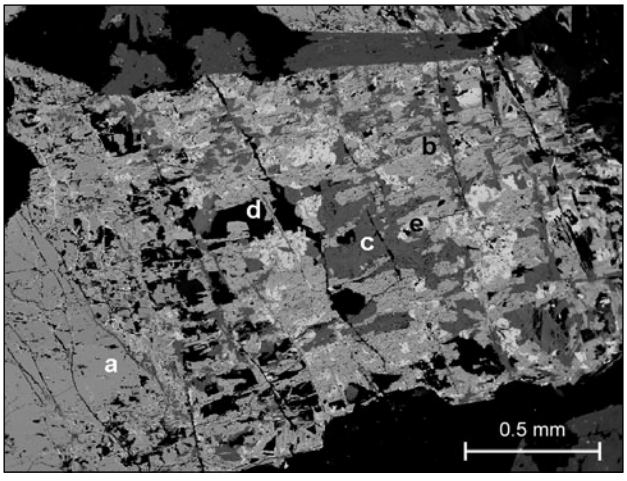

Fig. 2. A eudialyte crystal (a, grey, left part of the photo) has been completely altered (central and right part of the figure) into an aggregate of zircon (b, same grey shade as the unaltered eudialyte), aegirine (c, dark grey), analcime (d, black) and a heterogeneous mixture of fluorite, Ce-fergusonite, monazite and A1 (e, small white grains with a random distribution). These four minerals cannot be distinguished from each other in the photograph. The boundary between altered and unaltered eudialyte is rather well defined. (Sample GI 104380, locality A).

given eudialyte alteration aggregate. Figures 2-12 are all BSF images.

Paragenesis

Table 2 presents the minerals identified during the present study, their simplified formulae and references to localities and tables with compositional data. The common rock-forming minerals are not listed.

The Nb and the REE minerals generally occur as small rounded opaque or semi-transparent grains. The grain size rarely exceeds 10 microns. This excludes X-ray analytical work and optical examination in transmitted and reflected light. The minerals have been examined using the electron microprobe. Some of the observed minerals may be new mineral species, but insufficient mineralogical data prevent the proposal of new names for these minerals.

The catapleiite alteration type

At localities A and D, eudialyte is altered to extremely fine-grained aggregates of catapleiite and a number of other minerals: aegirine, analcime, minor amounts of fluorite, Y-fergusonite, apatite, monazite, nacareniobsite-(Ce), thorianite, neptunite and A1. A typical aggregate is pictured in Fig. 2.

The zircon alteration type

At localities B and C, eudialyte is altered to zircon, K-feldspar, albite, aegirine, fluorite and grossularite, together with small quantities of monazite, Ce-fergusonite, allanite, A1 and A2, and at locality C also Y-fergusonite, fersmite, Nb1, Nb2, Uk1 and Uk2. Coexisting catapleiite and zircon is rare and has only been observed at locality C.

A representative eudialyte decomposition aggregate is shown in Figs. 3, 4 and 5. Fig. 5 covers the left part of the aggregate in Fig. 4. The outlines of the original eudialyte crystal are marked by broken strings of very small zircon crystals. Zircon is always distinctly zoned and forms irregularly-shaped patches (Fig. 5). Euhedral zircon crystals have also been observed. Besides zircon, the aggregate is composed of microcline, aegirine, fluorite and monazite. An isolated monazite cluster close to the aggregate is shown in Fig. 6.

The aggregate in Fig. 7 is composed of K-feldspar, aegirine, zircon, Ce-fergusonite and allanite. On the left, patchily decomposed Ce-fergusonite lies isolated in analcime (Fig. 8). In the lower central part of Fig. 7, zircon is intergrown with allanite and two small grains of the unidentified mineral Uk1 (Fig. 9). In the bottom right part of Fig. 7, allanite crystals, which are associated with zircon (Fig. 10), contain inclusions of Nb1. This mineral also occurs as disseminated grains in K-feldspar in the central part of the aggregate in Fig.7.

The Y-fergusonite occurs in some aggregates as randomly distributed grains, in places as inclusions in Nb2 (Fig. 11). The Ce-fergusonite was found in three aggregates and A1 and A2 in two. Allanite occurs as aggregates of radiating crystals. Fersmite was found in association with zircon and grossularite. The pre-

Table 2. Minerals observed in altered eudialyte from the marginal pegmatite of the Ilímaussaq complex.

Mineral	Formula, based on chemical analyses this paper	Localities			
		A	D	B	C
Zircon	$Zr_{3.5}REE_{0.5}O_{10}Si_{4.0}O_{15..37}$			X	X
Catapleiite	$(Na,Ca,Fe)ZrSi_3O_8 \cdot nH_2O$	X	X		X
Ce-fergusonite	$(Fe,Nd)NbO_4$			X	X
Y-fergusonite	$(Ca,Fe)_{0.5}REE_{7.5}(Si,Ti)_{0.5}Nb_{10}O_{37.75}$	X			X
Fersmite	$CaNb_2O_6$				X
Allanite	$Ca(Ce, La, Ca)(Fe^{+2},Fe^{+3})(Al, Fe^{+3})Al(Si_2O_7)(SiO_4)O(OH)$			X	X
Nacareniobsite-Ce	$Na_3Ca_3REENb(Si_2O_7)_2OF_3$		X		
Monazite	$CeREEP_2O_8$	X		X	
Apatite	$Na_{0.5}Ca_{4.5}REE_{0.5}(PO_4)_3F(OH)$	X			
Thorianite with U	$(Th,U)O_2$ *	X	X		
A1	$(Na,Ca,Fe,Mn)_2Ce_3(REE)_3Si_6FO_{22.5}$	X	X	X	X
A2	$REE_3Si_4O_{12.5-y}(OH)_{2y} \cdot nH_2O$			X	X
Nb1	$(Fe,Mn,Ca)_{6.5}Nb_{10}REE_{10}Al_{3.5}Si_{7.5}O_{66.75}$				X
Nb2	$Mn_2Nb_2O_7$				X
Uk1	$(Fe,Mn,Ca)_{3.0}REE_{0.5}Al_{1.75}Si_4O_{14.38} \times nH_2O$				X
Uk2	$CeREEF_{1.5}O_{1.75-y}(OH)_{2y} \times nH_2O$				X

* Not analyzed for U.

sumed new mineral Uk2 was found in association with Ce-fergusonite (Fig. 12). The Uk2 grains in Fig. 12 are embedded in microcline and a mixture of calcite, a mineral with the proposed composition $Fe_6Mn_6Al_7Si_8O_{31.5-y}(OH)_y \bullet nH_2O$ and a mineral in such small grains that it could not be analyzed quantitatively.

The minerals

Selected and/or average compositions of identified and unidentified, possibly new minerals are listed in Tables 3 and 4, respectively. Analyses of eudialyte from different localities are listed in Table 1. The first author can supply detailed analytical data for all the minerals on request.

Identified minerals (Table 1)

Ce-fergusonite has a molar ratio Nb: REE close to 1:1. The proportions of the individual REE vary strongly and no obviously systematic substitutional relationships appear to exist. Based on the average value of all the Ce-fergusonites analyses, we have calculated the following empirical formula for the mineral, ignoring the small amounts of Th, Al, Cl and F: $Ca_{0.26}(Ce_{3.69}Y_{0.82}La_{0.85}Nd_{2.73}Pr_{0.60}Sm_{0.56}Gd_{0.25})_{\Sigma 9.50}(Si_{0.19}Ti_{0.02})Nb_{10.00}O_{39.95}$ or simplified: $(Ce,Nd)NbO_4$.

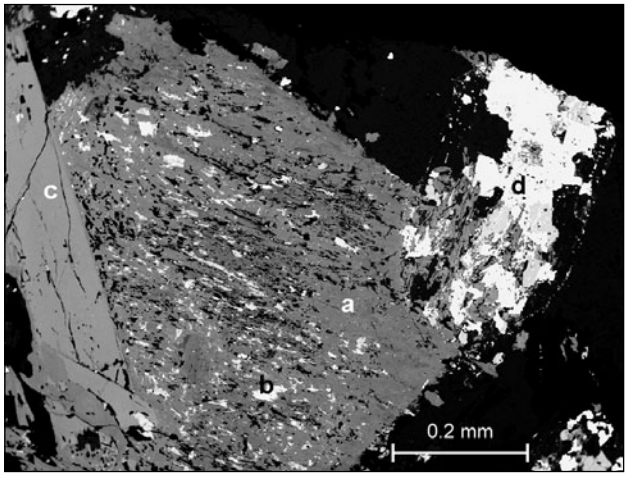

Fig. 3. The central part of the photo is composed of aegirine (a, grey) with numerous small inclusions of mainly hematite (b, white) after an original, now completely decomposed arfvedsonite crystal. To the left a primary aegirine lath (c) and to the right an eudialyte alteration aggregate (d). The latter has been enlarged in Fig. 4. (Sample GI 104361, localilty B).

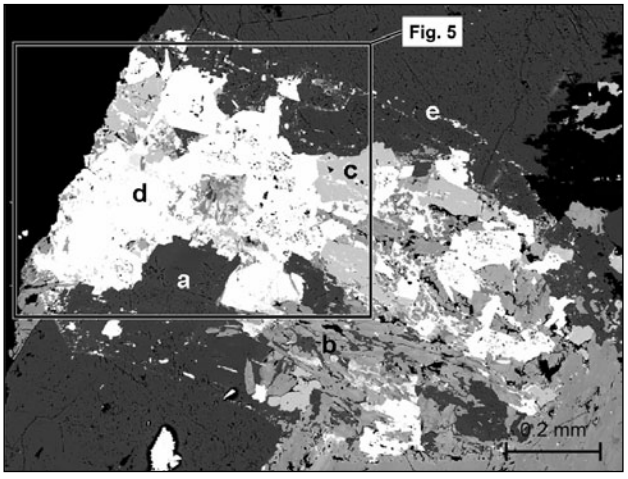

Fig. 4. Enlarged portion of Fig. 3 covering the eudialyte alteration aggregate. The aggregate is composed of microcline (a, dark grey), aegirine (b, grey), fluorite (c, light grey), monazite and zircon (d, both white). The left part of the aggregate is enlarged in Fig. 5. Very small zircon grains (e) mark the outline of the original eudialyte crystal. (Sample GI 104361).

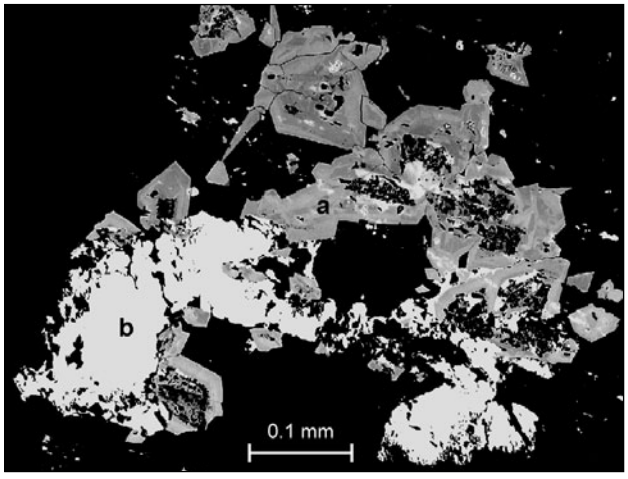

Fig. 5. In this image, the left portion of Fig. 4 is shown using a relatively low electron flux. Here (in contrast to Fig. 4) zoned zircon (a, grey) is easily distinguished from monazite (b, white). (Sample GI 104361).

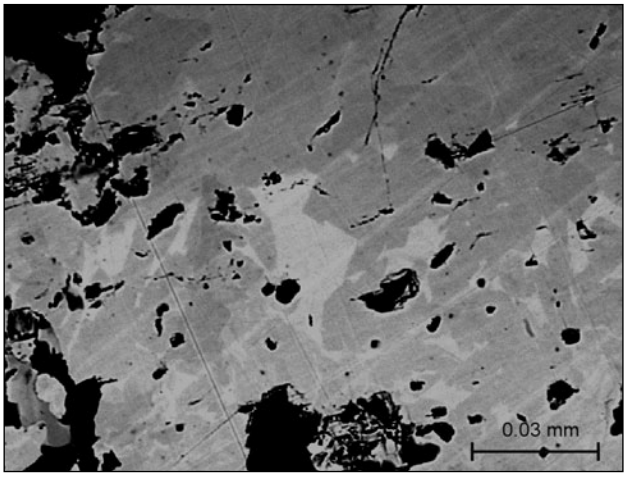

Fig. 6. Patchy aggregate of monazite. (Sample GI 104361, locality B).

Y-fergusonite does not vary as much in composition as Ce-fergusonite. The low totals are ascribed to the presence of HREE which, apart from Gd, have not been analysed. The REE values vary from sample to sample, but not as much as in Ce-fergusonite. The following empirical formula for the mineral, based on the average values of all analyses recorded is: $(Ca,Fe)_{0.56}(Ce_{0.45}Y_{5.06}La_{0.07}Nd_{0.71}Pr_{0.10}Sm_{0.40}Gd_{0.63})_{\Sigma 7.42}Si_{0.27}Ti_{0.10}Nb_{10.00}F_{0.18}Cl_{0.01}O_{37.25}$, or simplified: $(Ca, Fe)_{0.5}REE_{7.5}(Si, Ti)_{0.5}Nb_{10}O_{37.75}$ (plus HREE).

Allanite was found at localities B and C. A representative analysis of the mineral is listed in Table 3. Using the traditional allanite formula, its average composition from locality C may be written as:

$Ca_{0.57}(REE_{0.69}Ca_{0.31})(Fe_{0.55}Mn_{0.21}Ca_{0.24})(Al_{0.40}Fe_{0.60})Al(Si_2O_7)((Si_{0.95}Zr_{0.02}Ti_{0.03})O_4)O(OH)$.

For allanite from locality B, the average composition would be:

$Ca_{0.63}(REE_{0.69}Ca_{0.28}Na_{0.03})(Fe_{0.58}Mn_{0.26}Ca_{0.16})(Al_{0.64}Fe_{0.36})Al(Si_2O_7)((Si_{0.92}Zr_{0.01}Ti_{0.07})O_4)O(OH)$.

The two formulae have the same total REE content. However, the proportions between the individual REE vary significantly.

Nacareniobsite-(Ce) was only found at locality D and only in one eudialyte decomposition aggregate. Microprobe analyses of 11 grains show little variation from grain to grain. The following empirical formula may be written for the mineral:

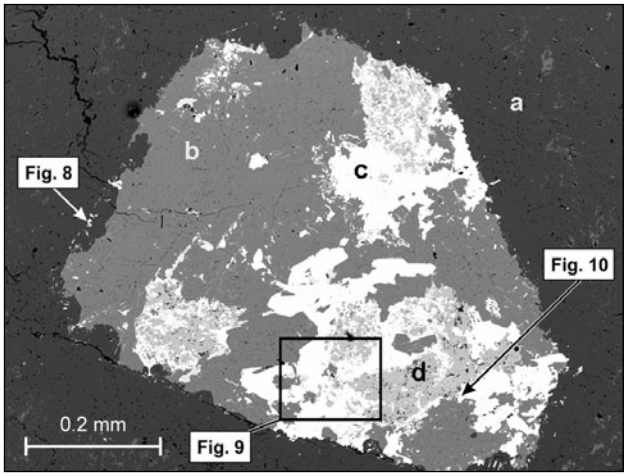

Fig. 7. Blocky eudialyte decomposition aggregate (strictly a pseudomorph after an original eudialyte crystal) in analcime (a, dark grey) is composed of K-feldspar (b, grey) and patchy areas of zircon, Ce-fergusonite and allanite (c, all three bright white) enclosing aegirine (d, light grey). For details see Figs. 8-10. (Sample GI 109302, locality C).

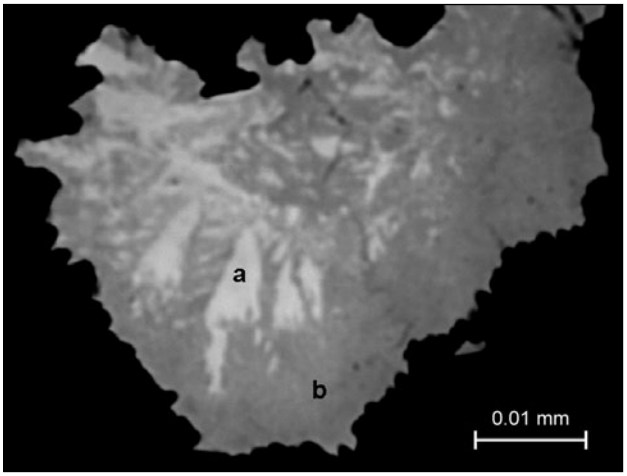

Fig. 8. Partly altered Ce-fergusonite. Primary Ce-fergusonite is white (a), the replacing variety is grey (b). (Sample GI 109302, localilty C).

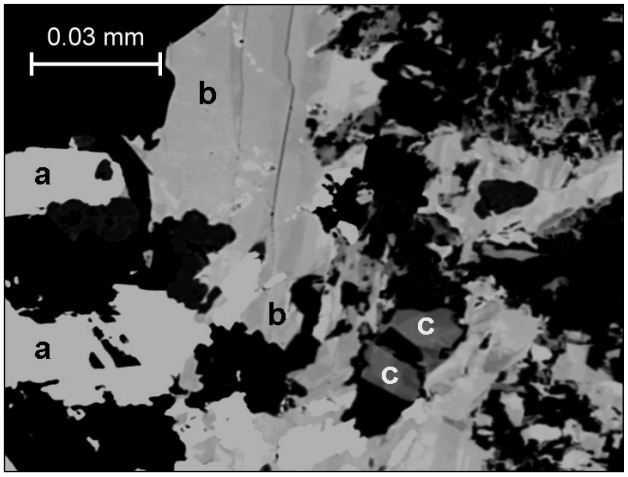

Fig. 9. Zircon (a, off-white), allanite (b, pale grey), and Uk1 (c, two dark grey grains in the lower central right part of the photo). The location of the figure is shown in Fig. 7. (Sample GI 109302, locality C).

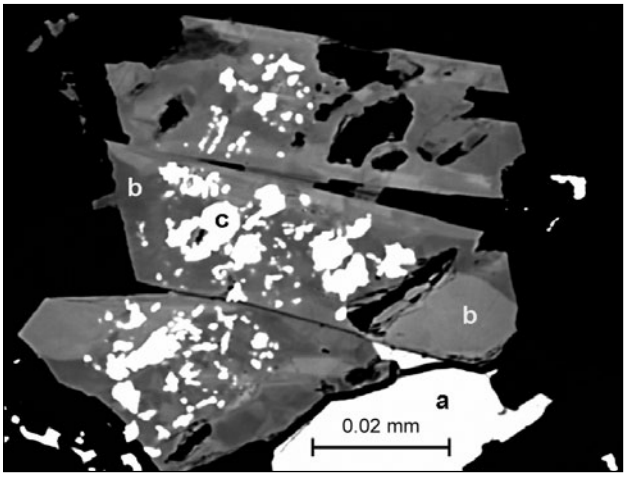

Fig. 10. A relatively large crystal of zircon (a, white, bottom right) and three crystals of allanite (b, mottled grey) enclosing grains of Nb1 (c, white), all embedded in K-feldspar (black). (Sample GI 109302, locality C).

$Na_{2.99}Ca_{2.94}(Ce_{0.37}Y_{0.13}La_{0.13}Nd_{0.22}Pr_{0.05}Sm_{0.05}Gd_{0.03})_{\Sigma 0.98}$ $Nb_{0.93}$ $Si_{3.98}Zr_{0.01}Ti_{0.01}F_{2.72}$ $O_{14.86}$ or simplified: $Na_3Ca_3REENb(Si_2O_7)_2OF_3$. Nacareniobsite-(Ce) was originally found at Kvanefjeld near locality A in Fig. 1 (Petersen et al. 1989).

Fersmite has the simplified composition $CaNb_2O_4$ and contains small amounts of TiO_2 (1.5 wt%), REE (2.7 wt%), FeO (0.9 wt%) and 0.2 wt % MnO and SiO_2.

Zircon is one of the major alteration products of eudialyte at localities B and C. A representative microprobe analysis is listed in Table 3. Zircon contains between 3.7 and 4.8 wt.% REE. The total content of FeO, MnO and CaO is less than 0.5 wt.%.

Catapleiite is the Zr-bearing member of the altera-

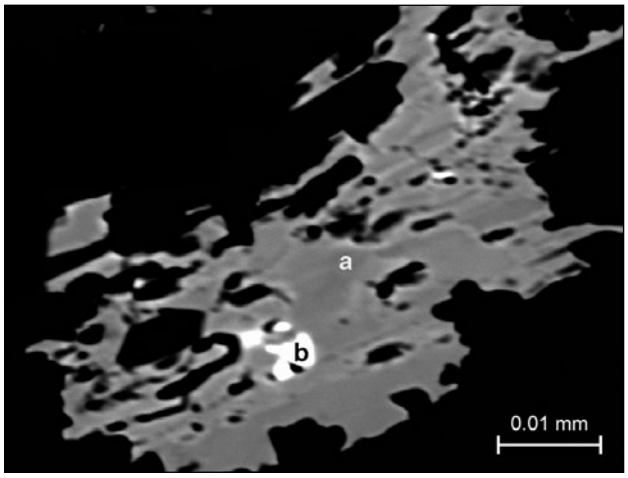

Fig. 11. Patchy grain of Nb2 (a) enclosing a grain of Y-fergusonite (b) lies in contact with allanite, zircon and K-feldspar (all black). (Sample 109302, locality C).

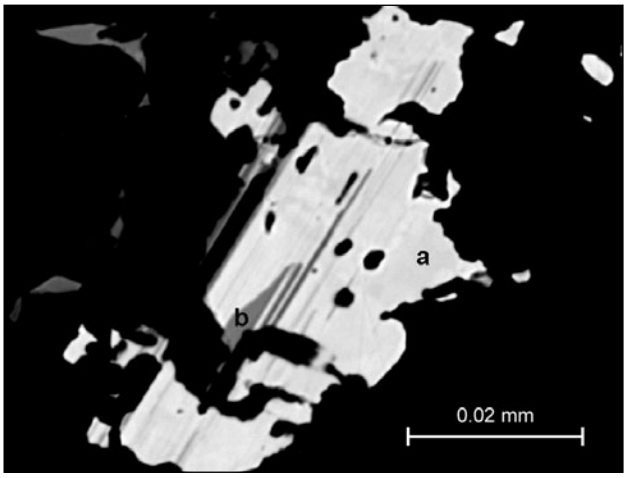

Fig. 12. Grain of mineral Uk2 (a, white), with grey lamellar phase (b). Secondary black unidentified phase replaces both Uk2 and the lamellar phase. (Sample GI 109304, locality C).

Table 3. Representative electron microprobe mineral analyses from the Ilímaussaq complex.

Oxide	Ce-Fergusonite	Y- Fergusonite	Allanite	Fersmite	Nacareniobsite-(Ce)	Zircon	Catapleiite	Grossularite	Monazite	Apatite
SiO_2	0.19	0.60	32.52	0.24	29.32	32.21	44.45	35.88	0.39	1.52
ZrO_2	n.d.	n.d.	n.d	n.d.	n.d.	58.30	33.66	n.d.	0.07	0.11
ThO_2	0.24	0.11	0.03	n.d.	n.d.	n.d.	n.d.	n.d.	n.d.	n.d.
TiO_2	0.08	0.28	1.55	1.53	0.08	0.08	1.04	0.30	n.d.	n.d.
Nb_2O_5	46.75	49.82	n.d.	76.49	14.95	n.d.	n.d.	0.25	n.d.	n.d.
La_2O_3	2.28	0.38	7.63	0.04	1.80	0.10	n.d.	0.03	24.04	5.87
Ce_2O_3	16.45	2.95	10.81	0.14	7.35	0.89	n.d.	0.03	34.30	7.47
Nd_2O_3	13.07	3.52	1.63	0.82	4.45	1.05	n.d.	0.05	7.93	1.61
Pr_2O_3	3.02	0.73	0.63	0.17	0.96	0.07	n.d.	0.07	2.37	0.42
Sm_2O_3	2.40	1.40	0.12	0.97	1.11	0.41	n.d.	n.d.	1.06	0.12
Gd_2O_3	1.42	3.06	0.07	0.43	0.76	0.38	0.26	n.d.	0.28	0.19
Y_2O_3	11.21	24.36	n.d.	0.29	1.73	2.70	0.39	0.16	0.04	0.06
Al_2O_3	n.d.	n.d.	15.09	n.d.	n.d.	0.40	n.d.	10.40	n.d.	n.d.
FeO	n.d.	0.07	12.41	0.88	n.d.	0.05	0.26	15.21	n.d.	n.d.
MnO	n.d.	n.d.	3.77	0.21	n.d.	0.08	n.d.	4.29	n.d.	n.d.
CaO	n.d.	0.53	11.05	16.87	20.06	0.06	0.35	31.97	0.08	42.89
Na_2O	n.d.	n.d.	0.12	n.d.	11.28	0.32	6.23	n.d.	n.d.	2.26
K_2O	n.d.	n.d.	n.d.	n.d.	n.d.	0.04	0.06	n.d.	n.d.	n.d.
P_2O_5	n.d	n.d.	n.d.	n.d.	n.d.	n.d.	n.d.	n.d.	31.44	36.54
Cl	0.24	0.06	n.d.	n.d.	n.d.	n.d.	n.d.	n.d.	n.d.	n.d.
F	n.d	0.13	n.d	n.d.	6.29	0.11	0.14	0.72	0.08	3.24
Totals	97.35	88.00	97.43	99.08	100.14	97.25	86.84	99.36	102.08	102.30

n.d. not detected

tion products of eudialyte at localities A and D, and is a minor constituent at locality C. A representative chemical analysis is presented in Table 3. Na easily burns away under the electron beam and the measurements for this element were therefore made with a sweeping beam over an area 30 square microns in size. The lowest content of CaO (0.24 wt.%) and highest content of Na_2O (10.51 wt.%) were recorded in catapleiite from locality A and the highest content of CaO (3.11 wt.%) and correspondingly lowest content of Na_2O (5.14 wt.%) were recorded at locality C.

Monazite was identified in samples from localities A and B and the average composition of the analyses recorded is listed in Table 3. The Ce content in the analyzed grains is fairly constant. However, the REE contents vary strikingly. With increasing content of La the content of the remaining REE decreases. Two extreme compositions recorded in dark and bright areas of the monazite aggregate shown in Fig. 6, were respectively:
(a): $Ce_{0.93}La_{0.44}(Nd_{0.36}Pr_{0.09}Sm_{0.05}Gd_{0.02})_{0.52}P_{2.00}F_{0.01}O_{7.84}$ and
(b): $Ce_{0.93}La_{0.88}(Nd_{0.07}Pr_{0.04}Sm_{0.01})_{0.12}P_{2.00}F_{0.01}O_{7.88.}$

Apatite. Three microprobe analyses gave the formula: $Na_{0.42}Ca_{4.46}Si_{0.15}REE_{0.56}(PO_4)_3F_{0.99}OH_{1.62,}$ or simplified: $Na_{0.5}Ca_{4.5}REE_{0.5}(PO_4)_3F(OH)$. This is very similar to the composition of apatite in naujaite (Rønsbo 2008).

Unidentified minerals (Table 4)

Mineral A1 is quite common. Most analyses have totals near 100 wt.%. The SiO_2 content is close to 23 wt.% and fairly constant. The following simplified formula is proposed: $(Na,Ca,Fe,Mn)_2Ce_3REE_3Si_6FO_{22.5}$. A detailed study of minerals A1 and A2 in the kakortokites is currently being carried out.

Mineral A2 was found at localities B and C. The average composition of A2 gives a total of only 82.84 wt.%, which suggests that it is a hydrated REE-silicate. The following simplified formula for the mineral is proposed: $REE_3Si_4O_{12.5-y}(OH)_{2y}\cdot nH_2O$.

Mineral Nb1 has only been found at locality C. Two groups of analyses were recorded for the mineral (Table 4). Characteristics for both groups are the nearly identical contents of Si, Nb, Al, Fe, Mn, and Ca. However, the proportions between the individual REE elements vary strikingly between groups, although the sum of the REE per formula unit is close to 10 (10.53 and 9.88) for both groups. We suggest the following simplified formula for the mineral:
$(Fe,Mn,Ca)_{6.5}Nb_{10}REE_{10}Al_{3.5}Si_{7.5}O_{66.75.}$

Mineral Nb2 has the simplified composition $Mn_2Nb_2O_7$. It contains 2.4 wt % TiO_2 and insignificant FeO, CaO and REE.

Mineral Uk1. Two small grains are associated with

Table 4. Average compositions of unidentified minerals from altered eudialyte in the marginal pegmatite of the Ilímaussaq complex

Mineral	A1	A2	Nb1	Nb1	Nb2	Uk1	Uk2
Locality	A,D,B,C	B,C	C	C	C	C	C
Element							
SiO_2	22.97	26.62	10.84	10.66	n.d.	3.68	n.d.
ZrO_2	0.16	n.d.	0.11	0.04	n.d.	n.d.	n.d.
TiO_2	n.d	n.d.	0.14	0.19	2.40	n.d.	n.d.
ThO_2	0.06	n.d.	0.05	0.06	n.d.	n.d.	n.d.
Nb_2O_5	0.06	n.d.	31.71	32.50	76.72	n.d.	n.d.
P_2O_5	0.63	n.d.	n.d.	n.d.	n.d.	n.d.	n.d.
Al_2O_3	n.d.	n.d.	4.45	4.14	n.d.	2.22	n.d.
Ce_2O_3	31.71	16.04	16.21	8.35	0.06	35.91	37.07
Y_2O_3	1.24	3.79	3.06	10.78	0.17	0.01	0.08
La_2O_3	16.02	1.80	5.29	2.72	n.d	12.28	23.24
Nd_2O_3	11.60	20.04	10.55	7.34	0.03	9.99	8.44
Pr_2O_3	2.89	3.31	1.96	1.15	n.d	3.50	2.53
Sm_2O_3	2.04	5.94	2.06	2.42	n.d	0.83	0.73
Gd_2O_3	0.88	3.97	1.43	2.57	n.d	n.d	0.18
FeO	1.14	n.d.	5.23	5.75	0.32	0.95	n.d.
MnO	0.47	n.d.	0.30	0.24	20.96	0.50	n.d.
CaO	5.65	1.17	4.15	4.79	0.12	5.63	0.39
Na_2O	0.35	n.d.	n.d.	n.d.	n.d.	n.d.	n.d.
F	1.09	0.16	n.d.	n.d.	n.d.	6.05	6.77
Total	98.96	82.84	97.54	93.70	100.78	81.55	79.43

allanite in the sample from locality C (Fig. 9). The sum of the elements is only 94.6 wt.%, which implies that the mineral is hydrous. The following simplified formula is proposed:
$(Fe,Mn,Ca)_{3.0}REE_{0.5}Al_{1.75}Si_4O_{14.38} \bullet nH_2O$.

Mineral Uk2. On the basis of the average of nine analyses of this presumably new mineral, the following formula is proposed:
$Ce_{1.00}(La_{0.63}Nd_{0.22}Pr_{0.07}Sm_{0.02}Gd_{0.01})_{\Sigma 0.95}Ca_{0.03}F_{1.58}O_{1.75y}(OH)_{2y} \bullet nH_2O$
or simplified: $CeREEF_{1.5}O_{1.75-y}(OH)_{2y} \bullet nH_2O$.

Discussion

The present study of the alteration of eudialyte from the Ilímaussaq complex confirms the observations of Ussing (1898) and Bøggild (1953) of two distinct types of alteration, one leading to zircon- and the other to catapleiite-bearing assemblages. In both cases, eudialyte is pseudomorphed by aggregates of minerals which, at the time of Ussing and Bøggild, were too fine-grained for detailed identification. Electron microprobe study has revealed a number of minerals, some of which are reported for the first time from the Ilímaussaq complex, and some may be new minerals (Table 4).

The zircon alteration type was found in thoroughly altered agpaitic rocks; nepheline and potassium feldspar being substituted by analcime and sericite, amphibole and primary aegirine by late aegirine. This type of alteration was identified in rocks of the marginal pegmatite close to the external contacts of the complex. At locality B they are penetrated by a network of lujavrite dykes and at locality C by a swarm of parallel pegmatite dykes. The eudialyte alteration aggregates consist of zircon, alkali feldspar, aegirine, analcime, grossularite and fluorite and the secondary REE- and Nb-minerals Ce- and Y-fergusonite, allanite, fersmite and some unidentified phases. The fluids responsible for this alteration may have been introduced along fractures and may have been derived from later lujavritic intrusions, or may be of external origin.

The catapleiite alteration type was found throughout the complex in rocks that are less thoroughly altered or almost unaltered. This type of alteration varies from single catapleiite plates in eudialyte in practically unaltered rocks, to pseudomorphs after eudialyte dominated by catapleiite in the most altered rocks. In naujaite, large eudialyte grains may be completely replaced by catapleiite whereas small crystals in the same rocks are unaltered. In lujavrites, eudialyte is generally altered to aggregates of catapleiite, aegirine, mica, analcime, neptunite, carbonates and other minerals (Rose-Hansen & Sørensen, 2002). In the most altered lujavrites, dusty aggregates have pseudomorphed eudialyte (Ussing 1898). In the marginal pegmatite, catapleiite is accompanied by minor monazite, apatite, nacareniobsite-(Ce) and feldspar, aegirine, neptunite, analcime and fluorite. The catapleiite alteration type appears to have been caused by low-temperature late magmatic interstitial fluids.

The late- and post-magmatic alteration is distinctly different from the hyperagpaitic orthomagmatic formation of lovozerite and steenstrupine of the Ilímaussaq complex (Sørensen 1962; Sørensen & Larsen 2001), and the formation of zirsinalite, lovozerite and terskite from the Lovozero agpaitic complex of the Kola Peninsula (Khomyakov 1995; Pekov 2000). These minerals are orthomagmatic, having formed from portions of the agpaitic magma which were enriched in Na, water and other volatiles. The formation of catapleiite appears to have been caused by low-temperature late magmatic interstitial fluids.

The zircon type of alteration has been reported by Bøggild (1953) from the mineral locality Narssarssuk in the Igdlerfigsalik centre of the Igaliko Complex located about 50 km east of the Ilímaussaq complex, and by Coulson (1997) from the North Qoroq centre from the same complex, where eudialyte is replaced by zircon, allanite, aegirine, natrolite, titanite, rinkite, mosandrite and wöhlerite, besides zirfesite. This type of alteration has been described from the Pilansberg complex, South Africa, by Mitchell & Liferovich (2006): zircon, Ce-fergusonite, Ce- and La-allanite, Ce-britholite, titanite, pyrochlore, natrolite, feldspars and a number of Ba and Mn minerals and REE carbonates. The alteration is judged to have been caused by low-temperature Na- and Cl-rich hydrothermal fluids. At Tamazeght, Morocco, eudialyte is replaced by aggregates of zircon, feldspar, aegirine, fluorite and calcite (Khadem Allah et al. 1998). In the Lovozero complex, zircon, vlasovite and woehlerite replace eudialyte in some albitized contact rocks (Pekov 2000).

The catapleiite type of alteration has been described from all eudialyte-carrying complexes. At Tamazeght pseudomorphs after eudialyte consist of aggregates of catapleiite, feldspar, aegirine, natrolite, vlasovite, rinkite, calcite, rhodochrosite, fluorite and pyrophanite. The eudialyte in pegmatites intruding the sedimentary country rocks can be altered into zircon, and there are also cases of eudialyte overgrowing zircon (Khadem Allah *et al.* 1998). Some secondary minerals after eudialyte contain Zr, Nb and REE, whereas others display a sharp separation of Zr from REE and Nb.

In Fig. 13 spider diagrams have been normalized against eudialyte in order to show the movement of elements during the eudialyte alteration process.

Fig.13a shows the minerals belonging to the catapleiite alteration type and Fig.13b those belonging to the zircon alteration type. Sharp separation of Zr has taken place and most of the secondary minerals are enriched in Nb-REE-Y and F, and depleted in Si, Th, Ti and Zr.

Zirconium is almost exclusively found in zircon and catapleiite, and Th in uranothorianite, whereas the REE are located in allanite, Ce- and Y-fergusonite, monazite and most of the unidentified minerals; Nb is held by fersmite, Ce- and Y-fergusonite, nacareniobsite-(Ce) and the unidentified minerals Nb1 and Nb2. Thus the Zr/Nb ratio, which varies from 10 to 17 in eudialyte, is very high in catapleiite and zircon and low or zero in all the other minerals containing these elements (Table 5). Na, Ca, Al, Fe and Mn are located in the feldspars, grossularite, aegirine, analcime, natrolite, grossularite, as well as in catapleiite, fersmite, allanite, apatite, nacareniobsite-(Ce), A1 and A2.

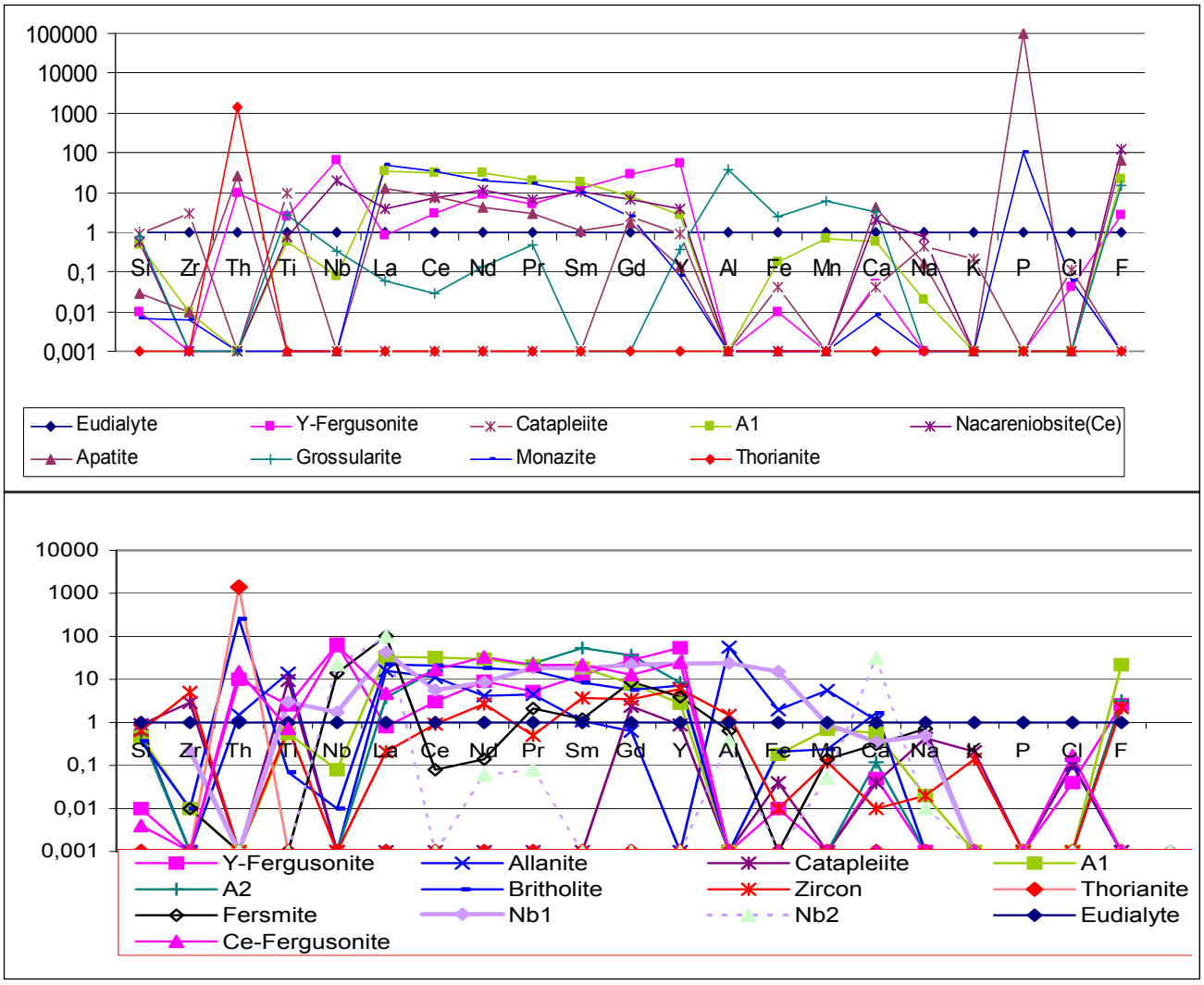

Fig. 13 a+b. Eudialyte normalized spider diagrams. The upper diagram (a) shows the catapleiite alteration type and the lower diagram (b) the zircon alteration type. Values at 0.001 represent analyses below detection limit and lines joining these 'points' can be disregarded.

Table 5. Zr/Nb, La/Nd, Ce/y and La/Gd rations in minerals from the Ilímaussaq complex

	Eudialyte	Catap-leiite	Zircon	Ce-Fergu-sonite	Y-Fergu-sonite	Fersmite	A1	A2	Nb1	Nb2	Uk1	Uk2
Zr/Nb	10.91 - 17.84	10.71		0	0	0	0.33 - 7.00		0.001 - 0.003		1.23	2.75
La/Nd	0.98 - 1.26		0.05 -0.19	0.17 - 1.19	0.03 - 0.27	0.05 - 0.21	0.79 - 2.62	0.07 - 0.28	0.37 - 0.50		3591	463.4
Ce/Y	1.95 - 2.74			1.40 - 30.92		0.48 - 0.25	6.03 - 313.8	2.36 - 18.36	0.77 - 6.30	0.35		129.1
La/Gd	3.43 - 7.83		0.26 – 5.0	1.61	0.12	0.09	41.07	0.39	3.70			

Ussing (1898, p.174) demonstrated that the bulk Zr content remained in the pseudomorphs. This may indicate that the bulk chemical composition of eudialyte is preserved in the pseudomorphs, although there has evidently been loss of Cl and Na and addition of F and P. Buchwald & Sørensen (1961), in a fission track examination of Ilímaussaq minerals, found that minute pigment particles in altered eudialyte are quite radioactive, which means that U, and probably also Th, released during alteration of the eudialyte was bound to the pigmentary material.

The alteration of eudialyte resulted in pronounced REE fractionation (Fig. 13).

Our microprobe set-up provided Gd as the only HREE. The LREE/HREE ratio and possible Eu anomaly therefore cannot be calculated; instead the La/Gd and Ce/Y ratios are presented in Table 5, together with the La/Nd ratio. The La/Nd ratio is close to 1.0 in eudialyte and Ce-fergusonite and is very low in zircon, Y-fergusonite, fersmite, A2 and Nb1. It is high in apatite and monazite and variable in allanite.

The Ce/Y and La/Gd ratios show lower values than eudialyte in zircon, Y-fergusonite and fersmite, higher values in A1, apatite, monazite and Ce-allanite, and variable values in Ce-fergusonite, A2 and Nb1.

In the eudialyte-normalized diagrams (Fig.13) it is evident that all the analyzed minerals, with the exception of Nb2, are enriched in REE relative to eudialyte. Nacareniobsite-Ce, Nb1, Nb2, Uk1, zircon, Ce-fergusonite, A1 and A2 show the same REE pattern as eudialyte. Fersmite is depleted in La, Ce, Pr and the HREE and enriched in the intermediate REE relative to eudialyte. Apatite, monazite, allanite, Uk1 and Uk2 are enriched in LREE and depleted in HREE relative to eudialyte. Y-fergusonite is the only one of the examined minerals which shows marked enrichment in the HREE.

Europium was not determined, but eudialyte displays a pronounced negative Eu anomaly similar to that of the agpaitic rocks of the complex (Bailey et al. 1978; Sørensen 1992; Pfaff et al. 2008).

In Pilansberg, three stages of eudialyte crystallization and five stages of eudialyte alteration are distinguished (Mitchell & Liferovich 2006). Thus, zircon belongs to an early miaskitic stage. With increasing alkalinity, eudialyte is formed, followed by catapleiite, allanite, apatite at decreasing alkalinity.

In the rocks studied by us, only the catapleiite and zircon trends of alteration are distinguished, and we have seen no signs of successive stages of alteration. Rare catapleiite grains have only been observed in one zircon aggregate.

Identity of the unidentified minerals

The unidentified minerals described here have been compared with those from the Lovozero complex (Khomyakov 1995), Pilansberg (Mitchell & Liferovich 2006) and the Tamazeght complex (Kadar 1984; Khadem Allah, 1993). We have not succeeded in correlating the unidentified Ilímaussaq minerals with any of these minerals or with any minerals listed in *Min-Ident-Win*, Dec. 2001.

The chemical compositions of minerals A1 and A2 resemble the composition of Ce-britholite $(Ce,Ca)_{10}(SiO_4,PO_4)_6(OH,F)_2$, cerite $(Ce,Ca)_{10}(SiO_4)_6(OH,F)_5$ and the unnamed mineral mineral X (Kalsbeek et al. 1990) for which we have calculated the formula $NaCa_{1.5}REE_7(Si,P)_6O_{24}OH \bullet nH_2O$. Mineral X is regarded by Kalsbeek et al.. (1990) as a P_2O_5-poor member of the britholite group of minerals. Britholite is of widespread occurrence in the Ilímaussaq complex.

As we only have information on the chemical compositions and no structural data of minerals A1 and A2, we are unable to decide whether these two minerals are new species or members of the britholite or cerite groups of minerals. In britholite, and possibly also in cerite, there is complete solid solution between Si and P.

The minerals Nb1 and Nb2 appear to be related to fersmite. The chemical analyses of nacareniobsite-(Ce) and apatite are close to the analyses of these minerals published by Petersen et al. (1989) and Rønsbo (1989, 2008).

Conclusions

Eudialyte is a major constituent of the agpaitic rocks of Ilímaussaq. It may be perfectly fresh, but is generally altered. At least four types of alteration may be distinguished: the common catapleiite type, the rare zircon type described here, the "zirfesite" type mentioned here and the lujavrite type described by Ussing (1898, 1912).

A characteristic feature is that the crystal shape is preserved, even when the eudialyte has been completely altered, as is the case in the zircon, zirfesite and lujavrite types.

In the two first-named types, eudialyte has been pseudomorphed by alteration products, but in the lujavrite type only "shells" of eudialyte crystals are preserved. In the catapleiite type, alteration may be weak as described here, or complete as in some kakortokites where crystals are pseudomorphed by cata-

pleiite aggregates. Alteration results in a pronounced separation of elements, Zr is found only in zircon and catapleiite. REE are located in REE minerals such as monazite, apatite, allanite, A1, A2, and UK1 and UK2. Nb is bound in fersmite and Nb2. REE and Nb occur together in fergusonite, Nb1, and nacareniobsite-(Ce). Allanite and nacareniobsite-(Ce) act as collectors for REE and Ca. Allanite is low in Na and marks a miaskitic trend, nacareniobsite-(Ce) is high in Na and marks the agpaitic trend. Besides allanite and nacareniobsite, Ca is found in monazite, grossularite, fluorite, catapleiite and fersmite.

Ussing (1898) demonstrated that the Zr content of the eudialyte was most probably retained in the pseudomorphs. The same may be the case with REE, Nb and perhaps Ca. It was, however, not a completely closed system as Cl has certainly been lost and F and P introduced. A quantitative test is impossible where all the original eudialyte has disappeared, as is the case in the zircon type of alteration. The catapleiite type of alteration took place at a late magmatic stage by residual interstitial liquids, whereas the zircon type may have formed by liquids of external origin.

Acknowledgements

We are grateful for the technical assistance of B. Wensler and H. Diaz. Collaboration with H. Bohse in the field is greatly appreciated. Dr. J. C. Bailey carefully read the manuscript and made valuable comments to its content. The Danish Natural Science Research Council provided the microprobe facililties. The Carlsberg Foundation supported the field work.

References

Andersen, S., Bohse, H. & Steenfelt, A. 1988: The southern part of the Ilímaussaq complex, South Greenland, 1:20.000. Copenhagen: Geological Survey of Greenland.

Bailey, J., Gwozdz, R., Rose-Hansen, J. & Sørensen, H. 1978: Preliminary geochemical work on the Ilímaussaq alkaline intrusion, South Greenland. Rapport Grønlands Geologiske Undersøgelse 90, 75-79.

Bohse, H., Brooks, C.K. & Kunzendorf, H. 1971: Field observations on the kakortokites of the Ilímaussaq intrusion, south Greenland, including mapping and analyses by portable X-ray fluorescence equipment for zirconium and niobium. Rapport Grønlands Geologiske Undersøgelse 38, 43 pp.

Bøggild, O.B. 1953: The mineralogy of Greenland. Meddelelser om Grønland 149(3), 442 pp.

Buchwald, V. & Sørensen H. 1961: An autoradiographical examination of rocks and minerals from the Ilímaussaq batholith, South West Greenland. Bulletin Geological Survey of Greenland 28, 35 pp. (also Meddelelser om Grønland 162, 11).

Coulson, I.M. 1997: Postmagmatic alteration in eudialyte from North Qoroq center, South Greenland. Mineralogical Magazine. 61, 99-1009.

Ferguson, J. 1964: Geology of the Ilímaussaq intrusion, South Greenland. Description of map and structure. Bulletin Grønlands Geologiske Undersøgelse 39, 82 pp.

Johnsen, O. & Gault, R.A. 1997: Chemical variation in eudialyte. Neues Jahrbuch Mineralogische Abhandlungen 171, 3, 215-237.

Kadar, M. 1984: Minéralogie et implications petrologiques des pegmatites des syenites nepheliniques du massif alcalin du Tamazeght (Haut Atlas de Midelt-Maroc). These présentée à L'Université Paul Sabatier de Toulouse (Sciences), France (146pp).

Kalsbeek, N., Larsen, S. & Rønsbo, J. G. 1990: Crystal structures of rare earth elements rich apatite analogues. (1990): Zeitschrift für Kristallographie 191, 249-263.

Khadem Allah, B. 1993: Syénites et pegmatites néphéliniques du complexe alcalin du Tamazeght (Haut Atlas de Midelt, Maroc). These présentée devant L'Université Paul Sabatier de Toulouse III (Science), France. 240pp.

Khadem Allah, B., Fontan, F., Kader, M., M., Onchw P. & Sørensen, H.1998:

Reactions between agpaitic nepheline syenitic melts and sedimentary carbonate rocks – exemplified by the Tamazeght complex, Morocco. Geochemistry International 36, 569-581.

Khomyakov, A.P. (1995). Mineralogy of hyperagpaitic alkaline rocks. Oxford: Clarendon Press, 223 pp.

Kostyleva, E.E. 1945: Zirfesite, a new zirconium mineral of the hypergenic zon. Doklady Akademii Nauk SSR 48, 531-533 (in Russian).

Kogarko, L.N., Lazutkina, L.N. & Krigman, L.D. 1988: Conditions of concentration of zirconium in igneous processes, 121 pp. Moscow: Nauka (in Russian).

MinIdent-Win , December 2001 by Smith, D.G.W & Leibovitz, D.P.

Mitchell, R.H. & Liferovich, R.P. 2006: Subsolidus deuteric/hydrothermal alteration of eudialyte in lujavrite from the Pilansberg alkaline complex, South Africa. Lithos 91, 352-372.

Pekov, I.V. (2000): Lovozero Massif. History, Pegmatites, Minerals. Moscow: Ocean Pictures Ltd. 480 pp.

Petersen, O.V., Rønsbo, J. & Leonardsen, E. 1989: Nacareniobsite-(Ce), a new mineral species from the Ilímaussaq alkaline complex, South Greenland, and its relation to mosandrite and the rinkite series. Neues Jahrbuch Mineralogische Monatshefte 1989, 84-96.

Pfaff, K., Krumrei, TH. Marks, M., Wenzel, T.R. & Markl, G. 2008: Chemical and physical evolution of the "lower layered sequence" from the nepheline syenitic Ilímaussaq intrusion, South Greenland: Implications for the origin of magmatic layering in peralkaline felsic liquids. Lithos 106, 280-296.

Rose-Hansen, J. & Sørensen, H. 2002: Geology of the lujavrites

from the Ilimaussaq alkaline comlex South Greenland, with information from seven bore holes. Meddelser om Grønland. Geoscience 40, 58 pp.

Rønsbo, J. 1989: Coupled substitutions involving REEs and Na and Si in apatites in alkaline rocks from the Ilímaussaq intrusion, South Greenland, and its relation to mosandrite and the rinkite series. Neues Jahrbuch für Mineralogie 1989, 84-96.

Rønsbo, J. 2008: Apatite in the Ilímaussaq alkaline complex: Occurrence, zonation and compositional variation. Lithos 106, 71-82.

Semenov, E.I. 1969: Mineralogy of the Ilímaussaq alkaline massif (South Greenland). 165 pp. Moscow: Nauka (in Russian).

Sørensen, H. 1962: On the occurrence of steenstrupine in the Ilímaussaq massif, Southwest Greenland. Meddelelser om Grønland 167, 1, 251 pp.

Sørensen, H. 1992: Agpaitic nepheline syenites: a potential source of rare elements. Applied Geochemistry 7, 417-427.

Sørensen, H. 2006: The Ilímaussaq alkaline complex, South Greenland. An overview of 200 years of Research and an Outlook. Geoscience 45, 1-70.

Sørensen, H. & Larsen, L.M. 2001: The hyper-agpaitic stage in evolution of the Ilímaussaq alkaline complex, South Greenland. In: Sørensen H. (ed): The Ilímaussaq alkaline complex South Greenland: status of mineralogical research with new results. Geology of Greenland Survey Bulletin 190, 83-94.

Sørensen, H. Bohse, H. & Bailey, J.C. 2006: The origin and mode of emplacement of lujavrites in the Ilimaussaq alkaline complex, South Greenland. Lithos 91, 286-300.

Steenfelt, A. 1972: Beskrivelse af pulaskit, heterogen foyait, sodalitfoyait, naujait og kakortokit på Kvanefjeldsplateauet, Ilímaussaq. 52pp. + appendix. Unpublished cand.scient. Thesis. Geologisk Institut. Københavns Universitet, Danmark.

Steenfelt, A. & Bohse, H. 1975: Variations in the contents of uranium in eudialyte from the differentiated alkaline Ilímaussaq intrusion, south Greenland. Lithos 8, 39-45.

Stromeyer, F. 1819: Summary of meeting 16 December 1819. (Analyse einiger grönlandischen, von Prof Giesecke erhaltenen Fossilien). Göttingische gelehrte Anzeigen 3, 1993-2000.

Ussing, N.V. 1898: Mineralogisk-petrografiske Undersøgelser af grønlandske Nefelinsyenitter og beslægtede Bjergarter. Meddelelser om Grønland 14, 1-220.

Ussing, N.V. 1912: Geology of the country around Julianehåb, Greenland. Meddelelser om Grønland 38, 1-376.

Westergaard, [Steenfelt] A. 1969: The border pegmatite of the Ilímaussaq Intrusion. Rapport Grønlands Geologiske Undersøgelser rapport 19, 39-40.

The cyclic Rørdal Member – a new lithostratigraphic unit of chronostratigraphic and palaeoclimatic importance in the upper Maastrichtian of Denmark

FINN SURLYK, LARS STEMMERIK, MORTEN AHLBORN, RIKKE HARLOU, BODIL W. LAURIDSEN, SUSANNE L. RASMUSSEN, NIELS SCHOVSBO, EMMA SHELDON & NICOLAS THIBAULT

Surlyk, F., Stemmerik, L., Ahlborn, M., Harlou, R., Lauridsen, B.W., Rasmussen, S.L., Schovsbo, N., Sheldon, E. & Thibault, N. 2010-11-11. The cyclic Rørdal Member – a new lithostratigraphic unit of chronostratigraphic and palaeoclimatic importance in the upper Maastrichtian of Denmark. © 2010 by Bulletin of the Geological Society of Denmark, Vol. 58, pp. 89–98. ISSN 0011–6297. (www.2dgf.dk/publikationer/bulletin)

The Maastrichtian chalk of the Danish Basin has been referred to the Tor Formation of the North Sea, but this may not be tenable because this formation in its type area shows a much higher degree of redeposition than the Maastrichtian chalk of the Danish Basin. The onshore succession has not been lithostratigraphically subdivided due to its rather monotonous nature and the widely scattered outcrops. An exception is the uppermost Maastrichtian exposed at Stevns Klint which is been referred to the Sigerslev Member, comprising rather benthos-poor, deep-water pure chalk, and the overlying mound-bedded, bryozoan-rich chalk which is placed in the Højerup Member. In addition, a thin marly chalk bed, the Kjølby Gaard Marl Member, containing Tethyan planktonic foraminifers is known from localities in northern Jylland and from water wells around Køge, eastern Sjælland. The new Rørdal Member is a cyclic chalk-marl unit, about 10 m thick, sandwiched between pure white chalks. It is well exposed in the large Rørdal quarry in Aalborg, and is recognised in boreholes south of Aalborg and in the Stevns-1 and Karlslunde-1 boreholes south of Copenhagen. Coccolith and brachiopod data show that it belongs to the UC20b-c^{BP} nannofossil zone of the North Sea scheme for the Upper Cretaceous Boreal province, and the *semiglobularis-humboldtii* brachiopod zone, both indicating the lower upper Maastrichtian. Isotope data show that it represents a distinct early late Maastrichtian cooling event. The member thus has a basinwide distribution and is an important isochronous marker because it represents a significant change in sea-water temperature and not a progradational event.

Keywords: Lithostratigraphy, cyclicity, chalk, marl, Rørdal Member, Maastrichtian, Denmark.

Finn Surlyk [finns@geo.ku.dk], Lars Stemmerik [ls@geo.ku.dk], Morten Ahlborn [ma@geo.ku.dk] Rikke Harlou [rh@geo.ku.dk], Bodil W. Lauridsen [bodill@geo.ku.dk], Nicolas Thibault [nt@geo.ku.dk]. Department of Geography and Geology, University of Copenhagen, Øster Voldgade 10, DK-1350 Copenhagen K, Denmark. Susanne L. Rasmussen [slr@geus.dk], Niels Schovsbo [nsc@geus.dk], Emma Sheldon [es@geus.dk]. The Geological Survey of Denmark and Greenland, Øster Voldgade 10, DK-1350 Copenhagen K, Denmark.

Corresponding author (finns@geo.ku.dk)

All outcropping Upper Cretaceous chalk of the Danish Basin belongs to the Maastrichtian Stage (Surlyk 1984). Lower Maastrichtian chalk is well exposed at Møns Klint, upper Maastrichtian chalk is exposed in quarries around Aalborg in northern Jylland, and uppermost Maastrichtian chalk is exposed along the length of the 14 km long coastal cliff, Stevns Klint, and in small outcrops in northern Jylland (Fig. 1).

The Maastrichtian chalk of the Danish Basin is referred to the rather unfortunately named Chalk Group but has not been systematically lithostratigraphically classified and subdivided due to the monotonous lithology, scattered nature of the outcrops, and lack of long continuous outcrop sections. It has with some hesitation been referred to the Tor Formation of the North Sea (Surlyk *et al.* 2003, 2006) but ongoing work on the fully cored scientific Stevns-1 and -2 boreholes (Stemmerik *et al.* 2006; Schovsbo *et al.* 2008; Thibault *et al.* 2009; Thibault 2010) will hopefully allow a detailed lithostratigraphic subdivision of the upper Campanian – Maastrichtian chalk of the Danish basin. The top Maastrichtian exposed at Stevns Klint has recently been referred to the Sigerslev Member, comprising rather benthos-poor, deep-water pure chalk,

and to the overlying mound-bedded, bryozoan-rich chalk of the Højerup Member (Surlyk *et al*. 2006). A thin but distinctive marl bed, the Kjølby Gaard Marl Member of Troelsen (1955), containing Tethyan planktonic foraminifers is known from the uppermost Maastrichtian at several localities in northern Jylland and from water wells and other wells around Køge and Copenhagen, eastern Sjælland.

The outcropping Maastrichtian chalk of Denmark was subdivided into a total of ten brachiopod zones by Surlyk (1970, 1972, 1984). This zonation has been extended to Hemmoor and Kronsmoor in northern Germany (Surlyk 1970, 1982), Norfolk in eastern England (Johansen & Surlyk 1990), and was correlated with the brachiopod zones of Steinich (1965) on the island of Rügen in north-eastern Germany. The Danish Maastrichtian is also referred to belemnite zones (Birkelund 1957; Christensen 1996, 1997; Schulz & Schmid 1983) but belemnites are only common in the lower Maastrichtian chalk of Hvide Klint and Møns Klint; they are very rare in the uppermost Maastrichtian of Stevns Klint, and virtually absent in the Maastrichtian of western Denmark. Recent work on coccoliths from the Stevns-1 and Rørdal-1 cores (Sheldon 2008; Thibault *et al*. 2009) has allowed correlation with the Boreal coccolith zonation of the North Sea established by Burnett (1998) and Fritsen (1999). A $\delta^{13}C$ curve has been established for the Stevns-1 and Rørdal-1 cores and this makes it possible to undertake detailed chronostratigraphic correlations of the upper Campanian – Maastrichtian chalk of the Danish Basin (R. Harlou unpublished data; Schovsbo *et al*. 2008; Thibault *et al*. 2009). Stevns-1 provides an excellent $\delta^{13}C$ standard reference curve for this stratigraphic interval in the Boreal Realm.

The new Rørdal Member defined here represents a marked deviation from the otherwise rather monotonous Maastrichtian chalk in that it is markedly cyclic with alternating chalk and marl beds (Lauridsen & Surlyk 2008; Schovsbo *et al*. 2008). It is well exposed in the large Rørdal quarry in Aalborg and is identified in boreholes south of Aalborg and in the Stevns-1 and -2 and Karlslunde-1 boreholes south of Copenhagen (Fig. 1). The aim of the present study is to define the cyclic unit as a formal member, to demonstrate its chronostratigraphic significance, and to highlight its importance as a palaeoclimatic signal.

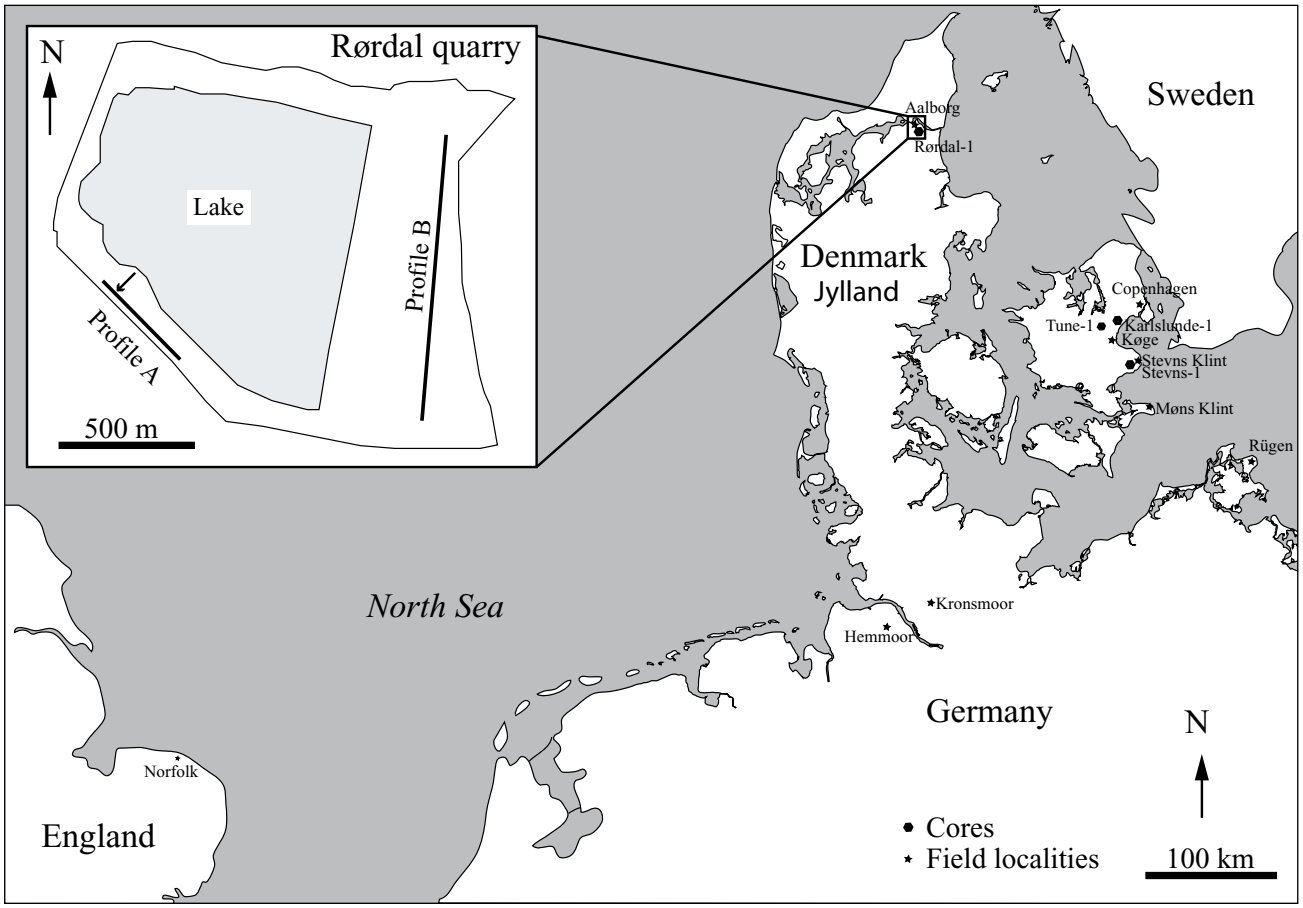

Fig. 1. Map showing position of localities mentioned in the text. Inset a map of the Rørdal quarry. Profiles A and B are illustrated in Figure 2. Arrow pointing at profile A indicates the position of the type section (Fig. 2A).

Lithostratigraphy

Rørdal Member

New member

Name

After the large Rørdal quarry situated in eastern Aalborg, northern Jylland (Fig. 1).

History

The member was first identified by Surlyk (1970) but at that time only the lowest thin marl bed was exposed. It was correlated with marl bands at Rügen and Hemmoor on the basis of brachiopod stratigraphy and was interpreted as a possible bentonite. A few years later the full cyclic succession became exposed (F. Surlyk and E. Stenestad, unpublished data, 1976) and was figured by Stenestad (2005, 2006). Recently it formed the basis for palaeoecological studies of the benthic invertebrates and trace fossil assemblages and their response to the cyclic changes in substrate lithology (Lauridsen & Surlyk 2008; Lauridsen *et al.* in press).

Type and reference locality

The uppermost part of the south-western wall of the Rørdal quarry is designated as the type section (Figs 1, 2A, B, 3). It is somewhat overgrown and weathered, but marks the final extent of the quarry and will not be further excavated. Excellent exposures are at present (2009) seen in the eastern quarry wall which, however, is subject to ongoing quarrying (Fig. 2C). The Karlslunde-1 and Stevns-1 boreholes (Stemmerik *et al.* 2006; Bonnesen *et al.* 2009) serve as reference localities (Figs 1, 4).

Thickness

The member is about 9 m thick in the type section as estimated from the thickness of the interval, comprising eight distinctive peaks on the gamma-ray profile (Fig. 3). A slightly different thickness was measured in the field due to difficulties in adequate estimations in the trench of the sloping quarry wall exposing slightly dipping beds (Fig. 3). The marl beds are 30–60 cm thick and the intervening chalk beds are 60–120 cm thick in the type section. In the gamma ray log the marl beds are measured as 30–65 cm thick and the intervening chalk beds as 50–110 cm thick (Fig. 3). The carbonate content is 71–82% in the marl beds and 82–92% in the chalk beds (Fig. 3).
In the Stevns-1 reference section, the correlative succession shows up to ten gamma ray peaks. However, only the lowermost five of these are associated with marly beds and are referred to the Rørdal Member. The member is approximately 9 m thick, from 105.05–96.20 m, and is characterised by only five marl beds, 5–10 cm thick, separated by 20–220 cm thick beds of

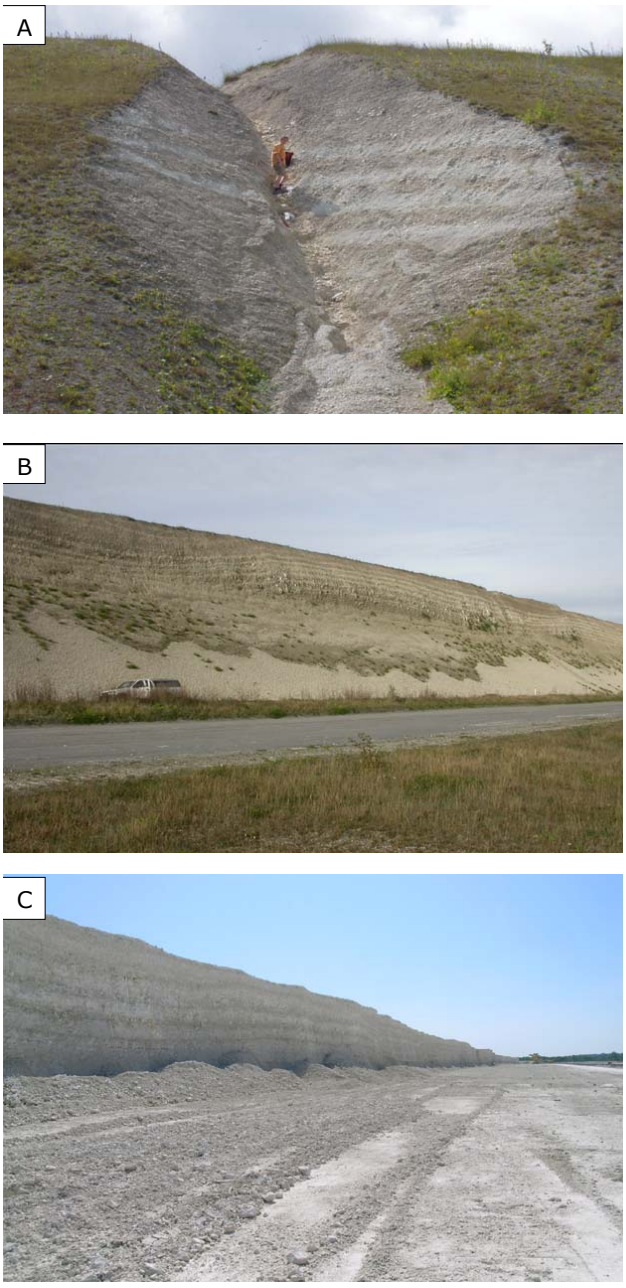

Fig. 2. (A) The type section of the Rørdal Member in the south-western wall of the Rørdal quarry. Position indicated on Figure 1. The exposed section is about 7 m high. (B) The south-western wall of the Rørdal quarry (profile A in Figure 1). Note the gentle glaciotectonic folding of the succession. The wall is about 23 m high. (C) The member is well exposed in the eastern quarry wall which at present (autumn 2009) is being intensely quarried (profile B in Figure 1). The quarry wall is 7 m high.

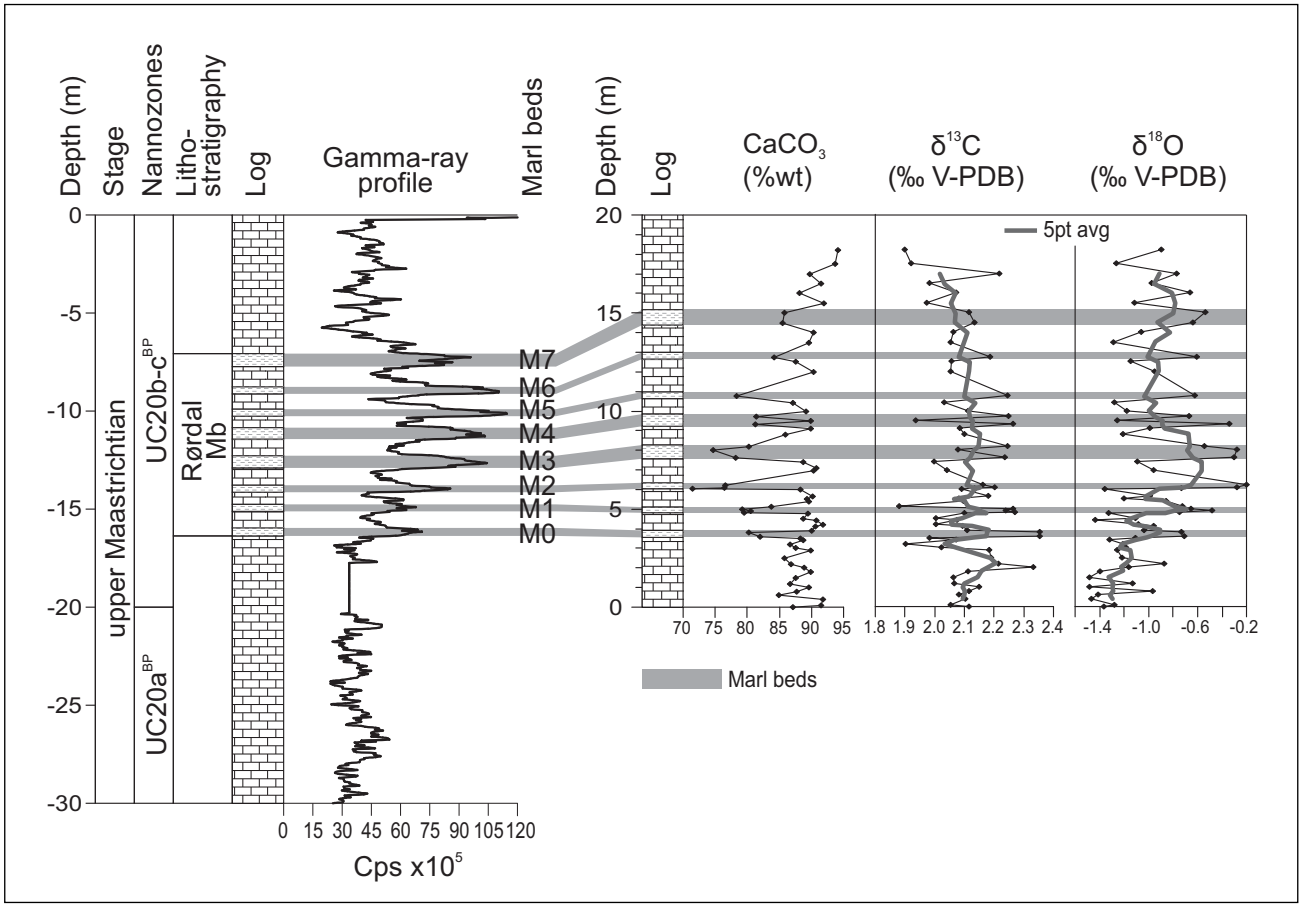

Fig. 3. Stratigraphy, gamma ray log, carbonate content and bulk stable isotopes from the Rørdal quarry section. The Rørdal Member comprises eight marl beds, M0 to M7.

bioturbated chalk (Fig. 4). In the greatly expanded reference section in Karlslunde-1, the eight marl beds are 4–50 cm thick, most being 6–13 cm thick (Fig. 4). The intervening bioturbated chalk beds are mainly 330–480 cm thick, but the uppermost bed is 690 cm thick.

Lithology and fossils

The member comprises a cyclic chalk-marl unit sandwiched between pure white chalks. A total of six marl beds have been identified in the somewhat weathered type section in the Rørdal quarry (Lauridsen & Surlyk 2008). Eight marl beds are visible in the eastern quarry wall and eight beds can be identified in gamma ray logs in a borehole drilled immediately adjacent to the type section (Figs 2, 3, 4). In fresh outcrop and in cores the marl beds are light grey and the intervening chalk is white but in weathered outcrops these colours are reversed and the marl beds are whitish, whereas the chalk beds are light grey (Fig. 2 A, B).

XRD-analyses of the marls indicate that they have a very uniform composition being dominated by smectite and quartz with some illite and minor analcime. Kaolinite is only present in marls from the boreholes in eastern Denmark. The silt fraction is dominated by quartz and dolomite with small amounts of mica, orthoclase and microcline. REE data indicate a very uniform composition of all the marl beds in Stevns-1 and Karlslunde-1 and are characterised by a slight Eu-anomaly (Fig. 5) which is not evident in the marls from the type locality at Rørdal (Ahlborn 2008).

The cyclic occurrence of the marl beds, the clay mineral assemblage, high quartz content, absence of volcanic phenocrysts in the silt fraction, and the lack of a marked negative Eu-anomaly make it unlikely that the marls are weathered volcanic ash-beds, i.e. bentonites. This is further supported by EDX-analyses of individual smectite grains, showing that they are Ca-rich rather than Mg-rich which would be expected if they were authigenic (Ahlborn 2008).

The generally millimetre-sized benthic invertebrate fauna obtained by washing of bulk samples is extremely diverse (Fig. 6). It is dominated by bryozoans estimated to comprise several hundred species, followed by 20 species of echinoderms, 16 species of

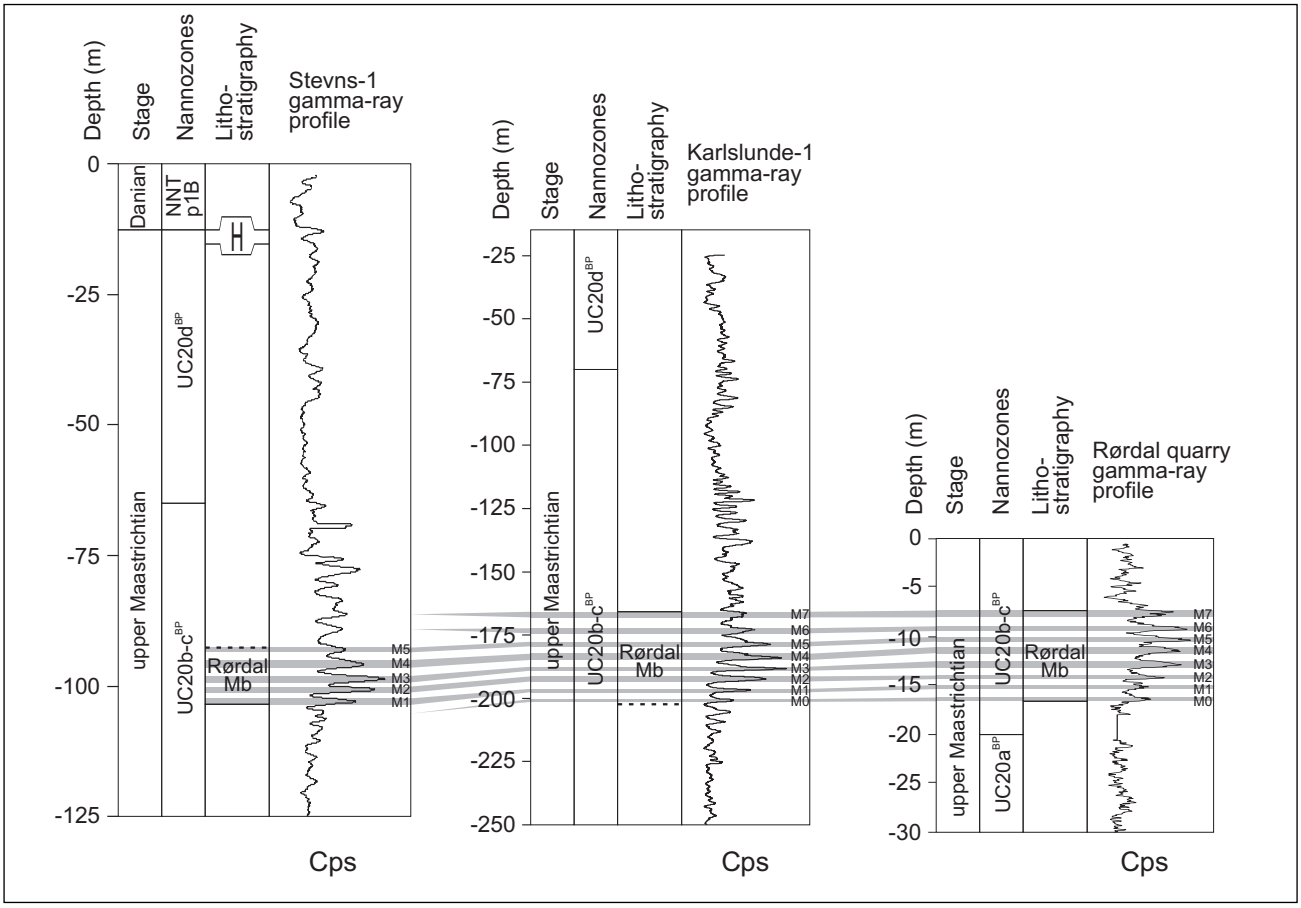

Fig. 4. The Rørdal-1, Stevns-1 and Karlslunde-1 boreholes, showing correlation of gamma ray logs of the Rørdal Member. The two latter boreholes serve as reference localities of the new Rørdal Member. Stratigraphic position of the member is indicated. Based on Stemmerik *et al.* (2006), Schovsbo *et al.* (2008), and Bonnesen *et al.* (2009).

brachiopods, 14 species of bivalves, and 13 species of serpulids (Lauridsen & Surlyk 2008). The member is strongly bioturbated throughout but burrows are more clearly visible and better defined in the marl beds (Fig. 7) (Lauridsen *et al.* in press). The ichnofauna represents the normal spectrum of trace fossils described from the Danish chalk and includes the upper, middle and lower tiers of Ekdale & Bromley (1991).

Stable isotope geochemistry

Oxygen and carbon isotopic composition of bulk carbonates were measured on 63 samples from the type section. The analysis was carried out at the Department of Geography and Geology, University of Copenhagen. The extraction of CO_2 was executed by reaction with anhydrous orthophosphoric acid at 70°C. Analyses were performed with a micromass isoprime spectrometer. The oxygen and carbon isotope values are expressed in per mil (‰) relative to the V-PDB standard reference. The analytical precision is estimated at 0.1‰ for oxygen and 0.05‰ for carbon.

The $\delta^{13}C$ values range between 1.9 and 2.4‰ and show an overall linear trend around 2.1‰ throughout the Rørdal Member (Fig. 3). The marl beds tend to have higher $\delta^{13}C$ values than the chalk beds with a mean difference of 0.3‰ between the two lithologies (Fig. 3).

The $\delta^{18}O$ values range between -0.2 and -1.5‰ and show a progressive overall increase upwards through the Rørdal Member from mean values of -1.3‰ at the base to values around -0.8‰ at the top (Fig. 3). This trend is interrupted by a positive excursion with values around -0.6‰ between marl beds M2 and M4 (Fig. 3). The marl beds show systematically heavier values than chalk beds with differences that vary between 0.5 and 1‰ between the two lithologies (Fig. 3).

Boundaries

The base of the member is defined by the base of the lowest marl bed in a succession of cyclically interbedded marl and chalk beds. The top of the member is defined by the top of the highest of the marl beds.

Distribution

The member is known from the Rørdal quarry, boreholes south of Aalborg, the Stevns-1, -2 and Karlslunde-1 boreholes south of Copenhagen (this study; Stemmerik *et al.* 2006; Ahlborn 2008; Schovsbo *et al.* 2008). The marl beds have also been identified in water wells in the Aalborg area by the resistivity logs (Jan Jul Christensen, written communication, 2007; Kirsten Skov Nielsen, written communication, 2008) due to the higher conductivity of the clay minerals compared to carbonate.

Bio- and chronostratigraphy

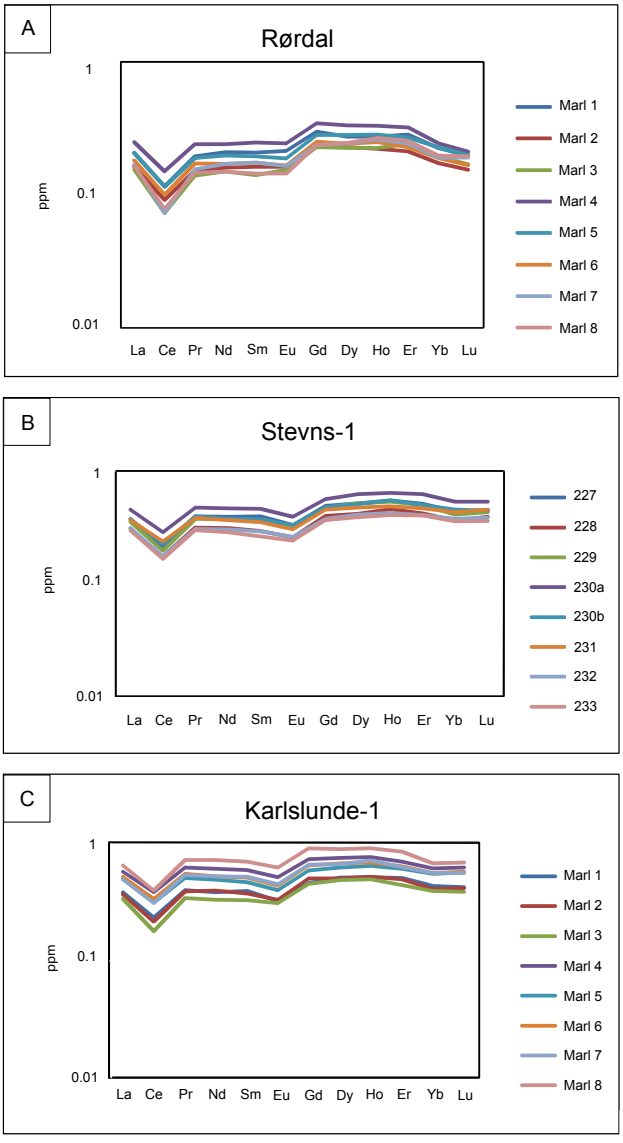

Fig. 5. Plots of REE from the eight marl beds of Rørdal Member from (A) Rørdal Quarry, (B) Stevns-1 and (C) Karlslunde-1. The REE have been normalized to Cody Shale for comparison with bentonite layers in the chalk of northeast England (Wray 1995, 1999). The lack of a defined negative Eu-anomaly in the REE data, combined with a lithology of mixed mineralogy, suggest an allochthonous origin of the marl beds.

The member is placed in the *semiglobularis-humboldtii* brachiopod zone of Surlyk (1970, 1984), and in the UC20b-c^{BP} nannofossil zone (Sheldon, 2008; Thibault 2010), corresponding to the lower upper Maastrichtian (Figs 3, 4).

Provenance

XRD and geochemical analysis of the mineralogy, major elements, trace elements and REE show a uniform composition of all marl beds, suggesting a common source area (Figs 5, 8). Plotting of the trace elements La, Th and Sc against each other reveals high Sc concentrations, suggesting a dominant volcanic contributor in the source area (Fig. 8). Zr/Nb ratios of 6.3–7.3 for all marl beds display a strong alkaline basalt signal while granitic basements would display ratios of 20–40, further strengthening this interpretation (Ahlborn 2008).

An obvious candidate as source area is the alkaline basalt necks and pipes in Skåne in southern Sweden to the east, where marked uplift of horsts took place during Late Cretaceous phases of inversion tectonics (Erlström *et al.* 1997). The stratigraphically younger Kjølby Gaard Marl has yielded similar results, showing that this area was a source of clay during much of the late Maastrichtian (Ahlborn 2008).

Environmental implications

The differences observed in the oxygen stable isotope values between marl and chalk beds may indicate differences in either temperature or salinity of the sea water during deposition, as well as diagenetic overprinting. Both lithologies are very soft and almost unlithified with only very minor signs of diagenetic influence confirmed by SEM examination of microbrachiopod valves. The borehole drilled adjacent to the type section was planned as a cored hole but yielded what looked like toothpaste, reflecting the soft nature of the sediments.

The overall progressively upwards increasing trend of the $\delta^{18}O$ values throughout the Rørdal Member thus seems to indicate an early late Maastrichtian cooling event with a fall in surface sea-water temperature of about 2° (Fig. 3). This interpretation is supported by a significant increase in the abundance of high-latitude calcareous nannofossil taxa in this interval at Rørdal quarry section and in the Stevns-1 borehole (N. Thibault, unpublished data). The variation in $\delta^{18}O$ between marl and chalk beds may be of primary environmental significance or can be attributed to differ-

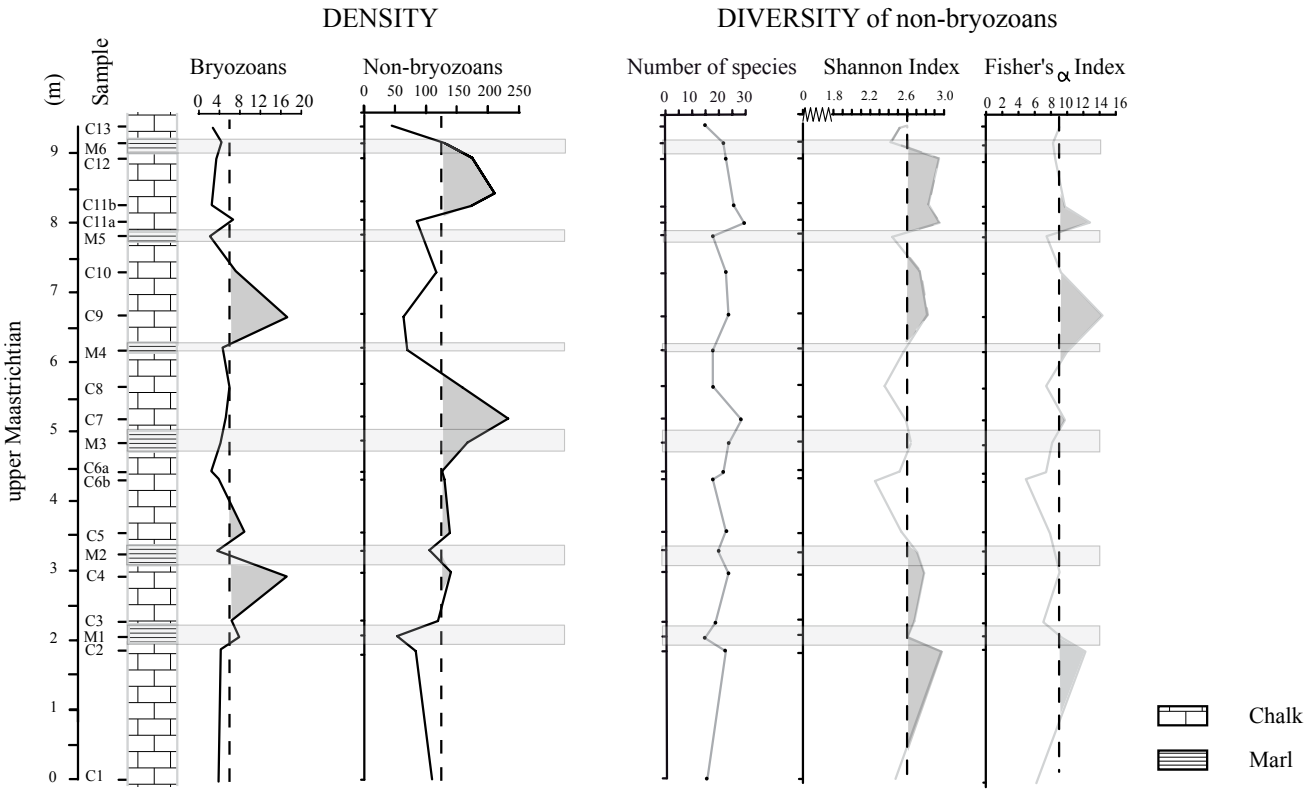

Fig. 6. Faunal density and diversity of the Rørdal Member based on data in Lauridsen & Surlyk (2008). The non-bryozoan group comprises echinoids, brachiopods, bivalves, serpulids, cirripedes, and sponges, which are all identified to species level, whereas the bryozoans are identified as morphotypes only. There is a pronounced difference in species diversity and density of bryozoan morphotypes between chalk and marl samples. Chalk samples are in most cases associated with higher bryozoan and non-bryozoan density and higher non-bryozoan diversity. The density of bryozoans is given g/kg sample due to the relatively high degree of fragmentation caused by sample preparation. The highest density is observed in the chalk between M1 and M2 with more than 14 g/kg. The density of bryozoans in the marl is in most cases below 5 g/kg, but there are slightly more bryozoans in M1. The density of the non-bryozoan macrofauna is also highest in the chalk beds. The density of the well-preserved non-bryozoans is quantified as number of specimens/kg sample. Marl samples are indicated by grey horizontal bars. Dark grey shaded areas indicate density and diversity values above the mean.

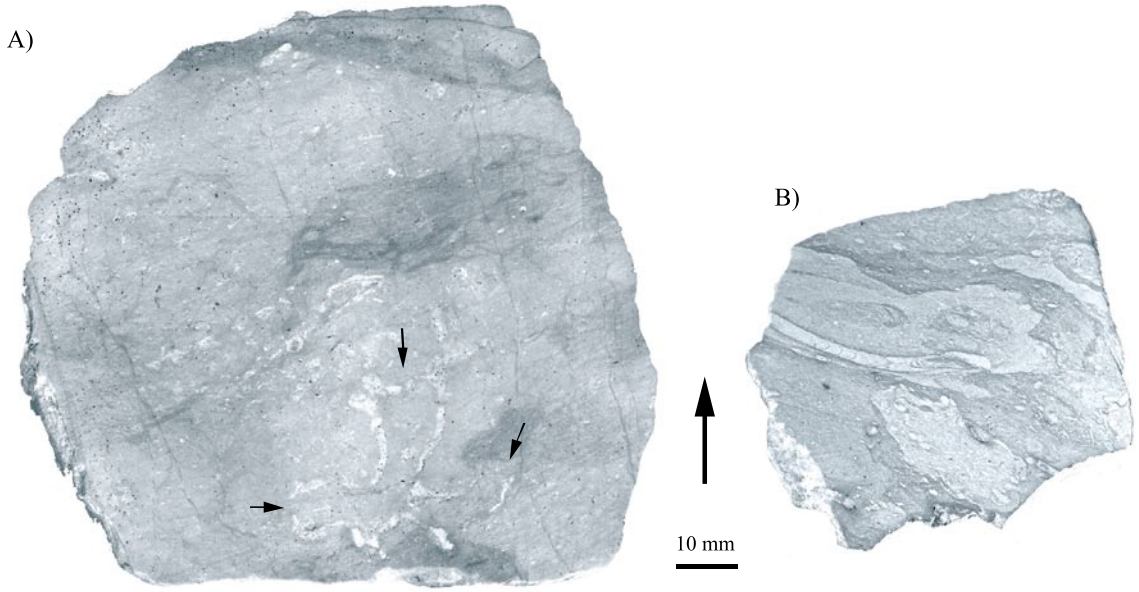

Fig. 7. Bioturbated chalk and marl samples from the Rørdal Member. The arrow indicates stratigraphic way up. (A) Chalk from sample 757, situated 2 m below M1. A possible operculum from a dissolved sponge is marked with small arrows. Note the very low diversity of trace fossils. (B) Marl from sample 722 (M4) shows a very high degree of reburrowing. Several *Thalassinoides* occur and the burrow fills are reburrowed by *Taenidum*, *Zoophycos* and *Chondrites*. *Zoophycos* displays a well-developed reverse backfill.

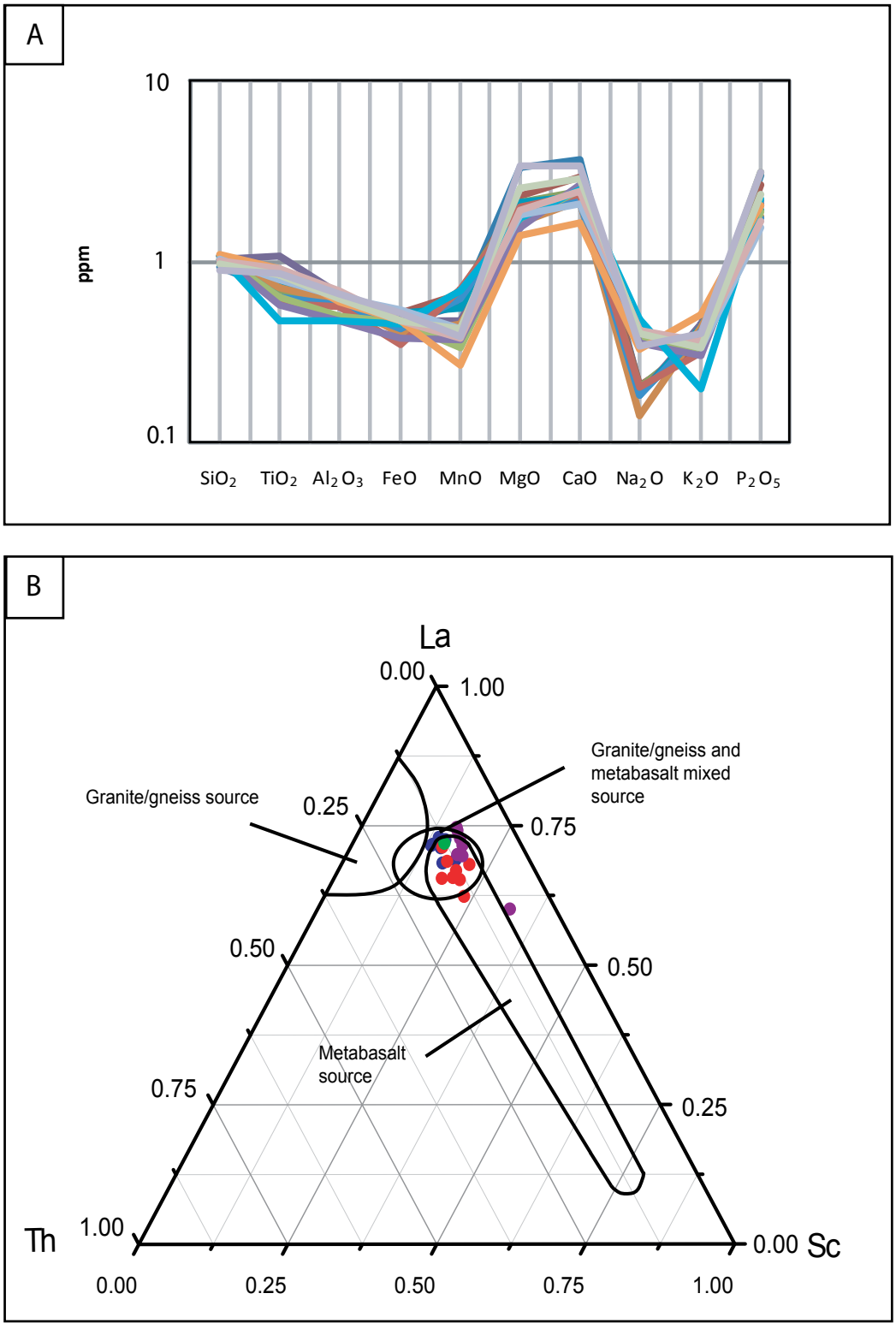

Fig. 8. (A) Plot of major elements from eight marl beds of the Rørdal Member from Stevns-1 and Karlslunde-1, and the Kjølby Gaard Marl Member from the Tune-1 borehole. The oxides are normalised after the Baltic, Ukrainian and Russian platform following Taylor & McLennan (1985). All marl beds show relative uniform curve patterns which suggest similar source areas. (B) Plot of the ternary relationship between the trace elements La-Th-Sc. All examined marl beds in Stevns-1 (blue), Karlslunde-1 (red), Rørdal (violet) and the Kjølby Gaard Marl (green) are characterised by compositions that deviate from the geochemical signature of a granite/gneiss basement. The plot illustrates an influence from a Sc-rich source, strongly suggesting a contribution from a volcanic source area. The compositions of the different source areas are from Lee & Lee (2003) and Sinha *et al.* (2008).

ential diagenesis between the two lithologies; ongoing work aims at solving this problem.

The wide distribution of the member in the Danish Basin suggests that the cooling event may be recognised in a larger region and adds to the knowledge of climate changes during the end of the Cretaceous Period.

Acknowledgements

We are grateful to Aalborg Portland Cement for allowing us access to the quarry, and Jan Jul Christensen and Kirsten Skov Nielsen for useful information. We thank Erik Thomsen for constructive comments. The study was supported by the Danish Natural Science Research Council.

References

Ahlborn, M. 2008: Et sedimentologisk studie af kridtlagserien i boringen Rørdal-2 fra Nordjylland, samt detaljerede leranalyser af mergellag i boringerne Rørdal-2, Stevns-1 og Karlslunde-1, Danmark. Cand. scient. thesis, University of Copenhagen.

Birkelund, T. 1957: Upper Cretaceous belemnites from Denmark. Biologiske Skrifter. Det Kongelige Danske Videnskabernes Selskab 9, 69 pp.

Bonnesen, E.P., Larsen, F., Sonnenborg, T.O., Klitten, K. & Stemmerik, L. 2009: Deep saltwater in Chalk of North-West Europe: origin, interface characteristics and development over geological time. Hydrogeology Journal. DOI 10.1007/sl10040-009-0456-9

Burnett, J.A. 1998: Upper Cretaceous. In: Bown, P.R. (Ed.): Calcareous Nannofossil Biostratigraphy. Norwell, Massachusetts, Kluwer Academic, 132–199.

Christensen, W.K. 1996: A review of the Upper Campanian and Maastrichtian belemnite biostratigraphy of Europe. Cretaceous Research 17, 751–766.

Christensen, W.K. 1997: The Late Cretaceous belemnite family Belemnitellidae: Taxonomy and evolutionary history. Bulletin of the Geological Society of Denmark 44, 59–88.

Ekdale, A.A. & Bromley, R.G. 1991: Analysis of composite ichnofabrics; an example in uppermost Cretaceous chalk of Denmark. In: Bottjer, D.J. (Ed.): 13th International Sedimentological Congress, Ichnologic symposium. Palaios. Society of Economic Paleontologists and Mineralogists, Tulsa, OK, United States, 232–249.

Erlström, M., Thomas, S.A., Deeks, N. & Sivhed, U. 1997: Structure and tectonic evolution of the Tornquist Zone and adjacent sedimentary basins in Scania and the southern Baltic Sea area. Tectonophysics 271, 191–215.

Fritsen, A. 1999: A Joint Chalk Stratigraphic Framework. Volume 1. Joint Chalk Research Program Topic V. Norwegian Petroleum Directorate. 206 pp.

Johansen, M.B. & Surlyk, F. 1990: Brachiopods and the stratigraphy of the Upper Campanian and Lower Maastrichtian chalk of Norfolk, England. Palaeontology 33, 823–873.

Lauridsen, B.W., Surlyk, F. & Bromley, R.G. in press: Trace fossils in cyclical chalk of the upper Maastrichtian Rørdal Member, Denmark. Cretaceous Research

Lauridsen, B.W. & Surlyk, F. 2008: Benthic faunal response to late Maastrichtian chalk–marl cyclicity at Rørdal, Denmark. Palaeogeography, Palaeoclimatology, Palaeoecology 269, 38–53.

Lee, J.I. & Lee, Y.I. 2003: Provenance of the lower Cretaceous Hayang Group, Gyeongsang Basin, southeastern Korea: Implications for continental-arc volcanism. Journal of Sedimentary Research 70, 151–158.

Schovsbo, N.H., Rasmussen, S.L., Sheldon, E., & Stemmerik, L. 2008: Correlation of carbon isotope events in the Danish Upper Cretaceous Chalk. Geological Survey of Denmark and Greenland Bulletin 15, 13–16.

Schulz, M.-G. & Schmid, F. 1983: Das Ober-Maastricht von Hemmoor (N-Deutschland): Faunenzonen-Gliederung und Korrelation mit dem Ober-Maastricht von Dänemark und Limburg. Newletters in Stratigraphy 13, 21–39.

Sheldon, E. 2008: Upper Campanian – Maastrichtian calcareous nannofossil biostratigraphy of the Stevns-1 borehole, Denmark. Journal of Nannoplankton Research 30, 39–49.

Sinha, S., Islam, R., Ghosh, S.K., Kumar, R. & Sangode, S.J. 2008: Geochemistry of Neogene Siwalik mudstones along Punjab re-entrant, India: Implications for source-area weathering, provenance and tectonic setting. Current Science 92, 1103–1113.

Stemmerik, L., Surlyk, F., Klitten, K., Rasmussen, S.L. & Schovsbo, N. 2006: Shallow core drilling of the Upper Cretaceous chalk at Stevns Klint, Denmark. Geological Survey of Denmark and Greenland Bulletin 10, 13–16.

Steinich, G. 1965: Die artikulaten Brachiopoden der Rügener Schreibkreide (Unter-Maastricht). Paläontologische Abhandlungen A 2, 1, 1-220.

Stenestad, E. 2005: *Heterohelix dentata* Biozonen i boringen Rørdal-1, øvre nedre Maastrichtien, Nordjylland, Danmark. Geologisk Tidsskrift 2005, 1–23.

Stenestad, E. 2006: Fluviokarst in the top of the Maastrichtian chalk at Rørdal, Northern Jutland, Denmark. Bulletin of the Geological Society of Denmark 53, 93–110.

Surlyk, F. 1970: Die Stratigraphie des Maastricht von Dänemark und Norddeutschland aufgrund von Brachiopoden. Newsletters in Stratigraphy 1, 7–16.

Surlyk, F. 1972: Morphological adaptations and population structures of the Danish chalk brachiopods (Maastrichtian, Upper Cretaceous). Det Kongelige Danske Videnskabernes Selskab Biologiske Skrifter 19, 2, 1–68.

Surlyk, F. 1982: Brachiopods from the Campanian–Maastrichtian boundary sequence, Kronsmoor (NW Germany). Geologis-

ches Jahrbuch A 61, 259–277.
Surlyk, F. 1984: The Maastrichtian Stage in NW Europe, and its brachiopod zonation. Bulletin of the Geological Society of Denmark 33, 217–223.
Surlyk, F., Damholt, T. & Bjerager, M. 2006: Stevns Klint, Denmark: Uppermost Maastrichtian chalk, Cretaceous–Tertiary boundary, and lower Danian bryozoan mound complex. Bulletin of the Geological Society of Denmark 54, 1–48.
Surlyk, F., Dons, T., Clausen, C. K. & Higham, J. 2003: Upper Cretaceous. In: Evans, D., Graham, C., Armour, A., & Bathurst, P. (Editors and co-ordinators). The Millennium Atlas: Petroleum Geology of the central and northern North Sea. London: The Geological Society of London 213–233.
Taylor, S.R. & McLennan, S.M. 1985: The continental Crust: Its Composition and Evolution. Blackwell, Boston, 312 pp.
Thibault, N., Schovsbo, N., Surlyk, F. & Stemmerik, L. 2009: Upper Campanian – Maastrichtian stable isotopes and calcareous nannofossil palaeoecology in the Boreal Realm (Stevns-1 well, Danish Basin Chalks): implications for climate change. EGU General assembly 2009, Vienna, Austria, 19–24 April 2009.
Thibault, N. 2010: Calcareous nannofossils from the Boreal upper Campanian – Maastrichtian Chalk of Denmark. Journal of Nannoplankton Research 31, 39–56.
Troelsen, J.C. 1955: *Globotruncana contusa* in the White Chalk of Denmark. Micropaleontology 1, 76–82.
Wray, D.S. 1995: Origin of clay-rich beds in Turonian chalks from Lower Saxony, Germany – a rare-earth element study. Chemical Geology 119, 161–173.
Wray, D.S. 1999: Identification and long range correlation of bentonites in Turonian–Coniacian (Upper Cretaceous) chalks of northwest Europe. Geological Magazine 136, 361–371.

The Skælskør structure in eastern Denmark – wrench-related anticline or primary Late Cretaceous seafloor topography?

FINN SURLYK, LARS OLE BOLDREEL, HOLGER LYKKE-ANDERSEN & LARS STEMMERIK

Surlyk, F., Boldreel, L.O., Lykke-Andersen, H. & Stemmerik, L. 2010-11-11. The Skælskør structure in eastern Denmark – wrench-related anticline or primary Late Cretaceous seafloor topography? © 2010 by Bulletin of the Geological Society of Denmark, Vol. 58, pp. 99–109. ISSN 0011–6297. (www.2dgf.dk/publikationer/bulletin)

Sorgenfrei (1951) identified a number of NW–SE oriented highs in the Upper Cretaceous – Danian Chalk Group in eastern Denmark, including the Skælskør structure and interpreted them as anticlinal folds formed by wrenching along what today is known as the Ringkøbing-Fyn High. Recent reflection seismic studies of the Chalk Group in Øresund and Kattegat have shown that similar highs actually represent topographic highs on the Late Cretaceous – Danian seafloor formed by strong contour-parallel bottom currents. Reflection seismic data collected over the Skælskør structure in order to test the hypothesis of Sorgenfrei show that the Base Chalk reflection is relatively flat with only very minor changes in inclination and cut by only a few minor faults. The structure is situated along the northern margin of a high with roots in a narrow basement block, projecting towards the northwest from the Ringkøbing Fyn High into the Danish Basin. The elevated position is maintained due to reduced subsidence as compared with the Danish Basin north of the high. The hypothesis of wrench tectonics as origin can be refuted. The seismic data show that the upper part of the Chalk Group is characterised by irregular mounded reflections, interpreted as representing contourite drifts, mounds and channels formed by strong, mainly late Maastrichtian bottom currents. The Skælskør structure of Sorgenfrei is thus in reality a Late Cretaceous topographic seafloor high formed by a combination of differential subsidence complemented by topographic features on the seafloor created by bottom currents in the late Maastrichtian.

Keywords: Skælskør structure, Chalk Group, wrenching, seafloor topography, bottom currents.

Finn Surlyk [finns@geo.ku.dk], Lars Ole Boldreel [lob@geo.ku.dk], Lars Stemmerik [ls@geo.ku.dk], Department of Geography and Geology, University of Copenhagen, Øster Voldgade 10, DK-1350 Copenhagen K, Denmark, Holger Lykke-Andersen [hla@geo.au.dk], Geological Institute, University of Aarhus, Høegh-Guldbergs Gade 2, bygning 1670, DK-8000 Aarhus C.

Corresponding author (finns@geo.ku.dk)

In a review of the topography, stratigraphy and tectonics at the base of the Quaternary in central and eastern Denmark Sorgenfrei (1951) noted the presence of NW–SE trending *en echelon* highs on and along the margins of what today is known as the Ringkøbing-Fyn High (Figs 1, 2). These highs were located at the north-eastern part of Stevns Klint, at Feddet south of Præstø, at Egesborg south of Næstved, at Rødby on southern Lolland, at Skælskør on western Sjælland, and at Nyborg and Ringe on western and central Fyn, respectively (Figs 1, 2). Sorgenfrei (1951) interpreted the highs as anticlinal folds formed by regional wrenching along the Ringkøbing-Fyn High which has a WNW–ESE orientation.

Similar highs are known from the Upper Cretaceous – Danian Chalk Group exposed in the 15 km long coastal cliff Stevns Klint where they are expressed by the position of the Cretaceous–Tertiary (K/T) boundary which varies from 5 m below to about 40 m above sea level along the length of the cliff (Rosenkrantz 1938; Lykke-Andersen & Surlyk 2004; Surlyk et al. 2006). An important lowermost Danian hardground situated up to about 1 m above the K/T boundary was interpreted as an originally horizontal marine abrasion

surface by Rosenkrantz (1938) who consequently interpreted the topographic relief of the boundary strata as a result of late or post-Danian Laramide folding. Reflection seismic data collected immediately offshore the cliff show, however, that the Base-Chalk reflection is remarkably planar, not folded, and has a gentle northward dip of 0.5° over at least 50 km in a S–N direction (Lykke-Andersen & Surlyk 2004; Esmerode *et al.* 2007a). The seismic profiles also show that a marked seafloor relief with ridges, valleys, drifts and channels was developed throughout deposition of the Chalk Group. The folding hypothesis was thus refuted and the relief of the K/T boundary was instead interpreted as representing a primary Late Cretaceous – Danian seafloor topography caused by long-lived bottom currents (Lykke-Andersen & Surlyk 2004). A similar high in the Danian carbonate succession is known from Øresund, the strait between Denmark and Sweden (Fig. 1) and has been interpreted as formed by post-Danian folding based on regional

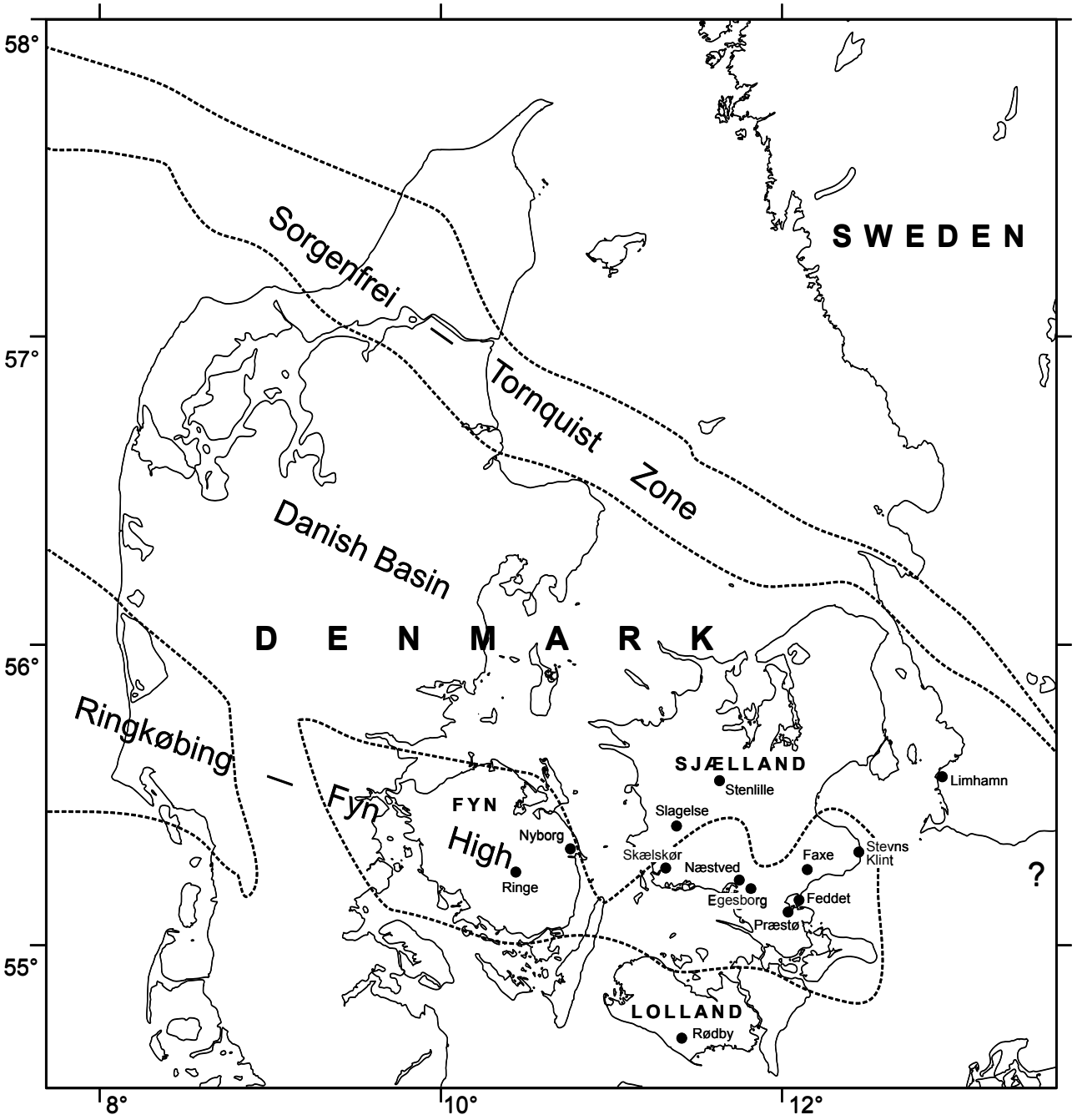

Fig. 1. Map showing the main structural elements of the Danish area and the position of localities mentioned in the text. Some of the localities are also shown in Figure 2.

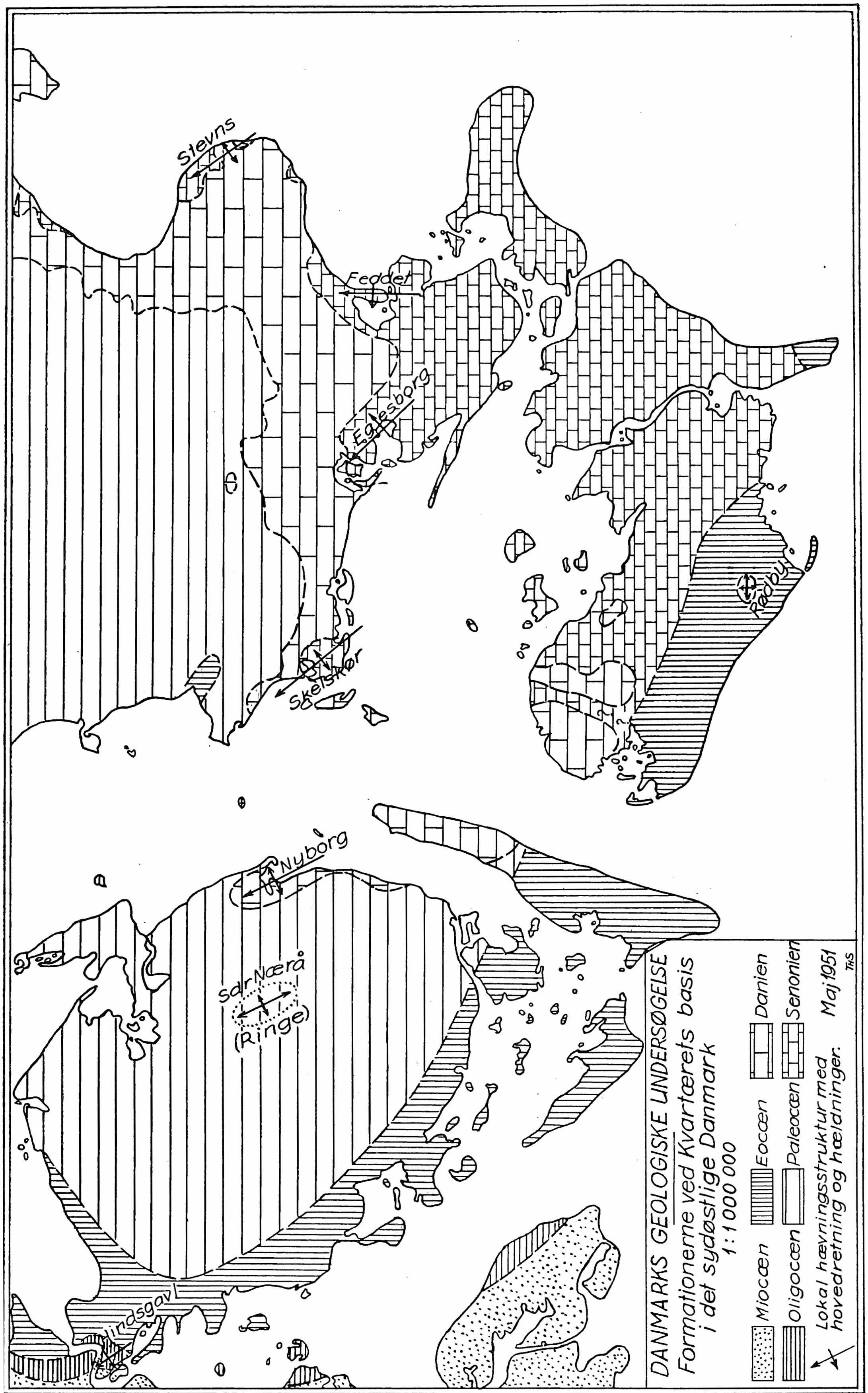

Fig. 2. Map prepared by Sorgenfrei (1951, p. 167), showing the geology of eastern Denmark at the base of the Quaternary. Note the presence of a number of mainly NW–SE oriented anticline-like structures. Sorgenfrei (1951) tentatively suggested that the structures were anticlinal folds formed during the Oligocene by wrenching along the margins of what today is known as the Ringkøbing-Fyn High (Fig. 1). Copied from Sorgenfrei (1951).

considerations (Hennig 1899), shallow boreholes (Brotzen 1959), and shallow seismic profiles (Knudsen *et al.* 1995). However, shallow and conventional deep seismic data supplemented by scuba-diving mapping of large excavations made for bridge piers, clearly show that the high also in this case represents a primary seafloor topography and is not due to folding (Bjerager *et al.* 2010).

The Danian of eastern Denmark comprises bryozoan limestone of the Stevns Klint Formation passing basinwards into chalk (Thomsen 1995; Surlyk 1997; Surlyk *et al.* 2006). At a few locations the bryozoan limestone is interbedded with coralline limestone formed by deep- and cool-water scleractinian corals. The largest occurrence of coralline limestone is in the Faxe quarry and smaller occurrences are known from the Limhamn quarry and from the Saltholm–Malmø High in the Øresund strait (Fig. 1). Coralline limestones are otherwise only known from a few shallow boreholes in southern Sjælland (Figs 1, 2). It is remarkable that these sites are all located over the highs identified by Sorgenfrei (1951). As a working hypothesis it has been proposed that formation of deep-water coral mounds in the Danian of the Danish Basin took place mainly on contemporaneous seafloor highs which were sites of intensified bottom currents, enabling extensive colonisation of azooxanthellate corals by supplying particulate nutrients (Bjerager *et al.* 2010). This is similar to the situation known from modern analogues (e.g. Freiwald *et al.* 1997, 2002).

The present study focuses on the large Skælskør structure of Sorgenfrei (1951). It is poorly known and the aim is to test if the structure is an anticline formed by post-Danian, possibly Oligocene wrenching along the northern margin of the Ringkøbing-Fyn High as suggested by Sorgenfrei (1951), or if it represents a local Late Cretaceous palaeobathymetric seafloor high formed by strong bottom currents.

Methods

The seismic data acquisition was performed on hard paved roads with a pulled geophone array system (72 geophones; separation 2.5 m; near offset 20 m). The seismic source was an IVI MiniVib, producing sweeps in the 10–300 Hz frequency band with four sweeps at each station located at intervals of 7.5 m along the line. The raw data were digitized, pre-processed (i.e. recorded sweeps correlated with sweep signal emitted from the vibrator) and recorded by a Geometrics Strataview recording system. The correlated field data were processed in Promax software to filtered stack sections with sea level as datum. A stack fold of ca. 12 was obtained at CMP-points with 1.25 m spacing. The Two Way Time (TWT) of the stacked sections were converted to depths by adopting a 1-D velocity model for the Chalk Group elaborated from refraction seismic data collected onshore along Stevns Klint (Nielsen *et al.* under revision). The stacked sections were geologically interpreted on PC-workstations with Kingdom Suite Software provided by Seismic Micro Technology.

Eight seismic lines were shot along the main, relatively straight roads around Skælskør but avoiding the main town (Fig. 3). The collected reflection seismic data are generally of excellent quality down to ca. 900–1000 m (600–700 msecs TWT) although parts of some profiles are disturbed by noise of various origins. The upper ca. 150 m (200 msecs TWT) show somewhat poorer reflectivity.

Results

The Quaternary cover is a few tens of metres thick in most of the study area and overlies Danian bryozoan limestone or Maastrichtian chalk. This means that the seismic profiles portray almost all of the Upper Cretaceous – Danian Chalk Group, the Danian part being only about 50 m thick in the area (Thomsen 1995). A strong reflection situated at depths down to about 600 msecs TWT, corresponding to a depth of about 900 m is interpreted as the Base Chalk reflection. It occurs at roughly the same depth as the Base Chalk reflection in seismic data onshore and offshore Stevns Klint where the group has a similar thickness (Lykke-Andersen & Surlyk 2004). The Chalk Group in the borehole Slagelse 1, situated 15–20 km north of the study area is close to 700 m thick (Sorgenfrei & Buch 1964); the position above a low salt pillow explains the somewhat lower thickness. The thickness of the Chalk Group in six boreholes at Stenlille 35–40 km NNE of the study area varies between 932 and 1062 m (Nielsen & Japsen 1991).

Seismic sections and a contour map of the Base Chalk reflection shows the planar, flat and undisturbed nature of the of the Base Chalk reflection (Figs 4, 5). It should be noted, however, that the wide spacing of the seismic lines does not allow detection of smaller topographic or structural features. The Base Chalk level is situated at a depth of about 800 m in the southern part of the study area and dips gently northwards starting with an inclination of about 1.3°. After two kilometres it flattens to about 0.8° until a low at about 900 m is reached north of Skælskør. Further northwards it rises again to a depth of about 850 m.

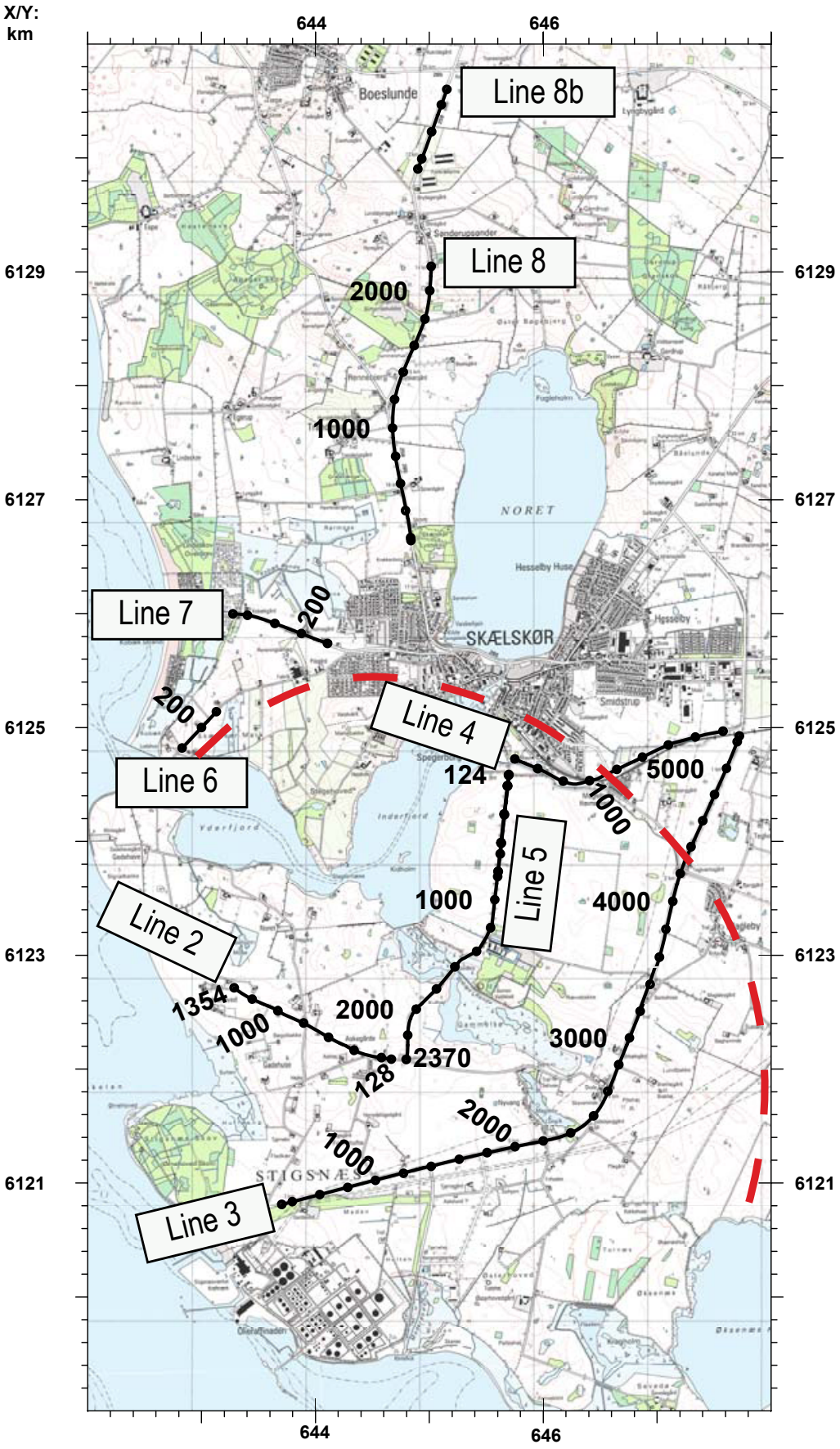

Fig. 3. Map showing the position of the seismic lines around the town of Skælskør. The numbers indicate shotpoints. The dashed red line gives the outline of the Skælskør high adapted from Sorgenfrei (1951), see also Figure 2.

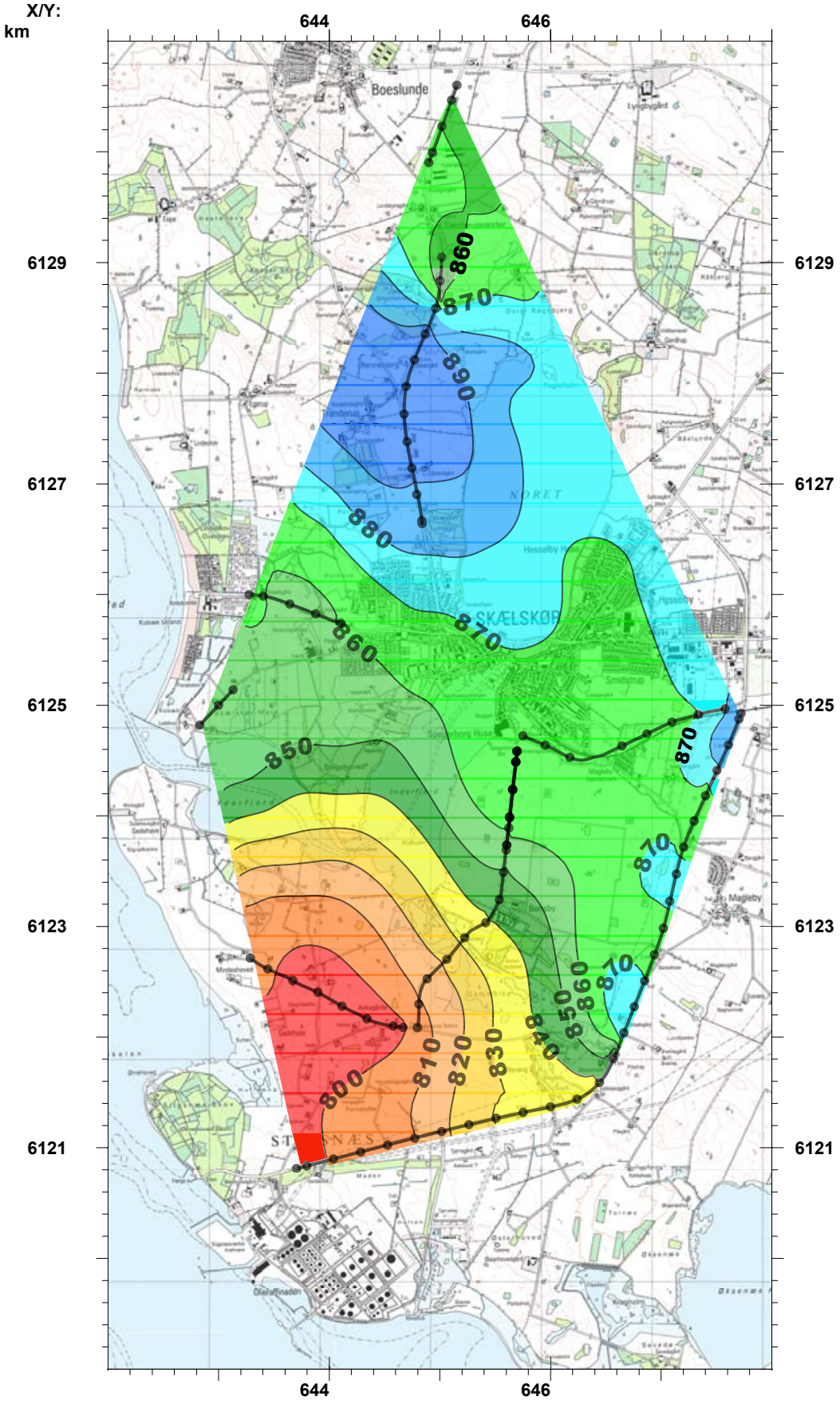

Fig. 4. Map showing the contours in metres below present sea level of the Base Chalk reflection. The contours are generated in the software package "The Kingdom Suite" provided by Seismic Micro Technology. Some of the features shown on the map are thus artefacts. Note the gentle northward dip of the reflection in most of the study area and a reversal to a S-ward dip in the northernmost part of the area. The latter is interpreted as the expression of low pillow of Zechstein salt (see also Figure 5).

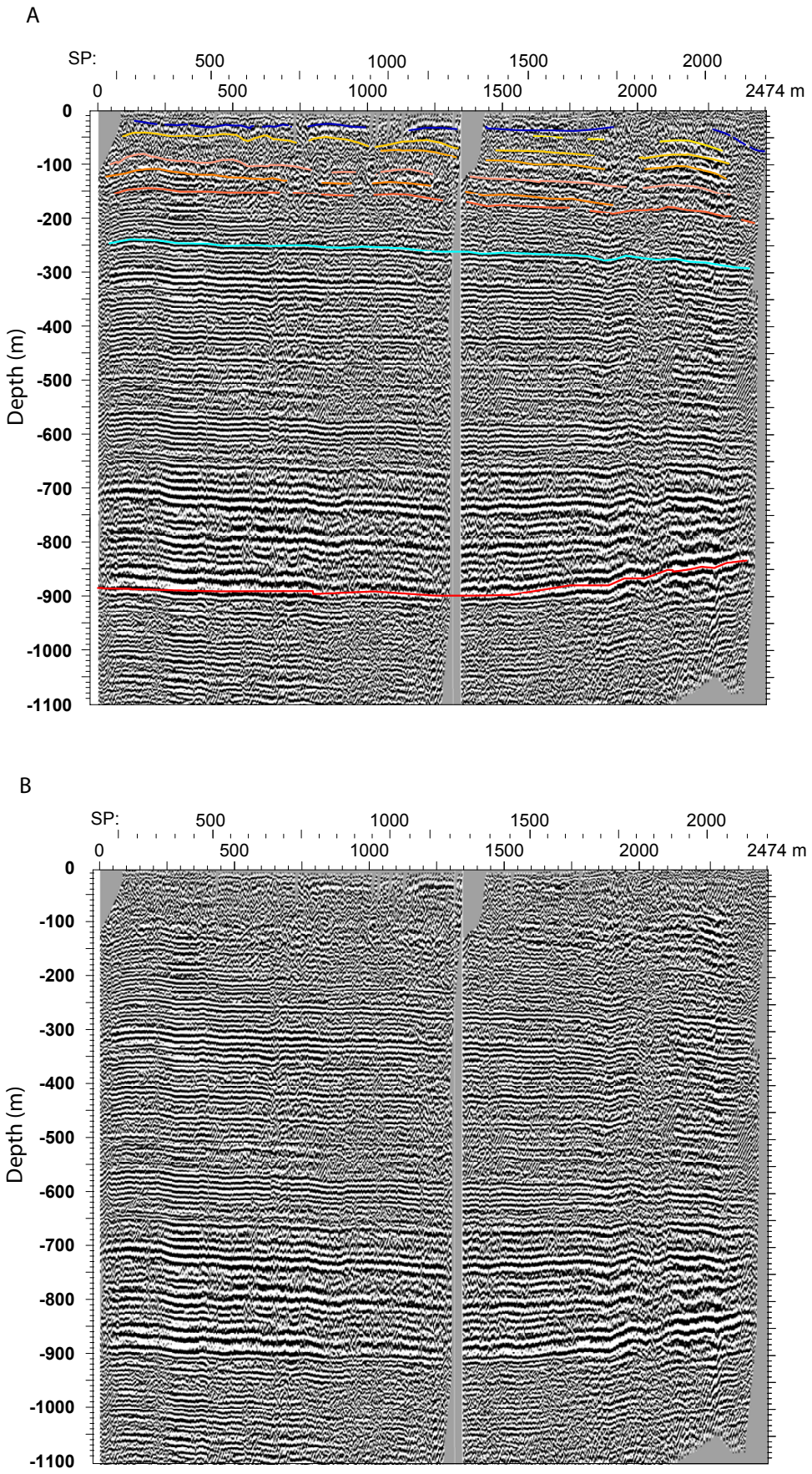

Fig. 5. N–S oriented seismic line 8 (position shown in Figure 3). Vertical scale is in metres below sea level. The unbroken and flat Base Chalk reflection (red, between 800 and 900 m depth) is close to horizontal from SP (shotpoint) 0 to SP 1600 where it starts to rise gently towards the N. This is interpreted as caused by the presence of a low pillow of Zechstein salt with a centre close to the northern end of the line (SP 2150).

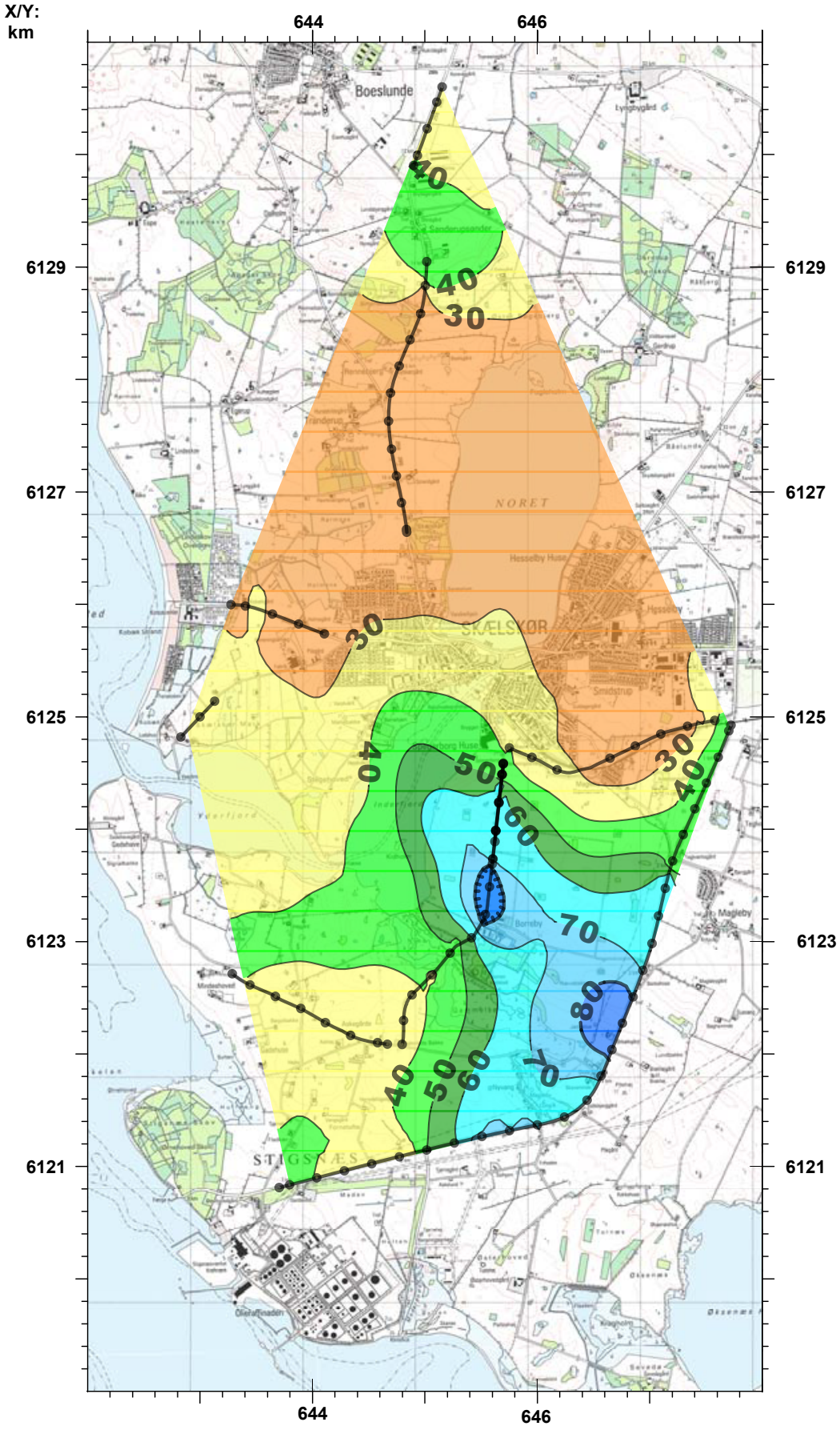

Fig. 6. Map showing contours in metres below present sea level of the top Top Chalk reflection. This surface was to some extent modified by Quaternary erosion and does not provide an exact picture of its original configuration. The contours are generated in the software package "The Kingdom Suite" provided by Seismic Micro Technology.

The southern high has a semicircular appearance in map view (fig. 4). Due to the sparse line coverage in the western part of the area it is believed that the real form is elongate in a direction parallel to the NW–SE trending coastline. The high is located along the NE-flank of a basement sliver protruding NW-wards from the Ringkøbing-Fyn High following the coastline between Skælskør and Stigsnæs as mapped by Vejbæk (1997). The high and the northward dip of the Base Chalk level is interpreted to be caused by increasing rates of subsidence from the basement sliver and out into the Danish Basin. The internal reflections in the Chalk Group diverge slightly basinwards towards the north, indicating that differential subsidence was active through the Late Cretaceous.

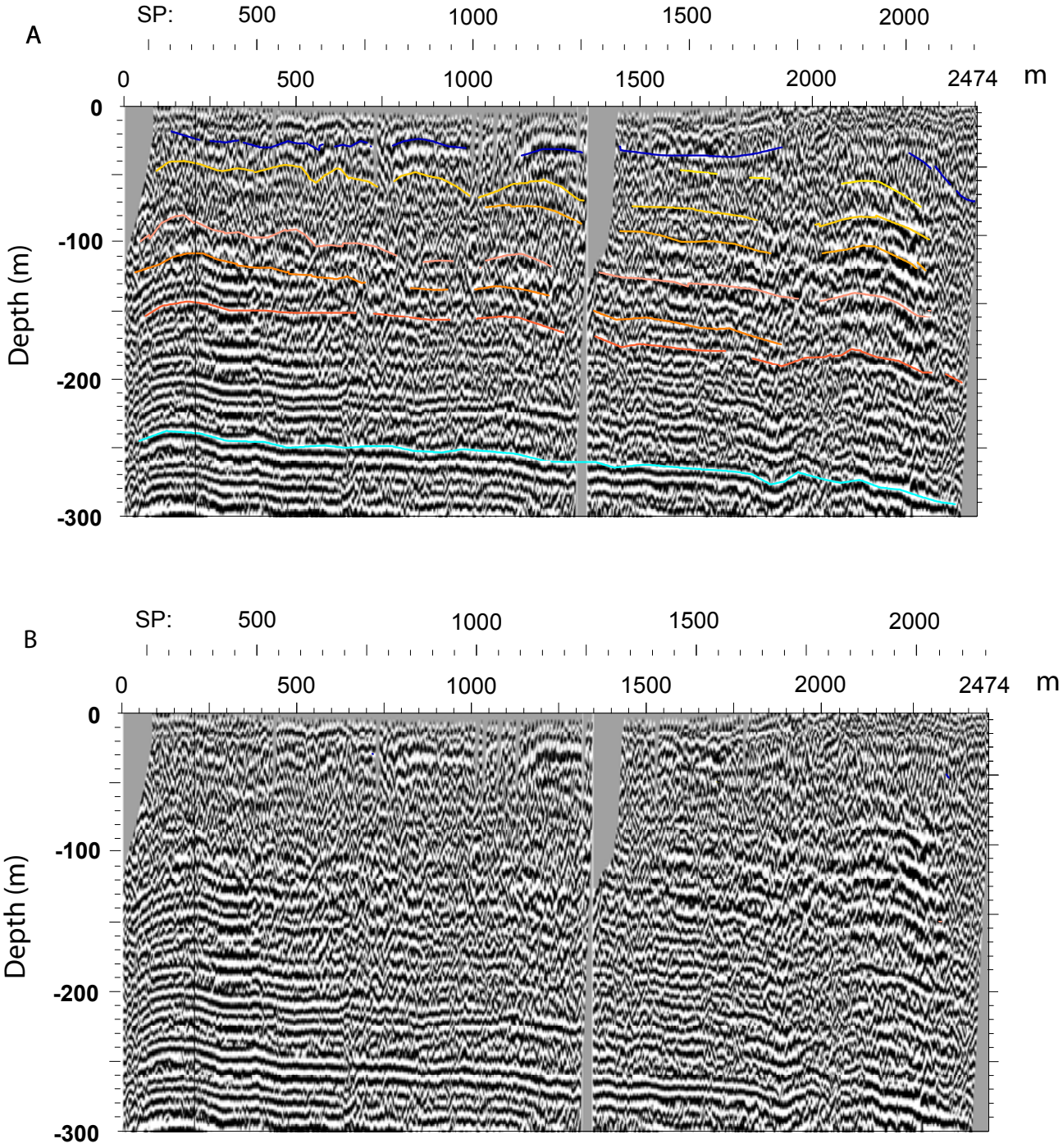

Fig. 7. Detail of the N–S oriented seismic section line 8 (Figs 3, 5). The top part of the Chalk Groups show mounded reflections representing development of a marked seafloor relief in the late Maastrichtian. Vertical scale in metres below sea level.

The Skælskør structure described by Sorgenfrei (1951) is located approximately above and to the north of the southern high (Figs 3, 4). The extent of the high mapped by Sorgenfrei (1951) was based on water wells penetrating into chalk, and the elliptic form depicted by Sorgenfrei shows the estimated outer limit of Upper Cretaceous chalk surrounded by Danian bryozoan limestone at the base of the Quaternary deposits. The Base Quarternary is an erosional surface and the observed distribution in map view of Maastrichtian chalk surrounded by Danian limestone proves the existence of a seafloor high at the the time of the K/T-boundary.

The location of the Skælskør structure indicates that differential subsidence took place at the southern edge of the Danish Basin. The hypothesis of wrenching as the cause of the Skælskør-high can therefore be rejected.

The change in dip in the northernmost part of the study area is clearly seen on line 8, where the reflection shows a very low dip towards the N in the southern part of the profile, changing to a S-ward dip at the northern end (Figs 4, 5). This rise in the position of the reflection is interpreted as caused by a deeper situated low pillow of Zechstein salt. Low salt pillows are common in the region, for example at the Stenlille boreholes (Japsen 1992).

The Top Chalk surface is to some extent modified by Quaternary erosion. The contour map shows a pronounced low in the SE part of the study area and an overall rise towards the NW and N. The highest part is found in the northernmost part of the study area and along seismic line 8 (Figs 5, 6).

The lower part of the Chalk Group is evenly bedded with parallel reflections (Fig. 5). Other seismic sections show slightly northwards diverging patterns. This pattern changes at depths of 150–200 m and the reflections above this level show a pronounced topographic relief with several scales of mound and channel-like features (Fig. 7). These features characterise the group all the way to the erosional top where it is overlain by Selandian siliciclastic sediments or Quaternary tills and outwash sands. Major palaeotopographic seafloor highs occur in the upper part of the Chalk Group in the southern, western and northernmost parts of the study area but the Base Chalk is flat and undisturbed beneath these highs and the intervening lows.

A similar development is seen elsewhere in NW Europe where a major palaeoceanographic change took place at the early–late Maastrichtian transition and the late Maastrichtian was characterised by strong bottom currents which sculpted the seafloor into drifts, channels and moats in several orders of magnitude, but commonly reaching amplitudes of more than 100 m and widths of several kilometres. These topographic features are parallel to the bathymetric contours of the seafloor in all areas where these can be estimated and they have thus been interpreted as formed by contour currents (Lykke-Andersen & Surlyk 2004; Surlyk & Lykke-Andersen 2007; Esmerode *et al.* 2007a, b; Surlyk *et al.* 2008; Esmerode & Surlyk 2009). The mounded reflections in the top part of the Chalk Group at Skælskør are likewise interpreted as representing a highly irregular seafloor relief formed mainly in the late Maastrichtian by bottom currents, possibly enhanced by bryoozoan growth as has been demonstrated for mounded chalk of the lower Sigerslev Member and the Højerup Member at Stevns Klint (Surlyk *et al.* 2006; Anderskouv *et al.* 2007).

Conclusions

- Reflection seismic data over the Skælskør structure clearly show that the Chalk Group has not been subjected to major syn- or post-depositional folding or faulting although a few minor faults have been detected.
- The Chalk Group shows differential subsidence across the northern flank of a basement high located in the southern part of the study area and forming a projection towards the northwest from the northern margin of the Ringkøbing-Fyn High. Subsidence thus increased from the high towards the north into the Danish Basin
- The Base Chalk reflection is essentially flat and undisturbed with only minor changes in inclination probably due to growth of a flat salt pillow in the northern part of the area.
- The upper part of the Chalk Group shows the development of a marked seafloor relief at the end of the Cretaceous, particularly in the late Maastrichtian.
- The hypothesis of Sorgenfrei (1951) that the high represents an anticline caused by wrenching along the Ringkøbing-Fyn High can thus be refuted.
- The high instead represents mounded drifts on the late Maastrichtian seafloor which were inherited into the Danian, and was superimposed on the northern flank of a small basement high south of the main study area.

Acknowledgements

This project was supported by Geocenter Denmark and the Danish Natural Science Research Council. We thank the seismic crew from the University of Aarhus for excellent work during data collection and Kresten Anderskouv and Erik Thomsen for useful comments on the manuscript.

References

Anderskouv, K., Damholt, T. & Surlyk, F. 2007: Late Maastrichtian chalk mounds, Stevns Klint, Denmark – combined physical and biogenic structures. Sedimentary Geology 200, 57–72.

Bjerager, M., Surlyk, F., Lykke-Andersen, H., Thibault, N. & Stemmerik, L. 2010: Danian cool-water coral reefs in southern Scandinavia localised over seafloor highs. Marine and Petroleum Geology 27, 455–466.

Brotzen, F. 1959: On *Tylocidaris* species (Echinoidea) and the stratigraphy of the Danian of Sweden. Sveriges Geologiska Undersökning ser. C 571, Årsbok 54, 1–81.

Esmerode E.V., Lykke-Andersen, H. & Surlyk, F. 2007a: Ridge and valley systems in the Upper Cretaceous chalk of the Danish Basin: contourites in an epeiric sea. In: Viana, A.R. & Rebesco, M. (eds): Economic and Palaeoceanographic Significance of Contourite deposits. The Geological Society, London, Special Publication 276, 265–282.

Esmerode, E.V., Lykke-Andersen, H. & Surlyk, F. 2007b: Interaction between bottom currents and slope failure in the Late Cretaceous of the southern Central Graben, North Sea. Journal of the Geological Society. London 165, 55–72.

Esmerode, E.V. & Surlyk, F. 2009: Origin of channel systems in the Upper Cretaceous Chalk Group of the Paris Basin. Marine and Petroleum Geology 26, 1338–1349.

Freiwald, A., Henrich, R. & Paetzold, J. 1997: Anatomy of a deep-water coral reef mound from Stjernsund, West Finnmark, Northern Norway. In: James, N.P. & Clarke, J.A.D. (eds.): Cool-water Carbonates. Special Publication – SEPM (Society for Sedimentary Geology) 56, 141–162.

Freiwald, E., Hohnerbach, V., Lindberg, B., Wilson, J.B. & Campbell, J. 2002: The Sula Reef Complex. Facies 47, 179–200.

Hennig, A. 1899: Studier öfver den baltiske Yngre kritans bildningshistoria. Kap. 5. Tertiäre dislokationer inom sydvestra Skånes Kritområde. Geologiska Föreningens i Stockholm Förhandlingar 21, 178–182.

Japsen, P. 1992: Landhævningerne i Sen Kridt og Tertiær i det nordlige Danmark. Dansk geologisk Forening, Årsskrift for 1990–91, 169–182.

Knudsen, C., Andersen, C., Foged, N., Jakobsen, P.R. & Larsen, B. 1995: Stratigraphy and engineering geology of København Limestone. Dansk Geoteknisk Forening Bulletin 11, 117–126.

Lykke-Andersen, H. & F. Surlyk 2004: The Cretaceous–Palaeogene boundary at Stevns Klint, Denmark: Inversion tectonics or sea-floor topography?: Journal of the Geological Society, London 161, 343–352.

Nielsen, L., Boldreel, L.O., Hansen, T.M., Lykke-Andersen, H., Stemmerik, L., Surlyk, F., Thybo, H. under revision. Integrated seismic analysis of the Chalk Group in eastern Denmark – implications for estimates of post-depositional uplift in southwest Scandinavia. Tectonophysics.

Nielsen, L.H. & Japsen, P. 1991: Deep Wells in Denmark 1935–1990. Lithostratigraphic subdivision. Geological Survey of Denmark, DGU Series A, 31, 1-179.

Rosenkrantz, A. 1938: Bemærkninger om det østsjællandske Daniens stratigrafi og tektonik. Meddelelser fra Dansk Geologisk Forening 9, 199–212.

Sorgenfrei, T. 1951: Oversigt over prækvartærets topografi, stratigrafi og tektonik i området Fyn-Sydsjælland-Lolland-Falster-Møn. Meddelelser fra Dansk Geologisk Forening 12, 166–171.

Sorgenfrei, T. & Buch, A. 1964: Deep Tests in Denmark 1935–1959. Danmarks Geologiske Undersøgelse 3. Rk., Nr. 36, 1–146.

Surlyk, F. 1997: A cool-water carbonate ramp with bryozoan mounds: Late Cretaceous – Danian of the Danish Basin. In: James, N.P. & Clarke, J.A.D. (eds.): Cool-water Carbonates. Special Publication – SEPM (Society for Sedimentary Geology) 56, 293–307.

Surlyk, F., Damholt, T. & Bjerager, M. 2006: Stevns Klint, Denmark: Uppermost Maastrichtian chalk, Cretaceous–Tertiary boundary, and lower Danian bryozoan mound complex. Bulletin of the Geological Society of Denmark 54, 1–48.

Surlyk, F., Jensen, S.K. & Engkilde, M. 2008: Deep channels in the Cenomanian–Danian Chalk Group of the German North Sea sector: Evidence of strong constructional and erosional bottom currents and effect on reservoir quality distribution. AAPG Bulletin 92, 1565–1586.

Surlyk, F. & Lykke-Andersen, H. 2007. Contourite drifts, moats and channels in the Upper Cretaceous chalk of the Danish Basin. Sedimentology 54, 405–422.

Thomsen, E. 1995: Kalk og kridt i den danske undergrund. In: Nielsen, O.B. (ed.): Danmarks geologi fra Kridt til idag. Aarhus Geokompendier 1, 31–67.

Vejbæk, O.V. 1997: Dybe strukturer i danske sedimentære bassiner. Geologisk Tidsskrift, 4, 1–31

Manuscript

Language – Manuscripts should be in English. Authors who are not proficient in English should ask an English-speaking colleague for assistance before submission of the manuscript.

Title – Titles should be short and concise, with emphasis on words useful for indexing and information retrieval. An abbreviated title to be used as running head must also be submitted.

Abstract – An abstract in English must accompany all papers. It should be short (no longer than 250 words), factual, and stress new information and conclusions rather than describing the contents of the manuscript. Conclude the abstract with a list of key words.

Danish summary – Authors are encouraged to deliver a short summary in Danish to follow the main text.

Main text – Use double spacing throughout, and leave a wide left margin (3.5 cm). Italics should be used only in generic and species names and in some Latin abbreviations (e.g. c., et al., ibid., op. cit). Use at most three grades of headings, but do not underline or capitalize. Indicate figure and table placement in pencil in the left margin.

References to figures, tables and papers – References to figures and tables in the text should have the form: Fig. 1, Figs 1–3, Table 3 or as (Smith 1969, fig. 3) when the reference is to a figure in a cited paper. – References to papers are given in the form Smith (1969) or (Smith 1969). Combined citations by different authors are separated by a semicolon; two or more papers by same author(s) are separated by commas. Citations are places chronologically and then alphabetically. Use 'et al.' for three or more authors, e.g. Smith et al. (1985).

Reference list

Danish letters æ, ø and å (aa) are treated as ae, o and a (aa), respectively. – Use following style:

Smith, A.A. 1989: Geology of the Bulbjerg Formation. Bulletin of the Geological Society of Denmark 38, 119–144. [Note that name of journal is given in full].

Smith, A.A.., Jensen, B.B. & MacStuff, C.C. 1987: Sandstones of Denmark, 2nd edition, 533 pp. New York: Springer Verlag [For more than 10 authors, use first author followed by et al.].

Smith, A.A.., Jensen, B.B. & MacStuff, C.C. 1992: Characterization of Archean volcanic rocks. In: Hansen, D.D. et al. (eds): Geology of Greenland. Geological Survey of Denmark and Greenland Bulletin 40, 1397–1438. [More than three editors – therefore et al. form is used].

References

1: Alphabetically by the first author's surname
2: Papers by one author: two or more papers are arranged chronologically
3: Papers by two authors: alphabetically after second author's name. Two or more papers by the same two authors: chronologically.
4: Papers by three or more authors: chronologically. Papers from the same year are arranged alphabetically after second, third, etc.author's name.

Authors themselves are responsible for the accuracy and completeness of their references. If incorrect references are detected the manuscript will be returned to the author for complete rechecking. The reference list must include all, and only, the references cited in the paper (including figures, tables etc).

Spelling – Geological units named after localities in Greenland, formal lithostratigraphical units and intrusions named after localities in Greenland remain unchanged even if the eponymous locality names have since been changed in accordance with modern Greenlandic orthography.

Illustrations

Illustrations – should be prepared for black and white printing: on one page unless author pays for the extra printing costs related to colour printing or foldouts. Horizontal illustrations are much to be preferred. Size of smallest letters in illustrations should not be less than 5.5 pt. Remember scale.

Submit copies of figures, tables, plates, etc. together with the manuscript. All figures (including photographs) should be submitted in electronic form ready for direct reproduction, i.e. having the dimensions of the final figure with a standard resolution of 300 dpi for photographs. Preferred formats are pdf, eps, tiff and jpg.

Size – The width of figures must 82 mm, 125 mm or 171 mm. Maximum height is 232 mm.

Captions – Captions to figures, tables and plates must be delivered on separate pages.

Colour charge – Colour figures are accepted, but imply a charge of DKK 3200 excl. VAT pr. article (max 16 pages).

Proofs and Offprints

Proofs – Authors receive one set of page proofs. Prompt return to the editor is requested. The cost of any alterations against the final manuscript will be charged to the author.

Offprint – One copy of the printed volume and a free pdf-file is supplied to the authors. Paper copies may be ordered at cost, when returning the proofs, stating carefully the number of copies and the address to which the offprints and invoice should be sent.

Content